Role of RAS signaling in Hedgehog-associated embryonal rhabdomyosarcoma

Dissertation
for the award of the degree
"*Doctor rerum naturalium"* (Dr.rer.nat.)
of the Georg-August-Universität Göttingen

within the doctoral program Molecular Medicine
of the Georg-August University School of Science (GAUSS)

submitted by
Julia Bauer

born in Göttingen

Göttingen 2018

Members of the Thesis Committee:

Supervisor
Prof. Dr. Heidi Hahn
Institute of Human Genetics, University Medical Center Göttingen

Second member of the thesis committee
Prof. Dr. Matthias Dobbelstein
Institute of Molecular Oncology, University Medical Center Göttingen

Third member of the thesis committee
Prof. Dr. Dieter Kube
Department of Haematology and Oncology, University Medical Center Göttingen

Members of the Examination Board:

Reviewer
Prof. Dr. Heidi Hahn
Institute of Human Genetics, University Medical Center Göttingen

Second reviewer
Prof. Dr. Matthias Dobbelstein
Institute of Molecular Oncology, University Medical Center Göttingen

Further members of the Examination Board:

Prof. Dr. Dieter Kube
Department of Haematology and Oncology, University Medical Center Göttingen

Prof. Dr. Peter Burfeind
Institute of Human Genetics, University Medical Center Göttingen

Prof. Dr. Frauke Alves
Department of Haematology and Oncology, University Medical Center Göttingen

Prof. Dr. Hubertus Jarry
Institute of Clinical and Experimental Endocrinology, University Medical Center Göttingen

Date of Disputation: 18th December 2018

Affidavit

Here I declare that my doctoral thesis entitled “Role of RAS signaling in Hedgehog-associated embryonal rhabdomyosarcoma” has been written independently with no other sources and aids than quoted.

……..

Julia Bauer

Göttingen, October 2018

Contents

I List of Figures

II List of Tables

III Abbreviations

µCT	Micro computed tomography
Ab	Antibody
AEC	3-Amino-9-ethylcarbazole
AKT	Protein kinase B
ALDH	Aldehyde dehydrogenase
ANG	Angiopoietin
ANOVA	Analysis of variance
ARF	ADP ribosylation factor
ARMS	Alveolar RMS
ATCC	American type culture collection
B6	C57BL/6N
Balb	BALB/c
BCA	Bicinchoninic acid
BCC	Basal cell carcinoma
BCL	B-cell lymphoma
BD	Binding domain
BLAST	Basic Local Alignment Search Tool
BOC	Brother of CDO
BrdU	5-bromo-2'-deoxyuridine
BSA	Bovine Serum Albumin Fraction V
bp	Base pairs
cAMP	Cyclic adenosine monophosphate
Casp 3	Caspase 3
CDK	Cyclin-dependent kinase
CDKN	Cyclin-dependent kinase Inhibitor
cDNA	Complementary DNA
CDO	Cell adhesion molecule-related/downregulated by oncogenes
ChIP	Chromatin immunoprecipitation
CM	Conditioned medium
CMV	Cytomegalovirus
COSMIC	Catalogue Of Somatic Mutations In Cancer
Cre	Cyclization recombination
CSC	Cancer stem cell
CT	Cycle threshold
CTNNB	Catenin beta-1 (β-catenin)
CXCR	C-X-C motif chemokine receptor
DAB	3,3'-Diaminobenzidine
DAPI	4′,6-diamidino-2-phenylindole
ddH_20	Double-distilled water
Del	Deleted
DHH	Desert Hedgehog
DISP	Dispatched
DMBA	1,3-Dimethylbutylamine

DMEM	Dulbecco's Modified Eagle Medium
DMF	Dimethylformamide
DMSO	Dimethylsulfoxide
DNA	Deoxyribonucleic acid
DNMT	DNA methyltransferase
dNTP	Deoxyribonucleotide triphosphate
DTT	Dithiothreitol
DYRK	Dual-specificity tyrosine-(Y)-phosphorylation-regulated kinases
ECL	Enhanced chemiluminescence
EDTA	Ethylenediamine tetraacetic acid
e.g.	*exempli gratia* (lat. for example)
EGF	Epidermal growth factor
EGFP	Enhanced green fluorescent protein
EGFR	EGF receptor
EGTA	Ethyleneglycol tetraacetic acid
ELISA	Enzyme-linked immunosorbent assay
ELK	ETS-like gene 1, tyrosine kinase
ERBB	Erb-B2 Receptor Tyrosine Kinase
ERK	Extracellular-signal regulated kinase
ERMS	Embryonal RMS
EtBr	Ethidium bromide
EtOH	Ethanol
FACS	Fluorescence-activated cell scanning
FCS	Fetal calf serum
FGF	Fibroblast growth factor
FGFR	FGF receptor
Fig.	Figure
fl	Floxed
FOXO1	Forkhead box protein O1
FU	Fused
GAP	GTPase activating protein
GAS1	Growth arrest specific 1
gDNA	Genomic DNA
GDP	Guanosine diphosphate
GLI	Glioma-associated oncogene
GLI^A	GLI activator form
Gli BS	Gli binding site
GLI^R	GLI repressor form
GOI	Gene of interest
GPCR	G-protein-coupled receptor
GTP	Guanosine triphosphate
GEF	Guanine nucleotide exchange factors
h	Hour
h	Human
HA	Hemagglutinin
HE	Haematoxylin and eosin

HEPES	4-(2-hydroxyethyl)-1-piperazineethanesulfonic acid
HH	Hedgehog
HhA	HhAntag
HHIP	HH interacting protein
HIS	Histidin
HRAS	Harvey rat sarcoma
HPRT	Hypoxanthine phosphoribosyltransferase
HRP	Horseradish peroxidase
HSC70	Heat shock cognate 71 kDa protein
HSV-TK	Herpes simplex virus thymidine kinase
i.e.	*id est* (lat. that is)
IgG	Immunoglobulin G
IGF	Insulin-like growth factor
IHC	Immunohistochemistry
IHH	Indian Hedgehog
IKK	Inhibitor of κB kinase
IL	Interleukin
i.p.	Intraperitoneally
ISH	*In situ* hybridization
i.v.	Intravenously
JNK	c-Jun N-terminal kinase
kb	Kilobase
KRAS	Kirsten rat sarcoma
kDa	Kilo Dalton
LB	Lysogeny broth
log	Logarithm to base 10
LOH	Loss of heterozygosity
LoxP	Locus of crossing-over of bacteriophage P1
m	Murine
mAb	Monoclonal antibody
MAPK	Mitogen-activated protein kinase
MB	Medulloblastoma
MDM2	Mouse double minute 2 homolog
MEK	Mitogen-activated kinase
MeOH	Methanol
MEKK1	Mitogen-activated protein kinase kinase kinase 1
min	Minute
MMP	Matrix metalloproteinase
MolTaq	Taq-Polymerase (named after *Thermus aquatius*)
MRF	Myogenic regulatory factor
mRNA	Messenger RNA
mTOR	Mammalian target of rapamycin
MYC	Avian myelocytomatosis virus oncogene cellular homolog
Myf	Myogenic factor
MyHC	Myosin heavy chain

MyoD	Myogenic differentiation antigen
N	Sample size
NC	Nitrocellulose
NCBI	National Center for Biotechnology Information
NF1	Neurofibromin 1
NFκB	Nuclear factor 'kappa-light-chain-enhancer' of activated B-cells
NLB	Nuclear lysis buffer
NIK	NFκB inducing kinase
NRAS	Neuroblastoma RAS viral oncogene homolog
n.s.	Not significant
OD	Optical density
OMIM	Online Mendelian Inheritance in Man
oncRAS	Oncogenic RAS
pAb	Polyclonal antibody
pAKT	Phosphorylated AKT
PAX	Paired box gene
PBS	Phosphate buffered saline
PBST	PBS-Tween 20
PCR	Polymerase chain reaction
PDGFR	Platelet-derived growth factor receptor
pDNA	Plasmid DNA
pERK	Phosphorylated ERK
PFA	Paraformaldehyde
pH	lat. *potentia hydrogenii*
PI	Propidium iodide
PI3K	Phosphatidylinositol-4,5-bisphosphate 3-kinase
PIK3CA	Phosphoinositide-3-kinase, catalytic, alpha polypeptide
PKC	Protein kinase C
PL	Phospholipase
pMSCV	Plasmid derived from Murine Stem Cell Virus
PRMS	Pleomorphic RMS
P/S	Penicillin/Streptomycin
pS6	Phosphorylated S6
PTCH	Patched
p-value	Probability value
qRT-PCR	Quantitative real-time PCR
RAF	Rat fibrosarcoma
RAG	Recombination activating gene
RAS	Rat sarcoma
Rb	Retinoblastoma
RBD	Ras-binding domain
RIPA	Radioimmunoprecipitation assay buffer
RLU	Relative light unit
RMS	Rhabdomyosarcoma
rpm	Rounds per minute

RPMI	Roswell Park Memorial Institute
RNA	Ribonucleic acid
RNAseq	RNA sequencing
rRNA	Ribosomal RNA
RT	Room temperature
RTK	Receptor tyorsine kinase
S6	Small subunit ribosomal protein S6
S6K1	S6 kinase beta-1
SAG	Smoothened agonist
SDS	Sodiumdodecylsulfate
sec	Second
SEM	Standard error of the mean
SFB	Subcellular fractionation buffer
SHH	Sonic Hedgehog
SMO	Smoothened
SMAD	Contraction of Sma (small) and Mad (Mothers against decapentaplegic)
S.O.C.	Super optimal broth with catabolite repression
SOS	Son of sevenless guanine nucleotide exchange factor
SOX	(sex determining region Y)-box
SPHK	Sphingosine kinase 1
SRMS	Sclerosing/spindle cell RMS
STE	Sodium Chloride-Tris-EDTA
SUFU	Suppressor of fused
Tab.	Table
TBE	Tris-boric acid-EDTA solution
TBP	TATA-binding protein
TBS	Tris buffered saline
TBST	TBS-Tween 20
TEA	Triethanolamine
TGFβ	Transforming growth factor β
TNF	Tumor necrosis factor
TP53/p53	Tumor protein p53
TPA	12-O-tetradecanoylphorbol-13-acetate
TRIS	Tris(hydroxymethyl)aminomethane
U	Enzymatic unit
UV	Ultraviolet
VEGF	Vascular endothelial growth factor
v/v	Volume/volume
WB	Western Blot
WHO	World Health Organization
WST-1	Water soluble tetrazolium salt 1
WT	Wildtype
w/v	Weight/volume
X-Gal	5-bromo-4-chloro-3-indolyl-β-D-galactopyranoside

1 Abstract

Rhabdomyosarcoma (RMS) are the most common pediatric soft tissue sarcomas. RMS of the embryonal subtype (ERMS) are characterized by high expression of markers of an activated Hedgehog (HH) signaling cascade, i.e. they overexpress *GLI1, GLI2* and *PTCH*. However, they very infrequently show pathway-activating mutations e.g. in PTCH, although inherited *PTCH/Ptch* mutations act as ERMS-drivers both in humans and mice. This is different for oncogenic mutations in the 3 *RAS* genes (H-, K-and NRAS; oncRAS), which are a very common in ERMS. Since the literature provides evidence for crosstalks between HH and RAS signaling in other tumor entities, this thesis aimed at a better understanding of a potential interaction of HH and RAS signaling in ERMS and of their roles in ERMS pathogenesis, growth and aggressiveness. This is particulary important for improvement of treatment strategies, which currently show only moderate efficiencies and sometimes cause severe side effects.

First, the role of oncRAS isoforms in regulation of HH targets and associated cellular responses were studied in human cell lines derived from sporadic (full-blown) ERMS. The *in vitro* data from TE617.T, RUCH-2 and RD highlight that oncRAS isoforms decrease the expression of the major HH-target *GLI1* in dependency of ERK. GLI1 downregulation was also seen on protein level in both the nucleus and cytoplasm. This indicates that oncRAS/ERK probably act on *GLI1* transcription. In addition, oncRAS/ERK also regulate the expression of other HH pathway members e.g. of *SHH*, *PTCH* and *GLI2*, which however depends on the oncRAS isoform and the individual cell line. Although oncRAS mutations can modify the expression of *SHH*, the cell lines are in all likeliness not able to secrete HH ligands and are not HH-responsive. Together, this supports an oncRAS-mediated non-canonical suppression of HH signaling, or at least of *GLI1*/GLI1 expression, in sporadic ERMS.

Interestingly, oncRAS isoforms increase proliferation and tumorigenicity of ERMS cell lines despite downregulation of *GLI1*/GLI1. This indicates that proliferation of the cells is independent of HH signaling or at least of *GLI1*/GLI1. Since oncRAS-mediated *GLI1*-downregulation is only moderate in xenografts, it is likely that the tumor microenvironment also influences HH signaling.

OncKRas and oncHRas also aggravate formation of *Hh/Ptch*-driven ERMS from heterozygous $Ptch^{del/+}$ mice. This is in contrast to oncNRas, which induces expression of myogenic markers without otherwise affecting the tumor. This suggests that the 3 oncRas isoforms have divergent functions in ERMS, at least in *Hh/Ptch*-driven tumors. Interestingly, these oncRas-mediated changes are only seen when the oncRas genes are expressed at a

very early ERMS stage, i.e. in ERMS precursor lesions. However, they do not occur when the mutations are induced at the full-blown tumor stage. Since, according to the literature, oncRas mutations themselves do not drive ERMS formation and since none of the oncRas genes significantly influence Hh signaling activity in *Hh/Ptch*-driven ERMS, these findings open the possibility that the mutational status of PTCH/Ptch may influence the importance of oncRAS mutations in ERMS. On the other hand it is possible that oncRAS mutations are rather passenger mutations, which only affect already initiated ERMS precursor cells and/or cancer stem cells (CSCs), but not the ERMS bulk populations. Indeed, a preliminary analysis shows that cell lines from sporadic (full-blown) ERMS have a subpopulation, which is positive for the CSC marker CD133. Of whether full-blown ERMS of heterozygous $Ptch^{del/+}$ mice lack this population is not clear at the moment and further experiments need to be done to shed light on these hypothesis. Together, these interesting results help to better understand the pathology of ERMS and hopefully will also be valuable to improve current therapies for this childhood sarcoma.

2 Introduction

2.1 Rhabdomyosarcoma

Soft tissue sarcomas are a very heterogeneous group of over 50 rare tumor entities that occur throughout the lifespan [1]. They account for about 2 % of malignant tumors in adults and 7 % of pediatric malignancies [2,3]. In children, rhabdomyosarcoma (RMS) account for approximately 50 % of all soft tissue tumors and thereby are the third most common extracranial solid tumor [3,4]. RMS have an incidence of 4.5 cases per million children per year and most frequently occur in children younger than 10 years of age [5].

Originally RMS were thought to develop from cells committed to the skeletal muscle lineage, because they frequently show aberrant muscle differentiation and develop in the skeletal muscle. However, since these tumors can also arise from other anatomic sites, such as the genitourinary region, it is thought that they rather are of mesenchymal origin [1,6-8].

RMS represent a heterogeneous group of soft tissue sarcomas. They can be divided into several histopathological subtypes, which differ in their clinical and morphological phenotype and molecular features. The current classification from the World Health Organization (WHO) divides RMS into alveolar RMS (ARMS), which are characterized by tumor cells separated by thin fibrovascular septa and embryonal RMS (ERMS) with small round blue cells and partial rhabdomyoblastic differention. ERMS can also show botryoid and pleomorphic growth patterns. Other RMS variants are pleomorphic RMS (PRMS), and sclerosing/spindle cell RMS (SRMS) [5,9-11]. The two major RMS subtypes in children are ARMS and ERMS and they differ in their prevalence, clinical features and outcome [6].

ARMS account for approximately one-third of all RMS and frequently occur in adolescents. They are found most commonly in the deep tissue of the extremities and show an alveolar pattern in histology [5]. On molecular level they can be divided into fusion-positive and fusion-negative tumors. Fusion-positive ARMS (75 %) show chromosomal translocations [t(2;13)(q35,q14) or t(1;13)(p36;q14)] leading to Forkhead box protein O (FOXO)1-Paired box gene (PAX)3/PAX7 fusion proteins, which contribute to pathogenesis [12]. Fusion-negative ARMS, lacking PAX-FOXO1 fusion proteins, are clinically and biologically similar to ERMS [13].

ERMS account for approximately two-thirds of all RMS and occur mainly in young children. Histologically, they resemble undifferentiated embryonic mesenchyme with isolated immature myoblastic cells. They are often found in the head and neck region and in the genitourinary tract [5]. Whole-genome sequence projects reveal that ERMS in general possess a higher background mutation rate than ARMS [14,15]. On molecular level, ERMS frequently show loss of heterozygosity (LOH) at chromosome 11p15, which is the locus of *Insulin-like growth factor 2* (*IGF2)* [4]. In addition, mutations in the rat sarcoma (Ras) signaling pathway (*NRAS*,

KRAS, *HRAS* and *Neurofibromin 1(NF1*)) are frequently described for ERMS [5,6,15] (compare section 2.3.4). Moreover, they can carry mutations in *Myogenic differentiation antigen* (*MYOD)*, *Fibroblast growth factor receptor* (*FGFR)4*, *catalytic Phosphoinositide-3-kinase alpha polypeptide* (*PIK3CA*), *Catenin beta 1* (*CTNNB1*) genes and in the tumour suppressor genes *tumor protein 53* (*TP53)* and *Retinoblastoma* (*RB)1.* However and in contrast to ARMS, they are always fusion-negative [6,8,16].

RMS have been associated with several hereditary diseases. These include hereditary retinoblastoma, neurofibromatosis type 1, Li–Fraumeni syndrome, Rubinstein–Taybi syndrome, Beckwith–Wiedemann syndrome, Costello syndrome, Noonan syndrome and Gorlin (basal cell carcinoma nevus) syndrome [8,17-22]. However, most cases of RMS are considered sporadic in their origin [8,20].

2.1.1 Current prognostics and therapy strategies

The tumor size, age at diagnosis, histological type, tumor stage and already conducted therapies are significantly associated with the overall survival of RMS. In general, patients with RMS show a 10-year overall survival rate of 62 %. More precisely, the rates range between 75 % for fusion-negative ARMS, 65 % for ERMS and 20 % for fusion-positive ARMS [13,23]. This highlights that fusion-positive ARMS are associated with a poorer prognosis than ERMS and fusion-negative ARMS.

RMS are considered a systemic disease with the possibility of micro- and macrometastasis, which are found in 46 % of fusion-positive RMS and 17 % of fusion-negative RMS [1,13,24]. Thus an effective treatment should not only target the primary tumor but also distant tumor seeds. The currently available multimodal therapy, which encompasses surgery, radiation and chemotherapeutic drugs, leads to the recovery of 60 % of all RMS patients. However, less than 30 % of high-risk patients (metastatic or fusion-positive tumors, adults) are cured [13,25]. In addition, many patients suffer from adverse side effects and treatment-related late effects [8]. Thus, more effective and less harmful therapy options are needed, which requires a better understanding of biology and molecular mechanisms of RMS pathogenesis.

2.2 The Hedgehog signaling pathway

The Hedgehog (*Hh*) ligand and its receptor Patched (*Ptch*) were first discovered in a mutational screen in larvae of *Drosophila melanogaster*. The mutations in the respective genes lead to segmentation defects, which in case of *Hh* results in a surface reminding of hedgehog spines [26]. A few years later, Hh was shown to influence pattern formation in surrounding cells in a paracrine manner [27-29].

Today it is known, that the Hh signaling pathway is one of the most important signal transduction pathways during embryonic development. In general, Hh signaling is quiescent in the adult organism but it is implicated in cell differentiation, stem cell maintenance,

metabolic homeostasis, tissue homeostasis and repair [30,31]. As a consequence, pathological activation of the pathway plays a crucial role in initiation and formation of various cancers [32].

2.2.1 Canonical Hh signaling

In mammals 3 Hh homologs, namely Indian Hedgehog (Ihh), Desert Hedgehog (Dhh) and Sonic Hedgehog (Shh), with distinct expression patterns were discovered [33]. Shh, the best studied Hh ligand, has a high functional similarity to Hh of *Drosophila*. It affects cells of the developing embryo, especially during formation of the ventral neural tube, the anterior-posterior limb axis and the ventral somites. Furthermore and as already said, it controls tissue homeostasis, stem cell maintenance and differentiation processes of mesenchymal cells in adults [33,34]. Ihh is involved in chondrogenesis, whereas Dhh regulates germ-cell proliferation and development of peripheral nerves. Dhh is also expressed in adult nerves [33,35-37]. Hh proteins are synthesized as precursors and are matured by autocatalytic cleavage and posttranslational modifications. Thus, a cholesterol moiety is attached to the N-terminal product and thereby restricts the ligand to the cell surface. If required for signaling, the processed Hh ligands are secreted with the help of the transmembrane protein Dispatched (DISP) [32,38-40].

Two *Ptch* homologs *Patched1* (*Ptch*) and *Patched 2* (*Ptch2*) are present in mammals. Ptch is a 12-pass transmembrane protein and the major Hh receptor. It has 2 extracellular loops, which are required for Hh binding, a cytoplasmic C-terminus that is involved in signal transduction and a sterol-sensing domain that mediates the intracellular trafficking of Ptch. It constitutively represses Hh signaling and thereby acts as a tumor suppressor [41-43]. The binding of Hh ligands to Ptch is supported by its co-receptors Cell adhesion molecule-related/downregulated by oncogenes (Cdo), Brother of Cdo (Boc) and Growth arrest specific 1 (Gas1) [44]. In its unbound state, Ptch is localized in the primary cilium und suppresses the activity of its interaction partner Smoothened (Smo) via a poorly understood mechanism [45]. Smo is a seven transmembrane receptor of the G-protein-coupled receptor (GPCR) superfamily [46,47]. Its activation triggers processing and modifications of glioma-associated oncogene (Gli) proteins (Cubitus interruptus in *Drosophila melanogaster*) and thereby the activity of the Hh signaling cascade [42].

The Gli proteins act as activator or repressor of transcription, which is reliant on the availability of Hh ligands [48,49]. *Gli1* is a transcriptional target of Hh signaling and provides a positive feedback loop in the pathways activity, whereas Gli2 and Gli3 are the main mediators of Hh signaling [50]. Gli2 and Gli3 are bifunctional transcription factors, which can act as full length activator forms (Gli^A) or truncated repressor forms (Gli^R). The activator forms are stabilized in the presence of Hh ligands. Gli proteins are processed into their truncated repressor forms when Hh ligands are absent. The balance between activator and repressor forms is very important for the regulation of Hh signaling activity [51-53]. The

processing into truncated Gli proteins is triggered by phosphorylation of amino acids that are located N-terminally or C-terminally of the DNA binding domain. Strong phosphorylation of both regions promotes the processing into truncated Gli^R forms or triggers degradation. Partially phosphorylated Gli proteins are processed and act as weak Gli^A (phosphorylation C-terminally of the DNA binding domain) or weak Gli^R (phosphorylation N-terminally of the DNA binding domain). Dephosphorylated Gli proteins are not processed and act as strong Gli^A [54,55]. Since Gli1 misses the N-terminal region after the zinc-finger DNA binding domain, it is supposed to act only as a Gli^A form. Gli1 and Gli2 have strong activator functions when present as the full length Gli^A form. Gli2 can be processed into a Gli^R form with low efficiency in mouse embryos and it is therefore considered to have a weak repressor activity [56]. In contrast, full-length Gli3 protein, which acts as a weak Gli^A form especially in early developmental processes like spinal cord patterning and sclerotome development [56-58], is efficiently processed into its truncated Gli^R form that acts as a strong transcriptional repressor.

A simplified scheme of the Hh pathway is shown in Figure 1 (Fig. 1). Fig. 1A shows the pathway in its inactive state, whereas Fig. 1B shows the active pathway upon binding of the Hh ligand.

In the absence of Hh ligands, Ptch is located in the primary cilium of the cell where it represses the activity of its interaction partner Smo [45]. The Gli proteins are prevented from entering the nucleus through interactions with the serine/threonine kinase fused (Fu) and suppressor of fused (Sufu) [59]. The Gli proteins are phosphorylated, which results in their proteolytic cleavage to truncated $Gli3^R$ proteins. Gli^R proteins, mainly $Gli3^R$, translocate into the nucleus and repress target gene transcription. In addition, surplus Gli proteins are ubiquitinated and subsequently proteasomally degraded [60,61].

Upon binding of Hh ligands, Ptch is inactivated and its inhibitory effect on Smo is abrogated. This results in enrichment of Smo in the primary cilium. As a consequence Sufu is degraded and releases Gli proteins [62,63]. The Gli proteins are dephosphorylated and stabilized in their full length Gli^A form. Thereupon, Gli^A proteins, mainly $Gli2^A$, translocate into the nucleus and activate the transcription of Hh target genes [42,49,64]. Among others, the mammalian Hh target genes include *Gli1*, *Ptch* and Hh interacting protein (*Hhip*). Additionally, Gli proteins can regulate genes implicated in proliferation (*Igf2*, *Platelet-derived growth factor receptor* (*Pdgfr*)*, myelocytomatosis virus oncogene cellular homolog* (*Myc*)), cell cycle progress and apoptosis (*Cyclin D1, Cyclin D2, N-Myc, B-cell lymphoma (Bcl) 2*), angiogenesis (*Vascular endothelial growth factor* (*Vegf*)*, Angiopoietin (Ang)1/2*), epithelial-mesenchymal transition (*Matrix metalloproteinase (Mmp)9, Snail*) or in regulation of stem cells (*Nanog,* (*sex determining region Y)-box 2* (*Sox2*)) [31,32,42,60,65-67]. However, the most reliable and robust readout of an active Hh signaling pathway is considered to be *Gli1* expression [46,68,69]. The activity of the Hh signaling pathway is not only regulated by its ligands, but partly also

through its targets genes. Whereas expression of *Gli1* amplifies the Hh signal, expression of *Ptch* and *Hhip* decreases the signal in a negative feed-back loop.

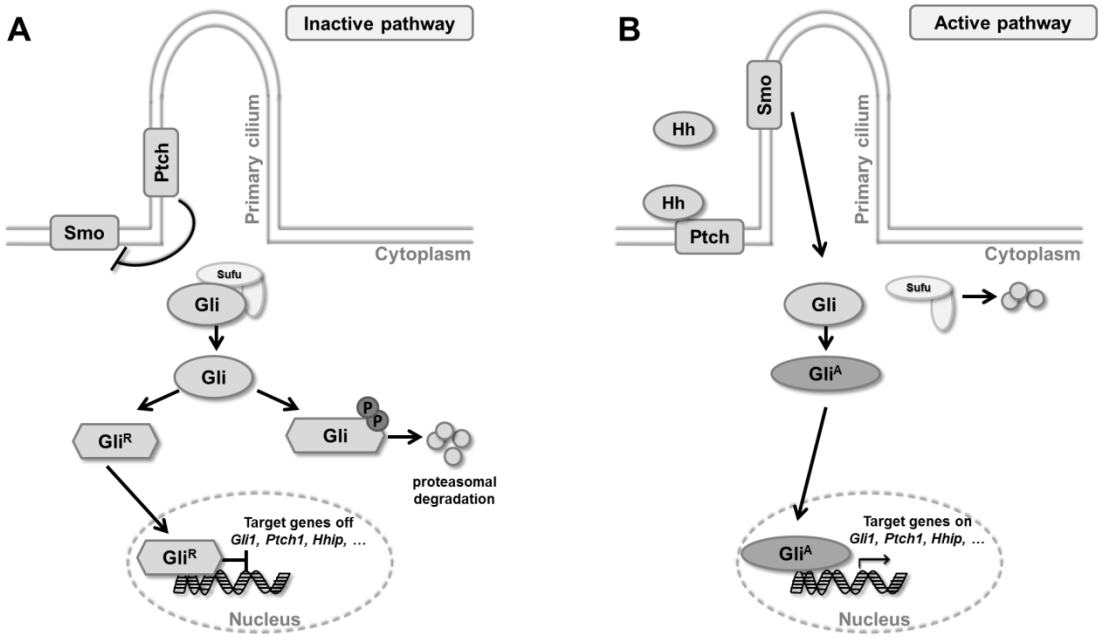

Figure 1: The Hh signaling pathway
(A) In the absence of its ligands the Hh signaling pathway is inactive. The transmembrane protein receptor Patched (Ptch) inhibits the activity of its interaction partner Smoothened (Smo). As a consequence, the glioma-associated oncogene (Gli) transcription factors, which are downstream targets of Smo, are kept in the cytoplasm by interaction with suppressor of fused (Sufu). Gli proteins are processed and act in their truncated repressor forms (Gli^R), which block target gene expression. Additionally, Gli proteins are proteasomally degraded. Consequently, transcription of Hh target genes is repressed. **(B)** Hh ligands bind to their receptor Ptch. This inactivates Ptch, which results in activation of Smo and the stabilization of Gli activator forms (Gli^A). Gli^A translocates into the nucleus and activates the transcription of Hh target genes. One of these targets is *Gli1*, which can amplify the Hh signal and provides a reliable marker of the pathway's activity. Additionally, Hh siganling promotes proteasomal degradation of Gli inhibitor Sufu. For more details see text. Modified according to [32].

2.2.2 Non-canonical Hh signaling

Besides canonical regulation (see section 2.2.1), Hh signaling can be regulated in a non-canonical manner. Non-canonical Hh signaling is divided into signaling processes, which do not require Smo (see section 2.2.2.1) and those which do not require Gli transcription factors (see section 2.2.2.2) [70].

2.2.2.1 Smo-independent Hh signaling

Smo-independent Hh signaling summarizes the regulation of expression, stability and transcriptional activity of Gli transcription factors by interaction with other signaling pathways or regulatory proteins. Smo-independent regulation of Gli proteins by other oncogenes and tumor suppressors is particularly involved in cancers [51,52,69,71].

The tumor suppressor p53 can inhibit Gli transcriptional activity because it can hamper the nuclear localisation of Gli1. This has been shown in melanoma [72]. *Vice versa*, Gli1 can also repress the activity of p53 in mouse embryonic fibroblasts by upregulation of the p53 inhibitor Mouse double minute 2 homolog (Mdm2). This results in degradation of p53 [73].

The transforming growth factor β (Tgfβ) can indirectly induce *Gli1* and *Gli2* expression in

different cell lines without involving the Ptch/Smo axis. Thus, activation of Tgfβ can cooperate with Smad3 or β-catenin, which in turn bind to the Gli2 promotor and thereby regulate the activation of Gli2 and Gli1 [74].

The phosphatidylinositol-4,5-bisphosphate 3-kinase (PI3K)/ protein kinase B (Akt)/ mammalian target of rapamycin (mTOR) signaling cascade can enhance nuclear localization and transcriptional activity of Gli1 and Gli2 in different human an murine model systems [75-78]. Thus, activated mTOR/Small subunit ribosomal protein S6 kinase beta (S6K1) signaling downstream of PI3K/Akt can modify phosphorylation and enhance activity of Gli1 [79]. Additionaly, *AKT1* itself is a transcriptonal target of the HH signaling cascade in B-cell lymphoma. This connection is a hint for a regulatory feed-back mechanism between Akt and Hh signaling [80].

Furthermore, the dual-specificity tyrosine-(Y)-phosphorylation-regulated kinases (Dyrk) 1A and 1B and also Dyrk2 can regulate Gli1 and Gli2 activity by phosphorylation [81-83]. As already mentioned above, phosphorylation of Gli proteins leads to processing into the respective Gli^A or Gli^R forms [54]. Dyrk1A can phosphorylate GLI1, which promotes its nuclear localization [81,82]. Dyrk1B was reported to either inhibit or stimulate Hh signaling, dependent on the *Dyrk1B* expression level and the used model systems [84-87]. It was suggested that Dyrk1B activates mTOR/Akt, which promotes Gli1 stabilization [87]. Finally, Dyrk2 can phosphorylate Gli2, thereby inducing its degradation in mouse embryonic fibroblasts and COS1 cells [83].

Finally, oncogenic Ras (oncRas) isoforms can directly influence Gli transcription factors with diverse outcomes in different tumor entities. This is reviewed in detail in section 2.4.

2.2.2.2 Gli-independent Hh signaling

The Hh receptor Ptch can regulate cell survival through apoptosis induction. This does not involve Hh ligands, Smo or Gli, but the formation of a caspase-activating complex [88,89]. Furthermore, Ptch can regulate cell cycle progression through interaction with Cyclin B1 without the involvement of the Smo/Gli axis [90,91].

In addition, Hh ligands can alter cell morphology and migratory capacity without Gli transcription activity in murine and human cells. However, this requires Smo activity, which in turn can activate PI3K or small guanosine triphosphate (GTP)ases like RhoA resulting in cytoskeletal changes [89,92]. The Smo-mediated cytoskeletal rearrangements and migration requires the metabolism of arachidonic acid through the 5-lipoxygenase pathway [92,93]. Moreover, Shh can stimulate Src kinases to control guidance of murine commissural axons. This also requires Smo, but not Gli proteins [94]. Additionally, Shh stimulates intracellular Ca^{2+} spike activity in neurodevelopment [95]. *Vice versa,* intracellular Ca^{2+} release and Protein kinase c (Pkc) activation can stimulate Shh gene expression [96] and these activities do not require Gli proteins. Finally, Smo can trigger intracellular signaling via second messengers like Ca^{2+} and cyclic adenosine monophosphate (cAMP) [97]. Indeed, Smo is supposed to

influence physiological Ca^{2+} fluctuation and Ca^{2+}-dependent signaling pathways in a Gli-independent manner [96]. Moreover, Smo, Ca^{2+} and cAMP are involved in Warburg-like metabolic reprogramming in muscles and brown fat [98].

2.2.3 Canonical HH signaling in human cancer

Several cancers are caused by pathological activation of the Hh signaling pathway. Indeed, the first link between a predisposition to tumors and mutations within the HH signaling pathway was the discovery of *PTCH* mutations in patients with Gorlin syndrome [99-102]. Besides developmental defects, patients with Gorlin syndrome develop basal cell carcinoma (BCC) and have an increased risk of developing other cancers such as medulloblastomas (MB), RMS, fibromas, glioma and meningioma [21,66,102-107].

Subsequently, aberrant activation of the HH signaling cascade due to inactivating mutations in *PTCH* or *SUFU*, activating mutations in *SMO* or mutations of other HH pathway molecules have been shown in the majority of both familial and sporadic forms of BCC and a subset of MB [108-117]. In the latter cancer entity a signature of the HH pathway activation status (*GLI1*, *SPHK1*, *SHROOM2*, *PDLIM3*, *OTX2*) has been established and serves as a diagnostic tool in the treatment of these tumors with HH inhibitors [118]. In addition, mutations in members of the HH signaling pathway have also been reported in other cancers associated with Gorlin syndrome, including RMS (see section 2.2.4) and meningiomas [119,120].

Thereupon, pathological activation of HH signaling was detected in a huge variety of other cancer types. As in BCC and MB, the dysregulation of the signaling pathway can be mutation-driven (Fig. 2A). However, it also can be ligand-driven (Fig. 2B) or can be dysregulated due to amplification of *GLI* (Fig. 2C). This dysregulation can occur tumorintrinsically or in the surrounding stromal tissue, or in both.

Examples for mutation-driven HH-associated tumors are BCC and MB, as already said. In contrast, lymphomas are ligand-driven tumors and show constitutive activation of the HH pathway due to overexpression of SHH [121]. Similarly, the expression of *SHH* and *GLI1* is increased in a subset of small lung cell carcinoma [122]. An amplification of GLI transcription factors has been described in glioblastoma, BCC and bladder cancer [123-125].

However, in the majority of tumor entities showing HH signaling activity, both mutations and overexpression of the ligands can be responsible for pathological activation of the pathway. For example tumors of the foregut, oesophagus, stomach and biliary tract can either show an increased level of SHH or IHH or genetic alterations in *PTCH*, *SMO* or *SUFU* [126,127]. In a subgroup of pancreatic adenocarcinoma and its precursor lesions, HH ligands are abnormally expressed or the HH signaling cascade is deregulated due to overexpression of *PTCH* [128]. Overexpression of HH ligands is also frequently observed in bladder cancer, which also can show amplification of *GLI1* or overexpression of GLI2 [129,130]. A subset of melanoma has mutations in *PTCH*, *SMO*, *SUFU*, *GLI1* or *GLI2*. In addition, the vascularization of these

tumors is regulated by SHH [75,131-133]. In a subset of advanced human prostate cancers, activation of the HH pathway occurs due to HH ligands that act in an autocrine or paracrine manner. In another subset this is due to mutations in *PTCH* and *HHIP* [125,134]. Similarly, the HH signaling pathway is activated due to mutations in *PTCH* or *SUFU* in a subset of breast cancer patients [135] and overexpression of *SHH*, *GLI1* or *PTCH* [136] is associated with poor prognosis [136].

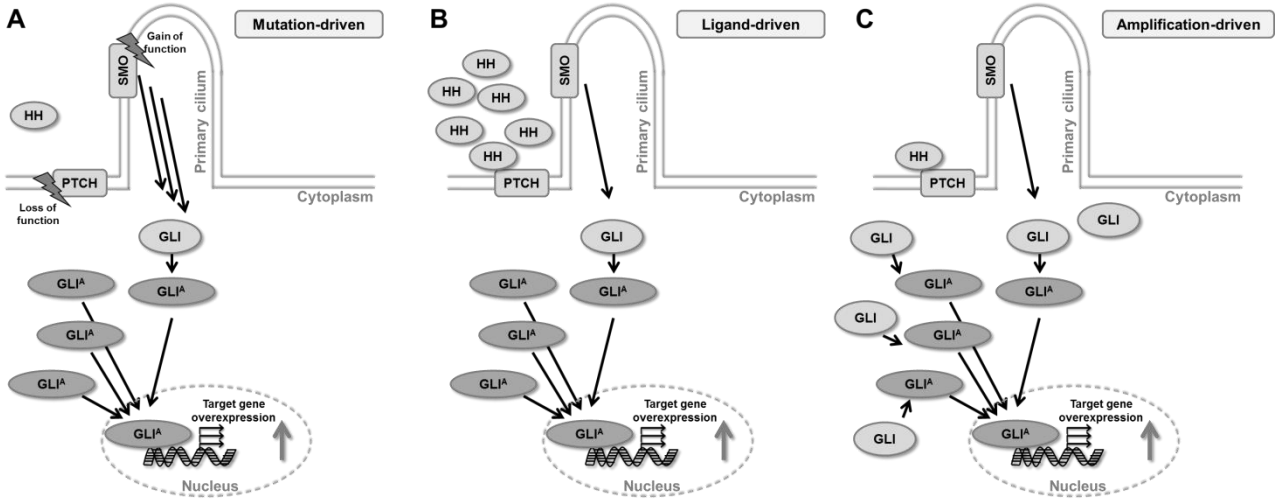

Figure 2: Canonical HH signaling in human cancer
Pathological activation of the HH signaling pathway plays a role in initiation, formation and progression of tumors (for details, see text). **(A)** Mutation-driven activation of the HH signaling pathway can be due to loss of function mutation in PTCH or gain of function mutations in SMO, which results in a permanent activation of the pathway. **(B)** Ligand-dependent dysregulation of the HH signaling pathway occurs due to overexpression of HH ligands. **(C)** Amplification-driven activation of the HH signaling pathway occurs due to amplification of *GLI*, which results in higher level of the respective proteins.

Taken together, a pathological activation of the canonical Hh signaling pathway can be caused by several mechanisms. These include mutations in members of the Hh signaling pathway (Fig. 2A), overexpression of Hh ligands (Fig. 2B) or amplification of Glis (Fig. 2C). Besides these modifications, Gli activity and thus Hh signaling can also be regulated in a non-canonical manner (see section 2.2.2).

2.2.4 Hh signaling and RMS

The spectrum of tumors found in Gorlin patients includes RMS, showing that germline mutations in *PTCH* enhance the susceptibility to this tumor entity (see section 2.2.3). This is similar in *Ptch*-heterozygous mice that develop RMS-like tumors [21]. These murine tumors resemble the embryonal RMS subtype in humans and as human ERMS, they show a strong expression of the Hh targets *Gli1* and *Igf2.* In addition, they express terminal myogenic differentiation markers, like *Desmin* and *MyoD* [66,137,138]. Moreover, a heterozygous deletion of *Sufu* in combination with loss of p53 or a constitutive activation of *Smo* leads to ERMS formation in mice [139,140].

Besides *GLI1*, the average expression level of *GLI2*, *GLI3* and *PTCH* are consistently elevated in human ERMS compared to normal skeletal muscle [141,142]. In addition, the level of

these genes is higher in ERMS and fusion-negative ARMS compared to fusion-positive ARMS. It also seems to correlate with a worse outcome and survival rate [143]. However, mutations in the coding regions of the HH pathway genes that can activate HH signaling, are very rare in RMS [15,144,145].

Nevertheless, genomic loss of the *PTCH* locus on 9q22 has been identified in 30 % (4/12) of ERMS cases [146,147]. In other studies, LOH of the *PTCH* or *SUFU* loci has also been detected in ERMS (3/8 tumors showed LOH of the *PTCH* and 2/4 tumors of the *SUFU* locus; in a different RMS subset 1/14 tumors showed LOH of the *PTCH locus*) [142,148].

On the other hand, genomic gain of 12q13.3 and 2q14.2, which contain the *GLI1* and *GLI2* loci, respectively, have been reported in up to 54 % (*GLI1*) and 92 % (*GLI2*) of ERMS [141,149]. Consequently, multiple copies of *GLI1* or *GLI2* have been detected in the tumor samples [141]. Additionally, increased protein level of GLI1 were observed [149]. However, there are also studies, which describe no mutations in RMS [15,144].

In addition, HH ligands were investigated in human RMS. Interestingly, SHH levels are not increased in ERMS [141]. However, DHH and IHH are expressed, which implicates a role of these ligands in this tumor entity [150-152].

Taken together, these data show that the Hh pathway plays an important role in RMS. However, its activation in RMS on molecular level is not fully understood. Nevertheless, inhibitors of the HH signaling pathway are under investigation for targeted therapy of RMS. The Gli1/2 inhibitor GANT61 shows promising results in cultured RMS cells [153-155]. Unfortunately, this inhibitor is unstable under acetic conditions and thus cannot be used in the clinics [156]. In addition, small molecule inhibitors for Smo are under investigation for RMS treatment. Cyclopamine, the first discovered natural Smo inhibitor, effectively reduces growth of different RMS cell lines [157]. However, in full-blown murine ERMS, application of cyclopamine does not inhibit tumor growth despite effectively inhibiting Hh signaling. In fact, cyclopamine rather induces tumor growth [158]. Recent analyses by our group with the Smo inhibitors cyclopamine, vismodegib, sonidegib and HhAntag (HhA) revealed that Smo inhibitors induce strong antitumoral effects in murine ERMS with a *Ptch* mutation, whereas cell lines derived from ERMS without *Ptch* mutation responded heterogeneously to Smo inhibition[159,160]. Therefore, Smo inhibitors are considered a good treatment option for ERMS that are caused by mutations upstream of Smo [159,160].

2.3 The Ras signaling pathway

The Ras genes were originally discovered in the genome of Harvey and Kirsten rat sarcoma viruses in the 1960/70s. In 1982, different research groups described mutated *RAS* alleles in human tumors, which resulted in an enormous interest in these genes [161]. Today, 3 Ras isoforms have been identified in mammals, which are H-*ras*-l (HRas), K-*ras*-2 (KRas) with

2 splice variants (K-*ras*-4a and the predominant splice variant K-*ras*-4b) and N-*ras* (NRas). Additionally, 2 pseudogenes, H-*ras*-2 and K-*ras*-l, have been characterized. All *Ras* genes are highly conserved during evolution [162]. The Ras proteins are low-molecular-weight GTP-binding proteins (21 kDa), which are activated in response to different extracellular stimuli through their receptors. To deploy their biological activity the Ras proteins need to be localized at the inner plasma membrane. In addition, they need to be posttranscriptionally modified by farnesyltransferases. Then they interact with lipid groups, which stabilizes their position at the plasma membrane [163-166].

Ras proteins control diverse cellular signaling pathways, which are involved in transcriptional regulation, translation, posttranslational modification and cellular processes, like growth, differentiation, survival, cell cycle progression, cytoskeletal remodeling, endocytosis and calcium signaling [167]. A simplified overview of Ras signaling and its different downstream axes is depicted in Fig. 3.

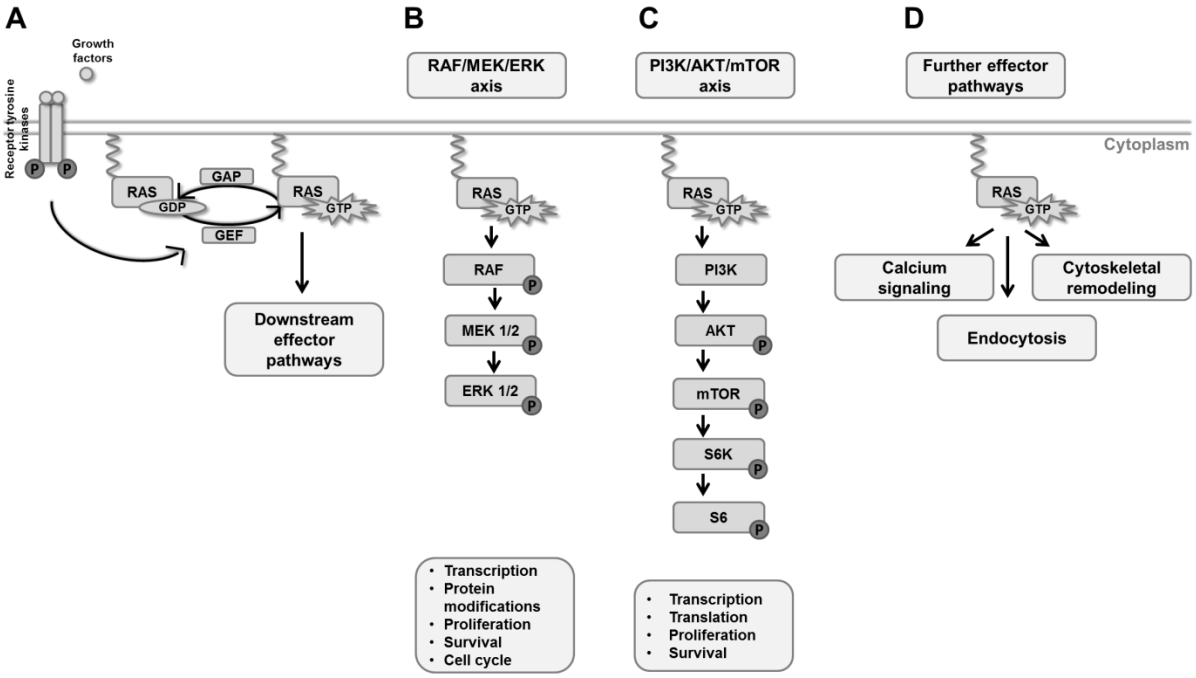

Figure 3: Activation of RAS and its downstream effector pathways
(A) RAS proteins are activated by various extracellular stimuli, which are mediated by receptor tyrosine kinases, G-Proteins or others. Consequently, guanine nucleotide exchange factors (GEF) promote the formation of active, GTP bound RAS. The return to the inactive state is controlled by GTPase activating proteins (GAP), which promote the hydrolysis of RAS-bound GTP. Active RAS controls the activity of several downstream signaling pathways. **(B)** The major effector pathway of active RAS is the RAF/MEK/ERK pathway. It predominantly controls transcription, posttranslational modifications, cellular proliferation and growth, as well as cell survival, differentiation and cell cycle progression. The signal is transmitted by sequential phosphorylation of the RAF, MEK and ERK kinases. **(C)** Another prominent effector pathway, which interacts with RAS, is the PI3K/AKT/mTOR signaling pathway. This effector pathway controls transcription, translation, proliferation and survival. The signal is transmitted by sequential phosphorylation of the kinases AKT, mTOR, S6K and of S6. **(D)** Other downstream effector pathways of the RAS signaling cascade control calcium signaling, cytoskeletal remodeling and endocytosis. For more details, see text. Modified according to [167].

As shown in Fig. 3A, the activity of Ras proteins is regulated by guanosine di- or triphosphate (GDP/GTP) binding, whereby GDP-bound Ras is inactive and GTP-bound Ras is active. The hydrolysis of GTP into GDP is catalyzed by GTPase activating proteins (GAPs) and the

exchange of GDP by GTP is catalyzed by guanine nucleotide exchange factors (GEFs) [168-171]. Ras is activated through GEFs in response to activation of different receptor tyorsine kinases (RTK) or GCPRs [172]. Under physiological conditions, Ras activation is transient and strictly regulated. However, mutations in codon 12, 13, or 61 convert the Ras genes into active oncogenes. This is due to the fact that mutations at these conserved sites prevent the hydrolysis of GTP to GDP and are thereby promote constitutive activation of Ras [173]. Besides activating mutations errors in GDP/GTP regulation, loss of GAPs or persistent RTK activation of GEFs are additional mechanisms of Ras activation in cancer [174]. Activated Ras binds preferentially to its downstream Ras-binding-domain (RBD)- or Ras-association-domain-containing targets and triggers the activity of other downstream effectors [175].

The major target of Ras is rat fibrosarcoma (Raf), which in turn triggers the phosphorylation and activation of the downstream mitogen-activated protein kinase (Mapk) signaling pathway (Fig. 3B). In mammalian cells, 4 major Mapk kinases have been characterized, which are extracellular-signal regulated kinase (Erk) 1/2, c-Jun N-terminal kinase (Jnk), p38 and Erk5 [176]. Ras activates Raf by recruiting it to the plasma membrane. Three Raf isoforms exist, which are called Raf-1, A-Raf and B-Raf. B-Raf has a higher intrinsic kinase activity than Raf-1 and A-Raf. Nevertheless, all Rafs are activated by multiple dephosphorylation and phosphorylation processes by Ras when recruited to the membrane [177,178]. Activated Raf in turn triggers serine phosphorylation of several proteins [179,180]. Main targets of Raf are the mitogen-activated kinases (Mek)1 and Mek2. Activated Mek in turn phosphorylates and activates the Erk, which itself has several substrates [180,181]. This signaling cascade controls cellular growth, differentiation, proliferation and migration of cells. Moreover, it regulates cell cycle progression and cellular differentiation processes [167,176,182-184]. Additionally, this cascade can have tumor suppressor properties by promoting selective protein stabilization or degradation and cellular senescence [185-188].

Ras signaling can also activate the PI3K/Akt/mTOR pathway [189] (Fig. 3C). PI3K converts phosphatidylinositol (4,5)-bisphosphate into phosphatidylinositol(3,4,5)-trisphosphate and thereby stimulates the activity of Akt by phosphorylation at Thr308. For full activation Akt must also be phosphorylated at Ser473 in its C-terminal region. Akt can trigger various cellular responses and is embedded in a complex network of activators, inhibitors and second messengers [190]. For example, Akt can phosphorylate different kinases such as mTOR that in turn activates S6 kinase. This affects cell proliferation and survial, as well as transcriptional and translational events [167,191-193]. Ras can interact with PI3K in a direct manner through its RBD without involving any other proteins. Depending on the cellular context, activation of the PI3K signaling pathway can lead to an activation or inhibition in Raf/Mek/Erk signaling at the level of Raf. *Vice versa*, Raf can activate or inhibit the PI3K/Akt/mTOR at the level of Akt (not visualized in Fig. 3) [189,194].

In addition to these two main effector pathways, Ras also regulates a large amount of other pathways (Fig. 3D). For example, Ras phosphorylates and thus activates phospholipases (PL), i.e. PLCε. Activation of PLs influences the generation of bioactive lipid mediators and leads to the mobilization of calcium, generation of diacylglycerol and activation of PKC [195-197]. Additionally, RAS can stimulate endocytosis and hence influence cellular trafficking of specific molecules [198,199]. Moreover, Ras signaling can regulate actin cytoskeleton dynamics in cells. This remodeling process is required for cellular growth [200,201].

2.3.1 Specific features of different Ras isoforms

The *Ras* genes show high homology and are co-expressed in most of mammalian tissues. However, whereas *HRas* level are high in brain, muscle and skin and low in liver of mice, *KRas* transcripts are most abundant in gut, lung and thymus and low in skin and skeletal muscle. *NRas* transcripts are elevated in testis and thymus. Additionally, the highest *NRas* level is observed at day 10 of gestation in mice, whereas *KRas* expression is highest at the beginning of gestation [202,203]. In general, the translation and protein expression of KRas messenger RNA (mRNA) is reduced relative to that of other Ras isoforms due to a high frequency of rare codons in *KRas*. These rare codons apparently enhance oncRas-driven tumorigenesis, because their conversion into common codons results in fewer tumors after carcinogen exposure in mice. [204,205].

The 3 Ras proteins share 85 % of their amino acid sequence, are activated through the same receptors and can exhibit functional redundancy. Nevertheless, activation of the Ras isoform can also have non-redundant functions [206-208].

The 3 Ras proteins differ in their N-terminal amino acids, which contain membrane binding and trafficking informations [209]. They are differently lipidated and show a different intracellular distribution [174,208]. For example, at an inactive state, HRas and NRas are localized at the plasma membrane and Golgi membranes, whereas KRas is preferentially present at the plasma membrane [210]. Within the plasma membrane, Ras isoforms are located in different microdomains. KRas is located within non-lipid-raft plasma membrane, irrespective of its activation state. In contrast, HRas is distributed equally between the raft and non-raft regions, but GTP-loading increases its localization within the non-lipid-raft plasma membrane [165,210]. Besides this differential compartmentalization, ubiquitination can influence the ability of Ras proteins to activate their downstream effectors [206].

In vitro experiments indicate that oncHRas might be a better activator of PI3K, whereas oncKRas and oncNRas activate predominantly Raf and Rac. This could result in different biological responses [211-215]. Additionally, the expression of oncHRas, but not oncKRas, can induce senescence [174]. On the other hand, oncNRas exerts anti-apoptotic effects, which are suppressed by oncKRas [216,217].

Furthermore, the biological outcome of a *Ras* mutation is strongly dependent upon the cellular context. For example, *NRAS* mutations are common in leukemia. Indeed, hematopoetic cells are easier transformed by oncNRas than by oncKRas or oncHRas. However, fibroblasts are more efficiently transformed by oncHRas than by oncKRas or oncNRas [218]. In addition, oncNRAS, but not oncKRAS, is able to transform melanocytes [219]. On the other hand, oncKRAS transforms colonic epithelial cell lines, whereas oncNRAS does not [216]. Similarly, oncKRas suppresses differentiation and promotes proliferation of murine colonic tumors. However, oncNRas does not promote proliferation, but rather suppresses apoptosis in this model (the effect of oncHRas was not investigated) [220]. Moreover, oncKRas promotes proliferation and maintains stem cell characteristics of endodermal progenitors. In contrast, oncHRas promotes differentiation and growth arrest of these cells, whereas oncNRas has no impact on none of these parameters [221].

Finally, besides overlapping and redundant functions, isoform-specific differences of the *Ras* genes are also obvious during developmental processes in mice. Thus, a *KRas* knockout in the germline is embryonic lethal at day 12 to 14 of gestation [222,223]. In contrast, mice with a *HRas* or an *NRas* knockout in the germline are viable [222,224]. This could be due to the fact that *KRas* is essential for normal fetal liver erythropoiesis [225]. However, HRas can replace the function of KRas when it is expressed from the *KRas* locus. The resulting mice are viable despite a dilated cardiomyopathy associated with arterial hypertension [226,227]. This suggests that HRas can functionally substitute for KRas during development. However, a homozygous deletion of *NRas* is lethal in developing $KRas^{+/-}$ mice, because of severe anemia and growth delays of the embryos [222]. This suggest, that *NRas* and *KRas* have partly overlapping functions in fetal liver erythropoiesis and other developmental processes.

As already mentioned, *HRas* knockout mice grow normally and are fertile. Most interestingly, they show a decreased tumor load after carcinogenic (1,3-Dimethylbutylamine (DMBA)/12-O-tetradecanoylphorbol-13-acetate (TPA)) treatment. Thus, *HRas* knockout mice develop approximately six times less papillomas compared with wildtype (wt) mice after 20 weeks of treatment. In addition, 40 % of the tumors of *HRas*-deficient mice show oncKRas mutations, which are not common in papilloma. This indicates that oncKRas can replace HRas in the initiation of papilloma [224,228].

NRas knockout mice are viable, fertile and show no gross morphological or histological abnormalities. Nevertheless, these mice have an impaired immune response as measured by decreased thymocyte proliferation and lower numbers of $CD8^+$ thymocytes upon an infection with influenza virus [229,230]. However, this immune defect was not seen in another model, in which *NRas* was knocked-out together with *HRas* [224]. Thus it remains open whether NRas is involved in a normal immune response.

2.3.2 Ras signaling in cancer

Approximately 25 % of all human tumors harbor oncogenic *RAS* mutations (*HRAS*: 2 %, *KRAS*: 18 %, *NRAS*: 5 %; according to COSMIC v86). These mutations create active Ras proteins and result in abberant proliferation or survival of tumor cells [231,232]. In the majority of cases (98 %), oncRas mutations are single base missense mutations at the residues G12, G13 or Q61. Interestingly, the predominant mutated *Ras* isoform and the respective mutated residue are specific for individual cancer types. However, in general G12 mutations occur more often in *KRAS* and *HRAS,* whereas Q61 mutations are predominant in *NRAS* [233].

In pancreatic ductal adenocarcinoma (90 % of all pancreatic cancers) and lung adenocarcinoma (35 % of all lung adenocarcinoma) *KRAS* is the predominantly mutated *RAS* isoform whereas mutations in *HRAS* or *NRAS* are very rare. This is similar in colorectal cancers, in which *KRAS* is also the primarily mutated isoform (45 % of all colorectal cancers) and in which *HRAS* and *NRAS* mutations are infrequent. In melanomas (15 % of all melanomas), liver cancer (30 % of all liver cancers) and acute myelogenous leukaemias (30 % of all acute myelogenous leukaemias), *NRAS* is the predominant oncRAS isoform and mutations within *HRAS* or *KRAS* are rarely observed. *HRAS* mutations are more common than *NRAS* or *KRAS* mutations in bladder cancer (10 % of all bladder cancers show *HRAS* mutations) and in head and neck squamous cell carcinomas (4 % of these cancers have *HRAS* mutations) [167,233,234]. Conversely, oncogenic *KRAS* and *NRAS* are observed at equivalent frequencies in multiple myeloma and seminoma, whereas mutations in *HRAS* are barely observed. In thyroid carcinomas, all 3 *RAS* isoforms are mutated at a similar frequency [167]. The impact of oncRAS mutations in RMS is described in detail in sections 2.3.4 and 2.4.1.

This highlights that most cancer types show mutations in a specific *Ras* isoform. As described above, differen Ras isoforms can regulate distinct signaling pathways [212-214]. In addition, a completive function of different Ras isoforms due to none-overlapping functions are described. For example, both wtKRas and wtNRas are required for transformation of mouse fibroblast. Whereas wtNRas regulates adhesion, wtKRas coordinates the motility of the cells [235]. However, recent studies also suggest collaborative effects between oncRas and different wtRas proteins, which supposedly is specific for individual cancer phenotypes. For example, in colorectal cancer cell lines an oncogenic *KRas* allele results in elevated levels of GTP-bound wtNRas [216]. In pancreatic cancer cell lines or colon cancer cells oncKRas activates wtHRas via the GEF Son of sevenless (Sos) and thereby stimulates cancer cell growth and tumor growth in xenografts [236]. Downregulation of wtHRas or wtNRas in pancreatic cancer cell lines or colon cancer cells expressing oncKRas leads to overactivation of the Erk and PI3K/Akt pathways [237]. In cancer cell lines (oncHRAS: T24 bladder cancer cell line, oncKRAS: MIA PaCa-2 pancreatic cancer cell line, oncNRAS: RD RMS cell line) expressing oncRas, oncRas activates basal Mapk signaling despite negatively regulating

RTK signaling on receptor level, whereas wtRas activates RTK signaling and acts as a driver of cell survival and proliferation [238]. In murine papilloma development, wtKRas acts cooperatively with oncHRas to promote papilloma development. Additionally, loss of wtNRas decreases the number of oncHRas-dependent papilloma [239].

Beside this tumorpromoting role of wtRas in oncRas-expressing cancers, other studies suggest that wtRas can act as a tumor suppressor. For example, tumorigenesis in the mouse skin is associated with an elevated copy number of oncHRas and/or a loss of wtHRas, indicating a tumor suppressive function of wtHRas [240]. Similar, loss of wtHRas increases the tumor load and reduces survival in murine pancreatic adenocarcinoma expressing oncKRas [241]. In addition, wtHRas inhibits oncKRas-dependent progression of murine lung cancers. Finally, loss of wtNRas increases the number of oncKRas-induced lung tumors [239].

2.3.3 RASopathies

Oncogenic mutations in *RAS* (or in other regulators of RAS signaling) are not only found in sporadic cancers. As germline mutations, they also can cause autosomal dominant genetic syndromes. These diseases are called RASopathies and are frequently associated with RMS [242,243]. Examples are Neurofibromatosis type 1, which is caused by germline mutations in *NF1*, which is a GAP that regulates GDP/GTP exchange of RAS [242,244,245]. Other examples are the capillary malformation–arteriovenous malformation syndrome, which is caused by haploinsufficiency of the RAS signaling regulator gene *RASA1* [246], the cardio-facio-cutaneous syndrome, which is caused by germline mutations in *BRAF*, *MAP2K1*, *MAP2K2* [247,248] and the Legius syndrome, which is caused by inactivating mutations in *SPRED1* that regulates the activation of the MAPK cascade [249]. Interestingly, 2 of the RASopathies, namely Noonan and Costello syndrome, can be caused by mutations in *RAS* and are associated with an increased susceptibility to RMS. Thus, patients with Costello syndrome have a dominant *HRAS* germline mutation [17,250], whereas Noonan syndrome can be caused by germline mutations in *KRAS* or *NRAS*. The latter disease also can show germline mutations in *PTPN11*, *SOS1*, *RAF1*, *SHOC2* and *CBL*, that, with the exception of *CBL* (E3 ubiquitin ligase), are all implicated in RAS signaling [251-258].

2.3.4 RAS signaling and RMS

As already mentioned, patients with Costello syndrome or Noonan syndrome are predisposed to the development of RMS, which are predominantly of the embryonal subtype [19,242,259-262]. Additionally, a few cases of RMS have also been described in patients suffering from Neurofibromatosis type 1 or from cardio-facio-cutaneous syndrome [263-265].

Interestingly, oncRAS mutations are also frequently found in sporadic RMS and are detected predominantly in the ERMS subtype [14,15]. Dependent on the analyzed tumor subset, 12 % [16], 22 % [266], 35 % [267] or even 46 % [141] of RMS show oncRAS mutations. Although these mutations can occur in all 3 *RAS* genes, *NRAS* mutations are the most common

ones [14,15,141,266,267]. With regard to the analyzed tumor subset, oncRAS mutations can positivity or negatively influence the outcome for patients with ERMS. On the one hand, activating mutations in *HRAS*, *KRAS*, *NRAS* or *NF-1* genes were described in 75 % of high-risk ERMS tumors [5,6,15]. On the other hand, gain-of-function mutations within the *RAS* genes were described to occur more frequently in ERMS patients with a better outcome [267]. Nevertheless mutations within the *RAS* genes at positions G12 and Q61 are more frequent than G13 mutations [15,141,231,232,267] (and according to COSMIC v86). Furthermore, whole-exome/-transcriptome sequencing, copy number and DNA methylome analyses of 60 RMS revealed activation of the FGFR4/RAS/AKT axis in up to 40 % of the tumors (24/60 tumors, with 10/60 tumors showing mutations in *HRAS*, *KRAS* or *NRAS*), which was predominantly detected in ERMS. However, mutations affecting PI3K directly are very rare [14,268]. Together, these results led to the conclusion that the RAS signaling pathway could be a druggable target in RMS. Indeed, inhibition of MEK or combined inhibiton of MEK and PI3K/mTOR block proliferation and trigger apoptosis of RMS cells [269-272].

Finally, it was proposed that oncRas mutations can either act as RMS-driver or as RMS-modifiers. However, this point is still a matter of debate [273-277]. Precisely, oncRas mutations were proposed to be necessary to convert normal primary human skeletal muscle myoblasts into tumorigenic cells mimicking ERMS [278]. This was shown by activation of oncKRas under the control of the *recombination activating gene 2* (*rag2)* promotor, which is active in myoblasts in zebrafish [274]. On the other hand, microarray-based data of RMS samples suggest, that a RAS signature occurs only in combination with signatures of other activated pathways [275]. In support of an RMS-modifier is also the observation that oncKRas in combination with heterozygous p53 mutations induces pleomorphic RMS, whereas p53 mutations alone induce an other RMS subtype. RMS in oncKRas mice have not been described so far [279-283]. Similarly, xenografts from murine satellite cells with oncKRas result in a pleomorphic RMS phenotype, but only in combination with a *Cyclin-dependent kinase inhibitior* (*Cdkn) 2a* knockout [273].

To sum up, these results show that active Ras signaling plays an extraordinarily important role in RMS pathogenesis. However, the precise role of oncRas mutations in ERMS pathogenesis is not well understood.

2.4 Interaction of Hh and Ras signaling

A non-canonical interaction between the Hh and Ras signaling pathways has been described frequently [284]. For example, the Shh/Ptch axis can stimulate activation of Erk in human mammary epithelial cells and in Shh Light II fibroblasts, which however does not require Smo [285]. *Vice versa*, Mek influences the transcriptional activity of *Gli1* in murine fibroblasts. In this setting, the N-terminal domain of Gli1 is phosphorylated in a Mek-dependent manner, which however does not involve Erk2 [286]. Additionally, Gli1 and Gli3 have been identified as

potential substrates of the Mapks Jnk and Erk in computational prediction and peptide binding arrays [287]. Indeed, Mapks can phosphorylate Gli1, Gli2 and Gli3 on residues located near the binding site for Sufu [288]. Furthermore, Gli proteins are stabilized by Epidermal growth factor receptor (EGFR)-mediated inhibition of proteasomal degradation in keratinocytes [289]. Therefore, it is speculated that Mapks can activate Gli transcription factors in a Hh/Ptch/Smo-independent manner.

Activated Hh signaling and simultaneous oncRas mutations are found in several tumor entities [284]. This suggests a cooperation of both signaling pathways in tumor development, maintenance or progression. An overview of known interactions between Hh and Ras signaling in different tumor entities is depicted in Fig. 4.

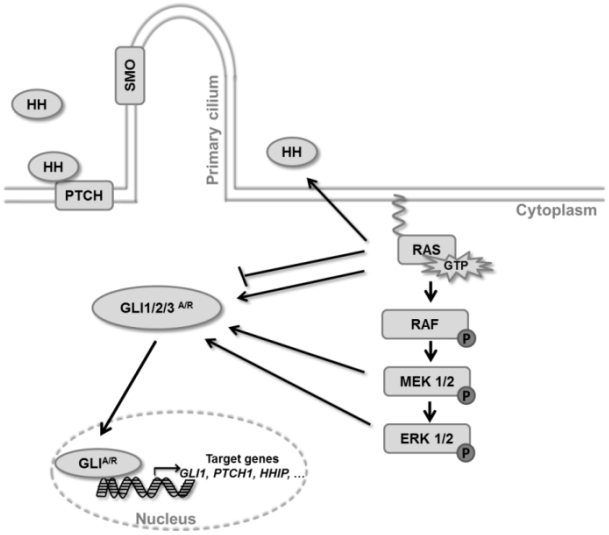

Figure 4: Interactions of HH and RAS signaling in cancer
HH signaling activity can be modified by RAS signaling in a non-canonical manner. In this setting, oncgenic actiovation of members of the RAS pathway induce or inhibit GLI transcription factors. In addition, oncRAS can induce secretion of HH ligands. The MEK/ERK casacde was shown to regulate GLI transcription factors. For more details, see text.

Hh/Ras interaction occurs for example in BCC, in which Hh and Egfr signaling synergistically contribute to oncogenic transformation via the Raf/Mek/Erk axis [290,291] and synergistically regulate the expression of genes necessary for tumor growth (*Sox2*, *Sox9*, *Jun*, C-X-C motif chemokine receptor (*Cxcr*)*4* and *Fgf19*) [292]. Additionally, Egfr/ADP ribosylation factor (Arf)6 signaling triggers Hh signaling and tumor growth in a *Drosophila* oncRas-driven tumor model. Tumor growth in this model depends on oncRas and oncRas in turn induces the expression of Egfr ligands [293].

In addition, oncRas-mediated modulation of Gli transcription factor can have oppositional outcomes in different tumor entities. Examples for activation of Hh signaling by oncRas are e.g. melanoma. In this tumor entity oncNRAS or oncHRAS can stimulate nuclear localization and transcriptional activity of *GLI1* [75]. In gastric cancer cells an active MEK/ERK cascade has a positive regulatory role in GLI1 transcriptional activity [294]. Another example is pancreatic cancer, in which GLI1 is required for oncKRAS-induced tumorgenesis [295,296]. Moreover,

oncKRAS blocks proteasome-mediated GLI1 degradation and thereby activates the HH signaling cascade in pancreatic cancer cells [297]. OncRAS also triggers ligand-independent HH signaling activation in thyroid cancer cells via the MEK/ERK axis [298]. However, in contrast, Lauth and colleagues observed that oncKRAS can also abrogate HH signaling activity in pancreatic cancer cells by inhibition of GLI2 function and promotion of the formation of the GLI3 repressor form. Thus, oncRAS tumor-intrinsically blocks HH signaling. However, since oncKRAS tumorintrinsically also induces SHH expression and secretion, HH signaling activity is induced in neighboring stromal cells [84].

In addition to the Ras/Mek/Erk axis, the PI3K/Akt/mTOR axis (which can also be regulated by Ras) can regulate Gli proteins and thus Hh signaling activity. For example, AKT enhances nuclear localization and activity of GLI1 in melanoma model systems [75]. In murine fibroblasts, PI3K/Akt/ signaling is required for Shh signal transduction and subsequent Gli activation [76].

In summary, the literature provides evidence for both, positive and negative crosstalks between Hh and Ras signaling in that oncRas either positively or negatively influences transcriptional activity of Gli transcription factors. The outcome of regulation depends on the experimental setting and on the tumor entity. *Vice versa*, Shh can regulate Erk activity in non-cancerous epithelial cells.

2.4.1 HH and RAS signaling in RMS

As described in sections 2.2.4 and 2.3.4, Hh and Ras signaling play crucial roles in RMS. Although interactions of these pathways have been described for several tumor entities, almost nothing is known about an interaction in RMS. Preliminary work from our group indicates that there is indeed a crosstalk between both pathways in RMS. Thus, the expression of any oncRAS isoform decreases *GLI1* expression in the ERMS cell line RUCH-2 and in the ARMS cell line RMS-13. However, the mechanism behind this downregulation is different. Whereas the oncRAS-dependent decrease in *GLI1* expression is mediated by MEK in RUCH-2 cells, MEK is not involved in *GLI1*-suppression in RMS-13 cells. Moreover, preliminary xenotransplantation studies and a genetic approach in the mouse indicate that oncRas isoforms change the growth behavior of Hh-associated RMS precursor lesions [299].

3 Aim of this study

RMS is the most common malignant soft tissue sarcoma in children. The efficiency of currently available multimodal therapies is limited and many patients suffer from severe adverse side effects and fatal long-term consequences. This indicates that it is of uttermost importance to better understand the tumor's pathology and to establish new therapeutic approaches.

The Hh signaling cascade and the Ras signaling pathway are frequently activated in RMS. This is in the first instance obvious in human ERMS that strongly express HH target genes and concurrently can show oncogenic *H*-, *K*- or *NRAS* (collectively named oncRAS) mutations. Surprisingly, and as already mentioned, preliminary work from our group indicates that all oncRAS isoforms decrease the expression of the major HH-target *GLI1* in an ERMS and also in an ARMS cell line. In ERMS the decrease apparently is mediated via MEK.

The main focus of this thesis was to investigate the role of oncRAS isoforms in regulation of HH targets and associated cellular responses of ERMS in more depth and thereby to validate the already gained results. Additionally, the consequences of a crosstalk between RAS and HH signaling for ERMS pathogenesis, growth and aggressiveness were analyzed.

For this purpose, the proliferation status and the activity of RAS and HH signaling were investigated in 3 different ERMS cell lines expressing oncRAS isoforms. In addition, it was examined whether the oncRAS-mediated decrease in *GLI1* was caused downstream of MEK at the level of ERK. Moreover, the subcellular localization and the protein level of all 3 GLI transcription factors were investigated. Finally, the cell lines were transplanted into immunosuppressed mice and the impact of oncRAS and the concomitant downregulation of *GLI1* on tumor growth and HH signaling activity was analyzed.

In a second approach, the impact of oncRas signaling on growth, differentiation status and on Hh signaling genes was analyzed in genetically engineered *Hh/Ptch*-driven ERMS mouse models. For this purpose, $Ptch^{del/+}oncRas^{fl/+}Myf5^{CreER/+}$ mice were generated. In these mice, the expression of either oncHRas, oncKRas or oncNRas can be induced at different stages of tumor development. Using this model, the impact of the respective oncRas mutation on tumor incidence, tumor latency time or multiplicity and on proliferation, Hh signaling activity and myyogenic differentiation was investigated. The experiments were perfomed in mice, in which the mutation was induced either in tumor precursor lesions or in full-blown ERMS. The aim of this study was to analyze the impact of oncRas mutations on different developmental stages of ERMS.

4 Material

4.1 Technical equipment

Table 1: Technical equipment

Technical equipment	Supplier
7900HT Fast Real-Time PCR System	Applied Biosystems, Waltham, MA, USA
Agarose gel electrophoresis chamber	Peqlab Biotechnology GmbH, Erlangen, Germany
Autoclave (9216E)	Fedegari Autoclavi SpA, Albuzzano, Italy
Autoclave (Systec DX-150)	Systec GmbH & Co. KG, Linden, Germany
Centrifuges (Biofuge pico, fresco, primo, Multifuge 3LR)	Heraeus Holding GmbH, Hanau, Germany
Centrifuge (5427 R)	Eppendorf AG, Hamburg, Germany
CO_2-Incubator (CB220-230V-G)	Binder GmbH, Tuttlingen, Germany
CO_2-Incubator (6000, BBD, 6220)	Thermo Fisher Scientific Inc., Waltham, MA, USA
Cooling plate (EG1150 C)	Leica Microsystems GmbH, Wetzlar, Germany
Digital monochrome thermal video printer (P91D)	Mitsubishi Electric Co., Tokyo, Japan
Digital photocamera (PowerShot G2)	Canon Deutschland GmbH, Krefeld, Germany
Dispersing tool for homogenizer (DS-8/P)	Miccra GmBH, Heitersheim, Germany
Dissection tools	Karl Hammacher GmbH, Solingen, Germany
Flow cytometer (BD LSR II)	BD Biosciences, San Jose, CA, USA
Flow cytometer (FACS Calibur)	BD Biosciences, San Jose, CA, USA
Freezer (-20 °C)	Liebherr GmbH, Bulle, Switzerland
Freezer (-80 °C)	Sanyo Electric Co., Ltd., Osaka, Japan
Freezing container (Mr. Frosty™)	Thermo Fisher Scientific Inc., Waltham, MA, USA
Fridge (4 °C)	Robert Bosch GmbH, Stuttgart, Germany
Heating block shaker (ThermoMixer©)	Eppendorf AG, Hamburg, Germany
High-precision scales (Sartorius Basic plus 2100)	Sartorius AG, Göttingen, Germany
Homogenizer (Miccra D-1)	Miccra GmBH, Heitersheim, Germany
Hybridization oven (HB-1000 Hybridizer)	Analytik Jena US, Upland, CA, USA
Gas burner	Campingaz, Hattersheim, Germany
Inverted fluorescence microscope (Axiovert 25)	Carl Zeiss GmbH, Jena, Germany
Inverted research microscope (IX71)	Olympus Optical Co., Ltd., Tokyo, Japan
Cryostat (CM 1900-1-1)	Leica Microsystems GmbH, Wetzlar, Germany

Liquid nitrogen tank	L'air liquid S.A., Paris, France
Magnetic stirrer (MR3000/3001)	Heidolph Instruments GmbH & Co. KG, Schwabach, Germany
Micro computed tomography (µCT) system (QuantumFX)	PerkinElmer Health Sciences, Hopkinton, MA, USA
Microplate reader (SynergyMx)	BioTek Instruments GmbH, Bad Friedrichshall, Germany
Microscope (Olympus BX 60)	Olympus Optical Co., Ltd., Tokyo, Japan
Microtome (HN 40)	Leica Microsystems GmbH, Wetzlar, Germany
Microwave oven (Dimension 4)	Panasonic Corp., Kadoma, Japan
Neubauer counting chamber	Brand GmbH & Co KG, Wertheim, Germany
Neon™ Transfection system	Thermo Fisher Scientific Inc., Waltham, MA, USA
Paraffin dispenser (PAG12)	Medite Medizintechnik GmbH, Burgdorf, Germany
Paraffin tissue floating bath	Medax GmbH & Co. KG, Rendburg, Germany
PCR Thermocycler (Mastercycler®)	Eppendorf AG, Hamburg, Germany
PCR Thermocycler (Labcycler Basic, Labcycler Gradient)	SensoQuest GmbH, Göttingen, Germany
pH-meter (inoLab, pH Level 1) and electrode (SenTix 91)	WTW, Weilheim, Germany
Pipette controller (accu-jet® pro)	Brand GmbH & Co. KG, Wertheim, Germany
Pipettes (Multi- and single-channel pipettes)	Eppendorf AG, Hamburg, Germany
Platform shaker (Unimax1010)	Heidolph Instruments GmbH & Co. KG, Schwabach, Germany
Precision weighing balance (ALC-210.4)	Sartorius AG, Göttingen, Germany
Power supply for agarose gel electrophoresis	Peqlab Biotechnology GmbH, Erlangen, Germany
Power supply for Western Blot transfer	Cleaver Scientific ltd., Rugby, United Kingdom
Spectrophotometer (NanoDrop 8000)	Thermo Fisher Scientific Inc., Waltham, MA, USA
Stereo microscope (Stemi 2000)	Carl Zeiss GmbH, Jena, Germany
Sterile workbench (Euroflow EF/A 5)	Clean Air Techniek, Woerden, Netherlands
Tab. centrifuge (Micro Centrifuge SD)	Carl Roth GmbH & Co. KG, Karlsruhe, Germany
Tissue processor (TP1020)	Leica Microsystems GmbH, Wetzlar, Germany
Ultraviolet (UV) light -Transilluminator	INTAS Science Imaging Instruments GmbH, Göttingen, Germany
Vacuum pump (EcoVac)	Schuett-biotec GmbH, Göttingen, Germany
Vortex mixer (Vortex-Genie2®)	Scientific Industries Inc, Bohemia, NY, USA
Water bath (1083)	GFL mbH, Burgwedel, Germany

Water purification system (Arium® 611 VF)	Sartorius AG, Göttingen, Germany
Western Blot imaging system (FluorChem™Q)	Bio-Techne Corp., Minneapolis, MN, USA
Western Blot transfer system (Trans-Blot® SD semi-dry electroblotting system)	Bio-Rad Laboratories GmbH, Munich, Germany
Western Blot transfer system (Tank electroblotting system OwlTM VEP-2 Mini)	Thermo Fisher Scientific Inc., Waltham, MA, USA

4.2 Consumables

Table 2: Consumable materials

Consumable	Supplier
6 well cell culture plate	Sarstedt AG & Co., Nürnberg , Germany
24 well cell culture plate	Corning Incorporated, New York City, NY, USA
96 well assay plate (black plate, clear bottom)	Corning Incorporated, New York City, NY, USA
384 well plate black & adhesive seal sheet	4titude® Ltd., Surrey, UK
Cell scraper	Sarstedt AG & Co., Nürnberg , Germany
Centrifuge tubes (15 ml, 50 ml)	Greiner Bio-One International GmbH, Kremsmünster, Austria
Coverslips	Thermo Fisher Scientific Inc., Waltham, MA, USA
Disposable needles (Sterican Ø 0.45 x 12 mm or Ø 0.30 x 12 mm)	B.Braun AG, Melsungen, Germany
Disposable syringes (BD DiscarditTM II 2, 10, 20, 50 ml)	BD Biosciences, San Jose, CA, USA
Combitips advanced® (0.2 ml, 0.5 ml, 2.5 ml, 5 ml, 10 ml)	Eppendorf AG, Hamburg, Germany
CryoPure tubes	Sarstedt AG & Co., Nürnberg, Germany
Delicate task wipes	Kimberly-Clark Europe Ltd., Surrey, UK
Disposable cups (100 ml)	Sarstedt AG & Co., Nürnberg, Germany
Filter tips (Biosphere® 20 µl, 100 µl, 200 µl, 1000 µl)	Sarstedt AG & Co., Nürnberg , Germany
Flow cytometry tube	Sarstedt AG & Co., Nürnberg , Germany
Fluted filters	Sartorius AG, Göttingen , Germany
Glassware	Schott AG, Mainz, Germany
Insulin syringe (BD Microfine + Demi)	BD Biosciences, San Jose, CA, USA
Microscope slides & Superfrost® plus microscope slides	Thermo Fisher Scientific Inc., Waltham, MA, USA
Nitrocellulose membrane (Hybond ECL), 0.2 µM and 0.45 µM pore size	GE Healthcare Europe GmbH, Freiburg, Germany
Nunclon™ disposables for cell culture (10 cm cell culture dish, 96-well plate)	Thermo Fisher Scientific Inc., Waltham, MA, USA
NuPAGE Novex 3-8 % Tris-Acetate Gel	Invitrogen, Carlsbad, CA, USA
NuPAGE Novex 4-12 % Bis-Tris Gel	Invitrogen, Carlsbad, CA, USA

Parafilm® laboratory film	Bemis Company, Inc., Neenah, WI, USA
Pasteur pipettes	TH. Geyer GmbH & Co. KG, Renningen, Germany
PCR tear-a-way plates & cap strips	4titude® Ltd., Surrey, UK
Petri dishes	Ochs GmbH, Bovenden/Lenglern, Germany
Pipette tips (20 µl, 200 µl, 1000 µl)	Sarstedt AG & Co., Nürnberg, Germany
Reaction tubes (1.5 ml, 2 ml, 5 ml)	Sarstedt AG & Co., Nürnberg, Germany
Safeseal microtubes (1.5 ml, 2 ml)	Sarstedt AG & Co., Nürnberg, Germany
Serological pipettes (2 ml, 5 ml, 10 ml, 25 ml)	Sarstedt AG & Co., Nürnberg , Germany
Softa-Man® hand disinfectant	B.Braun AG, Melsungen, Germany
Sterile filters (0.2 µm, 0.45 µm)	Sartorius AG, Göttingen, Germany
Surgical blades	Aesculap AG, Tuttlingen, Germany
Whatman® Blotting paper (GB 33 B003)	Heinemann Labortechnik GmbH, Duderstadt, Germany
Weighing paper	Macherey-Nagel GmbH & Co. KG, Düren, Germany

4.3 Reagents and chemicals

All chemicals, which are not listed in Table 3 (Tab. 3) were purchased from Merck KGaA, Darmstadt, Germany or Carl Roth GmbH & Co. KG, Karlsruhe, Germany.

Table 3: Reagents and chemicals

Reagent or chemical	Supplier
3-Amino-9-ethylcarbazole (AEC)	Sigma-Aldrich Co., St. Louis, MO, USA
Acetic acid	Carl Roth GmbH & Co. KG, Karlsruhe, Germany
Agarose	VWR International GmbH, Erlangen, Germany
Aluminium potassium sulfate dodecanhydrate	Merck KGaA, Darmstadt, Germany
Ampicillin sodium salt	Carl Roth GmbH & Co. KG, Karlsruhe, Germany
Boric acid	Carl Roth GmbH & Co. KG, Karlsruhe, Germany
Bovine serum albumin fraction V (BSA), protease free	Carl Roth GmbH & Co. KG, Karlsruhe, Germany
Chloroform	Carl Roth GmbH & Co. KG, Karlsruhe, Germany
Citric acid monohydrate	Carl Roth GmbH & Co. KG, Karlsruhe, Germany
Contrast reagent Imeron 300	Bracco Imaging GmbH, Konstanz, Germany
Cresol red, sodium salt	Aldrich Chemical Company Inc., Milwaukee, WI, USA
Cryoblock embedding medium	Medite Medizintechnik GmbH, Burgdorf, Germany

Dimethylformamide (DMF)	Sigma-Aldrich Co., St. Louis, MO, USA
Dimethylsulfoxide (DMSO)	Thermo Fisher Scientific Inc., Waltham, MA, USA
Dithiothreitol (DTT)	Thermo Fisher Scientific Inc., Waltham, MA, USA
Deoxyribonucleotide triphosphates (dNTPs)	Roche Diagnostics GmbH, Mannheim, Germany
Loading dye solution for DNA (6x)	Thermo Fisher Scientific Inc., Waltham, MA, USA
DNase/RNase-free distilled H_2O (ultrapure H_2O)	Invitrogen, Carlsbad, CA, USA
Eosin Y	Merck KGaA, Darmstadt, Germany
Ethanol (EtOH) 99 %	J.T. Baker B.V., Deventer, Netherlands
Ethanol 99%, denatured	TH. Geyer GmbH & Co. KG, Renningen, Germany
Ethidium bromide (EtBr) 0.07%	Inno-Train Diagnostik GmbH, Kronberg im Taunus, Germany
Ethylenediamine tetraacetic acid (EDTA) disodium salt dihydrate	Carl Roth GmbH & Co. KG, Karlsruhe, Germany
GeneRuler DNA ladder (50 base pairs (bp), 100 bp plus, 1 kilobase (kb))	Thermo Fisher Scientific Inc., Waltham, MA, USA
Glutaraldehyde	Sigma-Aldrich Co., St. Louis, MO, USA
Glycergel mounting medium	Dako North America Inc., Carpinteria, CA, USA
Haematoxylin crystalline, Mayer's	Merck KGaA, Darmstadt, Germany
Hydrochloric acid (37 %)	Carl Roth GmbH & Co. KG, Karlsruhe, Germany
Hydrogen peroxide (35 %)	Carl Roth GmbH & Co. KG, Karlsruhe, Germany
Immersion oil for microscopy (Immersion™ 518 N)	Carl Zeiss GmbH, Jena, Germany
Isoflurane (FORENE)	Abbott Laboratories Inc, Santa Clara, CA, USA
Isopropanol	Carl Roth GmbH & Co. KG, Karlsruhe, Germany
Kanamycin A	Sigma-Aldrich Co., St. Louis, MO, USA
Liquid barrier marker	Carl Roth GmbH & Co. KG, Karlsruhe, Germany
Matrigel basement membrane matrix phenol red free	Corning Incorporated, New York City, NY, USA
Methanol (MeOH)	Carl Roth GmbH & Co. KG, Karlsruhe, Germany
NuPAGE MES SDS running buffer, 20 x	Invitrogen, Carlsbad, CA, USA
NuPAGE Tris acetate SDS running buffer, 20 x	Invitrogen, Carlsbad, CA, USA
Paraformaldehyde (PFA)	Carl Roth GmbH & Co. KG, Karlsruhe, Germany

Pertex mounting medium	Medite Medizintechnik GmbH, Burgdorf, Germany
Phosphatase inhibitor cocktail Tab.ts (PhosSTOP)	Roche Diagnostics GmbH, Mannheim, Germany
Phosphate buffered saline (PBS) Tab.ts	Invitrogen, Carlsbad, CA, USA
Powdered milk	Carl Roth GmbH & Co. KG, Karlsruhe, Germany
Protease inhibitor cocktail (cOmplete Mini)	Roche Diagnostics GmbH, Mannheim, Germany
Primer “random” p(dN)6 Hexamer-oligonucleotides	Roche Diagnostics GmbH, Mannheim, Germany
ProLong Gold antifade mountant with 4′,6-diamidino-2-phenylindole (DAPI)	Thermo Fisher Scientific Inc., Waltham, MA, USA
RNaseZAP	Sigma-Aldrich Co., St. Louis, MO, USA
SeeBlue Plus2 Pre-Stained Protein Standard	Invitrogen, Carlsbad, CA, USA
S.O.C. (Super optimal broth with catabolite repression) medium	Invitrogen, Carlsbad, CA, USA
Sodium chloride	AppliChem GmbH, Darmstadt, Germany
Sodiumdodecylsulfate (SDS)	AppliChem GmbH, Darmstadt, Germany
Sodium hydroxide	Carl Roth GmbH & Co. KG, Karlsruhe, Germany
Spectra multicolor high range protein ladder	Thermo Fisher Scientific Inc., Waltham, MA, USA
Sucrose	Sigma-Aldrich Co., St. Louis, MO, USA
Tamoxifen	Sigma-Aldrich Co., St. Louis, MO, USA
Triethanolamine (TEA) hydrochloride	Sigma-Aldrich Co., St. Louis, MO, USA
Tris(hydroxymethyl)aminomethane (TRIS) base	AppliChem GmbH, Darmstadt, Germany
Triton™ X-100	Sigma-Aldrich Co., St. Louis, MO, USA
Tropix® I-BLOCK™	Applied Biosystems, Waltham, MA, USA
Tryptone (peptone ex casein)	Carl Roth GmbH & Co. KG, Karlsruhe, Germany
TWEEN® 20	Sigma-Aldrich Co., St. Louis, MO, USA
X-Gal (5-bromo-4-chloro-3-indolyl-β-D-galactopyranoside)	Carl Roth GmbH & Co. KG, Karlsruhe, Germany
Xylene	J.T. Baker B.V., Deventer, Netherlands
Yeast extract	Carl Roth GmbH & Co. KG, Karlsruhe, Germany

4.4 Buffers and solutions

If not indicated otherwise all buffers and solutions were prepared using double-distilled H_2O (ddH_2O).

Table 4: Buffers and solutions and their components

Buffer	Composition
2 x Laemmli buffer	65 mM Tris-HCl, pH 6.8 25 % (w/v) Glycerol 2 % (w/v) SDS 0.01 % (w/v) Bromophenol blue
6 x SDS loading buffer	375 mM Tris, pH 6.8 12 % (w/v) SDS 60 % (v/v) Glycerol 0.6 M DTT 0.01 % (w/v) Bromophenol blue
10 x PBS pH 7.4	1.4 M NaCl 65 mM Na_2HPO_4 27 mM KCl 15 mM KH_2PO_4
10 x Tris-boric acid-EDTA solution (TBE) pH 8.0	890 mM Tris/HCl, pH 8.0 730 mM boric acid 12.5 mM EDTA
10 x Tris-buffered saline (TBS) pH 7.4	150 mM NaCl 10 mM Tris/HCl, pH 8.0
AEC chromogen pH 5.2	70 mM Sodium acetate trihydrate 30 mM Acetic acid 16 mM 3-Amino-9 Ethylcarbazole Dissolved in DMF
Blotting buffer for semi-dry blotting	50 mM Tris 40 mM Glycine 20 % (v/v) Methanol 0.0325 % (w/v) SDS
Blotting buffer for tank blotting pH 8.3	200 mM Glycin 25 mM Tris 20 % (v/v) Methanol 0.1 % (w/v) SDS
BSA-azide	3 mM Sodium azide 2 % (w/v) BSA Dissolved in PBST
Casein	0.2 % (w/v) I-Block Dissolved in TBS
Citric acid buffer pH 3.0 or pH 6.0	10 mM Sodium Citrate
Cresol	0.1 % (w/v) Cresol red Dissolved in saturated sucrose-solution
dNTP-Mix	10 mM dATP 10 mM dCTP 10 mM dGTP 10 mM dTTP
Eosin solution	80 % (v/v) EtOH 1 % (w/v) Eosin y (water soluble)

Haematoxylin solution, Mayer's	300 mM Trichloro acetaldehyde hydrate 100 mM Potassium aluminum sulfate 50 mM Citric acid 35 mM Haematoxylin 75 nM Sodium iodate
Lysis buffer pH 8.8	150 mM NaCl 30 mM Tris/HCl, pH 7.5 10 % (v/v) Glycerol 1 % (v/v) Triton X-100 1 Tab.t/ 10 ml phosphatase inhibitor and protease inhibitor added before use: 2 mM DTT, 500 µM Phenylmethanesulfonylfluoride
LacZ buffer	2 mM $MgCl_2$ 0,02 % (v/v) NP-40 0,01 % (w/v) Natrium Deoxycholat Dissolved in PBS
LacZ-staining buffer	5 mM $K_3Fe(CN)_6$ 5 mM $K_4Fe(CN)_6$ 2 mM $MgCl_2$ 0.02 % (v/v) NP-40 0.01 % (w/v) Natrium Deoxycholat 500 µg/ml X-Gal Dissolved in PBS
Lysogeny broth medium (LB medium)	1 % (w/v) Bacto-tryptone 1 % (w/v) NaCl (pH7.0) 0.5 % (w/v) Yeast extract
Lysogeny broth agar (LB agar)	1.5 % (w/v) Agar Dissolved in LB medium
Modified radioimmunoprecipitation assay buffer (RIPA)	50 nM Tris/HCl, pH 7.4 1 % (v/v) NP-40 0.25% (v/v) Na-Deoxycholat 150 mM NaCl 1 mM EDTA 1 Tab.t/ 10 ml phosphatase inhibitor and protease inhibitor
Nuclear lysis buffer (NL buffer)	50 mM Tris-HCl, pH 8 150 mM NaCl 1 % (v/v) NP-40 0.5 M sodium deoxycholate 0.1 % (w/v) SDS 1 Tab.t/ 10 ml phosphatase inhibitor and protease inhibitor added before use: 10 % (v/v) Glycerol
Paraformaldehyde	4% (w/v) Paraformaldehyde Dissolved in PBS
PBS-Tween 20 (PBST)	0.1 % (v/v) Tween-20 Dissolved in PBS

Propidium iodide (PI) staining solution	10 µg/ml PI 100 µg/ml RNase A Dissolved in PBS
Proteinase K pH 8.0	50 mM Tris/HCl 5 mM EDTA 10 mg/ml Proteinase K
Subcellular fractionation buffer (SF buffer)	250 mM Sucrose 20 mM HEPES, pH 7.4 10 mM KCl 1.5 mM $MgCl_2$ 1 mM EDTA 1 mM Ethyleneglycol etraaceticacid (EGTA) 1 Tab.t/ 10 ml phosphatase inhibitor and protease inhibitor added before use: 2 mM DTT
Sodium Chloride-Tris-EDTA (STE) buffer	100 mM NaCl 50 mM Tris/HCl 1 mM EDTA 1 % (w/v) SDS
Stripping buffer	62.5 mM Tris, pH 6.7 2 % (w/v) SDS 100 mM ß-Mercaptoethanol
TBS-Triton X-100	0.1% Triton X-100 Dissolved in TBS
TBS-Tween 20 (TBST)	0.5 % (v/v) Tween-20 Dissolved in TBS
Tris-EDTA (TE) buffer pH 8.0	10 mM Tris 1 mM EDTA
Trypan blue staining solution	0.4 % (w/v) Trypan blue Dissolved in PBS
X-Gal stock solution	4 % (w/v) X-Gal Dissolved in DMSO

4.5 Kits and ready-to-use reaction systems

Unless indicated otherwise, all commercially available kits and ready-to-use reaction systems listed in Tab. 5 were used according to the manufacturer's instructions.

Table 5: Commercially available kits and ready-to-use reaction systems

Reaction system	Supplier
Amersham enhanced chemiluminescence (ECL) Western Blotting detection reagents	GE Healthcare Europe GmbH, Freiburg, Germany
Cell proliferation Enzyme-linked immunosorbent assay (ELISA), BrdU chemiluminescent	Roche Diagnostics GmbH, Mannheim, Germany
Dako REAL™ EnVision™ detection system, Peroxidase/3,3'-Diaminobenzidine (DAB) +, Rabbit/Mouse	Dako North America Inc., Carpinteria, CA, USA

Dual-Luciferase® Reporter assay system	Promega GmbH, Mannheim, Germany
NEON Transfection kit	Thermo Fisher Scientific Inc., Waltham, MA, USA
Pierce BCA Protein assay kit	Thermo Fisher Scientific Inc., Waltham, MA, USA
Platinum™ SYBR™ Green qPCR SuperMix-UDG w/ROX	Invitrogen, Carlsbad, CA, USA
PureLink®HiPure Plasmid Midiprep Kit	Invitrogen, Carlsbad, CA, USA
QIAamp DNA FFPE Tissue Kit	Qiagen GmbH, Hilden, Germany
QuantiTect SYBR® Green RT-PCR Kit	Qiagen GmbH, Hilden, Germany
Ras Pull-down activation assay biochem kit (bead pull-down format)	Cytoskeleton Inc, Denver, CO, USA
RevertAid™ H Minus First Strand cDNA Synthesis Kit	Thermo Fisher Scientific Inc., Waltham, MA, USA
TRIzol® Reagent	Life Technologies Co., Camarillo, CA, USA
Water soluble tetrazolium salt (WST-1) reagent	Roche Diagnostics GmbH, Mannheim, Germany

4.6 Enzymes

All enzymes were stored at -20 °C. Enzymatic reactions were performed according to the manufacturer's recommendations.

Table 6: Enzymes

Enzyme	Supplier
BamH1	New England Biolabs, Ipswich, MA, USA
BpmI	New England Biolabs, Ipswich, MA, USA
EcoRI	New England Biolabs, Ipswich, MA, USA
Hind III	New England Biolabs, Ipswich, MA, USA
KpnI	New England Biolabs, Ipswich, MA, USA
NheI	New England Biolabs, Ipswich, MA, USA
Not1	New England Biolabs, Ipswich, MA, USA
Proteinase K	Carl Roth GmbH & Co. KG, Karlsruhe, Germany
RNase A	Carl Roth GmbH & Co. KG, Karlsruhe, Germany
SuperScript™ II Reverse Transcriptase	Thermo Fisher Scientific Inc., Waltham, MA, USA
Taq-Polymerase (MolTaq)	Molzym GmbH & Co. KG, Bremen , Germany

4.7 Small molecule inhibitors

Table 7: Signaling pathway inhibitors

Inhibitor	Solvent	Applied concentration	Supplier
HhAntag (HhA)	DMSO	30 µM	Genentech, San Francisco, CA, USA
PI-103	DMSO	3 µM	Alexis Biochemicals, San Diego, CA, USA
SCH772984	DMSO	0.5 - 10 µM	Selleckchem, München, Germany
Smoothened agonist (SAG)	DMSO	100 - 150 nM	Cayman chemicals, Ann Arbor, MI, USA
U0126	DMSO	10 µM	InvivoGen, San Diego, CA, USA

4.8 Plasmids

Table 8: Plasmids and their application

Plasmid	Application	Supplier or Reference
pMSCVpuro	Transduction of cell lines	CLONTECH Laboratories Inc., Mountain View, CA, USA
pMSCVpuro-HRAS^{G12V}	Transduction of cell lines	[299]
pMSCVpuro-KRAS^{G12V}	Transduction of cell lines	[299]
pMSCVpuro-NRAS^{G12V}	Transduction of cell lines	[299]
pEGFP-N1	Transfection control	CLONTECH Laboratories Inc., Mountain View, CA, USA
pGL3 9×Gli-BS	Gli reporter assay	[300]
pCR3.1	Gli reporter assay	Invitrogen, Carlsbad, CA, USA
pCR3.1-mGli1	Gli reporter assay	[301]
pRL-CMV	Gli reporter assay	Promega GmbH, Mannheim, Germany

4.9 Antibodies

The primary antibodies (Ab) were monoclonal (mAb) or polyclonal (pAb) against their target. For Western Blot analyses horseradish peroxidase (HRP) conjugated IgG (immunoglobulin G) secondary antibodies were used. Antibodies for immunohistochemically stainings were used in combination with the Dako REAL™ EnVision™ detection system (Peroxidase/DAB+, Rabbit/Mouse).

Table 9: Primary antibodies

Primary antibody	Dilution	Readout	Supplier
mAb mouse anti-α-Tubulin (Clone DM1A)	1:10,000	WB band size: 55 kDa	Dianova, Hamburg, Germany
mAb mouse anti-AKT (Clone 55/PKBa/Akt)	1:1,000	WB band size: 60 kDa	BD Biosciences, San Jose, CA, USA
mAb mouse anti-Heat shock cognate 71 kDa protein (HSC70) (B-6)	1:10,000	WB band size: 70 kDa	Santa Cruz Biotechnology, Santa Cruz, CA, USA
mAb mouse anti-Ki67	1:50	IHC: Nuclear staining of dividing cells	BD Biosciences, San Jose, CA, USA
mAb mouse anti-pan-Ras	1:250	WB band size: 21 kDa	Cytoskeleton Inc, Denver, CO, USA
mAb mouse anti-S6 (54D2)	1:1,000	WB band size: 32 kDa	Cell Signaling Technology, Danvers, MA, USA
mAb rabbit anti-pAKT (Ser473) (193H12)	1:1,000	WB band size: 60 kDa	Cell Signaling Technology, Danvers, MA, USA
pAb goat anti-GLI3	1:200	WB band size: 190 kDa: full length form 85 kDa: truncated repressor form	R&D Systems, Minneapolis, MN, USA
pAb rabbit anti-Caspase 3	1:1,000	WB band size: 35 kDa Cleaved: 19/17 kDa	Cell Signaling Technology, Danvers, MA, USA
pAb rabbit anti-GLI1 (V812)	1:750	WB band size: 160 kDa	Cell Signaling Technology, Danvers, MA, USA
pAb rabbit anti-GLI2 (aa46-60)	1:1,000	WB band size: 185 kDa	Cell Signaling Technology, Danvers, MA, USA
pAb rabbit anti-ERK	1:1,000	WB band size: 42/44 kDa	Merck KGaA, Darmstadt, Germany
pAb rabbit anti-pERK (Thr202/Tyr204)	1:1,000	WB band size: 42/44 kDa	Cell Signaling Technology, Danvers, MA, USA
pAB rabbit anti-Lamin B1	1:1,000	WB band size: 68 kDa Cleaved: 45kDa	Cell Signaling Technology, Danvers, MA USA
pAb rabbit anti-pS6 (Ser240/244)	1:1,000	WB band size: 32 kDa	Cell Signaling Technology, Danvers, MA, USA
pAB rabbit anti-Ras	1:1,000	WB band size: 21 kDa	Cell Signaling Technology, Danvers, MA, USA

WB: Western Blot, IHC: Immunohistochemistry

Table 10: Secondary antibodies

Secondary antibody	Conjugation	Dilution	Supplier
pAb donkey anti-goat IgG	HRP	1:10,000	Jackson Immuno Research, Cambridgeshire, UK
pAb goat anti-rabbit IgG	HRP	1:10,000	Dianova, Hamburg, Germany
pAb rabbit anti-mouse IgG	HRP	1:10,000	Dianova, Hamburg, Germany

4.10 Synthetic Oligonucleotides

All synthetic deoxyribonucleic acid (DNA) oligonucleotides were obtained from Eurofins Scientific SE (Luxemburg, Luxembourg). For polymerase chain reactions (PCR) and quantitative real-time PCR (qRT-PCR) a 10 µM working solution of each primer was used. The appropriate dilutions and concentrations are described in sections 5.2.3 and 5.2.8.

Table 11: Oligonucleotides for PCR approaches

Primer name	Primer sequence (5'-3' orientation)	Amplicon size	Refe-rence
Primers for genotyping			
Exon 7-F Neo-R	AGGAAGTATATGCATTGGCAGGAG GCATCAGAGCAGCCGATTGTCTG	950 bp (mutated *Ptch*)	302
mPTCNx_f mPTCwt_r.2	TGGTAATTCTGGGCTCCCGT ACACAACAGGGTGGAGACCACT	445 bp (wt *Ptch*)	302
eCreRasF eCreRasR	GCCATCCCTCGCGTTCCTGTAGTC CCTGCCCCACCTGCCAATGAGAAG	622 bp (wt *Hras*) 667 bp (mutated *Hras*)	303
Kras-WT-UP1 Kras-URP_Lp1 KrasG12Dmut_UP	CACCAGCTTCGGCTTCCTATT AGCTAATGGCTCTCAAAGGAATGTA CCATGGCTTGAGTAAGTCTGC	270 bp (wt *Kras*) 170 bp (mutated *Kras*)	304
mNRas-WT-For mNRas-WT-Rev mNRas-Mut-Rev	AGACGCGGAGACTTGGCGAGC GCTGGATCGTCAAGGCGCTTTTCC AGCTAGCCACCATGGCTTGAGTAA GTCTGCA	487 bp (wt *Nras*) 345 bp (mutated *Nras*)	220
cF cR	GCATTTCTGGGGATTGCTTA CCCGGCAAAACAGGTAGTTA	241 bp (*Myf5^{CreER}*)	305
CK382 CK383	ACCCTCCAGCTCCAGACTTATC CCCTGTAATGGATTCCAAGCTG	454 bp (wt) Myogenic factor 5 (*Myf5*)	305
Rosa1 Rosa2 Rosa3	AAAGTCGCTCTGAGTTGTTAT GCGAAGAGTTTGTCCTCAACC GGAGCGGGAGAAATGGATATG	500bp (wt), 250bp (mutated)	306
Primers for recombination assays			
mHRasG12VrelF1 mHRasG12VrelR1	TGGGGCAGGAGCTCCTGGATT GGTGTTGTTGATGGCAAATAC	302 bp (*Hras* fragment)	299

Kras-WT_UP1 Kras-URP_Lp1	CACCAGCTTCGGCTTCCTATT AGCTAATGGCTCTCAAAGGAATGTA	270 bp (wt *Kras*), 304 bp (recombined *Kras*)	304
mNRas-WT-For mNRas-WT-Rev	AGACGCGGAGACTTGGCGAGC GCTGGATCGTCAAGGCGCTTTTCC	487 (wt *Nras*), 521 bp (recombined *Nras*)	220

Table 12: Oligonucleotides for qRT-PCR approaches

Trans-cript	Primer name	Primer sequence (5'-3' orientation)	Primer location	Ampli-con size
Primer for human and murine sequences				
18S	18S-fwd 18S-rev2	CGCAAATTACCCACTCCCG TTCCAATTACAGGGCCTCGAA	Exon 1 Exon 1	81 bp
Primer for human sequences				
HPRT	hHPRT1_F1 hHPRT1_R1	TGGCGTCGTGATTAGTGATG CGAGCAAGACGTTCAGTCCT	Exon 1/2 Exon 2/3	134 bp
GLI1	HsaGli1 tq F HsaGli1 tq R	AGCTACATCAACTCCGGCCA GCTGCGGCGTTCAAGAGA	Exon 11 Exon 12	116 bp
GLI2	hsGLI2F.1 hsGLI2R.1	AAGCCCTTCAAGGCGCAGTA TCGTGCTCACACACATATGGCTT	Exon 9 Exon 10	170 bp
GLI3	hsGLI3F.1 hsGLI3R.1	GCCAGCGCAGCCCCTAT CGGCCTGGCTGACAGCCT	Exon 6 Exon 7	128 bp
HHIP	HSA_Hhip_tq_FW1 HSA_Hhip_tq_RV1	ATGGTGGGTTGTGCTTTCCA CAGAAGCAGTTGTGTTTGTGCT	Exon 3 Exon 4	130 bp
PTCH	hsPTC1F.2 hsPTC1R.2	GAGGTTGGTCATGGTTACATGGA TGCTGTTCTTGACTGTGCCACC	Exon 6 Exon 7	196 bp
SHH	hSHH_forw hSHH_rev	GATGACTCAGAGGTGTAAGGAC CCTCGTAGTGCAGAGACTCC	Exon 1/2 Exon 2/3	147bp
Primer for murine sequences				
Hprt	mHPRT-FwQ mHPRT-RvQ	AGCCCCAAAATGGTTAAGGTTGC TTGCAGATTCAACTTGCGCTCAT	Exon 6 Exon 7	222 bp
Tbp	mTBP-QFwd mTBP-QRev	CACCAATGACTCCTATGACCCCTA CAGTTGTCCGTGGCTCTCTTATTC	Exon 3 Exon 5	210 bp
Gli1	mGli1-tq-F mGli1-tq-R	TACATGCTGGTGGTGCACATG ACCGAAGGTGCGTCTTGAGG	Exon 9 Exon 10	115 bp
Gli2	Gli2-RT-PCR-F Gli2-RT-PCR-R	GGTCATCTACGAGACCAACTGC GTGTCTTCAGGTTCTCCAGGC	Exon 8 Exon 9	272 bp
Gli3	Gli3F2 Gli3-sybrgree	GAAGGAACAACCCTATCAAGGAGGA CCAGCGGCACACGAACTCCTTCT	Exon 10 Exon 11	186 bp
Hhip	mHhipF.1 mHhipR.2	GGAGCCTTACTTGGACATTCACAA ACCGTTCCTGGTTGGTGGTATAA	Exon 4 Exon 5	143 bp

Ptch	mPtc10 mPtc11R	TACAGTCCGGGACAGCATACC GTACCCATGGCCAACTTCGGCTTT	Exon 5 Exon 6	151 bp
MyoD	MyoD-ScerjF MyoD-ScerjR	CCCCGGCGGCAGAATGGCTACG GGTCTGGGTTCCCTGTTCTGT	Exon 2 Exon 3	234 bp
Myo-genin	Myogenin-Scerj-F Myogenin-Scerj-R	GCAATGCACTGGAGTTCG ACGATGGACGTAAGGGAGTG	Exon 2 Exon 3	94 bp
Myosin heavy chain	MHC tq F MHC tq R	AACACGAAGCGTGTCATCCAGTA GTCTCGATGTCAGCAGATGCCAG	Exon 7 Exon 8	242 bp
Tropo-myosin 3	mTropo tq F mTropo tq R	GAGGATGAACTAGCAACCATGCA CCAGCTCCTCTTCAACCAGCT	Exon 2 Exon 3	181 bp
p21	mp21 tq F mp21 tq R	CCTTGTCGCTGTCTTGCACTC TCTCTTGCAGAAGACCAATCTGC	Exon 2 Exon 3	143 bp
p27	mp27 tq F mp27 tq R	AACTCTGAGGACCGGCATTTG CGGGGAACCGTCTGAAACAT	Exon 1 Exon 2	168 bp
HRas	mHras_tqF2 mHras_tqR2	CAGCCAAGACCCGGCAG CCTGAGCCTGGTGTCAGGA	Exon 4 Exon 5	150 bp
KRas	mKras_tqF2 mKras_tqR2	AGCGCCTTGACGATACAGC TCCAAGAGACAGGTTTCTCCATC	Exon 2 Exon 3	113 bp
NRas	mNras_tqF1 mNras_tqR1	CACAAAGCAAGCCCACGAAC TCGGTACTGGCGTATCTCCC	Exon 4 Exon 5	124 bp

4.11 Media

4.11.1 Media for cultivation of prokaryotic cells

Bacterial cells were cultured in LB medium or on LB medium agar plates. To erase untransformed cells appropriate antibiotics, namely ampicillin (100 µg/ml) or kanamycin (50 µg/ml), were added to the autoclaved and cooled media. Both, media and plates, were stored at 4 °C until use.

4.11.2 Media and reagents for cultivation of eukaryotic cells

Eukaryotic cell lines were cultured in medium according to Tab. 13. All media and reagents were sterile or were autoclaved. All reagents were stored at -20 °C or 4 °C until use.

Table 13: Media and reagents

Medium or reagent	Supplier
Accutase	GE Healthcare Europe, Freiburg, Germany
DMSO	Sigma-Aldrich Co., St. Louis, MO, USA
Dulbecco's Modified Eagle Medium supplemented with 4.5 g/L Glucose, L-Glutamine, Sodium Pyruvate (DMEM+++)	Invitrogen, Carlsbad, CA, USA
Dulbecco's Modified Eagle Medium supplemented with 4.5 g/L Glucose, L-Glutamine (DMEM++-)	Invitrogen, Carlsbad, CA, USA

Fetal calf serum (FCS)	Invitrogen, Carlsbad, CA, USA
G 418 disulfate salt solution (50 mg/ml)	Sigma-Aldrich Co., St. Louis, MO, USA
PBS Tab.ts for cell culture (1 Tab.t dissolved in 500 ml ddH_20, autoclaved before use)	Invitrogen, Carlsbad, CA, USA
Penicillin (10.000 U/ml) and Streptomycin (10 mg/ml) (P/S)	PAN Biotech GmbH, Aidenbach, Germany
Puromycin dihydrochloride (10 mg/ml)	Sigma-Aldrich Co., St. Louis, MO, USA
RPMI 1640 (RPMI)	Invitrogen, Carlsbad, CA, USA
TrypLE Express	Invitrogen, Carlsbad, CA, USA
Zeocin™ (100 mg/ml)	Thermo Fisher Scientific Inc., Waltham, MA, USA

4.12 Biological Material

4.12.1 Bacterial Strains

Chemical competent *Escherichia coli* DH5α cells were used for transformation and amplification of plasmid DNA (pDNA). The bacteria were stored at - 80 °C until use.

4.12.2 Eukaryotic cell lines

Different eukaryotic cell lines were used to perform cell culture experiments. If not indicated otherwise, the cells were obtained from the American type culture collection (ATCC). All cells were adeherent and they were cultured in appropriate cell culture media under constant conditions (37 °C, 5 % CO_2, humidified atmosphere) in a CO_2-incubator.

Table 14: Eukaryotic cell lines

Cell line	Specification	Culture medium	Reference and/or Supplier
B9 also named: *Ptch$^{flox/flox}$ERT2$^{+/-}$*	Adult, murine fibroblast cell line responsive to SHH	DMEM +++ 10 % FCS 1 % P/S	[307]
Daoy	Human medulloblastoma cell line	DMEM +++ 10 % FCS 1 % P/S	[308], kindly provided by Prof. Dr. Fritz Aberger
Daoy pMSCV	Daoy stably transduced with a *pMSCVpuro*-control vector	DMEM +++ 10 % FCS 1 % P/S 5 µg/µl Puromycin	This work
Daoy HRAS	DAOY stably transduced with a *pMSCVpuro-HRAS^{G12V}* vector	DMEM +++ 10 % FCS 1 % P/S 5 µg/µl Puromycin	This work

Daoy KRAS	DAOY stably transduced with a *pMSCVpuro-KRAS^{G12V}* vector	DMEM +++ 10 % FCS 1 % P/S 5 µg/µl Puromycin	This work
Daoy NRAS	DAOY stably transduced with a *pMSCVpuro-NRAS^{G12V}* vector	DMEM +++ 10 % FCS 1 % P/S 5 µg/µl Puromycin	This work
HEK293	Human embryonic kidney cell line	DMEM +++ 10 % FCS 1 % P/S	[309], ATCC, Manassas, VA, USA
HEK293 Shh-N	Stably transduced human embryonic kidney cell line, secreting Shh-N	DMEM +++ 10 % FCS 1 % P/S 0,4 µg/ml G-418	[310]
NIH/3T3	Adult, murine fibroblast cell line	DMEM +++ 10 % FCS 1 % P/S	[311], ATCC, Manassas, VA, USA
RD	Human ERMS cell line	DMEM +++ 10 % FCS 1 % P/S	[312], ATCC, Manassas, VA, USA
RMS-13	Human ARMS cell line	RPMI 1640 10 % FCS 1 % P/S	[313], ATCC, Manassas, VA, USA
RMS-13 pMSCV	RMS-13 stably transduced with a *pMSCVpuro*-control vector	RPMI 1640 10 % FCS 1 % P/S 0.5 µg/µl Puromycin	[299]
RMS-13 HRAS	RMS-13 stably transduced with a *pMSCVpuro-HRAS^{G12V}* vector	RPMI 1640 10 % FCS 1 % P/S 0.5 µg/µl Puromycin	[299]
RMS-13 KRAS	RMS-13 stably transduced with a *pMSCVpuro-KRAS^{G12V}* vector	RPMI 1640 10 % FCS 1 % P/S 0.5 µg/µl Puromycin	[299]
RMS-13 NRAS	RMS-13 stably transduced with a *pMSCVpuro-NRAS^{G12V}* vector	RPMI 1640 10 % FCS 1 % P/S 0.5 µg/µl Puromycin	[299]
RUCH-2	Human ERMS cell line	DMEM +++ 10 % FCS 1 % P/S	[314], ATCC, Manassas, VA, USA
RUCH-2 pMSCV	RUCH-2 stably transduced with a *pMSCVpuro*-control vector	DMEM +++ 10 % FCS 1 % P/S 8 µg/µl Puromycin	[299]

RUCH-2 HRAS	RUCH-2 stably transduced with a *pMSCVpuro-HRAS^{G12V}* vector	DMEM +++ 10 % FCS 1 % P/S 8 µg/µl Puromycin	[299]
RUCH-2 KRAS	RUCH-2 stably transduced with a *pMSCVpuro-KRAS^{G12V}* vector	DMEM +++ 10 % FCS 1 % P/S 8 µg/µl Puromycin	[299]
RUCH-2 NRAS	RUCH-2 stably transduced with a *pMSCVpuro-NRAS^{G12V}* vector	DMEM +++ 10 % FCS 1 % P/S 8 µg/µl Puromycin	[299]
SHH light II	NIH/3T3 stably transfected with a Gli-responsive luciferase reporter	DMEM +++ 10 % FCS 1 % P/S 0,4 µg/ml G-418 0,15 mg/ml Zeocin	[310]
TE617.T	Human ERMS cell line	DMEM ++- 10 % FCS 1 % P/S	[315]
TE617.T pMSCV	TE617.T stably transduced with a *pMSCVpuro*-control vector	DMEM ++- 10 % FCS 1 % P/S 0.8 µg/µl Puromycin	This work
TE617.T H-/NRAS	TE617.T stably transduced *pMSCVpuro-HRAS^{G12V}* and *pMSCVpuro-NRAS^{G12V}* vectors	DMEM ++- 10 % FCS 1 % P/S 0.8 µg/µl Puromycin	This work
TE617.T KRAS	TE617.T stably transduced with a *pMSCVpuro-KRAS^{G12V}* vector	DMEM ++- 10 % FCS 1 % P/S 0.8 µg/µl Puromycin	This work

4.12.3 Genetically modified mouse lines

All experiments using animals were performed in agreement with the legal and ethical requirements and have been approved by the Lower Saxony State Office for Consumer Protection and Food Safety (file numbers 33.9-42502-04-12/0805, 33.9-42502-04-17/2534, 33.9-42502-04-13/1284). All used mouse lines are listed in Tab. 15. Breeding, genotyping and experimental procedure are described in sections 5.5 and 5.2.3.1.

Table 15: Mouse strains

Mouse strain	International nomenclature	Genetic background	Genetic modification	Reference or Supplier
BALB/c	BALB/c	BALB/c	-	The Jackson Laboratory, Bar Harbor, ME, USA or Charles River Laboratories, Wilmington, MA, USA
C57BL/6N	C57BL/6N	C57BL/6N	-	The Jackson Laboratory, Bar Harbor, ME, USA or Charles River Laboratories, Wilmington, MA, USA
Ptch$^{del/+}$ *Balb*	-	BALB/c	Heterozygous deletion of exon 8 and 9 within the *Ptch* gene	[316]
HRasflox_B6	*Hras*^{tm1Jaf}	C57BL/6	Tandemly-arrayed murine *HRas1* genes with a wt copy flanked by loxP sites followed by a copy containing a *HRas*^{G12V} pointmutation	[303], kindly provided by Prof. Dr. James A. Fagin
KRasflox_B6	*Kras*^{tm4Tyj}	C57BL/6	A Lox-Stop-Lox behind exon 1 of wt *KRas* is followed by the *KRas*^{G12D} point mutation in exon 2	[304,317], kindly provided by Prof. Dr. Dieter Saur
NRasflox_B6	*Nras*^{tm1Tyj}	C57BL/6	A Lox-Stop-Lox behind exon 1 of wt *NRas* is followed by the *NRas*^{G12D} point mutation in exon 2	[220]
Myf5$^{CreER/+}$	*Myf5*$^{tm1(cre/Esr1*)Trdo}$	Mixed: 50 % BALB/c and 50 %: C57BL/6 + 129/Sv + FVB/N	Tamoxifen-inducible expression of the cyclization recombination (Cre) ER^{TM} fusion protein from the endogenous *Myf5* promoter/enhancer elements	[305], kindly provided by Prof. Dr. Thomas A. Rando

Myf5$^{CreER/+}$_Balbc	*Myf5$^{tm1(cre/Esr1*)Trdo}$*	BALB/c	Tamoxifen-inducible expression of the CreER^{TM} fusion protein from the endogenous *Myf5* promoter/enhancer elements	[305]
Nu/Nu	*Rj:NMRI-Foxn1$^{nu/nu}$*	outbred	Homozygous deletion of exon 3 of the *Foxn1* gene (causes thymic aplasia resulting in a lack of T cells)	Charles River Laboratories, Wilmington, MA, USA, [318,319]
R26R	*Gt(ROSA) 26Sor^{tm1Sor}*	C57BL/6	A neo cassette flanked by *loxP* sites is followed by a *lacZ* gene and a polyadenylation sequence inserted into the endogeneous *Rosa26* locus	[306]

4.13 Software and digital resources

Utilized software were licensed and, if possible, used in the latest version.

Table 16: Software

Software	Developer
4D	4D Deutschland GmbH, Eching, Germany
Adobe Photoshop CS5	Adobe Systems Incorporated, San Jose, USA
AlphaView Q SA 3.2.2	Cell Bioscience, Santa Clara, CA, USA
CellSens Dimension	Olympus Optical Co., Ltd., Tokyo, Japan
Endnote X5	Thomson ISI ResearchSoft, Carlsbad, CA, USA
Fiji	[320]
Flowing Software 2	Perttu Terho, Cell Imaging Core, Turku Centre for Biotechnology, Finland
FlowJo V10	Tree Star Inc., Oregon, OR, USA
Gen5	BioTek Instruments GmbH, Bad Friedrichshall, Germany
GraphPad Prism 6	GraphPad Software, Inc., La Jolla, CA, USA
Microsoft Office	Microsoft Co., Redmond, WA, USA
NanoDrop 800 V2.3	Thermo Fisher Scientific Inc., Waltham, MA, USA
Quantum FX µCT Software (Simple Viewer)	PerkinElmer Health Sciences, Hopkinton, MA, USA
SDS 2.2	Applied Biosystems, Waltham, MA, USA

All databases were used to get access to data and to perform further analyses.

Table 17: Databases

Database	Online access
Basic Local Alignment Search Tool (BLAST)	https://blast.ncbi.nlm.nih.gov/Blast.cgi
Broad-Novartis Cancer Cell Line Encyclopedia	https://portals.broadinstitute.org/ccle
Catalogue Of Somatic Mutations In Cancer (COSMIC)	https://cancer.sanger.ac.uk/cell_lines
ClinicalTrials.gov	https://clinicaltrials.gov
Ensembl genome browser	https://www.ensembl.org/index.html
ExPASy Bioinformatics Resource Portal	https://www.expasy.org/
MGI-Mouse Genome Informatics	http://www.informatics.jax.org/
National Center for Biotechnology Information (NCBI)	https://www.ncbi.nlm.nih.gov/
Online Mendelian Inheritance in Man (OMIM)	https://www.omim.org/
Primer-BLAST	https://www.ncbi.nlm.nih.gov/tools/primer-blast/
RepeatMasker	http://www.repeatmasker.org/

5 Methods

5.1 Cell culture methods

All described cell culture methods were performed under sterile conditions using appropriate laboratory equipment. Frequent microscopic examinations were performed with special attention given to morphological changes, confluence and possible contaminations of the cells.

5.1.1 Cultivation of eukaryotic cell lines

All used eukaryotic cell lines (see Tab. 14) were cultured in their respective media in a CO_2-incubator at 37 °C, 5 % CO_2 in a humidified atmosphere. For culture, the cells were seeded onto cell culture plates (ø 10 cm). The cell culture media with respective supplements (see Tab. 14) were renewed every fourth day at the latest. The cells were passaged and split when 90 % confluency was reached. For this purpose, media was removed, the cells were washed with PBS and the cell layer was covered with TrypLE Express. Cells were detached for 10 – 15 min within the cell culture incubator. The detachment process was stopped by adding FCS-containing cell culture media. The cell suspensions were collected from the plates and were pelleted at 300×g for 5 min. The supernatants were aspirated and cells were resuspended in fresh cell culture medium or PBS. Afterwards the cells were counted (see section 5.1.3) or split and then seeded onto new cell culture dishes containing fresh cell culture medium.

5.1.2 Cryoconservation of cells

Highly confluent cells at low passage numbers were detached as described above. After pelleting, the cells were resuspended in cell culture medium containing 5 % (v/v) DMSO. The cell suspensions were aliquoted in cryo-tubes and transferred into the freezing device Mr. Frosty for a slow freezing process. The cells were gradually frozen over night at -80 °C and afterwards moved into a liquid nitrogen tank for long term storage.

To restore the cells, aliquots of frozen cells were quickly thawed at room temperature (RT). Thawed cells were diluted in cell culture medium and pelleted at 300×g for 5 min. The supernatants, which contained DMSO, were removed and the resulting pellets were resuspended in supplemented cell culture medium. The cells were seeded onto new cell culture plates for further usage.

5.1.3 Counting of cells

Cell numbers of replicates were defined to ensure comparability of the respective experiments. The seeding densities were adjusted to the different experimental setups (Tab. 18).

The cells were detached and diluted in medium or PBS as described in section 5.1.1. Appropriate dilutions of cell suspensions containing trypan blue (0.004 %), that stains dead cells, were used for counting. Then, 10 µl of every dilution was pipetted onto a hemocytometer (0.100 mm depth, 0.0025 mm^2) and the cell numbers in all 4 big quadrants were counted manually. Dead/blue cells were not counted. The number of living cells was calculated using the following formula:

$$\frac{\text{Cells}}{\text{ml}} = \frac{\text{number of cells x } 10^4}{\text{number of counted big squares}} \text{ x dilution factor}$$

Afterwards, dilutions with desired cell amounts were prepared and the cells were seeded for experiments as described in Tab. 18.

Table 18: Conditions for *in vitro* assays

Experimental setup	Plate format	Technical replicates	Seeding density	Total volume of medium
Cell cycle analyses	ø 10 cm cell culture dish	Duplicates	1×10^6 cells/plate	8 ml/plate
Cell viability assay (WST-1 assay)	96 well plate	Triplicates - Sextuplicates	5×10^3 cells/well	100 µl/well
Co-culture experiments	96 well plate black	Triplicates	5×10^3 SHH light II cells + 7.5×10^3 cells/well	100 µl/well
Electroporation	6 well plate	Duplicates	5×10^5 cells/well	2 ml/well
Gene expression	6 well plate	Triplicates	2×10^5 cells/well	1 ml/well
GLI reporter assay	96 well plate black	Triplicates	5×10^3 cells/well	100 µl/well
Proliferation assay (BrdU assay)	96 well plate black	Triplicates - Sextuplicates	5×10^3 cells/well	100 µl/well
Protein expression	ø 10 cm cell culture dish	-	$1 \times 10^6 – 1.5 \times 10^6$ cells/plate	8 ml/plate

5.1.4 Stable transduction of cell lines

Stable transduction of RMS cell lines was part of a former doctoral thesis [299]. Briefly, virus particles with the expression plasmids *pMSCVpuro*, *pMSCVpuro-HRAS^{G12V}*, *pMSCVpuro-KRAS^{G12V}*, *pMSCVpuro-NRAS^{G12V}* were generated in collaboration with the Institute of Cellular and Molecular Immunology, University Medical Center Göttingen (RMS cell lines) or in collaboration with the Department of Biosciences, Paris-Lodron University of Salzburg (Daoy cell line). For this purpose, retroviral packaging cells were transfected with 3 µg of the plasmids. Cells were allowed to grow in fresh culture medium for 48 h. Afterwards, the virus particle containing supernatant was sterile filtered. For stable transduction 2 batches of each cell line were incubated with this supernatant. The virus containing media were refreshed daily. The cells with integrated viral genomes were selected by puromycin addition to the

media 3 days after transduction. Different amounts of puromycin were applied to determine adequate concentrations for efficient selection.

5.1.4.1 Plasmid identity verification

The identities of the transduced plasmids were analyzed using a complementary DNA (cDNA) based PCR approach [95 °C (4 min), 35 cycles of: 95° C (30 sec) + 55 °C (1 min) + 72 °C (1 min) and 72 °C for 5 min]. For this purpose, a forward primer located within the extended packaging sequence of the *pMSCVpuro* fragment and a mixture of 3 reverse primers located within the $HRAS^{G12V}$, $KRAS^{G12V}$ or $NRAS^{G12V}$ fragments were employed, which should result in plasmid specific amplificates (HRAS: 453 bp; KRAS: 596 bp; NRAS: 319 bp).

5.1.5 Proliferation assay

The cellular proliferation was measured using an ELISA-Kit according to the manufacturer's instructions. The assay itself is based on DNA incorporation of the thymidine analog 5-bromo-2'-deoxyuridine (BrdU) in DNA of proliferating cells and its detection via a chemiluminescent reaction. Briefly, 5×10^3 cells were seeded in black 96 well cell culture plates with clear bottom and were allowed to attach for 24 h. Afterwards the media were replaced by incubation medium for 24 h – 72 h. Simultaneously, the cells were labeled by addition of 10 µM BrdU to the respective incubation medium. Cells without BrdU labelling served as negative control. After the incubation, the cells were fixed and DNA was denatured by adding FixDenat solution for 30 min at RT. Fixed cells were incubated with a peroxidase conjugated anti-BrdU antibody (1:100) for 1 h at RT. The antibody solution was aspirated and wells were washed 3 times with the provided washing buffer. After removing the washing buffer, a peroxidase substrate solution was added sequentially by injectors of the SynergyMx microplate reader to all wells of the plate and luminescence was measured in the microplate reader with Gen5 software. Data were analyzed using Microsoft Excel and GraphPad Prism 6 software.

5.1.6 Cell viability assay

The sable tetrazolium salt WST-1 is cleaved into a soluble formazan by metabolically intact cells and was used to assess cell viability. The cells were seeded in a clear 96 well cell culture plate and were allowed to adhere for 24 h. Afterwards the media were replaced by medium containing respective drugs or reagents for 24 h – 72 h. At the end of treatment the incubation media were removed to prevent interactions between drugs and the tetrazolium salt. Then, the cells were incubated for 4 h at 37 °C with WST-1 reagent, which was diluted 1:25 in fresh cell culture medium. Empty wells served as negative control. Afterwards, absorbance was measured at 450 nm and 655 nm in the microplate reader with Gen5 software. The cell viability was calculated after subtraction of the reference wavelength

(655 nm) from the wavelength used for quantification of WST-1 cleavage (450 nm) using Microsoft Excel.

5.1.7 Cell cycle analyses

Cell cycle distribution was investigated by PI staining and subsequent fluorescence-activated cell scanning (FACS). The cells were seeded and allowed to grow for 48 h before harvest. Accutase was used to detach cells for 5 min at 37 °C. Then, cell culture medium was added to stop the reaction. The cell suspensions were pelleted at 300×g for 5 min and the supernatants were discarded. The pellets were resuspended in 1 ml of ice-cold PBS. The cells suspensions were transferred into pre-cooled (-80 °C) pure EtOH while shaking and then placed on dry ice. Afterwards, the cells were fixed in EtOH at –20 °C for at least 3 h. Fixed cells were pelleted at 600×g and 4 °C for 5 min. The cells were washed with ice-cold PBS and centrifuged again at 600×g and 4 °C for 5 min. The supernatants were discarded and the pellets were resuspended in 450 µl PI-staining solution (10 µg/mL PI and 100 µg/mL RNase A in PBS) and incubated for 30 min at 37 °C. Staining intensities were measured by flow cytometry (FACS Calibur) on the FL-3 channel. A minimum of 5×10^5 cells/sample were counted and data analysis was performed with Flowing Software 2.

5.1.8 Transfection

Cells were transfected with pDNA by electroporation using the Neon Transfection system according to the manufacturer's instructions. A few days ahead of electroporation, the cells were cultured until 70 % - 90 % confluency in culture medium without antibiotics. The cells were detached as described in section 5.1 and the cell pellets were resuspended and washed with PBS. Cell counting was performed as described in section 5.1.3. The cell suspensions containing the desired cell number (0.5×10^6 cells/electroporation) were transferred into new reaction tubes and pelleted again at 300×g for 5 min. The supernatants were removed and cells were resuspended in resuspension buffer R at a final density of 4.5×10^6 cells/ml. For transfection itself, 0.5×10^6 cells were mixed with 4.5 µg pDNA in a final volume of 110 µl. Electroporation was performed under conditions shown in Tab. 19.

Table 19: Electroporation conditions for ERMS cell lines

RD cells		RUCH-2 cell lines	
Pulse voltage (V)	1.000	Pulse voltage (V)	1.200
Pulse width (ms)	30	Pulse width (ms)	40
Pulse number	2	Pulse number	1

After electroporation, cells were seeded in 6 well plates with pre-warmed cell culture medium without antibiotics. Transfection with an enhanced green fluorescent protein (EGFP) expression plasmid served as transfection control. Cells treated with an electric field pulse only served as additional control. All cells were allowed to attach for at least 18 h and were checked for viability and EGFP expression before performing further experiments. The

mentioned transfection conditions for each cell line had been established with different amounts of the the *pEGFP-N1* plasmid using different electroporation conditions and cell amounts. They yielded over 70 % transfection efficiency as measured by flow cytometric analysis (BD LSR II flow cytometer and data evaluation by FlowJo).

5.1.9 GLI reporter assay

A luciferase-based GLI reporter system was used to measure transcriptional activity of GLI proteins. ERMS cell lines were transfected with a firefly luciferase reporter plasmid containing 9x GLI protein binding sites (*pGL-9xGli BS)* and a vector expressing constitutively active renilla (*pRL-CMV)* which served as an internal control. A plasmid overexpressing murine *Gli1* served as positive control, whereas its pCR3.1 backbone was used in the negative control. Additionally, *pEGFP-N1* transfected cells were included as transfection control. The transfections themselves were done by electroporation (see section 5.1.8). For transfection of cells that were grown ahead to > 75 % confluency, the plasmid concentrations in Tab. 20 were used.

Table 20: Plasmid composition for GLI reporter assay in ERMS cell lines

Positive control		**Treatment or treatment control**		**Negative control**	
Plasmid	**amount**	**Plasmid**	**amount**	**Plasmid**	**amount**
pGL-9xGli BS	3.5 µg	*pGL-9xGli BS*	3.5 µg	*pGL-9xGli BS*	-
pRL-CMV	0.5 µg	*pRL-CMV*	0.5 µg	*pRL-CMV*	0.5 µg
pCR3.1 mGli1	0.5 µg	*pCR3.1 mGli1*	-	*pCR3.1 mGli1*	-
pCR3.1	-	*pCR3.1*	0.5 µg	*pCR3.1*	4 µg

The transfected cells were detached after 24 h and seeded again in a black 96 well plate with clear bottom at a density of 5×10^3 cells/well (see section 5.1 for procedure). The cells were allowed to attach for at least 18 h before incubation with reagents/inhibitors for 24 h. Cells were checked for viability and EGFP expression microscopically before analyzing luciferase activity (see section 5.1.10).

5.1.10 Dual luciferase reporter assay

The dual luciferase reporter assay was performed according to the manufacturer's instructions. Briefly, the transfected cells were washed and lysed with 21 µl of passive lysis buffer per well of a 96 well plate. The lyses were performed at RT for 15 min on a shaker (250 rounds per minute (rpm)). Afterwards culture plates containing the lysates were frozen at –80 °C for a minimum of 15 min, thawed at RT and shaken at 250 rpm for 1 min. LARII and Stop'n'Glo reagents were prepared freshly for each measurement. Firefly and renilla activities were measured after serial injection of the 2 substrates and subsequent luminescence measurement of each well using the SynergyMx microplate reader and the Gen5 software. For determination of the relative luciferase activity, the readouts from firefly luciferase activity were normalized to renilla luciferase activity.

5.1.11 Generation of conditioned medium (CM)

Stably transfected HEK293 Shh-N cells and untransfected HEK293 cells were used to prepare Shh-CM and control-CM [310]. For this purpose, the cells were cultured to a confluency of about 70 %. Then, the media were aspirated, cells were washed with PBS and cell culture media were replaced by low serum cell culture medium containing 2 % FCS instead of 10 % FCS. After 24 h to 48 h the CM was removed from the cell layer and sterile filtered through a 0.2 µm pore filter. The CMs were selead with parafilm and stored at 4 °C for up to one month. Supernatants of ERMS cell lines were also used to generate CM under the same conditions.

5.1.12 Analyses of HH ligand secretion and responsiveness

In order to analyze whether cells were able to secrete HH ligands and thus to stimulate the HH pathway in surrounding cells, different cell culture approaches were applied.

5.1.12.1 Incubation of cells with CM

The Shh responsive B9 cells were seeded at a density of 2×10^5 cells in wells of a 6 well plate and allowed to attach for 24 h. Then, the culture media were replaced by CM derived from control and ERMS cell lines (see section 5.1.11) for 48 h. Afterwards RNA was isolated, reverse transcribed and analyzed for the expression of *18S*, *Hprt* and *Gli1* (see section 5.2.8). An increase in *Gli1* expression was indicative for secretion of HH ligands into the cell culture medium. The results from Shh-CM treatment served as positive control.

When responsiveness of ERMS cell lines to SHH was analyzed, the ERMS cells were seeded with a density of 2×10^5 cells/well in a 6 well plate and allowed to adhere for 24 h. Then the culture media were replaced by either Shh-CM or control-CM (see section 5.1.11) for 48 h. Afterwards RNA was isolated, reverse transcribed and the expression of *18S*, *Hprt* and *Gli1* was analyzed (see section 5.2.8). B9 cells were included in the experiments as a positive control.

5.1.12.2 Co-culture experiments with the SHH light II reporter cell line

Furthermore, the cells potentially secreting SHH were co-cultured with SHH light II cells, that harbor a Gli responsive luciferase reporter. For this purpose, SHH light II cells were seeded in a black 96 well plate with clear bottom at a density of 5×10^3 cells/well (see section 5.1.1 for procedure) together with 7.5×10^3 cells of either HEK293 cells, HEK293 Shh-N cells or ERMS cells. After 24 h the media were replaced by starvation medium containing 0.5 % FCS for further 24 h to enhance responsiveness of SHH light II cells to a potential HH stimulus. Afterwards the dual luciferase reporter assay was performed as described in section 5.1.10 to analyze HH signaling activity in the SHH light II cells. SHH light II cells stimulated with Smoothened agonist (SAG) and SHH light II cells co-cultured with HEK293 Shh-N cells served as positive controls, whereas co-culture of SHH light II cells with HEK293 cells served

as negative control. The culture of cells without a Gli responsive luciferase reporter was used as a further negative control.

5.2 Molecular biology

5.2.1 Plasmid cloning

All required equipment for bacterial transformation and plasmid amplification were sterilized by an autoclave or a gas flame.

5.2.1.1 Transformation of bacteria

For cloning applications the *Escherichia coli* strain DH5α was used. Aliquots of 50 µl of competent bacteria were thawed on ice and mixed with 1 µl of pDNA. After 20 min of incubation a 30 sec heat shock was performed at 42 °C. Samples were cooled down on ice for approximately 1 min before adding 450 µl S.O.C. medium. The suspensions were shaken at 400 rpm and 37 °C for 50 min. Afterwards 150 µl were plated on LB agar plates containing adequate antibiotics for selection (100 µg/ml ampicillin or 50 µg/ml kanamycin). After a short drying period the plates were incubated upside down at 37 °C overnight.

5.2.1.2 Plasmid amplification, isolation and purification

Single colonies of transformed DH5α were picked the day after transformation (see section 5.2.1.1) and inoculated into 100 ml LB medium containing the adequate selection antibiotic (100 µg/ml ampicillin or 50 µg/ml kanamycin). For plasmid amplification bacteria were grown overnight on a shaker at 155 rpm and 37 °C.

The PureLink HiPure Plasmid DNA Purification Kit was used for isolation and purification of pDNA according to the manufacturer's instruction. For this purpose, the bacterial suspensions were distributed into 50 ml reaction tubes and centrifuged at 10,000×g for 10 min at 4 °C. The supernatants were discarded and all pellets were resuspended in 4 ml of resuspension buffer (R3). Then, 4 ml of lysis buffer (L7) were added to each tube and the tubes were inverted once to mix the suspension. Lyses were performed for 5 min at RT and afterwards 4 ml precipitation buffer (N3) were added to the lysates. The suspensions were again mixed by inverting the tube. Then the tubes were centrifuged at 10,000×g for 10 min at 4 °C. Meanwhile the DNA extraction columns were equilibrated with 10 ml equilibration buffer (EQ1). The supernatants from the centrifuged suspensions were then loaded onto the columns and were allowed to drain by gravity flow. Afterwards the columns were washed twice with 10 ml of washing buffer (W8). The bound pDNA was eluted by adding 5 ml of elution buffer (E4). The eluates were collected in falcon tubes and aliquoted in 1 ml aliquots. To each reaction tube 1 ml of pure isopropanol was added to precipitate the pDNA. The precipitation was performed at -20 °C overnight or at -80 °C for 30 min. The reaction tubes were centrifuged for 30 min at 13,000 rpm and 4 °C. Supernatants were discarded and the pellets were dried at 55 °C for 5 min. The isolated pDNAs were dissolved in 20 µl of ultrapure

H_2O each by shaking at 42 °C with 1400 rpm for 10 min. pDNA concentration was quantified using the Nanodrop system (see section 5.2.6).

5.2.1.3 Restriction enzyme hydrolysis

The plasmid identity was analyzed by test-restriction hydrolysis. Based on the plasmid sequence, 2 adequate restriction endonucleases were chosen for hydrolysis. The digestions were performed using 500 ng of purified pDNA mixed with 3 units of the respective enzymes and hydrolysis buffer in a total volume of 10 µl. The incubation temperatures and times were chosen according to the manufacturer's recommendations. The reactions were stopped by a heat shock at 70 °C for 10 min followed by incubation on ice. The products were analyzed after addition of 6× loading dye solution by separation on an agarose gel (see section 5.2.4).

5.2.2 Isolation of genomic DNA (gDNA)

5.2.2.1 Biopsies

Biopsies from mouse tail tip, ear or tissue were used to isolate gDNA and to perform PCR-based genotyping of animals. The biopsies were digested in 500 µl of STE buffer with 0.25 mg proteinase K per sample at 55 °C overnight. The next day the samples were shaken thoroughly and afterwards they were centrifuged at 13,000 rpm at RT for 10 min. Then, 300 µl of the supernatant were transferred into 1 ml of pure denatured EtOH to precipitate the gDNA. The samples were centrifuged for 30 min at 13,000 rpm and 4 °C. The supernatants were discarded and the pellets were washed with 200 µl of 70 % EtOH and centrifuged again at 13,000 rpm and 4 °C for 10 min. The supernatants were discarded again and the pellets were dried upside down at 55 °C for approximately 10 min. The isolated gDNA was dissolved in 125 µl ultrapure H_2O and shaken at 1400 rpm 10 min at 42 °C.

5.2.2.2 Paraffin-embedded tissue

The isolation of gDNA from embedded tissue was performed using the QIAamp DNA FFPE Tissue kit according to the manufacturer's instructions. Briefly, 8 freshly cut sections with a maximal thickness of 10 µm of formalin-fixed and paraffin-embedded tissue were prepared. Excess paraffin was removed from the sections using a scalpel. The sections were transferred into a reaction tube and 1 ml of xylene was added. After vigorous mixing the samples were centrifuged at 13,000 rpm and RT for 2 min. The supernatants were discarded and the pellets were resuspended in 1 ml of 96 % pure EtOH. After a further mixing step samples were centrifuged again at 13,000 rpm and RT for 2 min. The supernatants were discarded and the remaining EtOH was allowed to evaporate at 37 °C. The completely dried pellets were resuspended in 180 µl of ATL buffer. After adding 20 µl of proteinase K and mixing, the samples were incubated at 56 °C until they were completely lysed. Subsequently, the formaldehyde modifications were reversed by incubating the samples in ATL buffer at 90 °C for 1 h. Afterwards, 200 µl of AL buffer were added to the samples. After a thorough

mixing step, 200 µl of 96 % pure EtOH were added and samples were mixed again and spun down. Then the lysates were transferred to elution columns (located in 2 ml collection tubes) and centrifuged at 8000 rpm for 1 min. The elution columns with bound gDNA were transferred into new 2 ml collection tube. After 2 washing steps with 500 µl of AW1 and 500 µl of AW2 buffer by centrifugation at 8000 rpm for 1 min, the elution columns were dried by centrifugation at 13,000 rpm and RT for 3 min. For elution of the bound gDNA the columns were transferred into new 1.5 ml reaction tubes and incubated with 50 µl of ATE buffer for 5 min at RT. Afterwards the columns were centrifuged at 13,000 rpm and RT for 1 min. The isolated gDNA was either used directly or stored at -20 °C.

5.2.3 Polymerase chain reaction

5.2.3.1 PCR-based genotyping analyses

Genotyping of mice was performed by different PCR approaches within a total volume of 10 µl. Each reaction contained 10-100 ng of gDNA template (0.75 µl - 1.25 µl), 0.5 µM forward primer (in 0.5 µl H_2O), 0.5 µM reverse primer (in 0.5 µl H_2O), 0.2 µM dNTPs (in 0.2 µl H_2O), 0.3 mM $MgCl_2$ (in 0.6 µl H_2O), 10 % (v/v) Cresol (1 µl), polymerase buffer (in 1 µl), 0.1 U MolTaq polymerase (in 0.1 µl buffer) and was filled with ultrapure H_2O to 10 µl. In case 2 reverse primers were needed the concentration of the forward primer was doubled (1 µM) and the amount of added H_2O was reduced. The cycling conditions used for genotyping are listed in Tab. 21. All used Primers and size of PCR products are described in Tab. 11.

Table 21: PCR approaches for genotyping

	Mutant *Ptch*			Wildtype *Ptch*			Wildtype *Myf5*			Mutant *Myf5*		
Step	**Temp.**	**Time**	**Cycles**	**Temp.**	**Time**	**Cycles**	**Temp.**	**Time**	**Cycles**	**Temp.**	**Time**	**Cycles**
First Denaturation	94 °C	5 min		95 °C	5 min		95 °C	5 min		95 °C	5 min	
	94 °C	1 min		95 °C	20 sec		95 °C	30 sec		95 °C	30 sec	
Amplification	62 °C	1 min	35 x	60 °C	20 sec	35 x	59 °C	30 sec	35 x	58 °C	40 sec	35 x
	72 °C	3 min		72 °C	45 sec		72 °C	90 sec		72 °C	40 sec	
Final Extension	72 °C	5 min		72 °C	5 min		72 °C	5 min		72 °C	5 min	

	Wildtype and mutant *HRas*			Wildtype and mutant *KRas*			Wildtype and mutant *NRas*			Wildtype and mutant *Rosa26*		
	Temp.	**Time**	**Cycles**	**Temp.**	**Time**	**Cycles**	**Temp.**	**Time**	**Cycles**	**Temp.**	**Time**	**Cycles**
First Denaturation	95 °C	5 min		95 °C	5 min		94 °C	5 min		95 °C	5 min	
	95 °C	30 sec		95 °C	30 sec		94 °C	30 sec		95 °C	20 sec	
Amplification	64 °C	30 sec	30 x	55 °C	30 sec	30 x	68 °C	1 min	25 x	60 °C	20 sec	30 x
	72 °C	1 min		72 °C	1 min		72 °C	1 min		72 °C	45 sec	
Final Extension	72 °C	5 min		72 °C	5 min		72 °C	5 min		72 °C	5 min	

5.2.3.2 PCR-based recombination assays

Recombination assays were performed to prove efficient recombination at the floxed *Ras* loci in tissue of genetically modified mice. For this purpose 1 µl of a gDNA (KRas and NRas) or

cDNA-template (HRas) was mixed with 0.5 µM forward primer (in 1 µl H_2O), 0.5 µM reverse primer (in 1 µl H_2O), 0.2 µM dNTPs (in 0.4 µl H_2O), 0.2 mM $MgCl_2$ (in 0.8 µl H_2O), 10 % (v/v) Cresol (2 µl), polymerase buffer (2 µl), 0.1 U MolTaq polymerase (in 0.2 µl buffer). The reaction was filled with ultrapure H_2O to 20 µl. The used primers for the different recombination assays and their sequences are listed in Tab. 11. The utilized PCR programs are listed in Tab. 22.

Table 22: PCR approaches for recombination assays

	HRas			KRas			NRas		
Step	**Temp.**	**Time**	**Cycles**	**Temp.**	**Time**	**Cycles**	**Temp.**	**Time**	**Cycles**
First Denaturation	95 °C	1 min		95 °C	5 min		94 °C	5 min	
	95 °C	30 sec		95 °C	30 sec		94 °C	30 sec	35 x
Amplification	65 °C	30 sec	45 x	55 °C	30 sec	40 x	68 °C	1 min	
	72 °C	45 sec		72 °C	1 min		72 °C	1 min	
Final Extension	72 °C	5 min		72 °C	5 min		72 °C	5 min	

5.2.3.2.1 KRas and NRas recombination assays

The PCR products from KRas and NRas recombination assays were analyzed directly by agarose gel electrophoresis (see section 5.2.4). For both assays a double band (Kras: 270 bp for wt and 304 bp for recombined KRas; NRas: 487 bp for wt and 521 bp for recombined NRas) indicated efficient recombination whereas a single band (KRas: 270 bp for wt KRas; NRas: 487 bp for wt NRas) indicated no recombination.

5.2.3.2.2 HRas recombination assays

The recombination assay for HRas comprised an enzymatic digestion of PCR-amplified *HRas* fragments with BpmI. The enzyme recognizes the wt sequence, whereas the mutant *HRas* sequence is not recognized by the enzyme due to the $HRas^{G12V}$ mutation [303].

For the recombination assay 12.5 µl of PCR-amplified HRas cDNA were mixed with 0.5 U BpmI (in 0.25 µl buffer) and 3.1 NEBuffer™ (2 µl), and the reactions were filled up with ultrapure H_2O to 20 µl. The enzyme hydrolyses were performed at 37 °C for 30 min and reactions were stopped by a heat shock at 65 °C for 2 min. The products were analyzed by agarose gel electrophoresis (see section 5.2.4). Not digested samples, lacking the restriction enzyme, were used as negative control. Potential results from the recombination assay are shown and explained in Fig. 5.

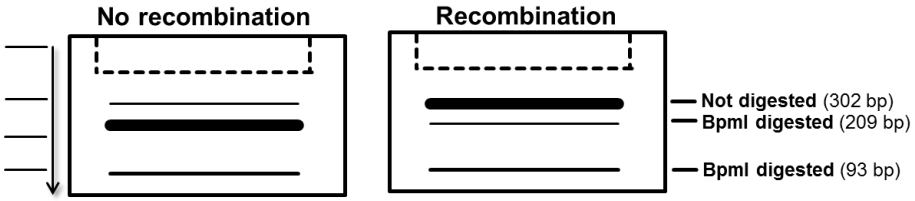

Figure 5: Potential readouts from HRas recombination assays
Heterozygous mice without recombination will show 2 strong digestion fragments (209 bp and 93 bp) and a weak undigested fragment (302 bp) (left cartoon). Heterozygous mice with successful recombination will show weak digestion bands (209 bp and 93 bp) and a strong undigested fragment (302 bp) (right cartoon). Since complete digestion was not feasible in this experimental setting an undigested fragment (302 bp) was always expected.

5.2.4 Agarose gel electrophoresis

DNA fragments were separated by agarose gel electrophoresis. Depending on the expected product sizes 1 % to 3 % (w/v) agarose gels were prepared in TBE buffer. The solutions were boiled for 3 min in a microwave oven at 1000 W to dissolve the agarose powder. The liquid gel was cooled down and a few droplets of ethidium bromide (0.07 %) were added. The agarose was poured into trays and combs were placed. After solidification, the combs were removed and the gels were covered with TBE buffer in an electrophoresis chamber. The samples were loaded and an electric field was applied (80-120 V, 500 mA, separation: 30 min-2.5 h). Appropriate markers were used to indicate the DNA size. Fragments were visualized in an UV transilluminator and documented using the INTAS GDS 3.39 software.

5.2.5 Ribonucleic acid (RNA) isolation

To protect RNA from degradation, the isolation was performed on ice if not indicated otherwise. Filter tips and equipment was RNAse-free. For isolation, the Trizol reagent was used according to the manufacturer's recommendations.

5.2.5.1 Isolation of total RNA from eukaryotic cell lines

The cultured cells were washed twice with ice-cold PBS and 1 ml of cold Trizol was added to one well of a 6 well plate. The suspensions were transferred into 2 ml tubes and were mixed thoroughly for 2 min on a shaker. After a 5 min incubation step at RT 200 µl chloroform were added to each sample. Again, the samples were mixed thoroughly for 20 sec on a shaker and incubated for 3 min at RT. A centrifugation step at 12,000 rpm and 4 °C for 10 min resulted in a phase separation. Approximately 600 µl/sample of the clear upper and aqueous phase were transferred into a tube with 700 µl of pre-cooled isopropanol. After precipitating overnight at -20 °C, the samples were centrifuged at 12,000 rpm and 4 °C for 30 min. The supernatants were discarded and the pellets were washed with 700 µl of pre-cooled 70 % pure EtOH. After 2 further washing steps (consisting of a centrifugation at 12,000 rpm and 4 °C for 15 min, the removal of the supernatants and the addition of 700 µl of pre-cooled 70 % pure EtOH) the RNA pellet was air-dried for about 1 h and solubilized in 15 µl – 45 µl ultrapure H_2O while shaking at 900 rpm and 56 °C for 10 min. The RNA concentrations were quantified (see section 5.2.6) and samples were stored at -80 °C.

5.2.5.2 Isolation of total RNA from tissue samples

Approximately 20 mg of frozen tissue sample were chopped in a petri dish on dry-ice using a scalpel blade. The chopped tissue was transferred into a 2 ml tube and covered with 1 ml of cold Trizol. Then the tissue samples were homogenized on ice using a disperser tool until a homogenous solution was achieved. The tool itself was cleaned after each sample. Further lyses were performed by incubation of the homogenates in Trizol for 5 min. The following steps were performed as described in section 5.2.5.1.

5.2.6 Photometric quantification of nucleic acids

The NanoDrop 8000 spectrophotometer was used to photometrically determine DNA and RNA concentrations. Optical densities (OD) of each sample were measured at 230 nm, 260 nm, 280 nm and 340 nm. OD_{260} provides the concentration of nucleic acids, whereby an OD_{260} of 1.0 reflects 50 µg/ml pure dsDNA or 40 µg/ml pure RNA. Thus, DNA or RNA concentrations were calculated by multiplying the measured OD_{260} values with 50 or with 40, respectively. OD_{230} of the sample provides a measurement of the concentration of sugars, salts and phenols, OD_{280} of the sample provides the concentration of proteins and OD_{340} measures turbidity and background signals. DNA and RNA samples with an OD_{260}/OD_{280} ratio between 1.8 and 2 and an OD_{260}/OD_{230} ratio ≥ 2, respectively, were considered as pure nucleic acids. OD_{340} values were optimally close to zero.

5.2.7 Reverse transcription

For cDNA synthesis, the SuperScript II Reverse Transcriptase kit was used based on the manufacturer's recommendations. In detail, 2 µg of total RNA (for isolation see section 5.2.5) were diluted in 7 µl of ultrapure H_2O and mixed with 250 ng of random hexamer oligonucleotides (in 5 µl H_2O) and incubated for 10 min at 70 °C. A mixture of 0.5 mM dNTPs (in 1 µl H_2O), 10 mM DTT (in 2 µl H_2O) and first strand buffer (4 µl) were added to the samples and the mixtures were incubated for 10 min at RT. After pre-warming at 42 °C for 2 min, 100 U (in 1 µl) of reverse transcriptase were added (final volume of 20 µl). The enzyme-driven cDNA synthesis was performed at 42 °C for 1 h. A heat inactivation step at 70 °C for 10 min stopped the synthesis. Assuming a reaction efficiency of 50 % the final cDNA concentration theoretically was 50 ng/µl. The samples were stored at -20 °C.

5.2.8 Quantitative real time PCR

Gene expression analyses were performed by SYBR-green based quantitative real time PCR (qRT-PCR). Dependent on the gene of interest (GOI) either the Platinum SYBR Green qPCR Super Mix (Invitrogen) or QuantiTect SYBR Green PCR (Qiagen) were applied using different qRT-PCR programs (see Tab. 23). For qRT-PCR reactions, 2 µl of diluted cDNA (see Tab. 24) were added to 8 µl of a prepared mastermix (see Tab. 23) resulting in a total reaction volume of 10 µl. Details of the used primer pairs are listed in Tab. 12. All

measurements were performed in triplicates in a sealed black 384 well plate on an ABI Prism 7900HT device using the SDS software.

The gene expression values were calculated using the standard curve method. To generate the standard curve a sample with high and constant expression of the GOI was chosen. Of this sample 20 ng/2 µl cDNA or 250 pg/2 µl cDNA were subjected to a 5-fold serial dilution row and amplified with primers specific for the GOI or *18S ribosomal RNA (rRNA)*, respectively. Logarithmic values of the calculated cDNA concentration from the dilution series were plotted against the corresponding measured cycle threshold (CT) from the same sample. A trend line was plotted and its formula was used to calculate the amount of GOI cDNA in the target samples. The resulting transcript levels of the GOI were normalized to those of *18S rRNA* of the same sample. Furthermore, the GOI transcript levels were also normalized to the reference genes *HPRT/Hprt* or *TBP/Tbp*. The standard curves for these genes were generated by 5-fold serial dilutions starting with 20 ng/2 µl cDNA. Further analyses were done using the SDS 2.2, Microsoft Excel and GraphPad Prism 6 software. Additionally, the results were relativized to experimental control samples, such as solvent controls.

Table 23: Mastermix and conditions for qRT-PCR

Mastermix	
Component	**Volume**
SYBR Green	5 µl
Forward primer	0.4 µl (0.4 µM)
Reverse primer	0.4 µl (0.4 µM)
H_2O	2.2 µl
cDNA template	2 µl

Qiagen		
Temp.	**Time**	**Cycles**
50 °C	2 min	
95 °C	15 min	
95 °C	15 sec	
60 °C	30 sec	40 x
72 °C	30 sec	
Dissociation stage (95 °C: 15 sec, 60 °C: 15 sec, 95 °C: 15 sec)		

Invitrogen		
Temp.	**Time**	**Cycles**
50 °C	2 min	
95 °C	2 min	
95 °C	30 sec	
60 °C	1 min	40 x
Dissociation stage (95 °C: 15 sec, 60 °C: 15 sec, 95 °C: 15 sec)		

Table 24: Assay informations for qRT-PCR

Human genes			
GOI	**Standard**	**Sample dilution**	**SYBR Green**
18S rRNA	E12.5	1:13,500	Qiagen, Invitrogen
HPRT	RMS-13	1:10	Invitrogen
GLI1	RMS-13	1:10	Invitrogen
GLI2	RMS-13	1:10	Qiagen
GLI3	RUCH-2	1:10	Qiagen
HHIP	RMS-13	1:10	Invitrogen
PTCH	RMS-13	1:10	Qiagen
SHH	MET-4	undiluted	Qiagen

Murine genes			
GOI	**Standard**	**Sample dilution**	**SYBR Green**
18S rRNA	E12.5	1:13,500	Qiagen, Invitrogen
Hprt	E12.5	1:20	Qiagen, Invitrogen
Tbp	E12.5	1:20	Invitrogen
Gli1	E12.5	1:20	Invitrogen
Gli2	E12.5	1:20	Qiagen
Gli3	RMS	1:20	Invitrogen
Hhip	E12.5	1:20	Qiagen
Ptch	E12.5	1:20	Qiagen
MyoD	RMS	1:20	Qiagen
Myogenin	RMS	1:20	Invitrogen
Myosin heavy chain (MyHC)	RMS	1:20	Qiagen
Tropomyosin 3	RMS	1:20	Qiagen
p21	RMS	1:20	Qiagen
p27	RMS	1:20	Qiagen

5.3 Protein biochemistry

The protein isolations were performed on ice if not indicated otherwise. Protein samples were stored at -80 °C.

5.3.1 Protein isolation from cell culture

Subconfluent cells grown on a 10 cm culture plate were used to detect the proteins pERK/ERK, pAKT/AKT, pS6/S6, pan-RAS, Caspase 3 and HSC70. For examination of nuclear and cytoplasmic GLI proteins 5 cell culture plates were pooled (see section 5.3.2).

The cell layers were washed twice with ice-cold PBS. Afterwards 500 µl of ice-cold PBS were added and the cells were scraped off the plate. The cell suspensions were transferred into cooled 2 ml tubes. The samples were centrifuged at 2,000 rpm and 4 °C for 5 min, afterwards the supernatants were discarded. The cell pellets were snap frozen in liquid nitrogen and thawed on ice. The pellets were resuspended in 50 µl – 100 µl of lysis buffer (depending on the pellet size) and passed several times through a 30G needle using a 1 ml syringe. Lysis was performed 45 min on ice and samples were gently mixed every 15 min. Then the lysates were centrifuged at 13,000 rpm and 4 °C for 30 min. The supernatants containing the cellular proteins were transferred into new tubes.

5.3.2 Subcellular fractionation of cellular lysates

The protocol for subcellular fractionation is based on other protocols described in the literature [321,322]. The cells were scraped off and washed as described in section 5.3.1. The pellets were resuspended in 500 µl PBS and the cell suspensions were split into 2 tubes to isolate cytosolic/nuclear proteins or the total protein fraction. Both tubes were centrifuged at 2,000 rpm and 4 °C for 5 min and the supernatants were discarded. Isolation of the total fraction was performed as described above (see section 5.3.1). The samples for isolation of the cytosolic and nuclear proteins were thoroughly resuspended in 250 µl of subcellular fractionation (SF) buffer and passed several times through a 30G needle using a 1 ml syringe. Lysis was performed 45 min on ice and the samples were gently mixed every 15 min. Afterwards the samples were centrifuged at 3,000 rpm and 4 °C for 15 min. The supernatants from this step were used to isolate cytosolic proteins, whereas the pellet was used to isolate nuclear proteins.

For isolation of cytosolic proteins, the supernatants were transferred into a new 1.5 ml tube and centrifuged at 8,000 rpm and 4 °C for 12 min. The resulting supernatant contained the cytosolic and membrane fractions.

To isolate nuclear proteins, the pellets were resuspended in 500 µl of SF buffer and washed by centrifugation at 3000 rpm and 4 °C for 10 min. The supernatants were discarded and the pellets were snap frozen in liquid nitrogen and thawed on ice. After thawing the pellets were resuspended in 50 µl of nuclear lysis buffer (NL buffer) and incubated for 45 min on ice and

gently mixed every 15 min. After lysis, the samples were centrifuged at 3000 rpm and 4 °C for 30 min and the supernatants containing the nuclear proteins were collected.

5.3.3 Protein isolation from murine tissue samples

Approximately 30 mg of a frozen tissue sample was chopped in a petri dish on dry ice using a scalpel blade. The chopped tissue was transferred into a 2 ml tube and covered with 200 µl of cold modified RIPA buffer. Tissue samples were homogenized on ice using a homogenizer. The homogenates were snap frozen in liquid nitrogen and thawed on ice. Afterwards the lysates were clarified by centrifugation at 10,000 rpm and 4 °C for 20 min. The supernatants, which contained cellular proteins, were collected and transferred into new tubes. The homogenizer was thoroughly cleaned before homogenizing another sample.

5.3.4 Quantification of isolated protein samples

The protein concentration was measured using the Pierce BCA (bicinchoninic acid) protein assay kit according to the manufacturer's recommendations. Briefly, the proteins were quantified in technical triplicates by adding 1 µl protein lysate to a well of a clear 96 well plate. Then, 200 µl of freshly prepared substrate solution was added to each well and the plate was incubated at 37 °C for 30 min to allow for the colorimetric reaction. A BSA dilution series in the respective lysis buffer was used to generate a standard curve. Absorbance was measured at 540 nm in a SynergyMx microplate photometer. The total protein concentration was calculated using the standard curve values.

5.3.5 Western Blot

For Western Blot analyses 20-45 µg of protein lysate were dissolved in 20 µl of ultrapure H_2O. SDS loading buffer was added and thereby diluted to a one fold concentration. The samples were denatured by boiling for 5 min at 96 °C and 500 rpm. After cooling on ice the samples were loaded onto appropriate SDS gels. The SDS gel electrophoresis was performed on ice.

5.3.5.1 Semi-dry blotting

Semi-dry blotting was used to detect smaller proteins with a maximal size of 100 kDa. For this purpose, proteins were separated on 4-12 % Bis-Tris gels using the MES SDS running buffer. The denaturated protein samples and an appropriate protein marker were loaded onto the gels and separated at 110-160 V and 160 mA for approximately 1.5 h. The separated proteins were blotted onto a nitrocellulose (NC) membrane with 0.2 µm pore size using semi-dry blotting buffer. The blotting itself was performed in a Trans-Blot® SD Semi-Dry Transfer Cell at 120 mA and 20 V for 1 h 25 min.

5.3.5.2 Tank blotting

The tank blotting was used to detect larger proteins. For this purpose, denaturated samples were loaded onto 3-8 % Tris-acetate gels. A high range protein marker was loaded to determine protein size. Separation by SDS gel electrophoresis was performed in Tris-acetate SDS running buffer at 100-110 V and 100 mA for approximately 2.5 h. The separated proteins were blotted onto a NC membrane with 0.45 µm pore size at 55 V and 300 mA for 2 h 35 min at 4 °C in a tank containing constantly stirred tank blotting buffer.

5.3.5.3 Antigen detection and visualization

After blotting, the membranes were blocked with 5 % (w/v) milk powder dissolved in TBST for 1 h at RT on a shaker. Afterwards the membranes were washed 3 x 10 min with TBST. The blocked membranes were incubated with primary antibodies dissolved in BSA-azide (for dilutions compare Tab. 9) at 4°C on a roller overnight. The membranes were washed again 3 × 10 min with TBST. Then HRP-conjugated secondary antibodies were added in 5 % (w/v) milk in TBST for 1 h at RT (see Tab. 10). After 3 washing steps with TBST, signals were detected using an enhanced chemiluminiescence reagent (ECL) in combination with the FluorChem Q system. For this purpose, luminol and peroxidase substrate were mixed 1:1 directly before use. The membranes were covered with the solution and after a short incubation time excess ECL was removed. Picture acquisition and processing was done with AlphaView Q SA and Adobe Photoshop CS5 softwares.

5.3.5.4 Stripping of membranes

For detection of multiple proteins of a similar size on the same membrane, the antibodies were stripped off. For this purpose, the membranes were washed with TBST for 2 × 10 min to remove the ECL reagent. The bound antibodies were stripped off by incubation of the membrane with stripping buffer at 55 °C for 30 min under constant rotation. Afterwards the membranes were washed thoroughly at least 4 times for 10 min in TBST. Then the membranes were blocked again and incubated with new primary antibodies solutions (section 5.3.5.3).

5.3.6 Ras pull-down activation assay

The Ras activation assay was strictly performed according to the manufacturer's instructions.

5.3.6.1 Cell culture samples

Subconfluent cells grown on a 10 cm cell culture plate were washed twice with ice-cold PBS and scraped off the plate using 500 µl of ice-cold PBS. The suspensions of 4 plates were pooled and centrifuged at 2,000 rpm and 4 °C for 5 min. The supernatants were discarded and cells were resuspended in 500 µl of the provided ice-cold lysis buffer. The lyses were performed for 10 min on ice and samples were centrifuged at 10,000 rpm and 4 °C for 2 min.

For protein quantification and detection of total Ras protein 60 µl of lysates were separated. The remaining cell lysates were immediately snap frozen in liquid nitrogen. Afterwards the protein concentrations were determined utilizing the BCA assay (see section 5.3.4).

As control, one sample was either loaded with GTPγS or GDP. For this purpose, 200 µg of protein were mixed with one-tenth volume of loading buffer. Immediately one-hundredth volume of supplied GTPγS or GDP was added. The samples were incubated at 37 °C for 30 min at 300 rpm on a shaker. Afterwards, the samples were mixed with one-tenth volume of stop buffer and stored on ice until the pulldown assay was performed. These GTPγS- or GDP-loaded samples were used to prove an efficient pulldown of active Ras protein. Furthermore, the kit supplied a pure His-Ras control protein, which was diluted in 2×Laemmli buffer and water before use. This protein served as a size marker. Moreover, 30 µg of total lysate of each analyzed sample was used to detect total Ras protein on a separate gel. These lysates were diluted in 20 µl of ultrapure H_2O and SDS loading buffer and seubjected to Western Blot analyses.

For the pulldown assay, 200 µg of protein were loaded onto 100 µg (30 µl) of Raf-RBD beads on platform shaker at 4 °C for 1 h. Afterwards, the beads were pelleted by centrifugation at 10,000 rpm at 4 °C for 2 min. The supernatant was carefully discarded and the beads were washed with 500 µl of supplied washing buffer and centrifuged again at 10,000 rpm and 4 °C for 3 min. The supernatant was discarded and the bead pellet was resuspended in 15 µl of 2×Laemmli buffer. All prepared samples were boiled at 96 °C and 400 rpm for 3 min and then rapidly cooled down on ice. Afterwards, samples were loaded onto 4-12 % Bis-Tris gels and semi-dry blotting was performed as described in section 5.3.5.1.

5.3.6.2 Tissue samples

Approximately 30 mg of a frozen tissue sample was chopped in a petri dish on dry ice using a scalpel blade. The chopped tissue was transferred into a 2 ml tube containing 200 µl of cold lysis buffer. Tissue samples were homogenized on ice. The homogenates were clarified by centrifugation at 10,000 rpm and 4 °C for 2 min. The supernatants containing the protein lysates were transferred into new tubes and immediately snap frozen. The following steps were identical to the procedure described above (see section 5.3.6.1) with the exception that 600 µg of protein were loaded onto 100 µg (30 µl) of Raf-RBD beads.

5.4 Immunohistochemical stainings

Tissue samples were fixed in 4 % (w/v) PFA in PBS for 24 h – 48 h at RT and then transferred into cold PBS and stored at 4 °C until embedding. The paraffin embedding was performed by Anke Frommhold and in cooperation with the Institute of Neuropathology, University Medical Center Göttingen.

The paraffin-embedded tissues were cut into 4-5 µm sections on a microtome. The sections were mounted onto microscope glass slides or superfrost glass slides and dried at 37 °C overnight prior immunohistochemical stainings.

5.4.1 Haematoxylin and eosin staining

For haematoxylin and eosin (HE) staining, sections were deparaffinized 2 times in xylene for 10 min and then rehydrated by a descending ethanol series (2 x 99 %, 96 %, 80 % and 70 %). After a thorough washing step under running ddH_2O, the slides were stained in hematoxylin solution for 20 min. Afterwards, the slides were washed under running warm tap water until hematoxylin was completely washed out from the cuvette. Then the slides were incubated with 1 % eosin solution for a maximum of 20 sec and shortly washed under running ddH_2O. Immediately after washing, the sections were dehydrated using ascending ethanol solutions (70 %, 80 %, 96 %, 99 %) and placed in fresh xylene twice in succession. Finally, the sections were mounted with Pertex and dried at least for 20 min at 55 °C.

5.4.2 Ki67 staining

For Ki67 staining the sections were deparaffinized 2 times in xylene for 10 min and were rehydrated by a descending ethanol series (2 x 99 %, 96 %, 80 % and 70 %). After washing under running ddH_2O, antigen-retrieval was performed by cooking the slides in citric acid buffer (pH 6) once for 4 min and 3 times for 3 min at 600 W in a microwave oven. Afterwards, the slides were cooled down to RT while shaking. Then the slides were washed 2 times in TBS buffer. Blocking of endogenous peroxidase activity was performed for 20 min on a shaker by incubating the sections in 3 % H_2O_2 in TBS buffer. The slides were washed for 5 min with ddH_2O and then placed in a moist chamber. A blocking against unspecific antibody binding was performed by adding 0.2 % casein in TBS buffer onto the slides. The primary antibody against Ki67 was diluted 1:50 in TBS and 50 µl of this solution were applied to each tissue section and incubated overnight at 4 °C. Then the slides were washed 3 times with TBST and afterwards they were incubated with the HRP-conjugated secondary antibody from the Dako EnVision kit for 30 min within a moist chamber at RT. After washing with TBST the staining was visualized by incubation with AEC staining solution. Haematoxylin was used for counter staining. Then, the slides were mounted with glycergel.

The results were evaluated by counting the number of $Ki67^+$ nuclei compared to the total number of nuclei. For this purpose, the staining was documented by 6 or 10 consecutive pictures of randomly chosen areas within the tumor tissue. The pictures were taken at 200 x magnification with the CellSens Dimension software and total number of nuclei, as well as $Ki67^+$ nuclei were counted manually using AlphaView Q SA software.

5.4.3 X-Gal staining

For X-Gal staining, the tissue samples were embedded in cryoblock media. For this purpose, freshly isolated tissue was fixed in 4 % PFA on ice for 2 h. Afterwards the tissue samples were washed 3 times with PBS for 20 min while shaking. The fixed tissues were equilibrated overnight in 25 % (w/v) sucrose in PBS at 4 °C. The next day, the tissue samples were embedded in cryoblock media on dry ice and cut into thin sections at -20 °C to -22 °C using a cryotome. The sections were mounted onto superfrost glass slides and were dried at RT for at least 2 h. The dried sections were incubated for 10 min with 0.2 % (v/v) glutaraldehyd in PBS on ice. Afterwards, the sections were washed 3 times with LacZ buffer (see Tab. 4) for 5 min on a shaker. Subsequently the sections were incubated with LacZ staining solution (see Tab. 4) at 30 °C overnight. If necessary, the staining solution was renewed after 24 h to enhance the signal intensity. The reactions were stopped by washing with PBS. Finally, the sections were mounted with mounting medium containing DAPI. Then pictures were taken at 600 x magnification using a Color View camera operated by CellSens software.

5.5 Animal experiments

All animal experiments were performed after approval of the Lower Saxony State Office for Consumer Protection and Food Safety and in accordance with all relevant ethical and legal requirements. Housing and breeding of animals was performed within the animal facility at the Institute of Human Genetics, University Medical Center Göttingen. In general, mice were housed at a 12 h light-dark cycle at 20 ± 2 °C and a relative humidity of 55 ± 10 % in individually ventilated Makrolon type 2 cages located in air-flow racks. Health checks were performed daily by animal caretakers. Mice received tap water and food pellets *ad libitum*. All used mouse lines are listed in Tab. 15.

5.5.1 Tumor xenografts

Immunodeficient *Nu/Nu* mice were used for transplantation studies and were purchased from Charles River Laboratories (Wilmington, USA). These mice were housed in autoclaved and individually ventilated type 2 cages and received sterilized food pellets as well as autoclaved water *ad libitum*. Genotypes of *Nu/Nu* mice were determined by the presence (*Nu/+*) or absence (*Nu/Nu*) of hairs.

For analyses of the *in vivo* growth behavior of oncRAS-expressing ERMS cell lines, cells harboring the control vector or cells expressing oncRAS were transplanted subcutaneously into the left and right flank of one *Nu/Nu* mouse, respectively. For the transplantation experiments animals of both genders at an age between 8 and 11 weeks were used.

Ahead of transplantation ERMS cell lines were grown in cell culture to 90 % confluence. One day before transplantation the cells were split 1:3 to ensure exponential growth. On the day of transplantation cells were collected and counted (compare sections 5.1.1 and 5.1.3).

Then, 2 × 10^6 TE617.T cells in PBS or 9 × 10^6 RUCH-2 cells in 1:1 Matrigel:PBS in a total volume of 200 µl were transferred into pre-cooled Sub-Q syringes and kept on ice. Mice were anesthetized with 1-3 % isoflurane in a 1:1 air/oxygen mix. Then the cells were injected subcutaneously. After transplantation mice were carefully monitored and tumor size was measured every second or every day by a caliper. The tumor volume was calculated by assuming an ellipsoid shape using de formula:

$$\text{Tumor volume} = \frac{\text{tumor width x height x length}}{2}$$

Mice were sacrificed when a tumor reached a diameter of 1.5 cm or latest 55 days after transplantation. The tumors were isolated, their exact size and weight was documented and then they were fixed in 4 % PFA in PBS. If possible, parts of the tumor tissue were frozen on dry ice and stored at -80 °C for further experiments.

Transplantation and tumor monitoring of TE617.T KRAS xenografts was part of the doctoral thesis of N. Cuvelier [299].

5.5.2 Breeding of mice

For ERMS monitoring studies *Ptch*$^{del/+}$ *Balb* mice were used. These mice harbor a heterozygous deletion of exon 8 and 9 within the *Ptch* gene and spontaneously develop RMS, which resembles human ERMS [137,143]. These mice were bred to conditional *HRasflox_B6* [303], *KRasflox_B6* [317] or *NRasflox_B6* [220] mice. The latter mice are heterozygous for a floxed oncogenic *Ras* allele that is expressed upon Cre-mediated recombination. The resulting *Ptch*$^{del/+}$*oncRas*$^{fl/+}$ offspring were crossed to *Myf5*$^{CreER/+}$ mice [305]. Since, as in humans, RMS of *Ptch*$^{del/+}$ *Balb* mice express high levels of *Myf5* [143,323], activation of the Cre recombinase in this model should result in expression of oncogenic *Ras* isoforms in the tumors. An overview of the breeding is displayed below (Fig. 6).

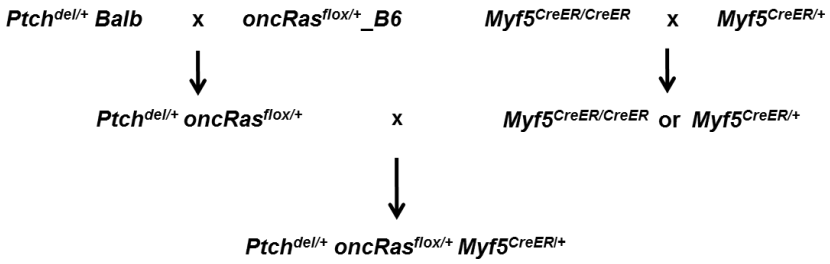

Figure 6: Breeding scheme for tumor monitoring studies
Overview of breeding strategies for generating and maintaining colonies of *Ptch*$^{del/+}$*oncRas*$^{fl/+}$*Myf5*^{CreER} mice. For details, see text.

When analyzing potential oncRas-dependent effects on ERMS precursor lesions the parental *Myf5*$^{CreER/+}$ mice were on a mixed C57BL/6 x *BALB/c* background, whereas those used for the analyses of oncRas-dependent effects in established ERMS were incipient-congenic and had been backcrossed 8 generations to BALB/c. Backcrossing had been done because the BALB/c background confers high susceptibility to ERMS [324,325].

5.5.3 Identification of mice

Mice were weaned at the age of 3 weeks and were numbered by ear clipping. Younger mice, which still were not weaned, were labeled by a tattoo code on their paws. At the same time tail tip biopsies were taken and were used for genotyping of the respective mice (see section 5.2.3.1).

5.5.4 Tamoxifen application

To induce recombination of the floxed *Ras* loci in *Ptch*$^{del/+}$*oncRas*$^{fl/+}$*Myf5*$^{CreER/+}$ mice 1 mg of tamoxifen in 100 µl solvent was injected intraperitoneally (i.p.) for 5 consecutive days resulting in a total dose of 5 mg tamoxifen per mouse. Tamoxifen was prepared by mixing 200 mg tamoxifen with 20 ml Sunflower seed oil and 800 µl pure EtOH. The solution without tamoxifen served as solvent control. The solutions were aliquoted into syringes and frozen at -20 °C until use.

5.5.5 Tissue isolation

Mice were euthanized by CO_2 or isoflurane narcosis and subsequent cervical dislocation. All tumors, skeletal muscles from the leg and back, cysts or suspicious tissues were taken and washed with PBS. If possible, tumors were weighed and measured using a caliper. Tumor tissue, cysts and suspicious tissues were fixed in 4 % PFA in PBS and were embedded in paraffin for immunohistochemical stainings (see section 5.4). The skeletal muscles and parts of the tumor samples were frozen on dry ice or snap frozen in liquid nitrogen and stored at -80 °C for protein and gene expression analyses.

5.5.6 Testing of the *Myf5*$^{CreER/+}$ deleter

To check the activity of the *Myf5*$^{CreER/+}$ deleter in ERMS, *Ptch*$^{del/+}$*Myf5*$^{CreER/+}$*R26R*$^{+/-}$ reporter mice were generated [299]. Tumor bearing mice were injected with 1 mg tamoxifen on 5 consecutive days and sacrificed 1 or 5 weeks thereafter. X-Gal stainings were performed on frozen sections of brain, heart, intestine, skeletal muscle and ERMS as described in section 2.4.3.

5.5.7 Tumor monitoring: induction of oncRas in ERMS precursor lesions

At the age of 4 weeks mice were injected with 1 mg. of tamoxifen i.p for 5 consecutive days to induce cre-mediated recombination at the respective *Ras* loci. Mice were monitored once a week for palpable tumors and were visually controlled for other abnormalities until the age of 200 days. The appearance of palpable tumors was recorded. Animals with poor general condition or those carrying tumors exceeding a size of 1.5 cm were sacrificed. Tissue was isolated as described in section 5.5.5. An overview of the study design is shown in Fig. 7.

Figure 7: Study design focusing on induction of Ras mutations in ERMS precursor lesions
Ptch$^{del/+}$ *or Ptch*$^{del/+}$*oncRas*$^{fl/+}$*Myf5*$^{CreER/+}$ mice at the age of 4 weeks were injected with tamoxifen for 5 consecutive days or left untreated. Afterwards mice were monitored weekly until the age of 200 days. For details, see text.

The studies were performed using tamoxifen-treated *Ptch*$^{del/+}$*HRas*$^{fl/+}$*Myf5*$^{CreER/+}$, *Ptch*$^{del/+}$*KRas*$^{fl/+}$*Myf5*$^{CreER/+}$ and *Ptch*$^{del/+}$*NRas*$^{fl/+}$*Myf5*$^{CreER/+}$ mice. Untreated siblings of the same genotype served as control. In order to analyze the effect of tamoxifen itself on tumor growth, ERMS-growth of tamoxifen- and untreated *Ptch*$^{del/+}$ mice from the same breeding were used. Part of these experiments have been done by N. Cuvelier and are described in her doctoral thesis [299]. Here, the already generated data were re-analyzed and the collected material was used for further analyses. Thus, the genotypes of each mouse were verified by a second round of genotyping PCR (see section 5.2.3.1). For this purpose, frozen and embedded tissue samples were used. In addition, recombination assays were performed using frozen or embedded samples from skeletal muscle and ERMS (see section 5.2.2). Finally, the study using *Ptch*$^{del/+}$*NRas*$^{fl/+}$*Myf5*$^{CreER/+}$ mice was completely repeated.

5.5.8 Tumor monitoring: induction of oncRas in already established ERMS

After weaning, mice were monitored once a week for palpable ERMS and were visually controlled for other abnormalities. Tumors occurred mainly at the extremities and the lower back and were observed until they reached a diameter of approximately 0.5 cm. Then the mice were subjected to micro computed tomography (µCT) measurement to determine the exact tumor volume (see section 5.5.9). Afterwards the mice were injected with 1 mg of tamoxifen for 5 consecutive days to induce the cre-mediated recombination at the *Ras* loci. After tamoxifen induction the mice were further monitored for changes in ERMS growth and general health conditions. Seven weeks after onset of the tamoxifen treatment, the mice underwent a second µCT measurement, which was defined as the end point of the study. Animals were euthanized, and tissue samples were taken as described in section 5.5.5. An overview of the study design is shown in Fig. 8.

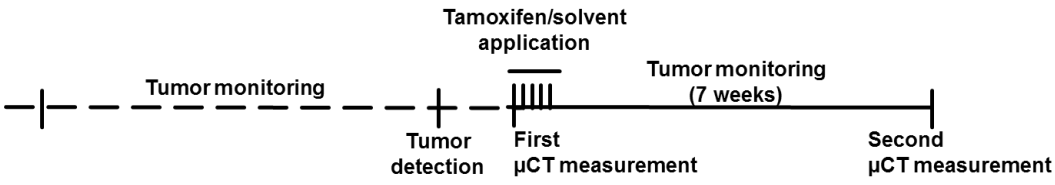

Figure 8: Study design focusing on induction of Ras mutations in established ERMS
After weaning, *Ptch*$^{del/+}$ *or Ptch*$^{del/+}$*oncRas*$^{fl/+}$*Myf5*$^{CreER/+}$ mice were monitored for palpable tumors. After tumor detection, mice were subjected to micro computed tomography (µCT) measurement and were injected with tamoxifen or solvent for 5 consecutive days. The mice were monitored for further 7 weeks and then subjected to a second µCT measurement. For more details, see text.

The study was performed with *Ptch*$^{del/+}$*HRas*$^{fl/+}$*Myf5*$^{CreER/+}$, *Ptch*$^{del/+}$*KRas*$^{fl/+}$*Myf5*$^{CreER/+}$ and *Ptch*$^{del/+}$*NRas*$^{fl/}$ *Myf5*$^{CreER/+}$ mice. Mice were injected with 1 mg of tamoxifen i.p. for 5 consecutive days to induce cre-mediated recombination or with solvent as a control. In addition, tamoxifen-treated or solvent-treated *Ptch*$^{del/+}$ siblings from each breeding cohort served as controls.

5.5.9 Tumor volume measurement by µCT

A low dose *in vivo* µCT (QuantumFX) was used to measure the tumor volume in living animals. The data acquisition was performed at 90 kVp tube voltage, 200 µA tube current and with 2 min total acquisition time. Mice were anesthetized with 1-3 % isoflurane in a 1:1 air/oxygen mix. Then the contrast agent Imeron 300 (5 ml/kg) was injected intravenously (i.v.) into the tail vain or into the retro-bulbar venous plexus. Approximately 30 sec later, the imaging was performed. Data sets were reconstructed with a voxel size of 80 µm and analyzed. Size of each tumor (precisely tumor width, height and length) at onset and end of the study was determined using simple viewer software.

The tumor volume was calculated by assuming an ellipsoid shape using the formula:

$$\text{Tumor volume} = \frac{\text{tumor width x height x length}}{2}$$

For data evaluation logarithmic values of the calculated tumor volume were plotted.

5.6 Statistical analyses

Statistical analyses were performed with MS Office Excel or GraphPad Prism 6 software. Data were considered significant when probability values (p-values) were < 0.05. Comparison of 2 samples or 2 groups was done by unpaired, non-parametric t-test (Mann Whitney) or Student's t-test. In order to compare more than 2 groups a one-way analysis of variance (ANOVA) and Dunn's multiple comparisons test were performed. Differences in ERMS-free survival were tested by Log-rank (Mantel-Cox) test and tumor latency time was tested by Gehan-Breslow-Wilcoxon test. Differences in tumor incidence and multiplicity were tested by Chi-square test. If not indicated otherwise graphs represent mean + standard error of the mean (SEM) values. Statistical significant results were visualized in graphs by * or $ (p-values < 0.05); ** or $$ (p-values < 0.01); *** or $$ (p-values < 0.001) and **** or $$$$ (p-values < 0.0001).

6 Results

6.1 Effects of oncogenic RAS mutations on human ERMS cell lines

Previous studies indicated a crosstalk of RAS and HH signaling in human RMS cell lines, whereby the interaction of the signaling pathways seemed to be differently regulated in cell lines of the embryonal and alveolar subtype. The studies showed that oncRAS isoforms can suppress the expression of the main HH target *GLI1* in a MEK-dependent manner at least in the ERMS cell line RUCH-2 [299].

In this work some of the already performed experiments were repeated and the role of oncRAS isoforms in regulation of HH targets and associated cellular responses of ERMS cells were analyzed in more depth. For this purpose, ERMS cell lines, originally wt for RAS, were stably transduced with different plasmids expressing oncogenic *HRAS*, *KRAS* or *NRAS* (collectively named oncRAS) isoforms (see section 5.1.4). Stably transduced cell lines with the empty plasmid (pMSCV) served as controls. In addition, experiments were performed with the human ERMS cell line RD, which harbors a $NRAS^{Q61H}$ mutation [312,326].

All described experiments within section 6.1 were also performed with untransduced (wt) cells. These experiments served as control for potential vector-dependent effects. Since no significant differences between wt cells and cells transduced with pMSCV were detected, the respective data were not included into the graphs of this thesis.

6.1.1 Characterization of stably transduced RMS cell lines with oncRAS isoforms

Ahead of all experiments, the stably transduced TE617.T, RUCH-2 and RMS-13 cell lines were analyzed to confirm successful transduction. In order to further characterize the cell lines, the impact of oncRAS isoforms on phosphorylation of downstream kinases, relative RAS activity and cell cycle distribution were analyzed.

6.1.1.1 Successful transduction of human RMS cell lines

The successful transduction of human RMS cell lines with the plasmids *pMSCVpuro* (pMSCV), *pMSCVpuro-HRAS*^{G12V} (oncHRAS), *pMSCVpuro-KRAS*^{G12V} (oncKRAS) or *pMSCVpuro-NRAS*^{G12V} (oncNRAS) was examined by PCR (see section 5.1.4.1). For this purpose, cDNAs from the stably transduced cell lines were analyzed with a common forward primer within the *pMSCVpuro* sequence and with 3 reverse primers specific for the transcribed oncRAS isoform (Fig. 9). All cell lines were screened using all primers to rule out potential contamination.

Successful transduction with vectors for pMSCV, oncHRAS, oncKRAS or oncNRAS was confirmed for the RMS-13 and RUCH-2 cell lines (Fig. 9B and Fig. 9C). The TE617.T cell line

(Fig. 9A) had been successfully transduced with oncKRAS. Unfortunately, oncHRAS and oncNRAS were expressed in one and the same TE617.T line probably due to a mix-up of the plasmids or a cross contamination of the cells during production. The PCR was also done on the pure single plasmids or on a mixture of all plasmids, which served as positive control (Fig. 9D).

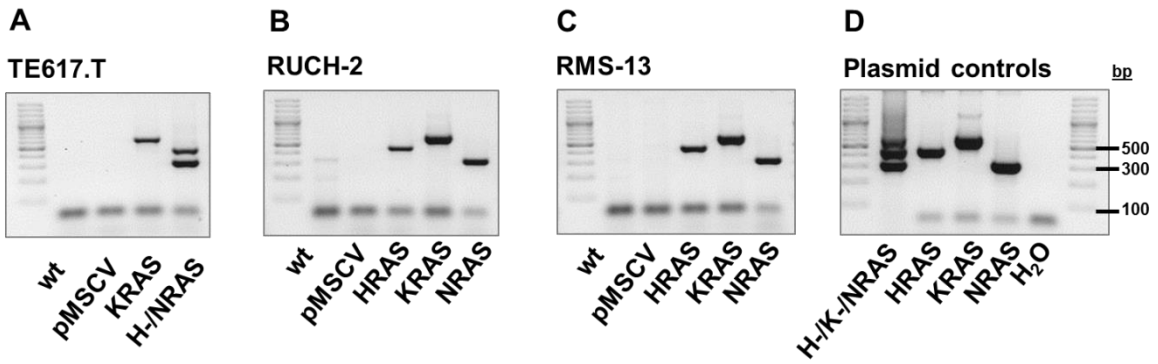

Figure 9: Successful transduction of RMS cell lines
RNA was isolated from TE617.T (A), RUCH-2 (B) and RMS-13 (C) cell lines, that have been stably transduced with the empty plasmid (pMSCV) or plasmids expressing oncHRAS (HRAS), oncKRAS (KRAS), oncNRAS (NRAS), or remained untransduced (wt). RNA were subjected to cDNA synthesis and analyzed by PCR with a common forward primer and isoform-specific reverse primers. Amplificates were separated by agarose gel electrophoreses and analyzed. Single plasmids or a mixture of the plasmids (100 ng/reaction) served as positive control (D). H-/NRAS indicate expression of oncHRAS and oncNRAS in one and the same cell line.

6.1.1.2 Transduction of RMS cell lines with oncRAS isoforms results in elevated protein level of RAS and pERK

Next, the stably transduced cell lines were analyzed by Western Blot for the general expression level of RAS proteins (pan-RAS), for the expression and activation of downstream kinases of RAS, which are pERK/ERK, pAKT/AKT, pS6/S6, and for caspase 3 cleavage to investigate apoptosis induction. Representative results for TE617.T cells (Fig. 10A), RUCH-2 cells (Fig. 10B) and RMS-13 cells (Fig. 10C) are shown.

In general, the level of RAS proteins were higher in all cell lines after transduction with any oncRAS isoform. Transduction with oncKRAS resulted in a protein double band, because *KRAS*^{G12V} expressed by the *pMSCVpuro-KRAS*^{G12V} plasmid contains a Hemagglutinin (HA)-tag sequence [299]. The transduction with oncRAS isoforms did not influence the protein level of pAKT/AKT and pS6/S6. It also did not influence caspase 3 cleavage, which was investigated as a readout for apoptosis. In contrast, pERK protein level were elevated in oncRAS-expressing RUCH-2 and RMS-13 cell lines. The exceptions were the oncRAS-transduced TE617.T cell lines and RUCH-2 KRAS cells, which did not show elevated level of ERK phosphorylation in comparison to pMSCV control cells.

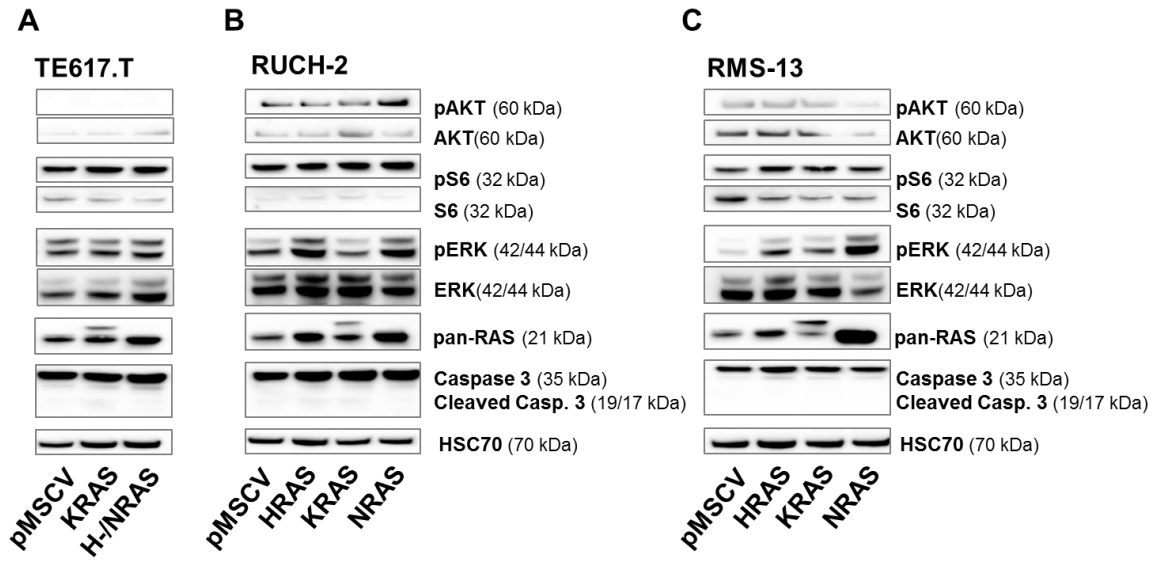

Figure 10: Characterization of protein expression of transduced RMS cell lines
Protein was isolated from TE617.T (A), RUCH-2 (B) and RMS-13 (C) cell lines, that have been stably transduced with the empty plasmid (pMSCV) or plasmids expressing oncHRAS (HRAS), oncKRAS (KRAS), oncNRAS (NRAS) or a mixture of oncHRas and oncNRAS (H-/NRAS). Western Blot analyses were done to detect the protein level of pAKT/AKT, pS6/S6, pERK/ERK, pan-RAS and caspase 3 cleavage (Caspase 3 and cleaved Casp. 3) with specific antibodies. HSC70 served as loading control. Protein names and sizes in kDa are displayed on the right side of the blots. The blots are representative for 2 independent experiments.

6.1.1.3 OncRAS isoforms are active in transduced RMS cell lines

Since not all cell lines showed phosphorylation of the RAS-downstream target ERK (see above), RAS activity in the cells was also investigated in an RAS activity assay (for experimental procedure compare section 5.3.6).

The analysis revealed that RAS activity was higher in all oncRAS-transduced cell lines in comparison to cell lines that have been transduced with the control vector. A densitometrical quantification (histograms in Fig. 11) indicated a 16-fold or 12-fold upregulation of RAS activity in TE617.T cells expressing oncKRAS or oncH-/NRAS, respectively, in comparison to cells harboring the pMSCV vector (Fig. 11A). For RUCH-2 cells a 2.5-fold (oncHRAS), 2.3-fold (oncKRAS) or 1.8-fold (oncNRAS) increase of RAS activity was measured after stable transduction with oncRAS isoforms (Fig. 11B). In the ARMS cell line RMS-13, stable transduction with oncRAS isoforms increased RAS activity approximately 4.7-fold (oncHRAS) 8.8-fold (oncKRAS) or 8.4-fold (oncNRAS) in comparison to RMS-13 pMSCV cells (Fig. 11C).

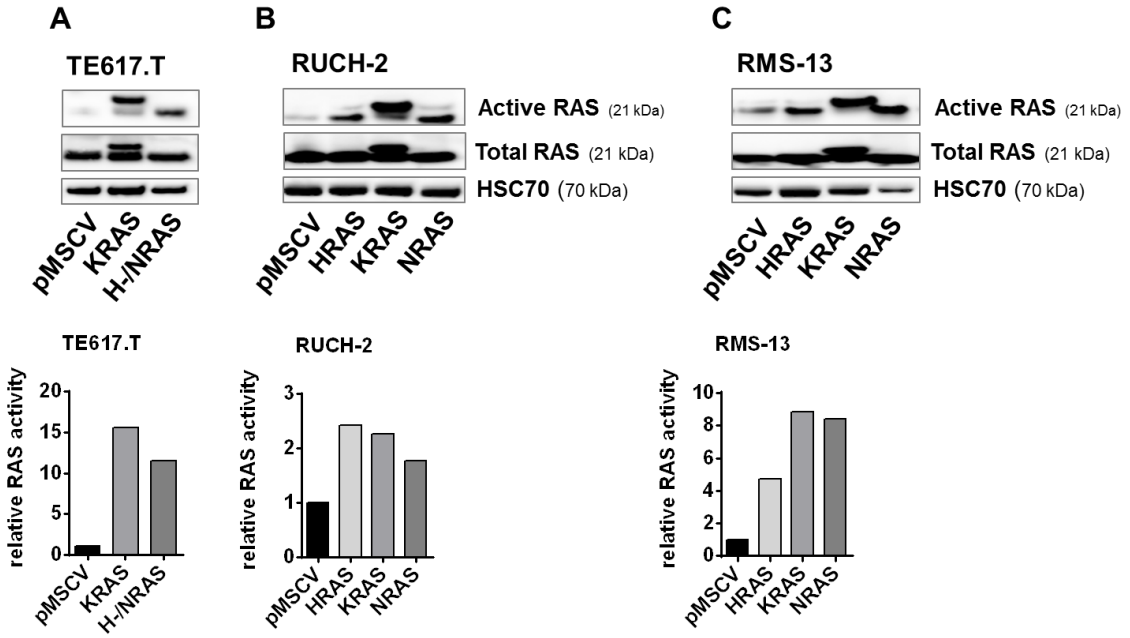

Figure 11: RAS activity assay of transduced RMS cell lines
Protein was isolated from TE617.T (A), RUCH-2 (B) and RMS-13 (C) cell lines, that have been stably transduced with the empty plasmid (pMSCV) or plasmids expressing oncHRAS (HRAS), oncKRAS (KRAS), oncNRAS (NRAS) or a mixture of oncHRas and oncNRAS (H-/NRAS). Afterwards cell lysates were subjected to a bead-based pull-down assay to precipitate active RAS. Whole lysates of the same cells were used to detect total RAS. Afterwards precipitated and not-precipitated lysates were analyzed by Western Blot to detect the protein level of active RAS and total RAS with specific antibodies. HSC70 served as loading control for total RAS. Protein names and sizes in kDa are displayed on the right side of the blots. The relative RAS activity was calculated by normalization of active RAS to total RAS/HSC70 and is displayed in histograms below the representative Western Blots. The results are representative for 1 or 2 independent experiments.

6.1.1.4 OncRAS isoforms do not influence cell cycle distributions of RMS cell lines

OncRAS isoforms are well-established modulators of cell cycle progression [183]. In order to investigate whether oncRAS modulate the cell cycle distribution of the stably transduced RMS cell lines, the cells were stained with PI and analyzed by flow cytometry 48 h after seeding (see section 5.1.7). An analysis of stably transduced RUCH-2 cell lines was not performed, because it was not possible to detach these cells with accutase.

OncRAS isoforms did not change cell cycle distribution in TE617.T cells (Fig. 12A). Thus, approximately 28.3 % (pMSCV), 25.3% (oncKRAS) or 33.9 % (oncH-/NRAS) of TE617.T cells were in G1/G0 phase, whereas 4.8 % (pMSCV), 6.5 % (oncKRAS) or 4.0 % (oncH-/NRAS) were in S phase and 17.6 % (pMSCV), 17.9 % (oncKRAS) or 22.4 % (oncH-/NRAS) were in G2/M phase. In the same experimental setup oncRAS isoforms did not change the cell cycle distribution of RMS-13 cells (Fig. 12B). Thus, approximately 37.9% (pMSCV), 33.9 % (oncHRAS), 34 % (oncKRAS) or 35.8 % (oncNRAS) of RMS-13 cells were in G1/G0 phase, whereas 6.9 % (pMSCV), 7.8 % (oncHRAS), 7.8 % (oncKRAS) or 5.5 % (oncNRAS) were in S phase and 27.9 % (pMSCV), 32.1 % (oncHRAS), 35.2 % (oncKRAS) or 24.5 % (oncNRAS) were in G2/M phase.

Taken together, there might be a difference in cell cycle distribution between TE617.T and RMS-13 cell lines. However, oncRAS isoforms do not influence cell cycle progression.

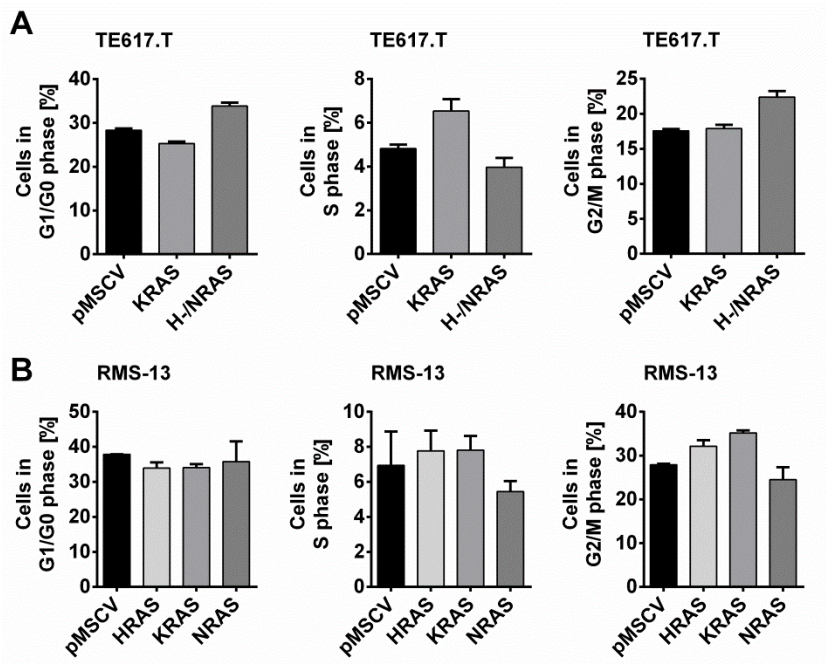

Figure 12: OncRAS isoforms do not influence cell cycle distribution of TE617.T and RMS-13 cells
TE617.T (A) and RMS-13 (B) cell lines that have been stably transduced with the empty plasmid (pMSCV) or plasmids expressing oncHRAS (HRAS), oncKRAS (KRAS), oncNRAS (NRAS) or a mixture of oncHRas and oncNRAS (H-/NRAS) were subjected to cell cycle analyses 48 h after seeding. Cells were detached, fixed and stained with PI. Cell cycle distribution was analyzed by flow cytometry and the relative amounts of cells resident in G1/G0 phase, S phase and G2/M phase were calculated. Bars represent the mean + SEM of 3 independent experiments performed in technical duplicates. For statistical analyses non-parametric t-tests (Mann Whitney) were performed.

In summary, the data presented in chapter 6.1 demonstrate that the human ERMS cell lines TE617.T and RUCH-2 and the human ARMS cell line RMS-13 express oncRAS isoforms after transduction with respective constructs. The activity of oncRAS isoforms in the cells was demonstrated by phosphorylation of the RAS-downstream kinase ERK and/or by a RAS activity assay. However, oncRAS isoforms apparently do not induce apoptosis as measured by caspase 3 cleavage in Western Blots. They also do not alter the cell cycle distribution of the cells. Moreover, no obvious morphological changes of the cells were detected microscopically (data not shown).

6.1.2 OncRAS isoforms modulate mRNA expression of HH signaling pathway members

6.1.2.1 OncRAS isoforms downregulate *GLI1* expression in RMS cell lines

Previous studies revealed an oncRAS-dependent downregulation of *GLI1* transcription in RUCH-2 and RMS-13 cell lines [299]. Here, the expression of the HH target *GLI1* was measured in stably transduced TE617.T. The measurement was also repeated in RUCH-2 and RMS-13 cell lines. Additionally, the HH-responsive medulloblastoma cell line Daoy [327], stably transduced with oncRAS-expressing plasmids, was analyzed for *GLI1* expression. *GLI1* was chosen as readout, because it is considered to be the most reliable marker for HH signaling activity [69]. For qRT-PCR analyses, *18S rRNA* and *HPRT* were chosen as suitable

reference genes [328]. The data confirmed that oncRAS decrease *GLI1* mRNA expression irrespective of the RMS subtype and the RAS isoform (see Fig. 13A for ERMS and Fig. 13B for ARMS cell lines) [299]. In contrast, oncRAS had no significant effect on *GLI1* mRNA level in Daoy cells (Fig. 13C). This indicates that oncRAS-mediated *GLI1* downregulation may be specific for RMS cell lines.

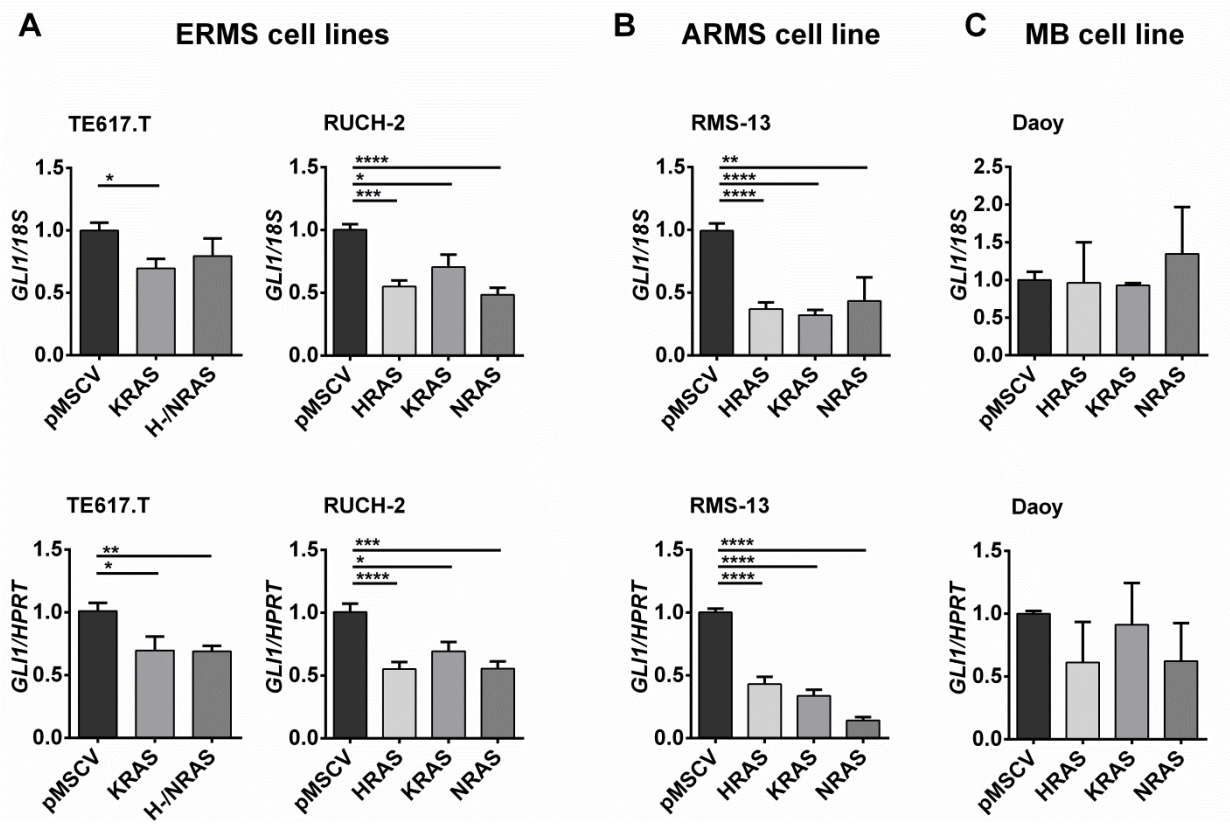

Figure 13: OncRAS isoforms downregulate relative *GLI1* expression in RMS cell lines
The ERMS cell lines TE617.T and RUCH-2 (A), the ARMS cell line RMS-13 (B) and the Medulloblastoma (MB) cell line Daoy (C) stably transduced with the pMSCV control vector or oncRAS isoforms (HRAS, KRAS, NRAS, H-/NRAS) were subjected to RNA isolation, cDNA synthesis and subsequent qRT-PCR analyses of the HH target gene *GLI1*. The expression data were normalized to *18S rRNA* (18S, upper row) and *HPRT* (lower row) and are shown as fold expression to respective pMSCV control cells that were set to 1. Bars represent the mean + SEM of 1 (Daoy), 3 (RUCH-2) or 4 (TE617.T, RMS-13) independent experiments performed in technical triplicates. For statistical analyses a non-parametric t-test (Mann Whitney) was performed. *p<0.05, **p<0.01, ***p<0.001, ****p< 0.0001 compared to expression level of pMSCV control cells.

6.1.2.2 Different oncRAS isoforms modify gene expression of *GLI3* and *SHH* in ERMS cells

In the following the focus is on the ERMS cell lines TE617.T and RUCH-2 stably transduced with oncRAS isoforms. After oncRAS-dependent downregulation of *GLI1* has been confirmed in these cell lines (see Fig. 13), the expression of other genes of the HH signaling pathway, namely *GLI2*, *GLI3*, *PTCH1* (in the following named *PTCH*), *HHIP* and *SHH*, was analyzed.

TE617.T cells expressing oncKRAS showed a moderate downregulation of the HH signaling activator *GLI2* and the HH ligand *SHH* in comparison to pMSCV control cells. In contrast, oncNRAS downregulated the HH signaling inhibitor *GLI3* and the HH ligand receptor *PTCH*

in comparison to pMSCV cells. The effects on *GLI2* and *PTCH* level were dependent on the reference gene used and were consequently considered as a trend in regulation. Relative gene expression of the HH signaling inhibitor protein *HHIP* was not significantly (n.s.) influenced by the oncRAS mutations (Fig. 14).

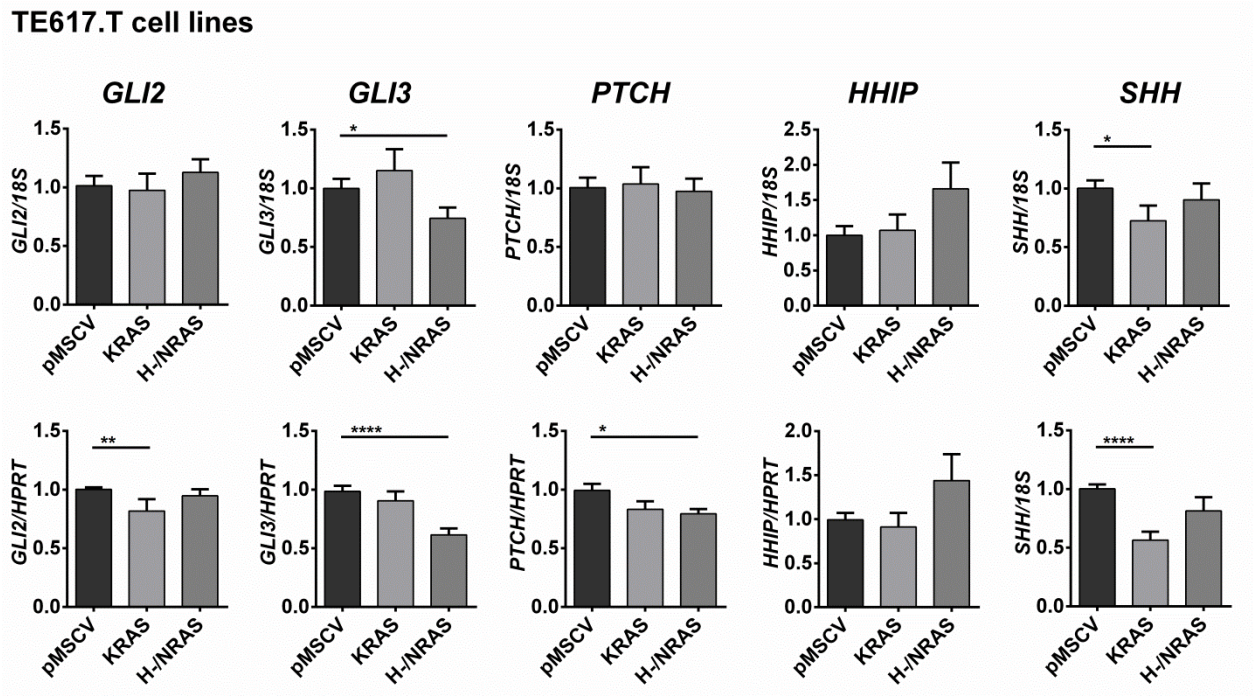

Figure 14: OncKRAS decreases *SHH*, whereas oncH-/NRAS decrease *GLI3* in TE617.T cells
TE617.T cells stably transduced with the pMSCV control vector or oncRAS isoforms (KRAS, H-/NRAS) were subjected to RNA isolation, cDNA synthesis and subsequent qRT-PCR analyses of the HH signaling pathway genes *GLI2*, *GLI3*, *PTCH*, *HHIP* and *SHH*. The expression data were normalized to *18S rRNA* (18S, upper row) and *HPRT* (lower row) and are shown as fold expression to TE617.T pMSCV control cells that were set to 1. Bars represent the mean + SEM of 4 independent experiments performed in technical triplicates. For statistical analyses a non-parametric t-test (Mann Whitney) was performed. *p<0.05, **p<0.01, ****p< 0.0001 compared to expression level of pMSCV control cells.

In RUCH-2 cells all oncRAS isoforms significantly downregulated *GLI2* expression in comparison to pMSCV control cells (Fig. 15). Interestingly, and in contrast to TE617.T cells, all oncRAS isoforms increased the expression of the HH ligand *SHH*. Furthermore, *GLI3* expression was decreased by oncNRAS. The oncogenic isoforms of HRAS and KRAS increased the expression of *PTCH,* while the expression of *HHIP* was not affected in any of the settings (Fig. 15).

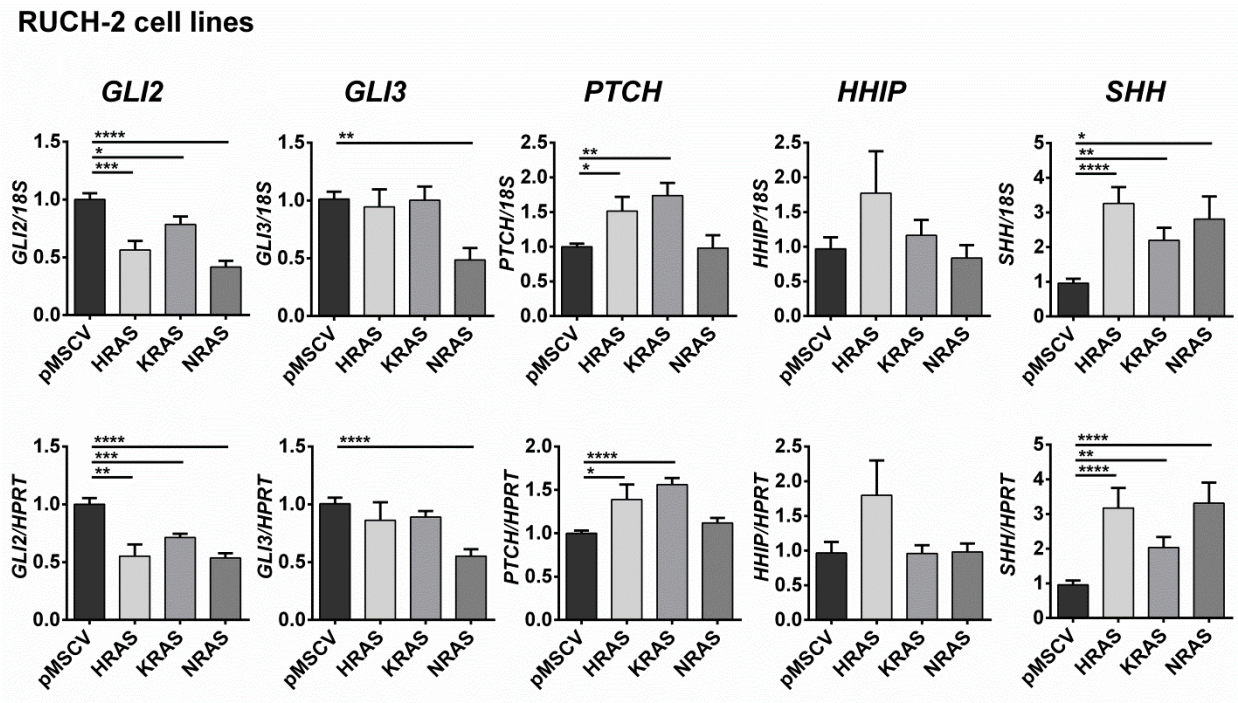

Figure 15: OncRAS isoforms modify *GLI2* and *SHH* expression in RUCH-2 cells
RUCH-2 cells stably transduced with the pMSCV control vector or oncRAS isoforms (HRAS, KRAS, NRAS) were subjected to RNA isolation, cDNA synthesis and subsequent qRT-PCR analyses of the HH signaling pathway genes *GLI2*, *GLI3*, *PTCH*, *HHIP* and *SHH*. The expression data were normalized to *18S rRNA* (18S, upper row) and *HPRT* (lower row) and are shown as fold expression to RUCH-2 pMSCV control cells that were set to 1. Bars represent the mean + SEM of 3 independent experiments performed in technical triplicates. For statistical analyses a non-parametric t-test (Mann Whitney) was performed. *p<0.05, **p<0.01, ***p<0.001, ****p< 0.0001 compared to expression level of pMSCV control cells.

Taken together, the results from chapter 6.1.2 highlight that oncRAS isoforms apparently inhibit HH signaling in RMS cell lines, because the expression of the main HH target gene *GLI1* decreases. This phenomenon is apparently specific for RMS cell lines, because it was not observed in medulloblastoma cells. Furthermore, oncRAS isoforms also modify the gene expression level of other central players of the HH signaling pathway such as *GLI2* (RUCH-2 cells only), *GLI3*, *PTCH* (RUCH-2 cells only) and *SHH*. However, the modulation is different between the ERMS cell lines TE617.T and RUCH-2.

6.1.3 Canonical HH signaling plays a subordinate role in ERMS cell lines

In oncRAS-transduced RUCH-2 and TE617.T cell lines the expression of *SHH* was up- or downregulated, respectively (see section 6.1.2.2). This suggested that oncRAS isoforms may affect canonical HH signaling in ERMS due to secretion of SHH. In order to test this hypothesis, the ability of the cells to secrete HH ligands was analyzed. In addition, it was analyzed whether the cells itself respond to the HH stimulus.

6.1.3.1 ERMS cell lines do not secrete HH ligands

In order to investigate whether ERMS cell lines are able to secrete HH ligands, CM of the transduced cell lines was prepared as described in section 5.1.11. Then, the murine HH-responsive cell line B9 was incubated for 48 h with the CM and expression of *Gli1* was measured by qRT-PCR. The supernatants from HEK293 or HEK293-Shh cells were used as

controls. Preliminary results already showed that oncRAS-transduced RUCH-2 cells are not able to secrete HH ligands [299]. As indicated here (Fig. 16), this was similar for oncRAS-transduced TE617.T cells. Thus, whereas HEK293-Shh CM strongly increased *Gli1* expression in B9 cells, incubation with CM from TE617.T pMSCV, TE617.T KRAS or TE617.T H-/NRAS cells did not influence the *Gli1* level of B9.

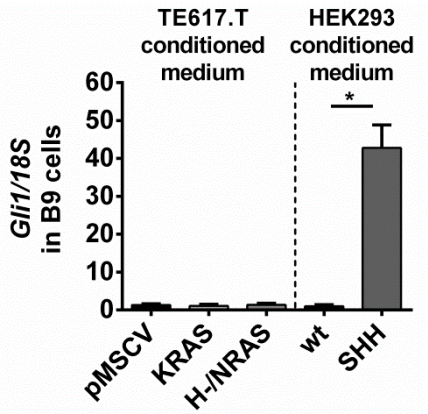

Figure 16: OncRAS-transduced TE617.T cells are not able to secrete HH ligands
B9 cells were incubated with conditioned media from TE617.T cells stably transduced with the pMSCV control vector or oncRAS isoforms (KRAS, H-/NRAS), or with media of HEK293 (wt) or HEK293-Shh (SHH) cells for 48 h. Afterwards B9 cells were subjected to RNA isolation, cDNA synthesis and subsequent qRT-PCR analyses of the HH target gene *Gli1.* The data were normalized to *18S rRNA* (18S) and are shown as fold expression in comparison to B9 cells incubated with TE617.T pMSCV (pMSCV) conditioned medium which was set to 1. Bars represent the mean + SEM of 3 independent experiments performed in technical triplicates. For statistical analyses a non-parametric t-test (Mann Whitney) was performed. *p<0.05, **p<0.01, ***p<0.001, ****p< 0.0001 compared to expression level of B9 cells were incubated with conditioned media from HEK293 cells.

The ability of stably transduced RUCH-2 cells or RD cells to secrete HH ligands was also tested by co-culture with the HH-responsive SHH light II reporter cell line. The activity of the HH signaling cascade in SHH light II reporter cells can be measured by a dual luciferase reporter assay, because these cells harbor a Gli responsive luciferase reporter system [310] (compare section 5.1.12.2).

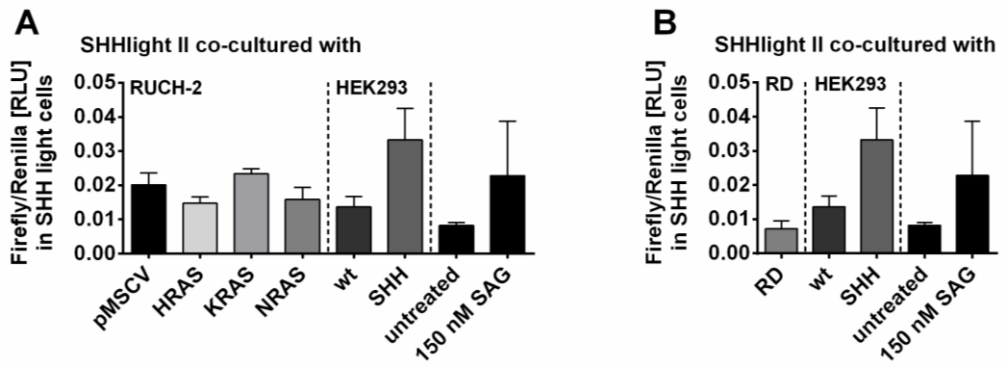

Figure 17: OncRAS-transduced RUCH-2 cells and RD cells do not stimulate Gli reporter activity in co-cultured SHH light II cells
SHH light II cells were either co-cultured with RUCH-2 cells (A) stably transduced with the pMSCV control vector or oncRAS isoforms (HRAS, KRAS, NRAS) or RD cells (B) for 24 h. SHH light II cells co-cultured with HEK293 Shh cells (SHH) or treated with 150 nM SAG served as positive controls, whereas SHH light II cells alone (untreated) or co-cultured with HEK293 cells (wt) served as negative controls. Afterwards the relative activity of the HH signaling cascade in SHH light II cells was determined by a dual luciferase assay. The luminescence readout from firefly luciferase activity was normalized to that of renilla luciferase activity and is displayed in relative light units (RLU). Bars represent the mean + SEM of 3 independent experiments performed in technical triplicates. For statistical analyses a non-parametric t-test (Mann Whitney) was performed.

Neither RUCH-2 cells with or without oncRAS (Fig. 17A) nor RD cells (Fig. 17B) were able to stimulate HH signaling in co-cultured SHH light II cells. Positive controls, i.e. stimulation with SAG or co-culturing with HEK293-Shh cells, increased the Gli reporter activity in SHH light II cells in comparison to the negative controls, which were untreated SHH light II cells or SHH light II cells co-cultured with HEK293 cells. However, the stimulation was not significant (Fig. 17A and Fig. 17B).

Taken together, the results demonstrate that the ERMS cell lines TE617.T, RUCH-2 and RD are in all likelihood not able to secrete HH ligands, regardless if they harbor a oncRAS mutation or not.

6.1.3.2 Moderate activation of HH signaling in ERMS cells by SHH-CM

Next, it was tested whether the HH signaling pathway could be activated in ERMS cells. For this purpose, stably transduced RUCH-2 cells were incubated for 48 h with CM from HEK293 or HEK293-Shh cells. Additionally, B9 cells were incubated with the same media and served as controls. Then the expression of *GLI1/Gli1* was measured. The results were dependent on the reference gene used for normalization (compare Fig. 18A and Fig. 18B). When the data were normalized to *18S rRNA* the results obtained from 3 independent experiments showed that the CM from HEK293-Shh cells moderately regulated the expression of *GLI1* in RUCH-2 HRAS and RUCH-2 KRAS cells, whereas it did not affect *GLI1* expression in RUCH-2 pMSCV and RUCH-2 NRAS cells. The functionality of Shh containing medium was proven by a strong *Gli1* induction in B9 cells.

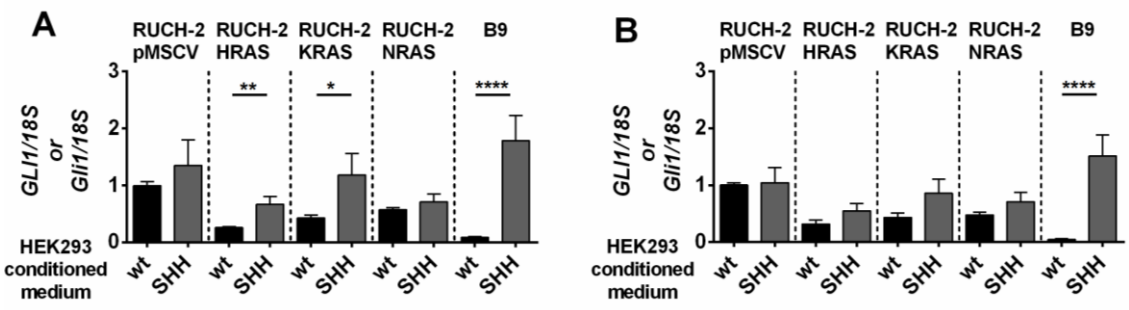

Figure 18: SHH moderately induces *GLI1* transcription in oncRAS-expressing RUCH-2 cells
RUCH-2 cells stably transduced with the pMSCV control vector or oncRAS isoforms (HRAS, KRAS, NRAS) were incubated with conditioned media from HEK293 (wt) or HEK293-Shh (SHH) cells for 48 h. B9 cells incubated with conditioned media from HEK293 or HEK293-Shh were used as negative and positive controls, respectively. Afterwards cells were subjected to RNA isolation, cDNA synthesis and subsequent qRT-PCR analyses of the HH target gene *GLI1/Gli1.* The data were normalized to *18S rRNA* (18S, A) or *HPRT* (B) and are shown as fold expression in comparison to RUCH-2 pMSCV cells incubated with HEK293 conditioned medium, which was set to 1. Bars represent the mean + SEM of 3 independent experiments performed in technical triplicates. For statistical analyses a non-parametric t-test (Mann Whitney) was performed. *p<0.05, **p<0.01, ****p< 0.0001 compared to expression level of control medium treated cell lines.

To sum up, the data from section 6.1.3 indicate that the ERMS cell lines TE617.T and RUCH-2 stably transduced with the pMSCV control vector or oncRAS isoforms, and RD cells probably are not able to secrete HH ligands. Additionally, stimulation with SHH may marginally regulate HH signaling activity, as measured by *GLI1* expression in RUCH-2 cell lines that express oncHRAS and oncKRAS isoforms.

6.1.4 OncRAS isoforms regulate *GLI1* expression in ERMS cells via the MEK/ERK axis

Next, it was investigated whether oncRAS isoforms regulate *GLI1* expression in a non-canonical manner via the PI3K/AKT/mTOR or the MEK/ERK axes. In order to inhibit PI3K/AKT/mTOR signaling the dual PI3K/mTOR inhibitor PI-103 [329] was used, whereas the

RAF/MEK/ERK axis was targeted with the specific MEK inhibitor UO126 [330] or the specific ERK1/2 inhibitor SCH772984 [331]. Additionally, the SMO inhibitor HhAntag (HhA) [332] was employed. The experiments were performed in accordance with previous work, which indicated an oncRAS-dependent regulation of the HH signaling pathway via the MEK axis in RUCH-2 cells [299].

The inhibitors HhA (30 µM), PI-103 (3 µM) and UO126 (10 µM) were applied in concentrations as described [299]. The concentration of the ERK inhibitor SCH772984 was first assessed in RUCH-2 cells in a range between 0.1 µM to 10 µM applied for 24 h. A Western Blot of RUCH-2 HRAS cells shows that all applied concentrations of SCH772984 inhibited phosphorylation of ERK protein level in comparison to solvent (DMSO) treated cells without showing an apoptotic effect (Fig. 19). The exception was 1 µM SCH772984, which only moderately inhibited ERK phosphorylation. This result was not only seen in RUCH-2 HRAS cells but also in other stably transduced RUCH-2 cell lines and in the MET-1 cell line, which is also used in our group. This effect is hard to explain. However, it is possible that specific concentrations of SCH772984 influence other signaling molecules that in turn phosphorylate ERK. Indeed, a similar scenario has been described for other small molecules such as the SMO Agonist SAG. Thus, SAG usually activates *GLI1* expression, but inhibits *GLI1* when used at concentration above 1 µM [310].

Based on these results and observations, a concentration of 0.5 µM SCH772984 was employed in subsequent experiments.

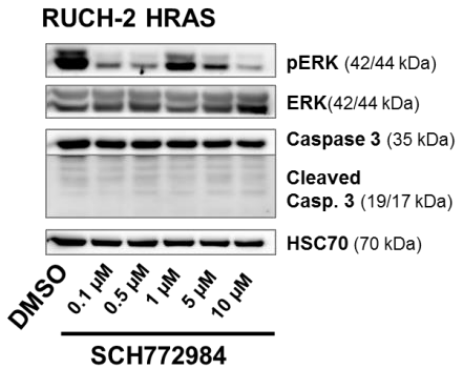

Figure 19: SCH772984 inhibits phosphorylation of ERK in different concentrations
Protein was isolated from RUCH-2 cells stably transduced with oncHRAS (RUCH-2 HRAS) after incubation with 0.1 µM to 10 µM SCH772984 for 24 h. The total cell lysates were analyzed by Western Blot for protein expression of pERK/ERK and caspase 3 cleavage (Caspase 3 and cleaved casp. 3) with specific antibodies. HSC70 served as loading control. Protein names and sizes in kDa are displayed on the right side of the blot. The depicted results were also obtained in experiments with RUCH-2 pMSCV and RUCH-2 KRAS and NRAS cells (data not shown).

The functionality of HhA, PI103, UO126 and SCH772984 was tested by analyses of protein level of pAKT/AKT, pS6/S6, pERK/ERK after treatment of the cells for 24 h (Fig. 20). Additionally, caspase 3 cleavage was analyzed. Representative Western Blots of TE617.T cells (Fig. 20A), RUCH-2 cells (Fig. 20B) and RD cells (Fig. 20C) show that in general SCH772984 effectively downregulated the pERK level in all cell lines. SCH772984 also slightly downregulated AKT level in TE617.T pMSCV cells, whereas it strongly reduced it in RUCH-2 cells stably transduced with oncRAS isoforms (Fig. 20B). However, this result is based on 1 biological replicate and needs further validation. Nevertheless, a downregulation of AKT protein level after SCH772984 treatment was also described for BxPC-3 and HPAC cells in the literature [333].

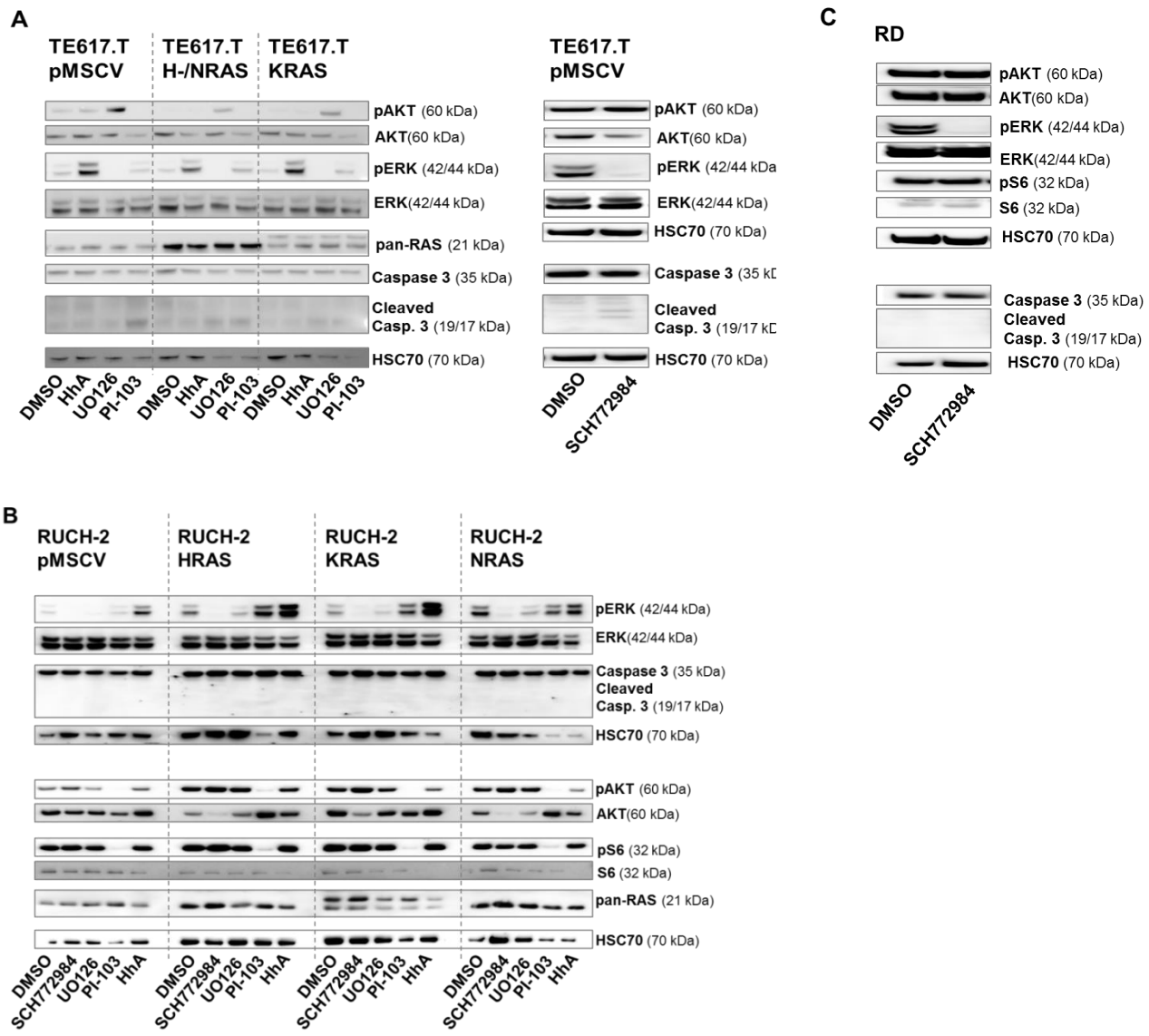

Figure 20: PI-103, UO126 and SCH772984 inhibit phosphorylation of their downstream kinases in TE617.T, RUCH-2 and RD cells

Protein was isolated from TE617.T (A) and RUCH-2 (B) cells stably transduced with the pMSCV control vector or oncRAS isoforms (HRAS, KRAS, NRAS, H-/NRAS) and RD cells (C) that have been incubated with HhA (30 µM), PI-103 (3 µM), UO126 (10 µM) or SCH772984 (0.5 µM) for 24 h. The total cell lysates were used for Western Blot analyses to detect the protein level of pAKT/AKT, pS6/S6, pERK/ERK, pan-RAS and caspase 3 cleavage (Caspase 3 and cleaved casp. 3) with specific antibodies. HSC70 served as loading control. Protein names and sizes in kDa are displayed on the right side of the blots. The results are representative for 1 (TE617.T + SCH772984, RUCH-2), 3 (TE617.T + HhA, PI-103 or UO126) or 4 (RD) independent experiments.

As expected, the MEK inhibitor UO126 decreased phosphorylation of ERK in all used cell lines and additionally increased phosphorylation of AKT in all TE617.T cell lines. This increase has already been described for other RMS cell lines [271]. These observations are already described in the literature, e.g. in breast cancer and RMS cells [271,333,334] . It has been suggested that the MEK inhibitor-induced activation of PI3K/AKT results from an inhibitory phosphorylation in conserved domains of the EGFR, which leads to hyperactivation of Erb-B2 Receptor Tyrosine Kinase 3 (ERBB3) that in turn upregulates the PI3K/AKT signaling pathway [335]. In RUCH-2 and TE617.T cells the dual PI3K/mTOR inhibitor PI-103 downregulated phosphorylation of AKT and S6 (Fig. 20A, Fig. 20B). Unfortunately,

phosphorylation of S6 was not measured in TE617.T cells. Additionally, PI-103 slightly induced phosphorylation of ERK and modified basal level of AKT in oncRAS-expressing RUCH-2 cells (Fig. 20B). Increased pERK level upon inhibition of mTOR has been described by others [336]. The SMO inhibitor HhA increased phosphorylation of ERK in all RUCH-2 and TE617.T cell lines (Fig. 20A, Fig. 20B). Furthermore, it decreased pAKT in all RUCH-2 cell lines (Fig. 20B). This phenomenon has already been described by our group [299,337]. These secondary actions of HhA were considered as an additional hint for an interaction of HH and RAS signaling, either via the PI3K/AKT/mTOR axis, or via the RAF/MEK/ERK pathway.

6.1.4.1 ERK inhibits *GLI1* expression in TE617.T cells, in oncRAS-expressing RUCH-2 cells and in RD cells

The above-mentioned inhibitors were then used to investigate if oncRAS-mediated downregulation of *GLI1* expression is regulated via the PI3K/AKT/mTOR axis or via the RAF/MEK/ERK pathway.

6.1.4.1.1 *GLI1* expression in TE617.T is inhibited by ERK without general involvement of oncRAS isoforms

The stably transduced TE617.T cells were treated for 24 h with HhA (30 µM), PI-103 (3 µM), UO126 (10 µM) or SCH772984 (0.5 µM) and *GLI1* expression was analyzed via qRT-PCR. The inhibition of SMO did not influence *GLI1* expression in any of the TE617.T cell lines (Fig. 21).

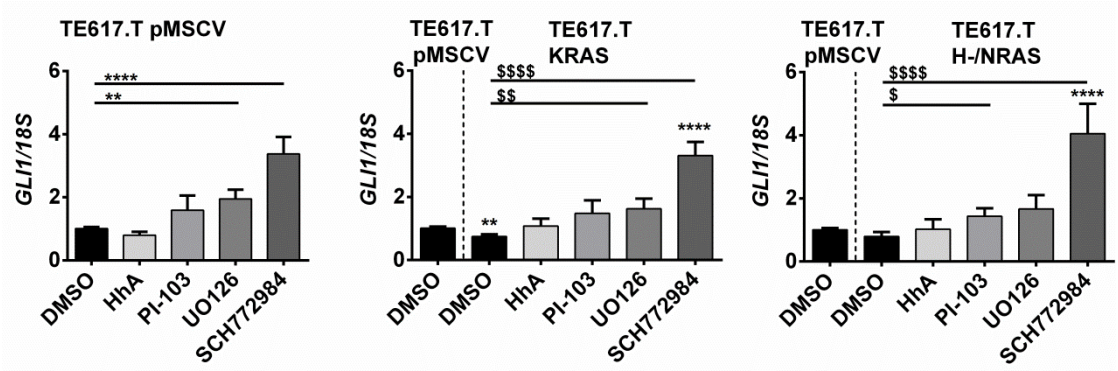

Figure 21: MEK and ERK suppress *GLI1* in TE617.T irrespective of oncRAS mutations
TE617.T stably transduced with the pMSCV control vector or oncRAS isoforms (KRAS, H-/NRAS) were incubated with DMSO, HhA (30 µM), PI-103 (3 µM) and UO126 (10 µM) or SCH772984 (0.5 µM) for 24 h. Afterwards cells were subjected to RNA isolation, cDNA synthesis and subsequent qRT-PCR analyses of the HH target gene *GLI1.* The data were normalized to *18S rRNA* (18S) and are shown as fold expression in comparison to TE617.T pMSCV cells incubated with DMSO, which was set to 1. The respective bar is shown in each histogram as a reference. Bars represent the mean + SEM of 4 independent experiments performed in technical triplicates. For statistical analyses a non-parametric t-test (Mann Whitney) was performed. * indicate significance compared to DMSO treated TE617.T pMSCV cells, whereas $ indicate significance compared to solvent control of the respective cell line. $ p<0.05, **/$$ p<0.01, ****/$$$$ p< 0.0001

This indicates again that it is not possible to modulate HH signaling via the canonical axis in these cells. PI-103 increased *GLI1* expression in oncH-/NRAS-expressing TE617.T cells, however not in oncKRAS-expressing or TE617.T control cells. The treatment with the MEK inhibitor UO126 increased *GLI1* level in oncKRAS-expressing and control cells, whereas inhibition of ERK increased *GLI1* in all TE617.T cell lines. Taken together, these data

indicate that inhibition of ERK (and also of MEK) results in a significant increase of *GLI1* expression in all TE617.T cells investigated. In fact, the observed effect was independent of oncRAS mutations, since it was also observed in control cells.

6.1.4.1.2 ERK mediates oncRAS-induced downregulation of *GLI1* expression in RUCH-2 cells

In RUCH-2 pMSCV control cells inhibition of PI3K/mTOR significantly decreased *GLI1* expression, whereas treatment with the other inhibitors had no significant effect (Fig. 22A).

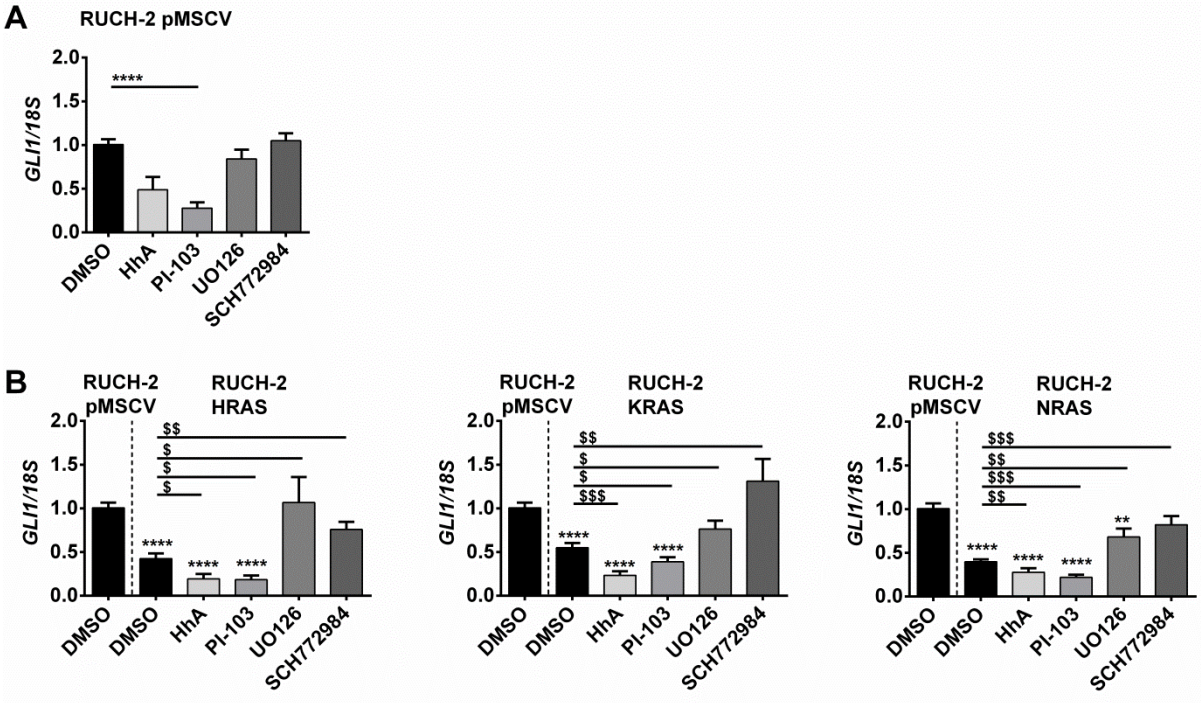

Figure 22: ERK mediates oncRAS-induced downregulation of *GLI1* in RUCH-2 cells
RUCH-2 cells stably transduced with the pMSCV control vector (A) or oncRAS isoforms (HRAS, KRAS, NRAS) (B) were incubated with DMSO, HhA (30 µM), PI-103 (3 µM), UO126 (10 µM) or SCH772984 (0.5 µM) for 24 h. Afterwards cells were subjected to RNA isolation, cDNA synthesis and subsequent qRT-PCR analyses of the HH target gene *GLI1.* The data were normalized to *18S rRNA* (18S) and are shown as fold expression in comparison to RUCH-2 pMSCV cells incubated with DMSO, which was set to 1. The respective bar is shown in each histogram as a reference. Bars represent the mean + SEM of 3 independent experiments performed in technical triplicates. For statistical analyses a non-parametric t-test (Mann Whitney) was performed. * indicate significance compared to DMSO treated RUCH-2 pMSCV cells, whereas $ indicate significance compared to solvent control of the respective cell line. $ p<0.05, **/$$ p<0.01, $$$ p<0.001, **** p< 0.0001

In contrast, in RUCH-2 cells stably transduced with oncRAS isoforms the incubation with HhA or PI-103 decreased the relative *GLI1* expression in comparison to solvent-treated cells, whereas treatment with UO126 or SCH772984 significantly increased *GLI1* in comparison to DMSO treated RUCH-2 oncRAS cell lines. Moreover, inhibition of MEK in RUCH-2 HRAS and RUCH-2 KRAS cells or inhibition of ERK in all oncRAS-expressing cells restored *GLI1* expression back to the basal level of control RUCH-2 pMSCV cells (Fig. 22B). These results show that oncRAS-dependent downregulation of *GLI1* in RUCH-2 cells is mediated by ERK.

6.1.4.1.3 ERK inhibits *GLI1* expression in RD cells

In addition to ERMS cell lines stably transduced with oncRAS isoforms, RD cells harboring an endogenous oncNRAS mutation were incubated with 0.5 µM SCH772984 for 24 h. In this cell line and as already demonstrated by our group, PI-103 treatment results in a decrease of *GLI1* expression whereas UO126 treatment increases *GLI1* [160]. Here, the ERK inhibitor SCH772984 increased the *GLI1* level (Fig. 23). This result indicates that the oncRAS mutation in RD cells might suppress *GLI1* expression via the ERK axis, which is similar to RUCH-2 cells (compare section 6.1.4.1.2).

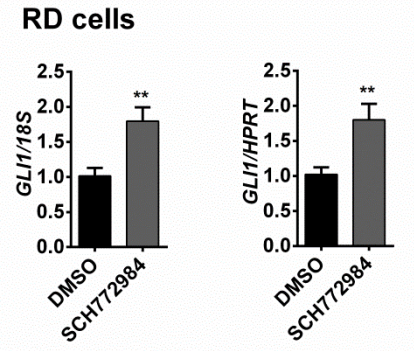

Figure 23: ERK inhibition increases *GLI1* expression in RD cells
RD cells were incubated with DMSO or SCH772984 (0.5 µM) for 24 h. Afterwards cells were subjected to RNA isolation, cDNA synthesis and subsequent qRT-PCR analyses of the HH target gene *GLI1.* The data were normalized to *18S rRNA* (18S, left) or *HPRT* (right) and are shown as fold expression in comparison to RD cells incubated with DMSO, which was set to 1. Bars represent the mean + SEM of 3 independent experiments performed in technical triplicates. For statistical analyses a non-parametric t-test (Mann Whitney) was performed. ** p<0.01 compared to expression level of DMSO treated RD cells

6.1.4.2 ERK regulates *PTCH* and *SHH* expression in TE617.T cells, *SHH* expression in oncRAS-expressing RUCH-2 cells and *GLI3* in RD cells

Next it was analyzed whether the ERK inhibitor SCH772984 also influences the gene expression level of *GLI2*, *GLI3*, *PTCH*, *HHIP* and *SHH* in stably transduced TE617.T and RUCH-2 cells and in RD cells.

6.1.4.2.1 *PTCH* and *SHH* expression in TE617.T cells is inhibited by ERK without general involvement of oncRAS

In TE617.T pMSCV control cells, ERK inhibition did not influence the expression of *GLI2* or *GLI3,* but generally increased transcription of *PTCH*, *HHIP* and *SHH* (Fig. 24).

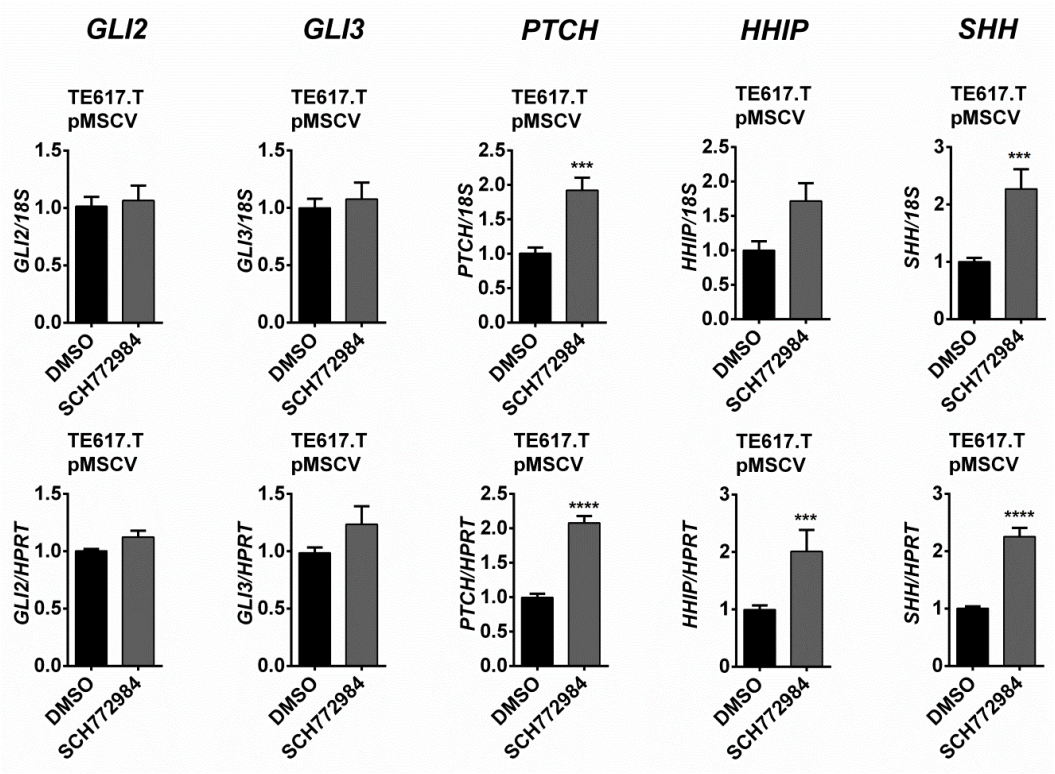

Figure 24: ERK inhibits *PTCH* and *SHH* expression in TE617.T pMSCV cells
TE617.T cells stably transduced with the pMSCV control vector were incubated with DMSO or SCH772984 (0.5 µM) for 24 h. Afterwards cells were subjected to RNA isolation, cDNA synthesis and subsequent qRT-PCR analyses of the HH signaling pathway genes *GLI2*, *GLI3*, *PTCH*, *HHIP* and *SHH*. The data were normalized to *18S rRNA* (18S, upper row) or *HPRT* (lower row) and are shown as fold expression in comparison to cells incubated with DMSO, which was set to 1. Bars represent the mean + SEM of 4 independent experiments performed in technical triplicates. For statistical analyses a non-parametric t-test (Mann Whitney) was performed. ***p<0.001, ****p< 0.0001 compared to expression level of DMSO treated cells

In TE617.T KRAS cells, which showed an oncKRAS-dependent downregulation of *SHH*, application of SCH772984 restored *SHH* back to basal level of pMSCV control cells. Furthermore, SCH772984 downregulated *GLI2* and upregulated *PTCH* transcription, whereas gene expression of *GLI3* and *HHIP* were not affected (Fig. 25).

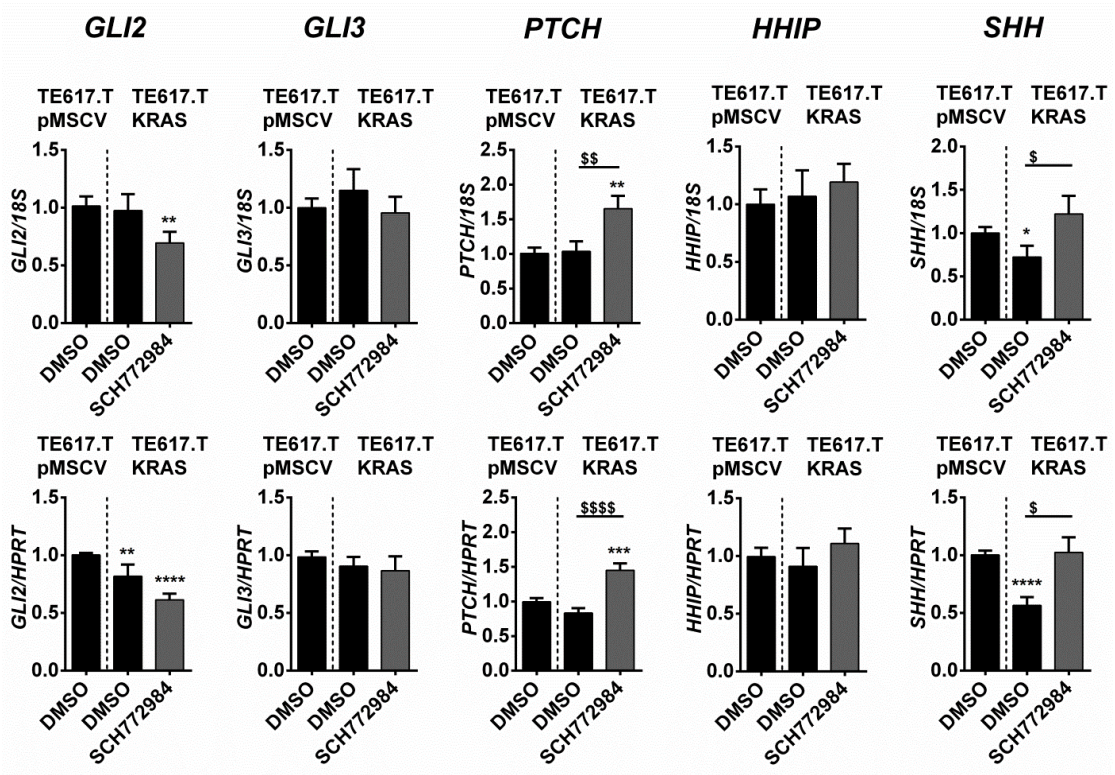

Figure 25: ERK activates *GLI2* and inhibits *PTCH* expression in TE617.T KRAS cells and restores oncKRAS–dependent decrease of *SHH* back to basal level

TE617.T cells stably transduced with the pMSCV control vector or oncKRAS (KRAS) were incubated with DMSO or SCH772984 (0.5 µM) for 24 h. Afterwards cells were subjected to RNA isolation, cDNA synthesis and subsequent qRT-PCR analyses of the HH signaling pathway genes *GLI2*, *GLI3*, *PTCH*, *HHIP* and *SHH.* The data were normalized to *18S rRNA* (18S, upper row) or *HPRT* (lower row) and are shown as fold expression in comparison to DMSO treated TE617.T pMSCV cells, which was set to 1. The respective bar is shown in each histogram as a reference. Bars represent the mean + SEM of 4 independent experiments performed in technical triplicates. For statistical analyses a non-parametric t-test (Mann Whitney) was performed. * indicate significance compared to DMSO treated TE617.T pMSCV cells, whereas $ indicate significance compared to TE617.T KRAS cells treated with DMSO.*/$ p<0.05, **/$$ p<0.01, *** p<0.001, ****/$$$$ p< 0.0001

In TE617.T H-/NRAS cells SCH772984 had no obvious impact on *GLI2* or *HHIP* level. It also had no clear-cut effect on *GLI3*, which is downregulated in these cells by oncH-/NRAS compared to the pMSCV control cells. Like in TE617.T pMSCV cells, SCH772984 increased the relative mRNA level of *SHH*. However, SCH772984 increased the expression of *PTCH.* The latter result was considered as a tendency, since the result was only significant upon normalization to *HPRT* but not to *18S rRNA* (Fig. 26).

Taken together, SCH772984 generally increases *PTCH and SHH* in TE617.T cells irrespective of an oncRAS mutation.

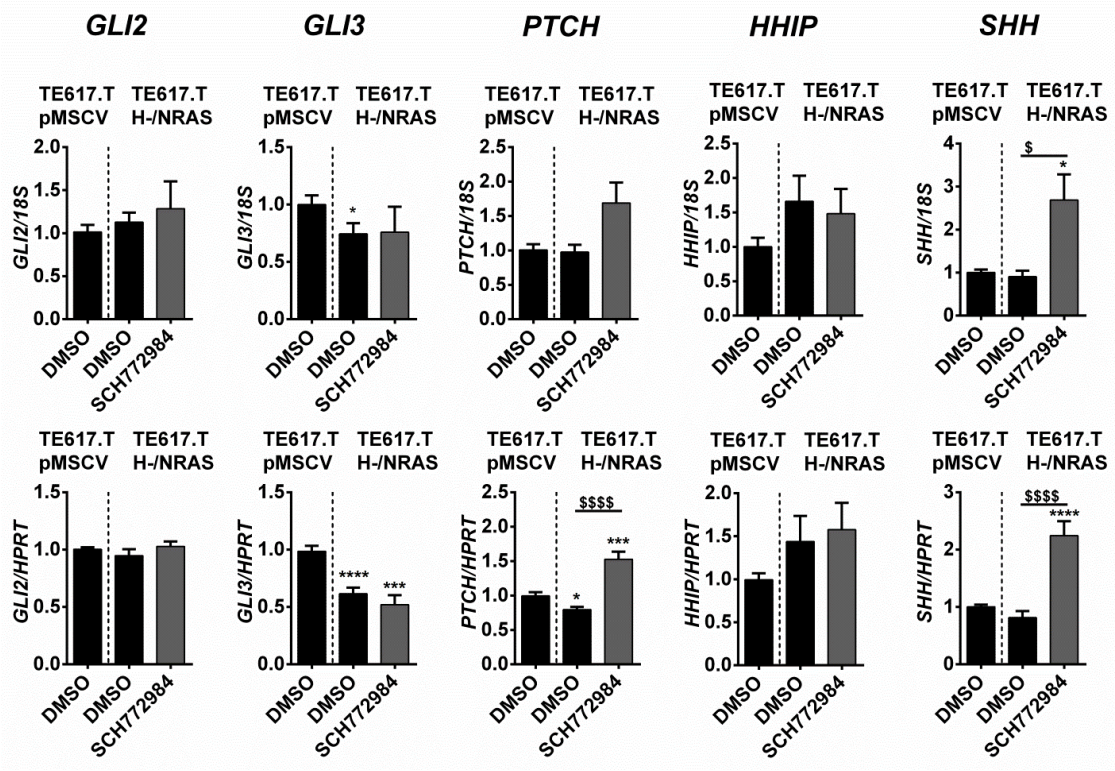

Figure 26: ERK inhibits *PTCH* and *SHH* expression in TE617.T H-/NRAS cells
TE617.T cells stably transduced with the pMSCV control vector or oncH-/NRAS (H-/NRAS) were incubated with DMSO or SCH772984 (0.5 µM) for 24 h. Afterwards cells were subjected to RNA isolation, cDNA synthesis and subsequent qRT-PCR analyses of the HH signaling pathway genes *GLI2*, *GLI3*, *PTCH*, *HHIP* and *SHH.* The data were normalized to *18S rRNA* (18S, upper row) or *HPRT* (lower row) and are shown as fold expression in comparison to DMSO treated TE617.T pMSCV cells, which was set to 1. The respective bar is shown in each histogram as a reference. Bars represent the mean + SEM of 4 independent experiments performed in technical triplicates. For statistical analyses a non-parametric t-test (Mann Whitney) was performed. * indicate significance compared to DMSO treated TE617.T pMSCV cells, whereas $ indicate significance compared to TE617.T H-/NRAS cells treated with DMSO.*/$ p<0.05, *** p<0.001, ****/$$$$ p< 0.0001

6.1.4.2.2 OncRAS-mediated upregulation of *SHH* expression in RUCH-2 cells depends on ERK

The expression of the HH signaling pathway genes *GLI2*, *GLI3*, *PTCH*, *HHIP* and *SHH* were also measured in RUCH-2 cell lines, which were treated with 0.5 µM of the ERK inhibitor SCH772984 for 24 h and 48 h. Since the results after 24 h and 48 h were identical, only the 24 h values are shown.

In RUCH-2 pMSCV control cells SCH772984 did not significantly influence expression of any of the analyzed genes (Fig. 27).

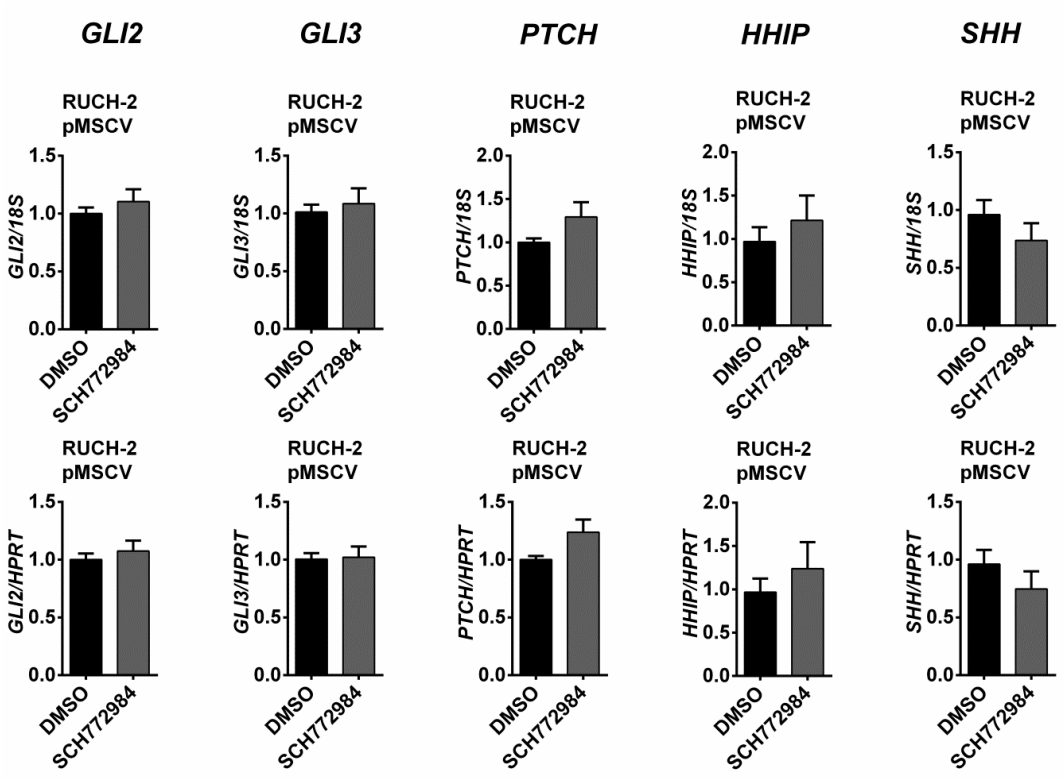

Figure 27: ERK inhibition does not influence expression of HH signaling genes in RUCH-2 pMSCV cells
RUCH-2 cells stably transduced with the pMSCV control vector were incubated with DMSO or SCH772984 (0.5 µM) for 24 h. Afterwards cells were subjected to RNA isolation, cDNA synthesis and subsequent qRT-PCR analyses of the HH signaling pathway genes *GLI2*, *GLI3*, *PTCH*, *HHIP* and *SHH*. The data were normalized to *18S rRNA* (18S, upper row) or *HPRT* (lower row) and are shown as fold expression in comparison to cells incubated with DMSO, which was set to 1. Bars represent the mean + SEM of 3 independent experiments performed in technical triplicates. For statistical analyses a non-parametric t-test (Mann Whitney) was performed.

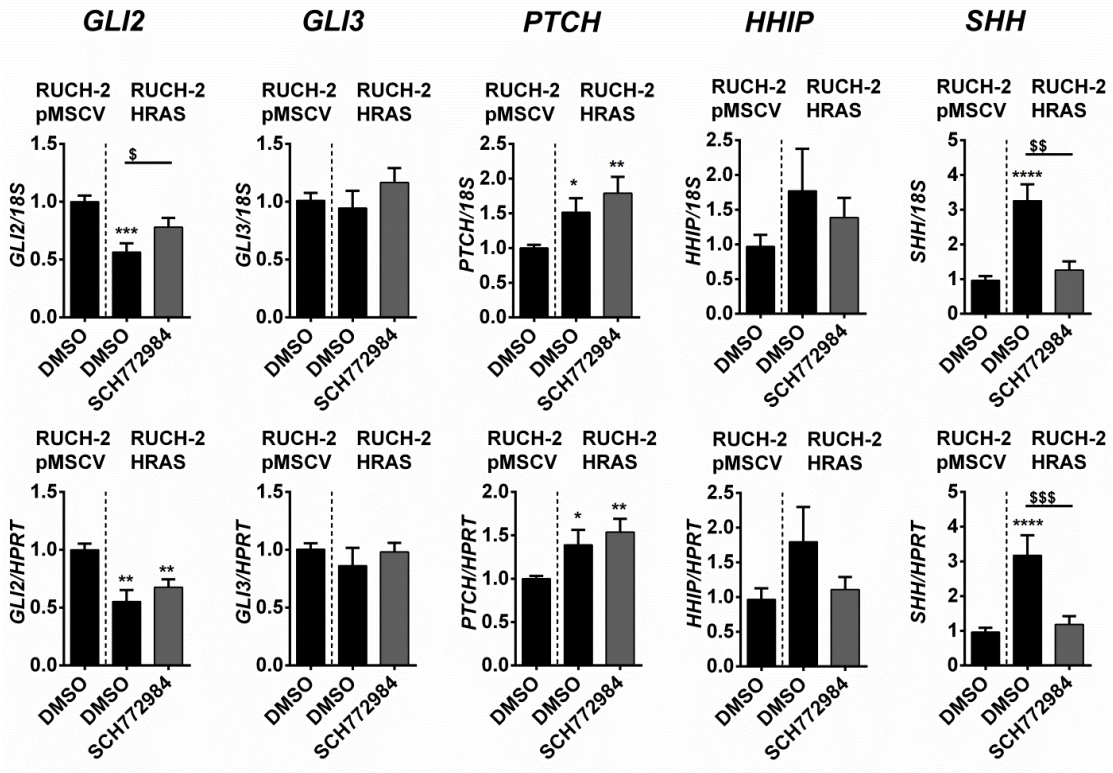

Figure 28: ERK mediates oncHRAS-dependent increase of *SHH* in RUCH-2 cells
RUCH-2 cells stably transduced with the pMSCV control vector or oncHRAS (HRAS) were incubated with DMSO or SCH772984 (0.5 µM) for 24 h. Afterwards cells were subjected to RNA isolation, cDNA synthesis and

subsequent qRT-PCR analyses of the HH signaling pathway genes *GLI2*, *GLI3*, *PTCH*, *HHIP* and *SHH.* The data were normalized to *18S rRNA* (18S, upper row) or *HPRT* (lower row) and are shown as fold expression in comparison to DMSO treated RUCH-2 pMSCV cells, which was set to 1. The respective bar is shown in each histogram as a reference. Bars represent the mean + SEM of 3 independent experiments performed in technical triplicates. For statistical analyses a non-parametric t-test (Mann Whitney) was performed. * indicate significance compared to DMSO treated RUCH-2 pMSCV cells, whereas $ indicate significance compared to RUCH-2 HRAS cells treated with DMSO.*/$ p<0.05, **/$$ p<0.01, $$$ p<0.001, **** p< 0.0001

Treatment of oncHRAS-expressing RUCH-2 cells, with SCH772984 restored oncRAS-mediated downregulation of *GLI2* back to the basal expression level of the control RUCH-2 pMSCV cells. However, this was only seen after normalization to *18S rRNA*, but not upon normalization to *HPRT.* In contrast, the oncHRAS-dependent increase in *SHH* transcription was significantly downregulated and did not differ from the expression level of the control RUCH-2 pMSCV cells. Finally, the oncHRAS-mediated upregulation of *PTCH* was not affected by application of SCH772984 (Fig. 28).

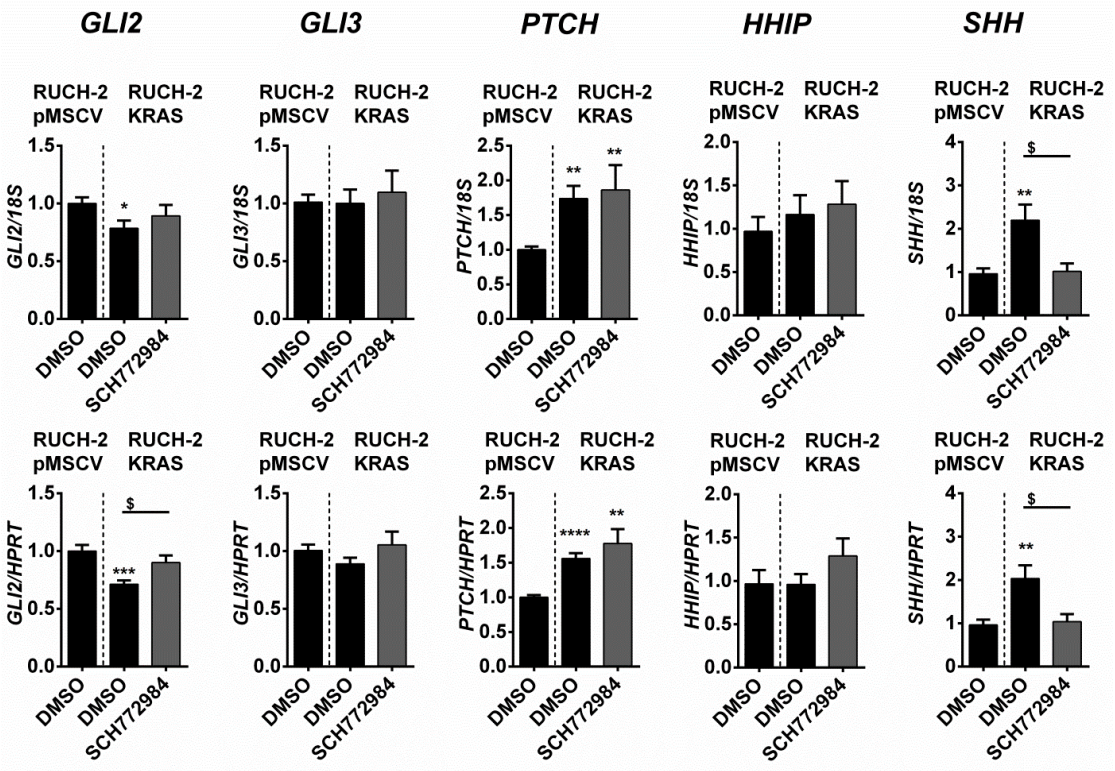

Figure 29: ERK mediates oncKRAS-dependent increase of *SHH* in RUCH-2 cells
RUCH-2 cells stably transduced with the pMSCV control vector or oncKRAS (KRAS) were incubated with DMSO or SCH772984 (0.5 µM) for 24 h. Afterwards cells were subjected to RNA isolation, cDNA synthesis and subsequent qRT-PCR analyses of the HH signaling pathway genes *GLI2*, *GLI3*, *PTCH*, *HHIP* and *SHH.* The data were normalized to *18S rRNA* (18S, upper row) or *HPRT* (lower row) and are shown as fold expression in comparison to DMSO treated RUCH-2 pMSCV cells, which was set to 1. The respective bar is shown in each histogram as a reference. Bars represent the mean + SEM of 3 independent experiments performed in technical triplicates. For statistical analyses a non-parametric t-test (Mann Whitney) was performed. * indicate significance compared to DMSO treated RUCH-2 pMSCV cells, whereas $ indicate significance compared to RUCH-2 KRAS cells treated with DMSO.*/$ p<0.05, ** p<0.01, *** p<0.001, **** p< 0.0001

OncKRAS-expressing RUCH-2 cells showed a downregulation of *GLI2* and an upregulation of *SHH* and *PTCH*, whereas *HHIP* and *GLI3* were not changed in comparison to the control

vector harboring cells. The treatment with SCH772984 did not alter *HHIP* level. It however restored *GLI2* and *SHH* level back to basal expression of the control RUCH-2 pMSCV cells, whereas *PTCH* expression was not affected by ERK inhibition (Fig. 29).

OncNRAS-expressing RUCH-2 cells showed a downregulation of *GLI2* and an upregulation of *SHH* and *PTCH*, whereas *HHIP* was not affected. Treatment with SCH772984 increased the *GLI2* expression level, however without reaching the basal expression level of control RUCH-2 pMSCV cells. The oncNRAS-mediated decrease in *GLI3* expression was not affected, whereas the oncNRAS-dependent upregulation of *SHH* was restored to basal level of the control. Additionally, SCH772984 increased the expression of *PTCH*, at least after normalization to *HPRT*. The relative expression of *HHIP* was not affected (Fig. 30).

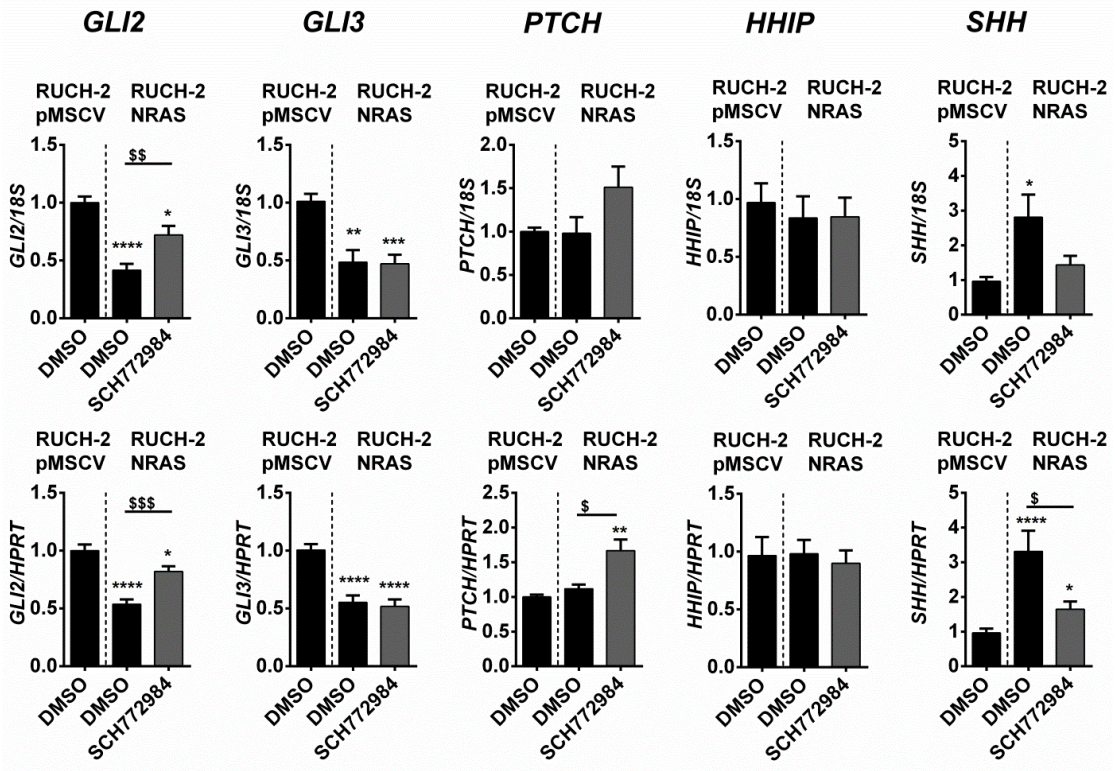

Figure 30: ERK mediates oncNRAS-dependent decrease in *GLI2* and increase in *SHH* in RUCH-2 cells
RUCH-2 cells stably transduced with the pMSCV control vector or oncNRAS (NRAS) were incubated with DMSO or SCH772984 (0.5 µM) for 24 h. Afterwards cells were subjected to RNA isolation, cDNA synthesis and subsequent qRT-PCR analyses of the HH signaling pathway genes *GLI2*, *GLI3*, *PTCH*, *HHIP* and *SHH.* The data were normalized to *18S rRNA* (18S, upper row) or *HPRT* (lower row) and are shown as fold expression in comparison to DMSO treated RUCH-2 pMSCV cells, which was set to 1. The respective bar is shown in each histogram as a reference. Bars represent the mean + SEM of 3 independent experiments performed in technical triplicates. For statistical analyses a non-parametric t-test (Mann Whitney) was performed. * indicate significance compared to DMSO treated RUCH-2 pMSCV cells, whereas $ indicate significance compared to RUCH-2 NRAS cells treated with DMSO.*/$ p<0.05, **/$$ p<0.01, $$$ p<0.001, **** p<0.0001

Taken together, ERK is responsible for the oncRAS-mediated upregulation of *SHH* in RUCH-2 cells, whereas (in contrast to *GLI1*) it's involvement in oncRAS-mediated downregulation of *GLI2* is not unambiguously clear. Furthermore, ERK is generally not involved in oncHRAS and oncKRAS-mediated induction of *PTCH* expression or in oncNRAS-dependent downregulation of *GLI3*.

6.1.4.2.3 ERK inhibits *GLI3* expression in RD cells

The data from section 6.1.4 show that ERK upregulates *GLI1* mRNA expression in RD cells. When analyzing the expression level of *GLI2*, *GLI3*, *PTCH*, *HHIP* and *SHH* after SCH772984 treatment, *GLI2* and *SHH* expression slightly increased, whereas the *GLI3* mRNA level was significantly upregulated. *PTCH* and *HHIP* expression level were not affected (Fig. 31).

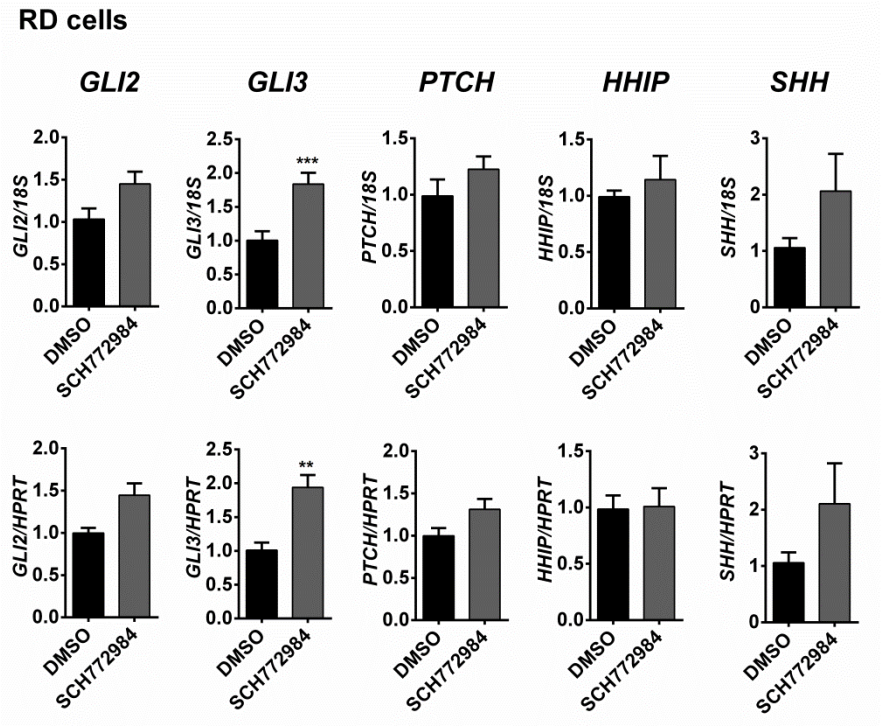

Figure 31: ERK inhibits *GLI3* expression in RD cells
RD cells were incubated with DMSO or SCH772984 (0.5 µM) for 24 h. Afterwards cells were subjected to RNA isolation, cDNA synthesis and subsequent qRT-PCR analyses of the HH signaling pathway genes *GLI2*, *GLI3*, *PTCH1*, *HHIP* and *SHH*. The data were normalized to *18S rRNA* (18S, upper row) or *HPRT* (lower row) and are shown as fold expression in comparison to cells incubated with DMSO, which was set to 1. Bars represent the mean + SEM of 3 independent experiments performed in technical triplicates. For statistical analyses a non-parametric t-test (Mann Whitney) was performed. **p<0.01, ***p<0.001 compared to expression level of DMSO treated RD cells.

To sum up, the results from sections 6.1.4.1 show that ERK (and MEK) inhibit *GLI1* in TE617.T cells and in RUCH-2 cells with oncRAS isoforms. Additionally, ERK inhibits *GLI1* in RD cells, harboring an oncNRAS mutation. In TE617.T cells ERK inhibits *PTCH and SHH* irrespective of an oncRAS mutation. Furthermore, the oncRAS-mediated upregulation of *SHH* in RUCH-2 cells is dependent on ERK. In RD cells, ERK inhibits *GLI3*. The implication of ERK in regulation of *GLI2* in these ERMS cell lines is not clear since statistical significance is not given in all cases. In contrast, ERK is not involved in oncHRAS and oncKRAS-mediated induction of *PTCH* expression in RUCH-2 cells. It is also not involved in oncNRAS- and oncH-/NRAS-dependent downregulation of *GLI3* in RUCH-2 and TE617.T cells, respectively.

6.1.4.3 ERK inhibits GLI transcriptional activity in RD cells

To investigate whether oncRAS itself or the inhibition of ERK indeed modifies the activation status of GLI transcription factors and thus of the HH signaling cascade, a GLI reporter assay

was performed as described in section 5.1.9. The cells were transfected with a firefly luciferase reporter plasmid and a constitutively active renilla expression plasmid. The transfected cells were incubated for 24 h with DMSO or SCH772984 and measurement of GLI reporter activity was performed.

ERK inhibition did not influence activity of the GLI reporter neither in wt RAS nor in RUCH-2 cells expressing oncRAS (Fig. 32A). This is in contrast to *GLI1* mRNA level that was suppressed by oncRAS in an ERK-dependent manner (compare section 6.1.4.1). On the one hand that may indicate that the suppression of *GLI1* level apparently is regulated independently of GLI transcription factors. On the other hand, and more likely, the assay did simply not work in this very cell line, because the luciferase activity in the positive control was also not significantly elevated over the negative control. However, electroporation with the *pEGFP-N1* control plasmid yielded over 70 % transfection efficiency in RUCH-2 cell lines (data not shown). This is sufficient and consequently other parameters of the assay need to be optimized.

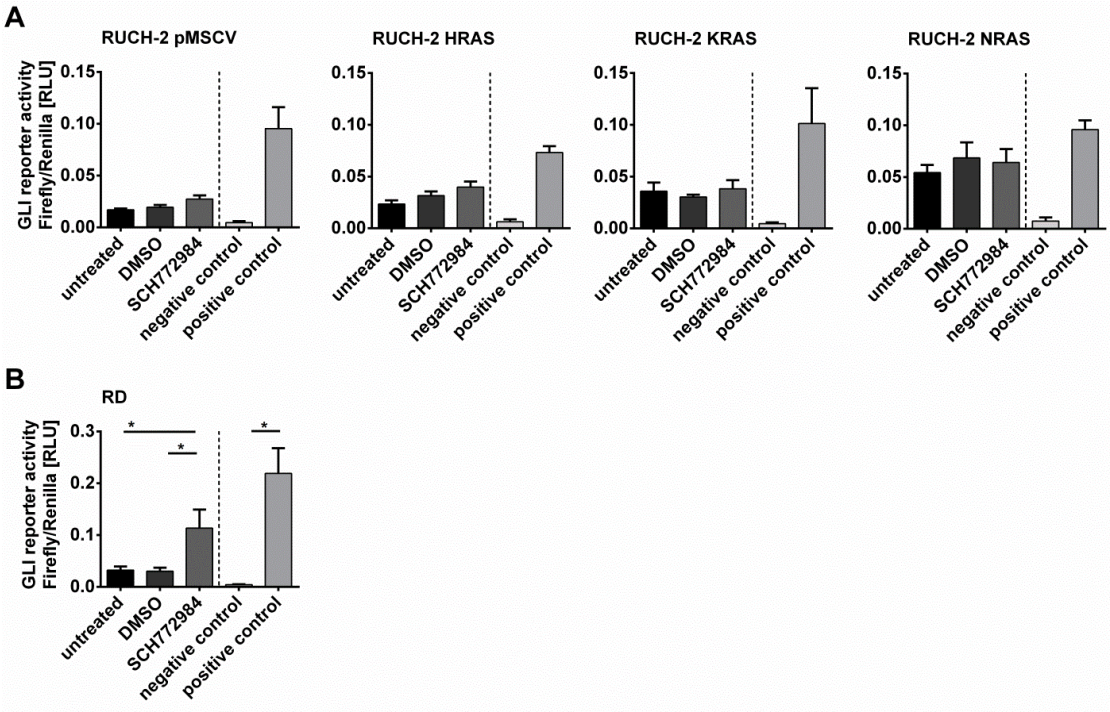

Figure 32: ERK suppresses GLI activity in RD cells but not in stably transduced RUCH-2 cell lines
RUCH-2 cells stably transduced with the pMSCV control vector or oncRAS isoforms (HRAS, KRAS, NRAS) (A) and RD cells (B) were transfected with plasmids for a GLI reporter assay. The cells were incubated with DMSO or 0.5 µM SCH772984 for 24 h. Afterwards, the relative GLI reporter activity was determined by a dual luciferase assay. The luminescence readout from firefly luciferase activity was normalized to renilla luciferase activity. The transfection with an mGli1 overexpressing plasmid (positive control), its pCR3.1 backbone (negative control) or untreated RMS cell lines transfected with the firefly luciferase reporter plasmid and the renilla vector served as controls. Bars represent the mean + SEM of 3 (RUCH-2) or 4 (RD) independent experiments performed in technical sextuplicates or triplicates. For statistical analyses a non-parametric t-test (Mann Whitney) was performed. *p<0.05

This was different in RD cells. In these cells SCH772984 significantly increased GLI reporter activity in comparison to DMSO treated or untreated cells. In addition, also the positive control revealed significant different results (Fig. 32B). In conclusion, ERK inhibits GLI

activity and thus HH signaling activity in RD cells. This is in line with gene expression analyses, which showed that ERK inhibits the transcription of *GLI1 and GLI3* (compare section 6.1.4.1.3 and section 6.1.4.2.3).

6.1.4.4 OncRAS decrease GLI1 protein level in RUCH-2 cells

Since oncRAS isoforms decreased *GLI1* mRNA expression in all ERMS cell lines, further experiments focused on examination of GLI protein level and on the translocation of GLI repressor and activator forms into the nucleus. For this purpose, protein lysates were fractionated into total, cytosolic and nuclear fractions and a Western Blot for GLI proteins was established and performed (see section 5.3.2 and 5.3.5.2).

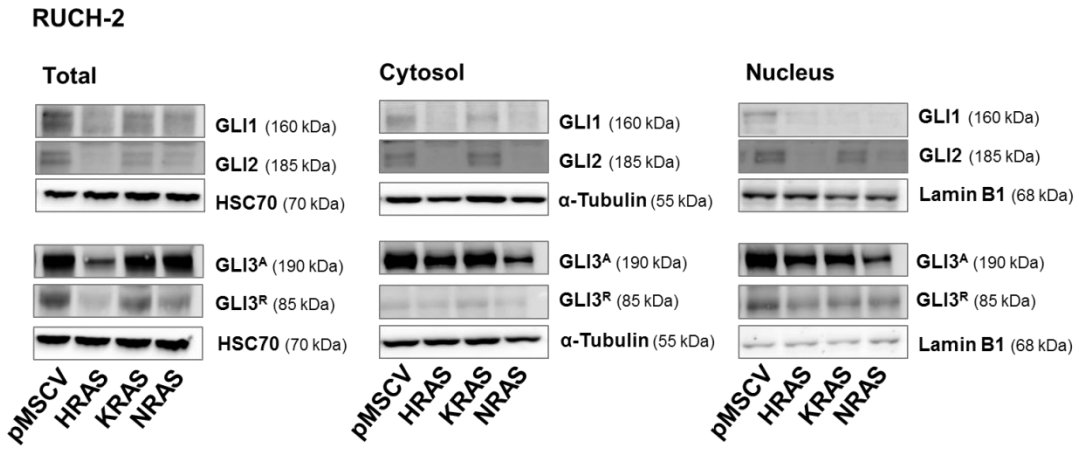

Figure 33: OncRAS isoforms modulate GLI protein expression in different cellular compartments in RUCH-2 cells
Protein was isolated from RUCH-2 cells stably transduced with the pMSCV control vector or oncRAS isoforms (HRAS, KRAS, NRAS). Afterwards the lysates were fractionated into total, cytosolic and nuclear lysates and subjected to Western Blot analyses. Protein level of GLI1, GLI2 and GLI3 activator ($GLI3^A$) and repressor forms ($GLI3^R$) were detected using specific primary antibodies. HSC70 served as reference protein for total fraction, α-Tubulin as reference for cytosolic fraction and LaminB1 as reference for nuclear fraction. Protein names and sizes in kDa are displayed on the right side of the blots. The results are representative for 3 independent experiments.

As seen in RUCH-2 cells, oncRAS isoforms downregulated GLI1 regardless of the cellular compartment (Fig. 33). This result was consistent in 3 independent experiments. Furthermore, a downregulation of the full length GLI2 activator form and probably also the GLI3 full length activator and truncated repressor proteins were detected regardless of the cellular compartment. However, these results were uniformly seen only in 2 out of 3 experiments and thus need to be considered with care.

6.1.4.5 OncRAS-dependent decrease of GLI1 is mediated by ERK in RUCH-2 cells

Next it was investigated whether ERK inhibition in RUCH-2 oncRAS cells restores GLI1 protein level and also that of GLI2, $GLI3^A$ and $GLI3^R$ back to basal level of RUCH-2 pMSCV control cells. For this purpose, the cells were incubated with SCH772984 for 24 h. The protein lysates of cytosolic and nuclear fraction were used for a Western Blot analyses. As controls, lysates from HH-responsive Daoy cells treated with DMSO or SAG, or lysates from RMS-13 cells, which show GLI1 amplification [326], were used. In most Western Blots the

efficient fractionation in the cytosolic and nuclear fraction was revealed by level of the reference proteins α-Tubulin and Lamin B1, respectively (Fig. 34). Unfortunately, the GLI2 and GLI3 data were not evaluable due to highly variable results between the 5 experiments. However, the experiments unambiguously showed that SCH772984 elevated GLI1 protein level in all oncRAS expressing cell lines (Fig. 34A: RUCH-2 HRAS, Fig. 34B: RUCH-2 KRAS, Fig. 34C: RUCH-2 NRAS) in both the cytosolic and nuclear fraction up to basal level detected in the control. This again confirms that oncRAS-mediated decrease of GLI1 is regulated by ERK.

RD cells were also treated with SCH772984 (data not shown). In this cell line ERK inhibition by SCH772984 did not change the protein level of any of the analyzed GLI proteins. However, similar to RUCH-2 cells the results were ambiguous and varied between the experiments and thus were not reliable.

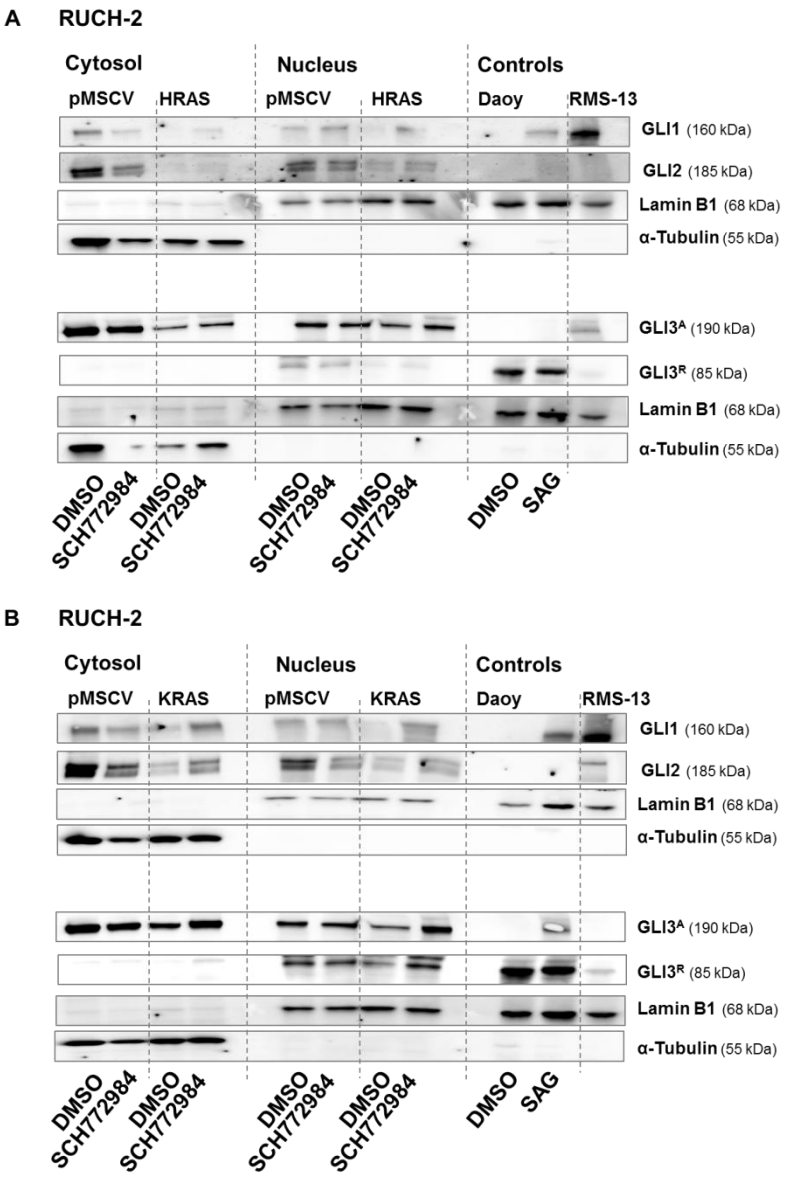

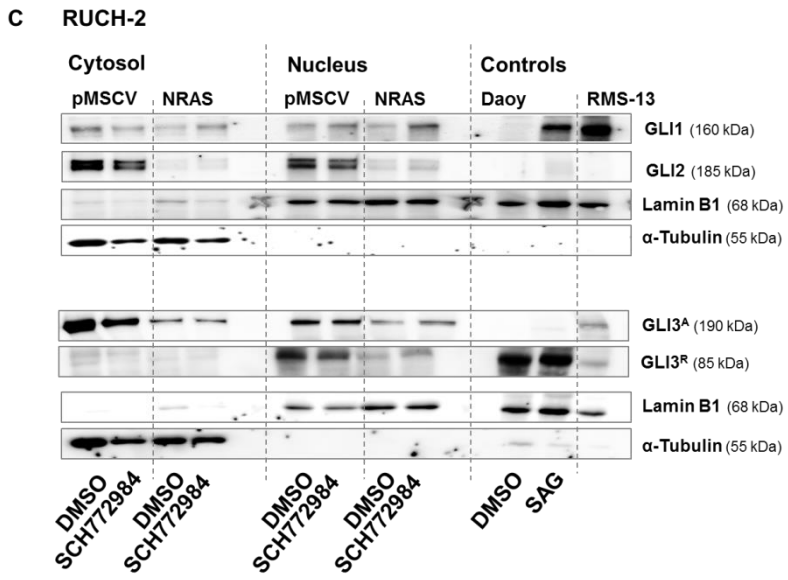

Figure 34: ERK inhibition reverses oncRAS-dependent decrease of GLI1 protein in RUCH-2 cells
RUCH-2 cells stably transduced with the pMSCV control vector or oncRAS isoforms (HRAS, KRAS, NRAS) were treated for 24 h with 0.5 µM SCH772984. Afterwards protein was isolated from RUCH-2 pMSCV, RUCH-2 HRAS (A), RUCH-2 KRAS (B) and RUCH-2 NRAS (C) and the lysates were fractionated into cytosolic and nuclear lysates and subjected to Western Blot analyses. Protein level of GLI1, GLI2 and GLI3 activator ($GLI3^A$) and repressor forms ($GLI3^R$) were detected using specific primary antibodies. Protein lysates from starved Daoy cells treated with DMSO served as size control for $GLI3^R$, whereas lysates from starved Daoy cells treated with 150 nM SAG and lysates of RMS-13 cells served as control for GLI1, GLI2 and $GLI3^A$. α-Tubulin served as reference for cytosolic fraction and LaminB1 as reference for nuclear fraction. Protein names and sizes in kDa are displayed on the right side of the blot. The results are representative for 5 independent experiments.

6.1.5 OncRAS isoforms induce proliferation of TE617.T and RUCH-2 cells

Next, the impact of oncRAS on the proliferative and metabolic activity of ERMS cell lines was investigated. For this purpose, BrdU incorporation assays and WST-1 based colorimetric assays (see section 5.1.5 and 5.1.6) were performed on TE617.T and RUCH-2 cells with and without oncRAS mutations. The assays were conducted 24 h after seeding for TE617.T cell lines. Analyses for RUCH-2 cell lines were performed in a serial experiment from 24 h to 72 h, because RUCH-2 cells are slow-growing.

The results show that oncRAS strongly induced proliferation (Fig. 35A) and increased metabolic activity (Fig. 35B) in TE617.T cells. In RUCH-2 cells expressing oncHRAS a significant increase in proliferation was detected 72 h after seeding, whereas proliferation of RUCH-2 cells expressing oncKRAS increased 48 h and 72 h after seeding in comparison to pMSCV control cells. The oncNRAS mutation apparently had no impact on proliferation within this time frame (Fig. 35C). Furthermore, none of the oncRAS mutations altered metabolic activity of RUCH-2 cells (Fig. 35D).

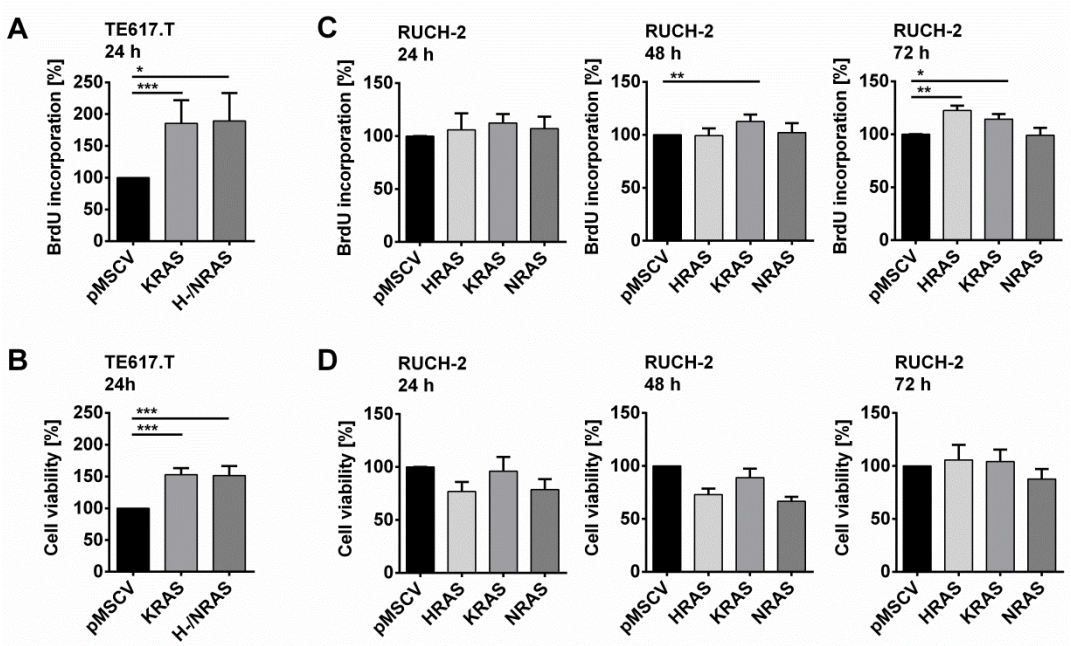

Figure 35: Impact of oncRAS on proliferation and metabolic activity of ERMS cell lines
In TE617.T stably transduced with the pMSCV control vector or oncRAS isoforms (KRAS, H-/NRAS) (A, B) and RUCH-2 cells stably transduced with the pMSCV control vector or oncRAS isoforms (HRAS, KRAS, NRAS) (C, D) the proliferative (A, C) and metabolic activity (B, D) were measured 24 h (TE617.T, RUCH-2), or 48 h and 72 h (RUCH-2) after seeding. BrdU incorporation and cell viability of pMSCV control cells were set to 100 %. Bars represent the mean + SEM of 3 (RUCH-2) or 7 (TE617.T) independent experiments performed in technical sextuplicates or triplicates, respectively. For statistical analyses a non-parametric t-test (Mann Whitney) was performed. *p<0.05, **p<0.01, ***p<0.001, ****p< 0.0001 compared to level of respective pMSCV control cells.

6.1.6 Chapter summary

In summary, the results of chapter 6.1 show that RMS cell lines, which are wt for RAS, have been successfully transduced with oncH-, oncK- or oncNRAS isoforms. A PCR using vector specific primers confirms successful transduction of all cell lines. Western Blot analyses confirm an increase in pERK and pan-RAS protein expression level. Additionally RAS activity is increased in these cell lines. Further analyses reveal that oncRAS mutations decrease *GLI1* mRNA expression irrespective of the RMS subtype and the RAS isoform. Additionally, oncRAS does not only influences *GLI1* expression, which is the major readout for HH signaling activity, but also the expression of other central stakeholders of the signaling pathway like *GLI2*, *PTCH* and *SHH*.

Since oncRAS isoforms increase or decrease *SHH* expression in RUCH-2 oncRAS or TE617.T oncKRAS cells, respectively, it was also investigated whether the cells secrete SHH or not. Medium transfer experiments demonstrate that none of the investigated ERMS cell line was able to secrete HH ligands, regardless of the oncRAS mutation status. In addition, the data show that it is not possible to significantly activate HH signaling at least in RUCH-2 cells. Together these data suggest a non-canonical regulation of HH signaling or at least of *GLI1* expression in ERMS by oncRAS.

Subsequent application of several kinase inhibitors shows that the oncRAS-mediated downregulation of *GLI1* in RD and RUCH-2 cell lines is ERK-dependent. In TE617.T cells,

GLI1 expression is inhibited already intrinsically by ERK and can be strengthened by oncRAS. A subsequent GLI reporter assay shows that ERK indeed regulates GLI activity in RD cells. However, this is not seen in RUCH-2 cells, in which the assay probably does not work efficiently.

Furthermore, Western Blot analyses reveal that oncRAS mutations indeed downregulate the protein level of GLI1 both in the cellular and nuclear compartment of RUCH-2 cells and that ERK inhibition restores the protein expression back to basal level. Unfortunately, the data for GLI2, $GLI3^A$ and $GLI3^R$ are too heterogeneous to make a final statement.

Finally, oncRAS induces proliferation of TE617.T and RUCH-2 cell lines despite downregulation of *GLI1*/GLI1. This indicates that the level of HH signaling, or at least of *GLI1*/GLI1, is not associated with the proliferative capacity of ERMS cells.

6.2 Effects of oncRAS isoforms on xenografts derived from ERMS cell lines

In vitro results described in section 6.1.5 and section 6.1.2.1 showed that oncRAS induces proliferation of ERMS cell lines despite *GLI1* downregulation. In order to see, if the tumor cells behave similarly in the *in vivo* situation, all stably transduced ERMS cell lines were transplanted subcutaneously into flanks of 8-10 weeks old *Nu/Nu* mice. In this experimental setting, pMSCV control cells were implanted into the left flank and oncRAS-expressing cells into the right flank of one and the same animal. The cohorts consisted of 8-12 animals. The approximate tumor volume was measured every or every second day with a caliper. When a tumor reached a diameter of 1.5 cm the mice were sacrificed. The exact tumor volume and the tumor weight were assessed after isolation. In order to see whether the tumor cells influence expression of HH target genes in the tumor microenvironment, species specific primers were used in qRT-PCR analyses of tumor samples.

6.2.1 OncRAS increase tumorigenicity of TE617.T cells

For the generation of tumors 2×10^6 TE617.T pMSCV, TE617.T KRAS or TE617.T H-/NRAS cells were injected into the animals. As already mentioned, all mice were sacrificed when a tumor reached a diameter of 1.5 cm or latest after 55 days. The transplantation studies were performed with either 8 (TE617.T pMSCV and TE617.T KRAS) or 12 (TE617.T pMSCV and TE617.T H-/NRAS) *Nu/Nu* mice.

6.2.1.1 OncRAS enhance tumor growth and weight of TE617.T xenografts

Transplanted TE617.T KRAS and TE617.T H-/NRAS cells resulted in a more aggressive tumor growth in comparison to simultaneously transplanted TE617.T pMSCV cells. Thus, the approximate tumor volume in living mice (measured by caliper), tumor weight and exact tumor volume after tumor isolation were significantly increased in comparison to the control (see Fig. 36A for TE617.T KRAS and Fig. 36B for TE617.T H-/NRAS).

These results are in line with cell culture experiments, which showed an increased proliferation rate of TE617.T cells with an oncRAS mutation in comparison to control cells (section 6.1.5).

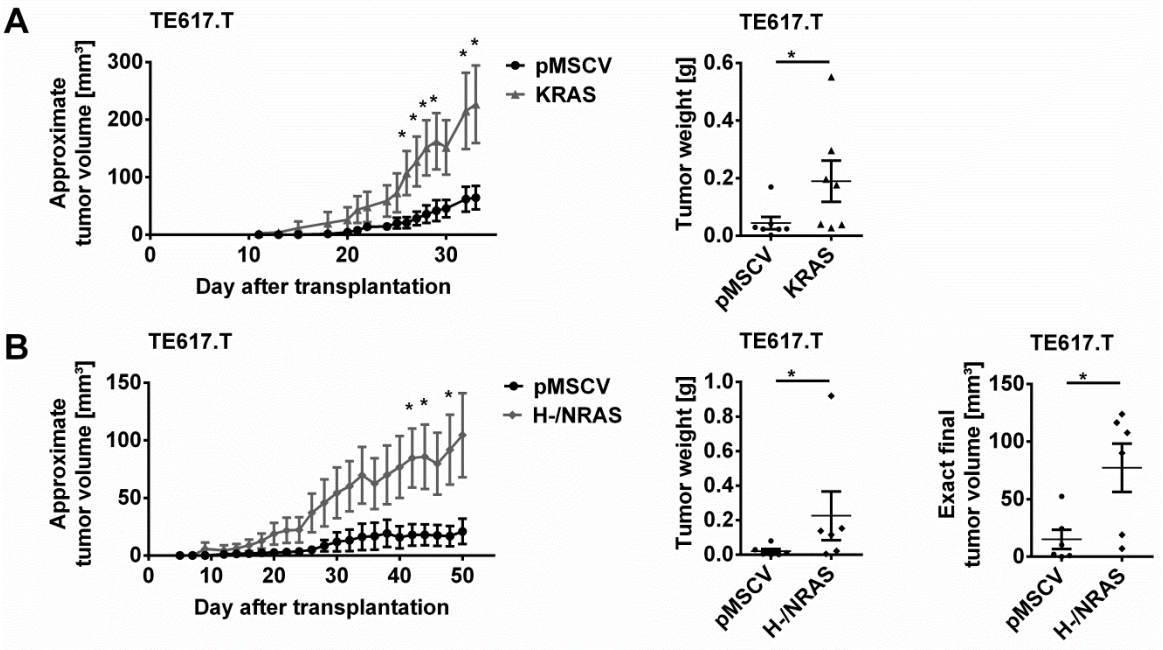

Figure 36: OncRAS isoforms increase tumor growth and weight of TE617.T xenografts
2 × 10^6 TE617.T pMSCV and 2 × 10^6 TE617.T KRAS (A) or 2 × 10^6 TE617.T H-/NRAS (B) cells in 200 µl PBS were transplanted into the left or right flanks, respectively, of *Nu/Nu* mice (n=8 for TE617.T pMSCV and TE617.T KRAS, n= 12 for TE617.T pMSCV and TE617.T H-/NRAS). Tumor size was measured with a caliper every or every second day after transplantation and the approximate tumor volume was calculated. The results are shown in the tumor growth curves in the left panels. At the end of the study tumors were isolated, weighed and measured to determine exact tumor volume. The results are shown in the respective middle and right panels. For statistical analyses multiple t-tests (growth curve) and non-parametric t-tests (Mann Whitney; for tumor weight and exact tumor volume) were performed. * indicate significance compared to characteristics of TE617.T pMSCV xenografts.* p<0.05

6.2.1.2 OncH-/NRAS may influence tumorintrinsic *SHH* expression in TE617.T xenografts

In cultured TE617.T cells the oncRAS mutations resulted in a slight decrease in *GLI1* and *SHH* mRNA level (compare section 6.1.2). In order to analyze, whether this is still true for transplanted cells, the expression of these genes was also measured in the xenografts using primers specific for the human transcripts (Fig. 37A). Although the cultured cells apparently did not secrete *SHH* (compare section 6.1.3.1), the potential effects of Hh signaling was also analyzed, i.e. on expression of murine *mGli1*, *mGli2* in the surrounding murine stroma cells using primers specific for murine transcripts (Fig. 37B).

The RNA was isolated from all available frozen tumor samples of TE617.T pMSCV (n=7), TE617.T KRAS (n=5) and TE617.T H/NRAS (n=6). Data were normalized to gene expression of TE617.T pMSCV tumors that have been transplanted simultaneously in the same animal. The results indicate that tumor-intrinsic *hGLI1* expression was slightly, but not significantly, decreased in tumors of oncKRAS and oncH/NRAS-expressing TE617.T cells in comparison to pMSCV control tumors. Additionally, a significant decrease of *hSHH* was

detected in oncH/NRAS tumors, whereas no influence on *hGLI2* was measured (Fig. 37A). Analyses of *mGli1* and *mGli2* expression in the tumor microenvironment indicated no significant changes induced by oncRAS-expressing tumors (Fig. 37B). These results partly reflect the situation in cell culture (at least for *SHH*; compare section 6.1.2.2). They also suggest that oncRAS-expressing TE617.T xenografts do not influence Hh signaling in the tumor microenvironment.

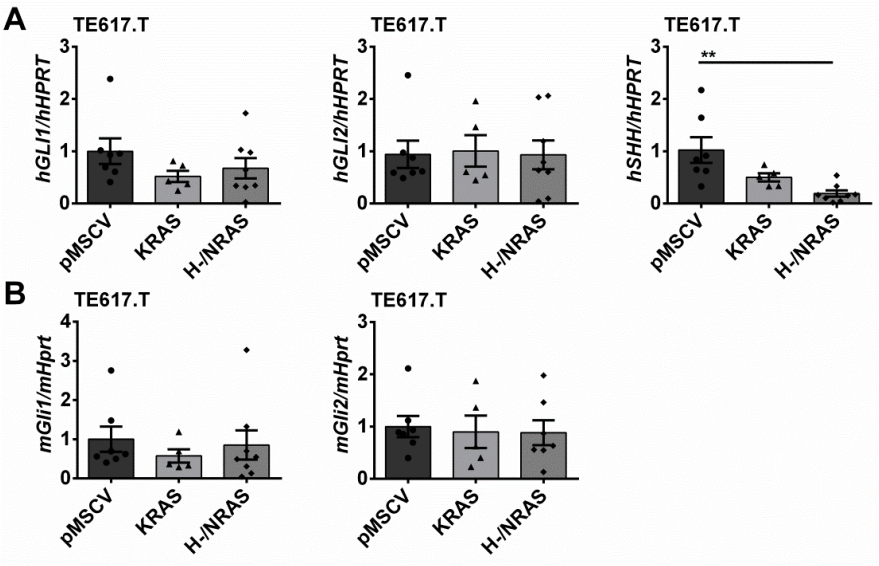

Figure 37: OncRAS do not significantly change the expression of *hGLI1/mGli1*, *hGLI2/mGli2* in TE617.T xenografts
Xenograft tumors were subjected to RNA isolation, cDNA synthesis and subsequent qRT-PCR analyses of the HH signaling pathway genes *hGLI1/mGli1*, *hGLI2/mGli2*, *hSHH* using species specific primers for human (A) and murine genes (B). The data were normalized to *hHPRT* for human gene expression (A) and to *mHprt* for murine gene expression (B) and are shown as fold expression to TE617.T pMSCV xenografts that were set to 1. Bars represent the mean ± SEM of 7(pMSCV), 5 (KRAS) or 6 (H/NRAS) isolated tumors. For statistical analyses non-parametric t-tests (Mann Whitney) were performed. **p<0.01 compared to expression level of TE617.T pMSCV xenografts.

6.2.2 OncKRAS and oncNRAS increase tumorigenicity of RUCH-2 cells

The transplantation of RUCH-2 cell lines were performed with 8 *Nu/Nu* mice for each cohort. In contrast to TE617.T cells, 9×10^6 RUCH-2 cells in matrigel were implanted. All mice were sacrificed when a tumor reached a diameter of 1.5 cm or latest after 21 days.

6.2.2.1 OncKRAS and oncNRAS increase tumor growth and weight of RUCH-2 xenografts

The transplantation of RUCH-2 KRAS (Fig. 38B) and RUCH-2 NRAS (Fig. 38C) cells resulted in a strongly enhanced tumor growth in comparison to simultaneously transplanted RUCH-2 pMSCV cells. In contrast, RUCH-2 HRAS cells did not grow and the tumor volume started to regress early after transplantation (Fig. 38A). However, since BrdU incorporation in cultured RUCH-2 HRAS cells was significant (see section 6.1.5) and since RUCH-2 KRAS and RUCH-2 NRAS xenotransplants grew very fast, it is likely that the RUCH-2 HRAS cells have died prior or during the transplantation procedure. Nevertheless, this study should be repeated to see whether this assumption is true or not.

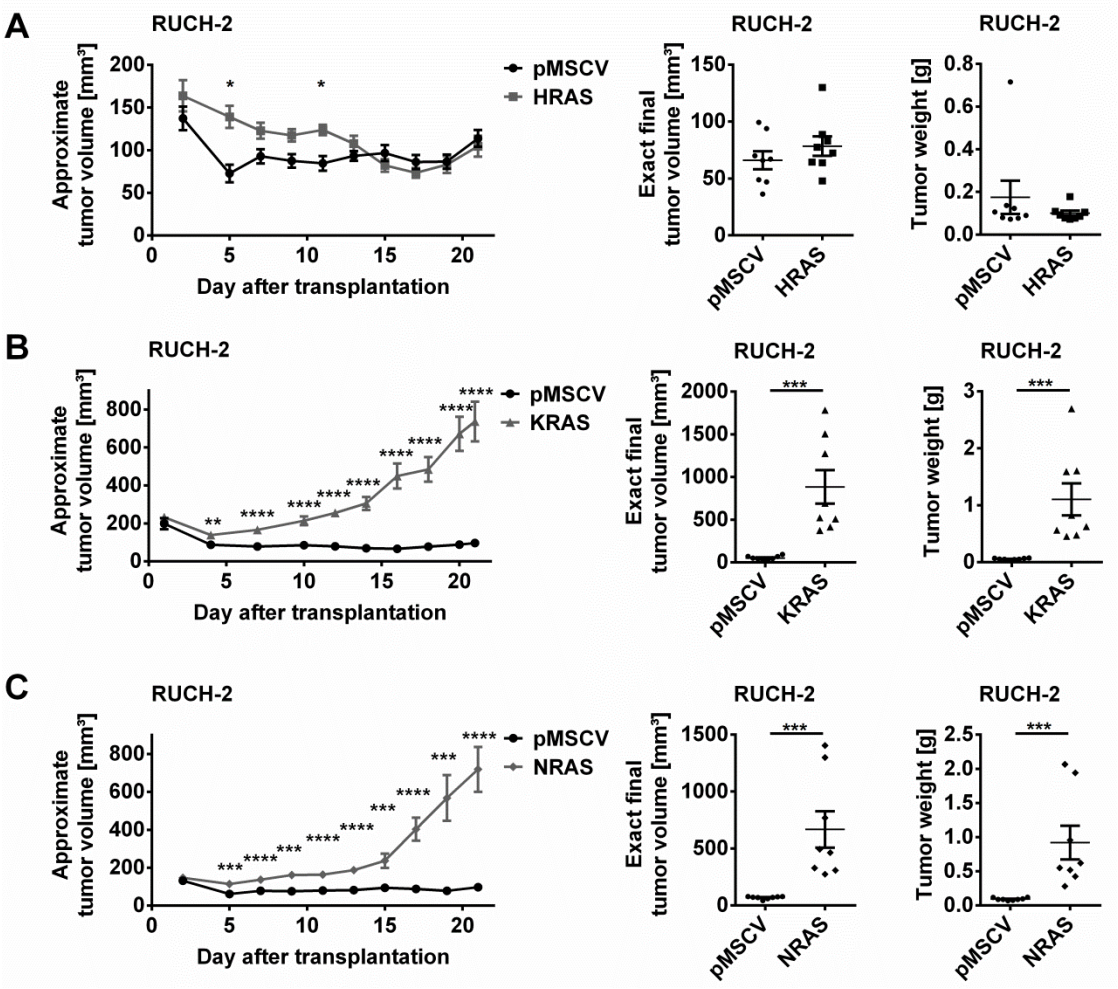

Figure 38: OncKRAS and oncNRAS increase tumor growth and weight of RUCH-2 xenografts
9×10^6 RUCH-2 pMSCV, RUCH-2 HRAS (A), RUCH-2 KRAS (B) or RUCH-2 NRAS (C) cells in 200 µl PBS were transplanted into the left or right flanks, respectively, of *Nu/Nu* mice (n=8 for each cohort). Tumor size was measured with a caliper every or every second day after transplantation and the approximate tumor volume was calculated. The results are shown in the tumor growth curves in the left panels. At the end of the study tumors were isolated, weighed and measured to determine the exact tumor volume. The results are shown in the respective middle and right panels. For statistical analyses multiple t-tests (growth curve) and non-parametric t-tests (Mann Whitney; for tumor weight and exact tumor volume) were performed. * indicate significance compared to characteristics of RUCH-2 pMSCV xenografts. *p<0.05, **p<0.01, ***p<0.001, ****p< 0.0001

The approximate tumor volume of RUCH-2 xenografts with oncKRAS or oncNRAS mutations in living mice, and their weight and exact tumor volume after tumor isolation were significantly increased, when compared to RUCH-2 pMSCV xenografts (Fig. 38). For oncKRAS this result fits to cell culture experiments, in which oncKRAS also increased the proliferation rate. However, the *in vivo* results for the oncNRAS-expressing RUCH-2 cell line are different from the *in vitro* situation, in which oncNRAS did not increase the proliferation rate, even not after 72 h of incubation with BrdU (compare section 6.1.5).

6.2.2.2 OncRAS may downregulate *GLI1* expression in tumor cells and upregulate *Gli2* expression in stromal cells of RUCH-2 xenografts

In vitro experiments using oncRAS-expressing RUCH-2 cell lines showed a decrease in *GLI1* and *GLI2* mRNA level and a simultaneous increase in *SHH* mRNA level in comparison to the control (compare section 6.1.2). The expression of these genes was also analyzed in the

xenografts. In addition and in order to see, whether RUCH-2 cell with oncRAS secrete SHH *in vivo*, the expression of *Gli1* and *Gli2* was measured in the tumor stroma.

In xenografts derived from oncKRAS-expressing RUCH-2 cells the expression of *hGLI1* and *hSHH* was somewhat lower in comparison to RUCH-2 pMSCV xenografts. However, these results were not significant. In addition, the level of *hGLI2* remained unchanged (Fig. 39A). When the expression level of *mGli1* and *mGli2* were measured, an increase in xenografts derived from oncKRAS-expressing RUCH-2 was detected, which was not significant for *Gli1* but significant for *Gli2*. This indicates a potential impact of oncKRAS-expressing tumor cells on HH signaling in surrounding stromal cells (Fig. 39B). However, since *SHH* was rather downregulated in these xenografts, the increase in *mGli1* or *mGli2* is rather not mediated by secretion of the SHH ligand by tumor cells.

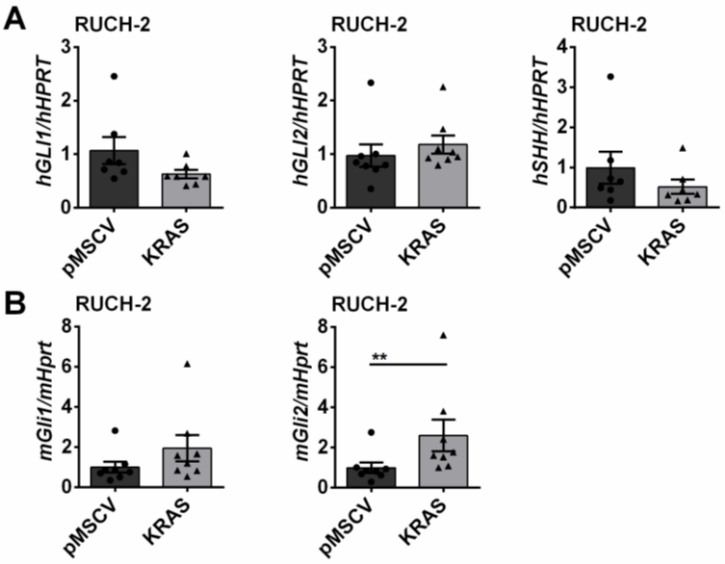

Figure 39: OncKRAS significantly induces *mGli2* expression in the stroma of RUCH-2 xenografts
Xenograft tumors were subjected to RNA isolation, cDNA synthesis and subsequent qRT-PCR analyses of the HH signaling pathway genes *hGLI1/mGli1*, *hGLI2/mGli2*, *hSHH* using species specific primers for human (A) and murine genes (B). The data were normalized to *hHPRT* for human gene expression (A) and to *mHprt* for murine gene expression (B) and are shown as fold expression to RUCH-2 pMSCV xenografts that were set to 1. Bars represent the mean ± SEM of 8 isolated tumors of each cohort. For statistical analyses non-parametric t-tests (Mann Whitney) were performed. **p<0.01 compared to expression level of RUCH-2 pMSCV xenografts.

Gene expression analyses of xenografts derived from oncNRAS-expressing RUCH-2 cells revealed that, as seen in cell culture, oncNRAS decreased *hGLI1* and *hGLI2* in the tumor cells. Whereas the decrease in *GLI1* was significant, the decrease in *hGLI2* was not. In contrast to cell culture, oncNRAS also decreased *hSHH* in comparison to RUCH-2 pMSCV xenografts (Fig. 40A). In the murine stroma, no significant changes in mRNA level of *mGli1* and *mGli2* were measured (Fig. 40B).

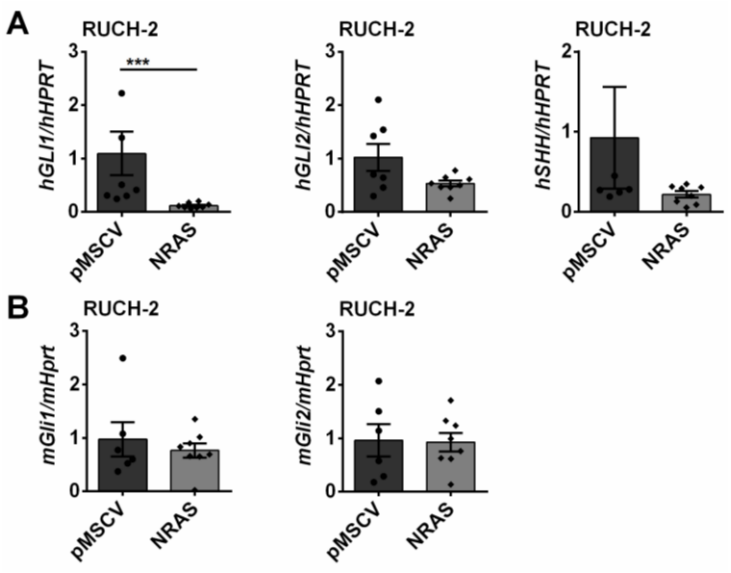

Figure 40: OncNRAS significantly decreases *hGLI1* expression in tumor cells of RUCH-2 xenografts
Xenograft tumors were subjected to RNA isolation, cDNA synthesis and subsequent qRT-PCR analyses of the HH signaling pathway genes *hGLI1/mGli1*, *hGLI2/mGli2*, *hSHH* using species specific primers for human (A) and murine genes (B). The data were normalized to *hHPRT* for human gene expression (A) and to *mHprt* for murine gene expression (B) and are shown as fold expression to RUCH-2 pMSCV xenografts that were set to 1. Bars represent the mean ± SEM of 8 isolated tumors of each cohort. For statistical analyses non-parametric t-tests (Mann Whitney) were performed. ***p<0.001 compared to expression level of RUCH-2 pMSCV xenografts.

Taken together, the results show that transplanted RUCH-2 cells with oncKRAS or oncNRAS behave somewhat different when compared to cell culture (compare section 6.1.2). Thus, *hGLI1* is only moderately decreased in RUCH-2 oncKRAS xenografts (it however is significantly decreased in RUCH-2 oncNRAS xenografts) and an upregulation of *hSHH* is observed in none of the analyzed xenografts. Nevertheless, the expression of *mGli2* in the tumor stroma is significantly increased, at least in oncKRAS xenografts.

6.2.3 Chapter summary

In chapter 6.2, the impact of oncRAS on growth and HH signaling activity in ERMS xenotransplants is described. As in cell culture, the tumor growth is significantly stimulated by oncRAS mutations in ERMS cell lines. In addition, oncRAS tend to decrease tumorintrinsic *GLI1* expression, although the respective results are only significant for oncNRAS-expressing RUCH-2 xenografts. In contrast, the transplantation of oncRAS cells rather results in a decrease in *SHH* expression (which was significant for oncH-/NRAS expressing TE617.T cells), whereas *SHH* expression of cultured oncRAS RUCH-2 or oncRAS TE617.T cells is elevated or decreased, respectively. Finally, tumor-extrinsic *Gli2* expression in oncKRAS-expressing RUCH-2 xenografts is increased, which may indicate that the transplanted tumor cells indeed secrete HH ligands and thus may affect HH signaling activity in the tumor microenvironment.

6.3 Effects of oncRas mutations on ERMS of *Ptch*$^{del/+}$ mice

In addition, a genetic approach was pursued to study possible interactions of Hh and Ras signaling in ERMS. For this purpose the *Ptch*$^{del/+}$ mouse model was used. These mice spontaneously develop RMS, which resemble ERMS in humans and show active Hh signaling [137,143,323,324]. *Ptch*$^{del/+}$ mice were crossed to mice which conditionally express one of the oncRas genes. In order to activate the expression of oncRas, the *Myf5*^{CreER} deleter [305] mouse was used.

6.3.1 Pilot testing and validation of the utilized mouse models

6.3.1.1 Testing the activity of the *Myf5*^{CreER} driver in ERMS using the *R26R*$^{+/-}$ reporter strain

In a pilot test, the activity of the *Myf5*^{CreER} driver was analyzed in ERMS of *Ptch*$^{del/+}$ mutant mice. This Cre driver was chosen, because human and murine ERMS from *Ptch* mutant mice highly express *Myf5* [323]. In order to ensure that the oncRas mutations indeed will be induced in ERMS of *Ptch*$^{del/+}$ mice, *Ptch*$^{del/+}$*Myf5*^{CreER} mice were bred to the cre-reporter strain *R26R*. When the mice developed a palpable tumor, they were injected i.p. with tamoxifen or solvent for 5 consecutive days and were sacrificed 1 or 5 weeks thereafter. ERMS and skeletal muscle (SM) as well as brain, heart (negative controls, not shown) and intestine (positive control due to endogenous β-galactosidase activity, not shown) were isolated and subjected to X-Gal stainings (see section 5.4.3). Another positive control was SM from *Rosa26-lacZ* mice. These mice express lacZ and thus show high β-galactosidase activity in every organ of the body [306].

Tissue sections of SM and ERMS from solvent-treated *Ptch*$^{del/+}$*Myf5*^{CreER}*R26R*$^{+/-}$ mice showed no X-Gal staining, whereas ERMS from tamoxifen-treated *Ptch*$^{del/+}$*Myf5*^{CreER}*R26R*$^{+/-}$ mice stained positive (Fig. 41). The galactosidase activity visualized by X-Gal staining was detected in ERMS 1 or 5 weeks after treatment. Since no staining was detected in SM, it was concluded that the *Myf5*^{CreER} driver is primarily active in ERMS and also does not show any leakiness i.e. it is not active without tamoxifen. Nevertheless, the staining itself was not as strong as expected from literature [305].

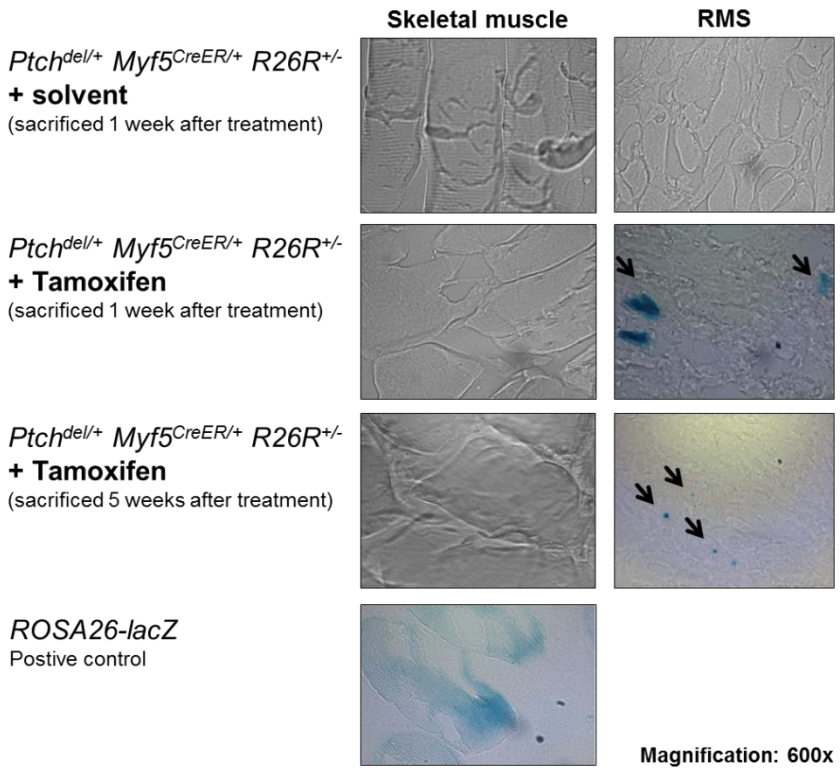

Figure 41: X-Gal staining of skeletal muscle and ERMS isolated from solvent- or tamoxifen-treated *Ptch$^{del/+}$Myf5$^{CreER/+}$R26R$^{+/-}$* mice
Cryo-embedded sections of skeletal muscle (SM) and ERMS (RMS) from solvent- or tamoxifen-treated *Ptch$^{del/+}$Myf5$^{CreER/+}$R26R$^{+/-}$* mice were subjected to X-Gal staining. Cryo-embedded sections of SM from *ROSA26-lacZ* mice served as positive control. The arrows point to areas of staining. Pictures were taken at 600x fold magnification.

6.3.1.2 *HRas*, *KRas* and *NRas* are expressed in SM and ERMS of *Ptch$^{del/+}$* mice

Next, the expression of *HRas*, *KRas* and *NRas* were analyzed by PCR and qRT-PCR in SM and ERMS from *Ptch$^{del/+}$* mice. These analyses were done to confirm that the Ras isoforms are expressed mainly in ERMS: if Ras should not be expressed in ERMS from *Ptch$^{del/+}$* mice, an activation of oncRas from the endogenous *Ras* locus is not possible. As shown in Fig. 42, *HRas*, *KRas* and *NRas* are expressed in SM and ERMS tissue, respectively (Fig. 42A, Fig. 42C and Fig. 42E, respectively). Moreover, qRT-PCR data showed that the level of *HRas* expression is equal in SM and ERMS, whereas *KRas* and *NRas* level are higher in ERMS compared to SM (Fig. 42B, Fig. 42D and Fig. 42F, respectively).

In addition, the *Ras* loci were sequenced to rule out endogenous mutations in the 3 genes. However, all 3 *Ras* loci were wt in more than 5 analyzed RMS from *Ptch$^{del/+}$* mice (data not shown).

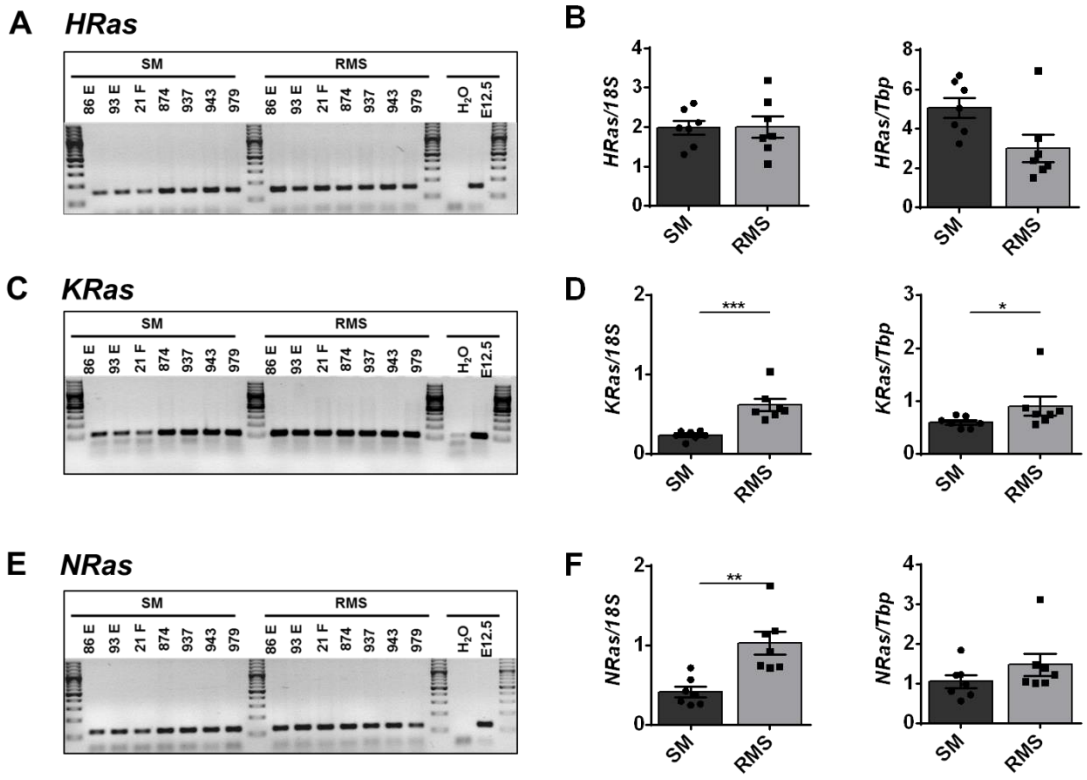

Figure 42: Ras isoforms are expressed in SM and ERMS tissue samples of *Ptch*$^{del/+}$ mice
The basal expression of *HRas* (A, B), *KRas* (C, D) and *NRas* (E, F) were analyzed in skeletal muscle (SM) and ERMS (RMS) tissue samples of *Ptch*$^{del/+}$ mice by PCR (A, C, E) and quantified by qRT-PCR (B, D, E). The numbers in A, C and E indicate the mouse identification number. The expression in embryos at E12.5 served as positive control. The histograms shown in B, D and F represent qRT-PCR analyses and show the mean gene expression ± SEM of 7 tissue samples for SM and ERMS. Data were normalized to 18S *rRNA* (18S, left) or *Tbp* (right). For statistical analyses non-parametric t-tests (Mann Whitney) were performed. *p<0.05, **p<0.01, ***p<0.001 compared to expression level within SM.

6.3.1.3 Testing *Myf5*^{CreER} activity at the *Ras* loci in ERMS of *Ptch*$^{del/+}$*oncRas*$^{fl/+}$*Myf5*$^{CreER/+}$ mice

After having checked the activity of the *Myf5*^{CreER} driver in ERMS (see section 6.3.1.1), it was tested whether this Cre driver also efficiently targets the 3 oncogenic *Ras* loci. This was done because it is well known that the recombination efficiency of one and the same Cre driver can vary at different loci [338-340]. The recombination assays were performed on frozen or paraffin-embedded tissue samples from SM and ERMS of *Ptch*$^{del/+}$*HRas*$^{fl/+}$*Myf5*$^{CreER/+}$, *Ptch*$^{del/+}$*KRas*$^{fl/+}$*Myf5*$^{CreER/+}$ and *Ptch*$^{del/+}$*NRas*$^{fl/+}$*Myf5*$^{CreRE/+}$ mice (compare section 5.2.3.2). Additionally, frozen tissue samples from these mice were used for a second round of genotyping to confirm the genetic setting (compare section 5.2.3.1).

The recombination assay for *HRas* was done on PCR-amplified cDNA by enzymatic digestion with BpmI. The enzyme recognizes the wt sequence (derived from the wt and the floxed locus), whereas the mutant *HRas* exon is not recognized due to the *HRas*^{G12V} mutation [303] (compare section 5.2.3.2.2). As already described, successful recombination was indicated by weak 209 bp and 93 bp digestion bands and a strong undigested fragment of 302 bp.

SM tissue samples from untreated, solvent-treated (not shown) and tamoxifen-treated *Ptch*$^{del/+}$*HRas*$^{fl/+}$*Myf5*$^{CreER/+}$ mice showed a weak band for undigested transcript and a strong band for the digested, wt transcripts. The same bands were also observed in ERMS samples from untreated and solvent-treated (not shown) *Ptch*$^{del/+}$*HRas*$^{fl/+}$*Myf5*$^{CreER/+}$ mice (Fig. 43). This might indicate that the *Myf5*^{CreER} driver is leaky at the *HRas* loci. However, it could also mean that the BpmI-mediated digestion of the cDNA was incomplete. Nevertheless, the recombination efficiency at the *HRas* locus increased in ERMS samples of tamoxifen-treated mice (Fig. 43). Thus, a strong band for the undigested, recombined transcript and a weak band for the digested, wt transcripts were observed, which indicated efficient recombination at the *HRas* locus in ERMS.

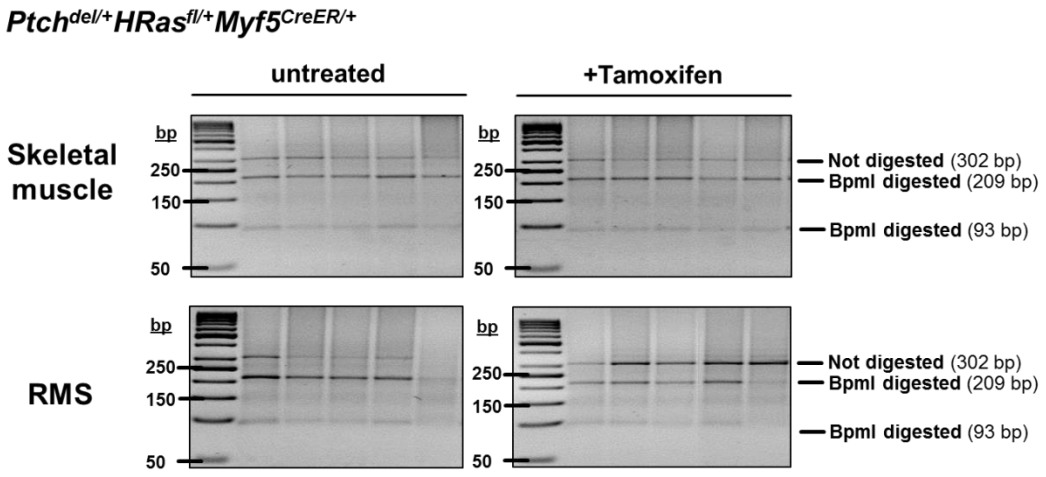

Figure 43: Recombination assays for the floxed *HRas* loci
Skeletal muscle (SM) and ERMS (RMS) tissue samples were subjected to RNA isolation and subsequent cDNA synthesis. Fragments of the *HRas* gene were PCR-amplified and then digested using BpmI. Products were separated by agarose gel electrophoresis. A successful recombination is indicated by weak digestion bands (209 bp and 93 bp) and a strong band for the undigested fragment (302 bp). No recombination should be indicated by strong digestion bands (209 bp and 93 bp) and lack of the undigested band (302 bp). However, due to either incomplete digestion or leakiness of the Cre driver at the floxed *HRas* locus the undigested band was always present. For more details, see text.

The recombination assay for *KRas* was done on PCR-amplified gDNA samples. A band of 304 bp represents the recombined *KRas* allele, whereas a band of 270 bp represents the wt *KRas* allele. Due to the fact that all mice were heterozygous for the floxed *Ras* alleles, efficient recombination at the KRas locus was demonstrated by the occurrence of the 304 bp fragment in addition to the 270 bp band. A double band was clearly observed in ERMS samples from tamoxifen-treated mice, whereas it was only detected in very rare cases of untreated or solvent-treated (data not shown) mice (Fig. 44). This suggests that the *Myf5*^{CreER} driver might be leaky at the floxed *KRas* locus in very few cases. Due to these data the ERMS incidence of tamoxifen- and untreated *Ptch*$^{del/+}$*KRas*$^{fl/+}$*Myf5*$^{CreER/+}$ mice were compared, whereas all untreated *Ptch*$^{del/+}$*KRas*$^{fl/+}$*Myf5*$^{CreER/+}$ mice showing spontaneous recombination have been excluded from analyses (see section 6.3.2.3).

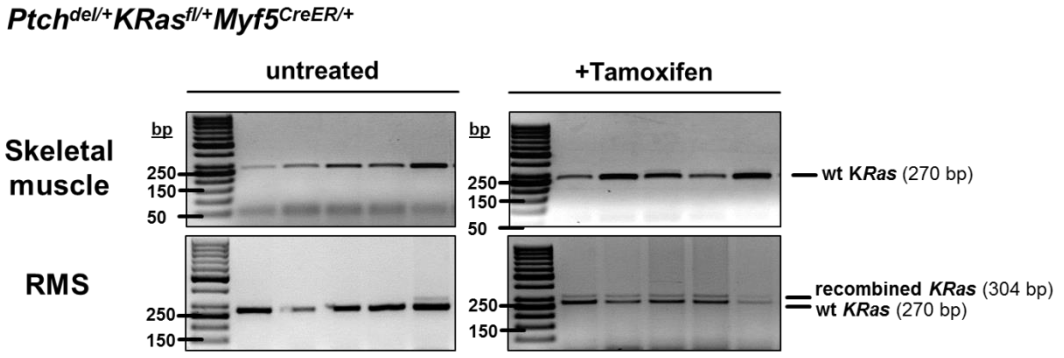

Figure 44: Recombination assays for the floxed *KRas* loci
Skeletal muscle (SM) and ERMS (RMS) tissue samples were subjected to gDNA isolation and subsequent PCR which was used to prove efficient recombination at the floxed *KRas* locus. Amplificates were separated by agarose gel electrophoresis and analyzed afterwards. A double band (270 bp for wt and 304 bp for the floxed *KRas* locus after recombination) indicated efficient recombination, whereas a single band (270 bp for wt *KRas*) indicated no recombination.

The recombination assay for *NRas* was also done with PCR-amplified gDNA samples. As already stated above, all mice were heterozygous for the floxed *Ras* alleles. Therefore, efficient recombination at the floxed *NRas* locus was demonstrated by the occurrence of the 521 bp fragment in addition to the 487 bp band that represents the wt *NRas* allele. The analysis revealed that the double band only occurred in ERMS samples isolated from tamoxifen-treated mice, whereas it was never seen in ERMS from untreated *Ptch*$^{del/+}$*NRas*$^{fl/+}$*Myf5*$^{CreER/+}$ mice (Fig. 45). However, in rare cases recombination also occurred in SM of tamoxifen-treated *Ptch*$^{del/+}$*NRas*$^{fl/+}$*Myf5*$^{CreER/+}$ mice (data not shown). Since the latter fact probably is of no importance for ERMS growth, all tamoxifen-treated *Ptch*$^{del/+}$*NRas*$^{fl/+}$*Myf5*$^{CreER/+}$ mice (and all untreated mice) with the correct genotype were included in the analysis described in section 6.3.2.4.

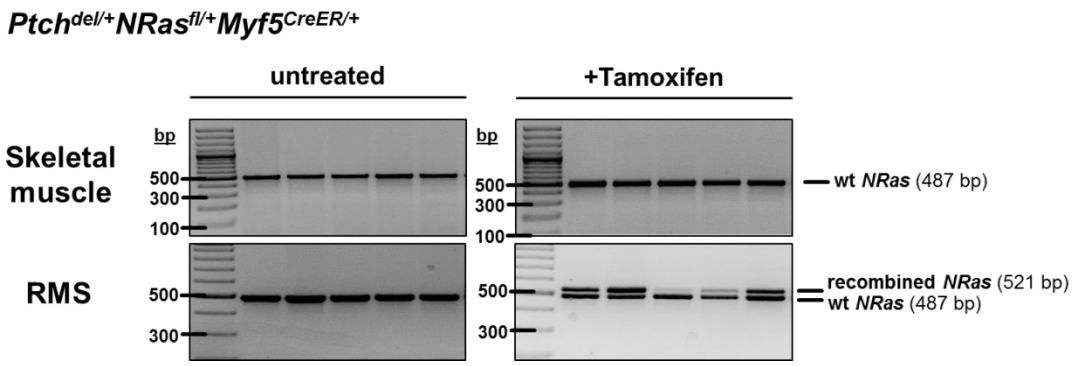

Figure 45: Recombination assays for the floxed *NRas* loci
Skeletal muscle (SM) and ERMS (RMS) tissue samples were subjected to gDNA isolation and subsequent PCR, which was used to prove efficient recombination at the floxed *NRas* locus. Amplificates were separated by agarose gel electrophoresis and analyzed afterwards. A double band (487 bp for wt and 521 bp for the recombined floxed *NRas* alleles) indicated efficient recombination, whereas a single band (487 bp for the wt *NRas* allele) indicated no recombination.

6.3.1.4 Testing Ras activity in ERMS of tamoxifen-treated *Ptch*$^{del/+}$*oncRas*$^{fl/+}$*Myf5*$^{CreER/+}$ mice

Next, the functionality of the expressed oncRas alleles was investigated. For this purpose, ERMS samples from tamoxifen-treated *Ptch*$^{del/+}$*oncRas*$^{fl/+}$*Myf5*$^{CreER/+}$ mice were analyzed in a Ras activity assay (experimental details are explained in section 5.3.6). The densitometrical analysis (Fig. 46A) of two independent experiments and a representative Western Blot (Fig. 46B) highlight an approximate twofold increase in Ras activity in tumor tissue of tamoxifen-treated *Ptch*$^{del/+}$ mice with oncRas mutation.

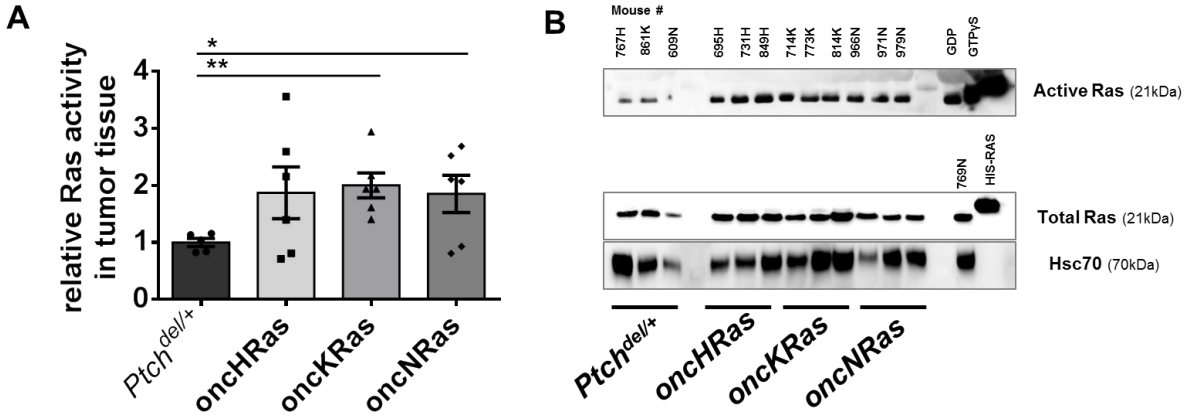

Figure 46: Ras is active in ERMS tissue samples of tamoxifen-treated *Ptch*$^{del/+}$*oncRas*$^{fl/+}$*Myf5*$^{CreER/+}$ mice
Protein was isolated from tumor samples of tamoxifen-treated *Ptch*$^{del/+}$ and *Ptch*$^{del/+}$*oncRas*$^{fl/+}$*Myf5*$^{CreER/+}$ (oncHRas, oncKRas, oncNRas) mice. Afterwards cell lysates were subjected to a bead-based pull-down assay to precipitate active Ras. Whole lysates of the same samples were used to detect total Ras. Afterwards, precipitated and whole lysates were analyzed by Western Blot to detect the protein level of active Ras and total Ras with specific antibodies. Hsc70 served as loading control for total Ras. The relative Ras activity was calculated by normalization of active Ras to total Ras/Hsc70 and is displayed in histograms showing the mean Ras activity of 6 tumors each cohort ± SEM. Ras activity in ERMS from *Ptch*$^{del/+}$mice served as control and was set to 1 (A). A representative Western Blot is shown in (B). Protein names and sizes in kDa are displayed on the right side of the blot. The depicted results are representative for 6 tumors of each cohort analyzed in two independent experiments. For statistical analyses unpaired non-parametric t-tests (Mann Whitney) were performed. *p<0.05, **p<0.01 compared to relative Ras activity within tumor tissue from *Ptch*$^{del/+}$ mice.

Taken together, the results described in section 6.3.1 show that ERMS of *Ptch*$^{del/+}$ mice express wt *HRas*, *KRas* and *NRas*. In order to activate oncRas expression in *Ptch*$^{del/+}$*oncRas*$^{fl/+}$ mice the *Myf5*^{CreER} driver was used. Indeed, tamoxifen-mediated activation of this driver induces recombination of the conditional floxed oncRas alleles primarily in the tumor tissue. Moreover, Ras activity assays verify the successful Ras activation in ERMS of tamoxifen-treated *Ptch*$^{del/+}$*oncRas*$^{fl/+}$*Myf5*$^{CreER/+}$ mice.

6.3.2 Activation of oncRas in ERMS precursor lesions

ERMS in *Ptch*$^{del/+}$ mice are initiated before birth and become conspicuous and palpable earliest at the age of approximately 7 weeks [323]. In order to analyze the impact of oncRas on ERMS precursor lesions, the expression of oncRas in *Ptch*$^{del/+}$*HRas*$^{fl/+}$*Myf5*$^{CreER/+}$, *Ptch*$^{del/+}$*KRas*$^{fl/+}$*Myf5*$^{CreER/+}$ or *Ptch*$^{del/+}$*NRas*$^{fl/+}$*Myf5*$^{CreER/+}$ mice was induced with tamoxifen at the age of 4 weeks. Untreated siblings of the same genotype or untreated or tamoxifen-treated *Ptch*$^{del/+}$ mice served as controls.

Breeding and tumor monitoring of the mice was part of another doctoral thesis [299]. Here, the data were evaluated again and the monitoring study of *Ptch*$^{del/+}$*NRas*$^{fl/+}$*Myf5*$^{CreER/+}$ mice was repeated entirely. Overall survival was defined as the percentage of mice, which remained alive within the time frame of monitoring. RMS-free survival indicated the time point of first detection of a palpable ERMS of a mouse. On this basis the mean ERMS-free survival and the median latency time until tumor detection of the cohort was calculated. The tumor incidence specifies the percentage of mice with a detected ERMS in the complete cohort. The tumor multiplicity was calculated as proportion of mice with 1 or more ERMS compared to all ERMS-bearing mice.

6.3.2.1 Tamoxifen does not influence growth or incidence of ERMS of *Ptch*$^{del/+}$ mice

First, it was tested whether tamoxifen itself modulates ERMS in *Ptch*$^{del/+}$ mice. For this purpose, *Ptch*$^{del/+}$ mice were treated with tamoxifen at an age of 4 weeks and monitored for ERMS development. All *Ptch*$^{del/+}$ mice were the siblings of all *Ptch*$^{del/+}$*oncRas*$^{fl/+}$*Myf5*$^{CreER/+}$ mice. The time point of first tumor detection was recorded for approximately 200 days. The details and characteristics of all animals are listed in Tab. 25. The respective Kaplan-Meier curves for overall survival and ERMS-free survival and graphs for tumor incidence and multiplicity are shown in Fig. 47A, Fig. 47B, Fig. 47C and Fig. 47D, respectively. The analyses did not reveal any significant differences between untreated and tamoxifen-treated *Ptch*$^{del/+}$ mice.

Table 25: Influence of tamoxifen treatment on ERMS development of 4 week old *Ptch*$^{del/+}$ mice
Absolute numbers, median survival, premature death, ERMS incidence, latency time and further observed abnormalities of *Ptch*$^{del/+}$ mice with and without tamoxifen injection. The respective Kaplan-Meier curves and graphs are shown in Fig. 47.

Treatment	Number of mice	Median overall survival (range)	Healthy // premature death	Mice with ERMS (incidence)	Mice with ≥ 2 ERMS (incidence)	Median latency time	Further observations
Untreated	27	200 days (60 – 206)	23 // 4	12 (44 %)	3 (11 %)	73 days	Cysts/ Cavernous angioma: 6 Medulloblastoma: 1
Tamoxifen	27	200 days (90 – 209)	21 // 6	13 (48 %)	4 (15 %)	105 days	Cysts/ Cavernous angioma: 4 Medulloblastoma: 1

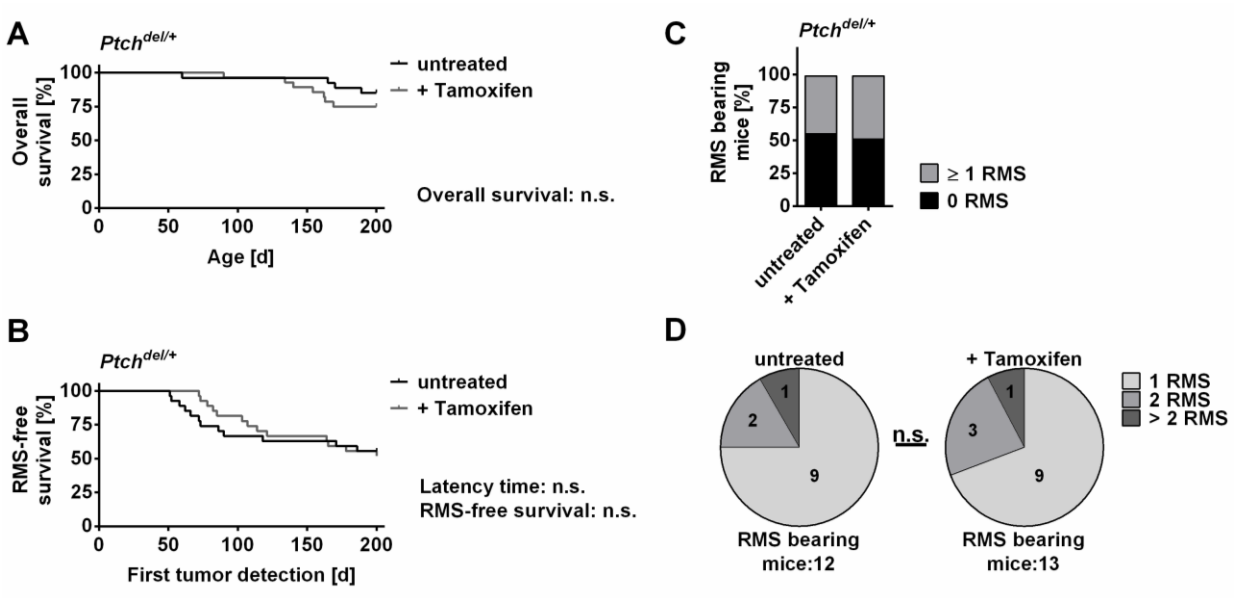

Figure 47: Tamoxifen treatment does not influence ERMS development in *Ptch*$^{del/+}$ mice
Ptch$^{del/+}$ mice were injected with tamoxifen at the age of 4 weeks or remained untreated. Mice were monitored until the age of approximately 200 days and the time point of first tumor detection and death were recorded. Kaplan-Meier curves of overall (A) and ERMS-free (B) survival of untreated (black) and tamoxifen-treated (grey) *Ptch*$^{del/+}$ mice are shown. The data were analyzed by Gehan-Breslow-Wilcoxon test for statistical differences in overall and ERMS-free survival. Differences in latency time were analyzed by Log-rank (Mantel-Cox) test. Differences in total number of animals with ERMS (C) and in tumor multiplicity (D) were analyzed by Chi square tests. For more details see Tab. 25.

6.3.2.2 OncHRas increases the ERMS incidence in *Ptch*$^{del/+}$ mice

Ptch$^{del/+}$*HRas*$^{fl/+}$*Myf5*$^{CreER/+}$ mice were treated with tamoxifen at an age of 4 weeks. Untreated animals served as controls. The details and characteristics of all animals of this cohort are listed in Tab. 26. The respective Kaplan-Meier curves for overall and ERMS-free survival are shown in Fig. 48A and Fig. 48B, respectively. The results show that the ERMS incidence was significantly higher in tamoxifen-treated *Ptch*$^{del/+}$*HRas*$^{fl/+}$*Myf5*$^{CreER/+}$ mice compared to untreated mice (Fig. 48C). In addition, the time until detection of palpable ERMS was shorter and just missed significance (Fig. 48B). However, no significant differences in the median overall survival, tumor multiplicity (Fig. 48D) or other abnormalities were observed (Tab. 26).

Table 26: Influence of oncHRas on ERMS development of 4 week old *Ptch*$^{del/+}$*HRas*$^{fl/+}$*Myf5*$^{CreER/+}$ mice
Absolute numbers, median survival, premature death, ERMS incidence, latency time and further observed abnormalities of *Ptch*$^{del/+}$*HRas*$^{fl/+}$*Myf5*$^{CreER/+}$ mice with and without tamoxifen injection. The respective Kaplan-Meier curves and graphs are shown in Fig. 48.

Treatment	Number of mice	Median overall survival (range)	Healthy // premature death	Mice with ERMS (incidence)	Mice with ≥ 2 ERMS (incidence)	Median latency time	Further observations
Untreated	32	200 days (65 – 211)	20 // 12	18 (56 %)	6 (19 %)	96 days	Cysts/ Cavernous angioma: 4 Medulloblastoma: 3 Papilloma: 1
Tamoxifen	32	200 days (76 – 204)	22 // 10	24 (74 %)	7 (22 %)	83 days	Cysts/ Cavernous angioma: 4 Medulloblastoma: 1 Papilloma: 1

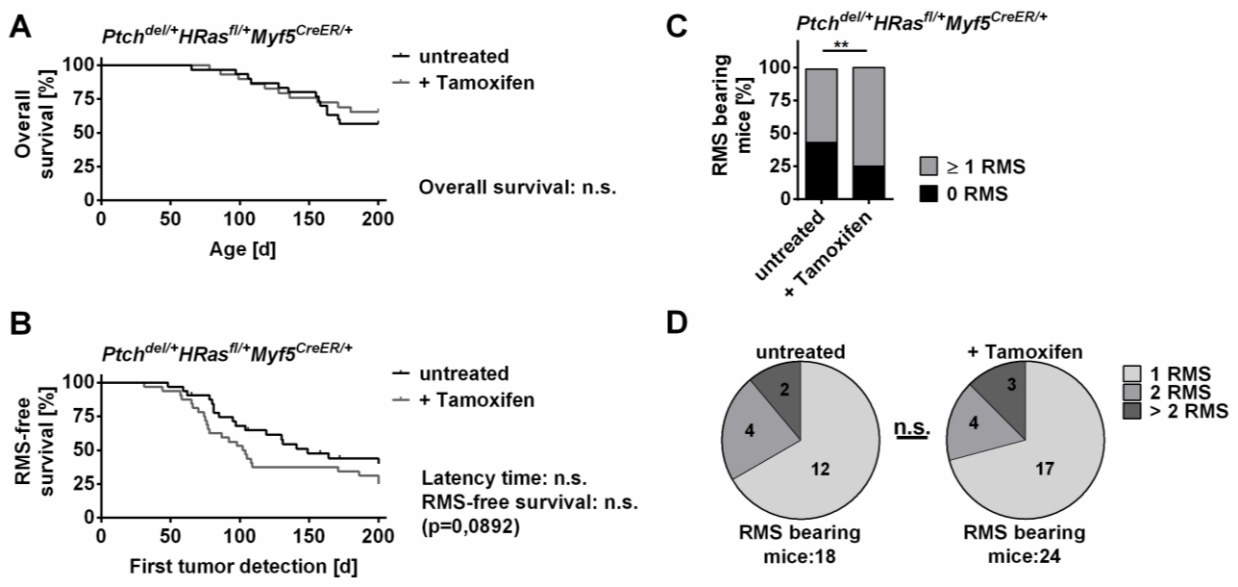

Figure 48: OncHRas increases tumor incidence and slightly reduces ERMS-free survival in *Ptch*$^{del/+}$ mice
Ptch$^{del/+}$*HRas*$^{fl/+}$*Myf5*$^{CreER/+}$ mice were injected with tamoxifen at the age of 4 weeks or left untreated. Mice were monitored until the age of approximately 200 days and the time point of first tumor detection and death were recorded. Respective Kaplan-Meier curves for overall (A) and ERMS-free (B) survival of untreated (black) and tamoxifen-treated (grey) *Ptch*$^{del/+}$*HRas*$^{fl/+}$*Myf5*$^{CreER/+}$ mice are shown. The data were analyzed by Gehan-Breslow-Wilcoxon test for statistical differences in overall and ERMS-free survival. Differences in latency time were analyzed by Log-rank (Mantel-Cox) test. Differences in total number of animals with ERMS (C) and in tumor multiplicity (D) were analyzed by Chi square tests. **p<0.01 compared untreated *Ptch*$^{del/+}$*HRas*$^{fl/+}$*Myf5*$^{CreER/+}$ mice. For more details see Tab. 26.

6.3.2.3 OncKRas increases tumor incidence and reduces ERMS-free survival in *Ptch*$^{del/+}$ mice

The *Ptch*$^{del/+}$*KRas*$^{fl/+}$*Myf5*$^{CreER/+}$ cohorts were treated as described above. Untreated mice served as controls. The details and characteristics of the animals are listed in Tab. 27 and are shown in Fig. 49. The data reveal that oncKRas significantly decreased the overall survival and ERMS-free survival (Tab. 27 and Fig. 49A, Fig. 49B). It also significantly increased the tumor incidence (Fig. 49C). On the other hand, oncKRas did not influence the occurrence of other abnormalities or tumor multiplicity (Tab. 27 and Fig. 49D).

Table 27: Influence of oncKRas on ERMS development of 4 week old *Ptch*$^{del/+}$*KRas*$^{fl/+}$*Myf5*$^{CreER/+}$ mice
Absolute numbers, median survival, premature death, ERMS incidence, latency time and further observed abnormalities of *Ptch*$^{del/+}$*KRas*$^{fl/+}$*Myf5*$^{CreER/+}$ mice with and without tamoxifen injection. The respective Kaplan-Meier curves and graphs are shown in Fig. 49.

Treatment	Number of mice	Median overall survival (range)	Healthy // premature death	Mice with ERMS (incidence)	Mice with ≥ 2 ERMS (incidence)	Median latency time	Further observations
Untreated	24	200 days (83 – 209)	17 // 7	10 (41 %)	4 (17 %)	109 days	Cysts/ Cavernous angioma: 3 Medulloblastoma: 3
Tamoxifen	29	122 days (69 – 201)	12 // 17	22 (76 %)	13 (45 %)	78 days	Cysts/ Cavernous angioma: 4 Medulloblastoma: 0

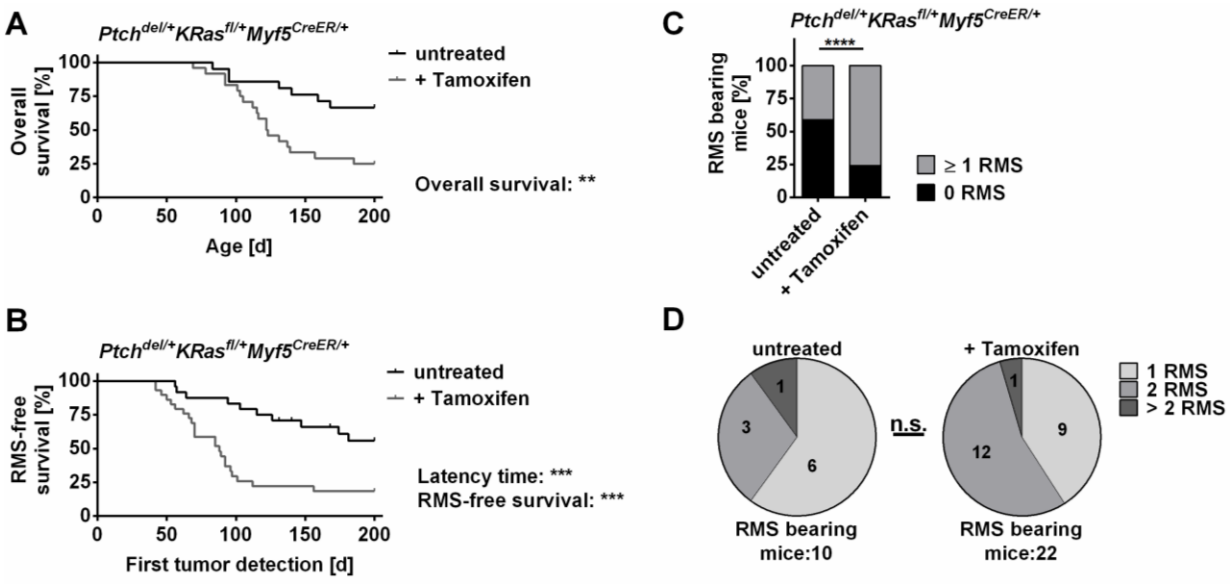

Figure 49: OncKRas increases tumor incidence and decreases ERMS-free survival in *Ptch*$^{del/+}$ mice
Ptch$^{del/+}$*KRas*$^{fl/+}$*Myf5*$^{CreER/+}$ mice were injected with tamoxifen at the age of 4 weeks or left untreated. Mice were monitored until the age of approximately 200 days and the time point of first tumor detection and death were recorded. Respective Kaplan-Meier curves for overall (A) and ERMS-free (B) survival of untreated (black) and tamoxifen-treated (grey) *Ptch*$^{del/+}$*KRas*$^{fl/+}$*Myf5*$^{CreER/+}$ mice are shown. The data were analyzed by Gehan-Breslow-Wilcoxon test for statistical differences in overall and ERMS-free survival. The data were analyzed for differences in latency time using the Log-rank (Mantel-Cox) test. Differences in total tumor incidence (C) or tumor multiplicity (D) were analyzed with Chi square tests. **p<0.01, ***p<0.001, **** p< 0.0001 compared to untreated *Ptch*$^{del/+}$*KRas*$^{fl/+}$*Myf5*$^{CreER/+}$ mice. For more details see Tab. 27.

6.3.2.4 OncNRas does not influence ERMS growth of *Ptch*$^{del/+}$ mice

Mice from the *Ptch*$^{del/+}$*NRas*$^{fl/+}$*Myf5*$^{CreER/+}$ cohorts were treated as described above. Untreated mice served as controls. The details and characteristics of the animals are shown below (Tab. 28 and Fig. 50A, Fig. 50B, Fig. 50C and Fig. 50D). The data show that oncNRas does neither significantly influence overall survival, ERMS free survival, ERMS latency time, tumor incidence nor multiplicity (Fig. 50A, Fig. 50B, Fig. 50C and Fig. 50D). It also does not influence the occurrence of other abnormalities (Tab. 28).

Table 28: Influence of oncNRas on ERMS development of 4 week old *Ptch*$^{del/+}$*NRas*$^{fl/+}$*Myf5*$^{CreER/+}$ mice
Absolute numbers, median survival, premature death, ERMS incidence, latency time and further observed abnormalities of *Ptch*$^{del/+}$*NRas*$^{fl/+}$*Myf5*$^{CreER/+}$ mice with and without tamoxifen injection. The respective Kaplan-Meier curves and graphs are shown in Fig. 50.

Treatment	Number of mice	Median overall survival (range)	Healthy // premature death	Mice with ERMS (incidence)	Mice with ≥ 2 ERMS (incidence)	Median latency time	Further observations
Untreated	26	200 days (131 – 212)	19 // 7	17 (65 %)	10 (38 %)	63 days	Cysts/ Cavernous angioma: 4 Medulloblastoma: 1
Tamoxifen	28	200 days (76 – 206)	22 // 6	20 (71 %)	8 (29 %)	94 days	Cysts/ Cavernous angioma: 6 Medulloblastoma: 1

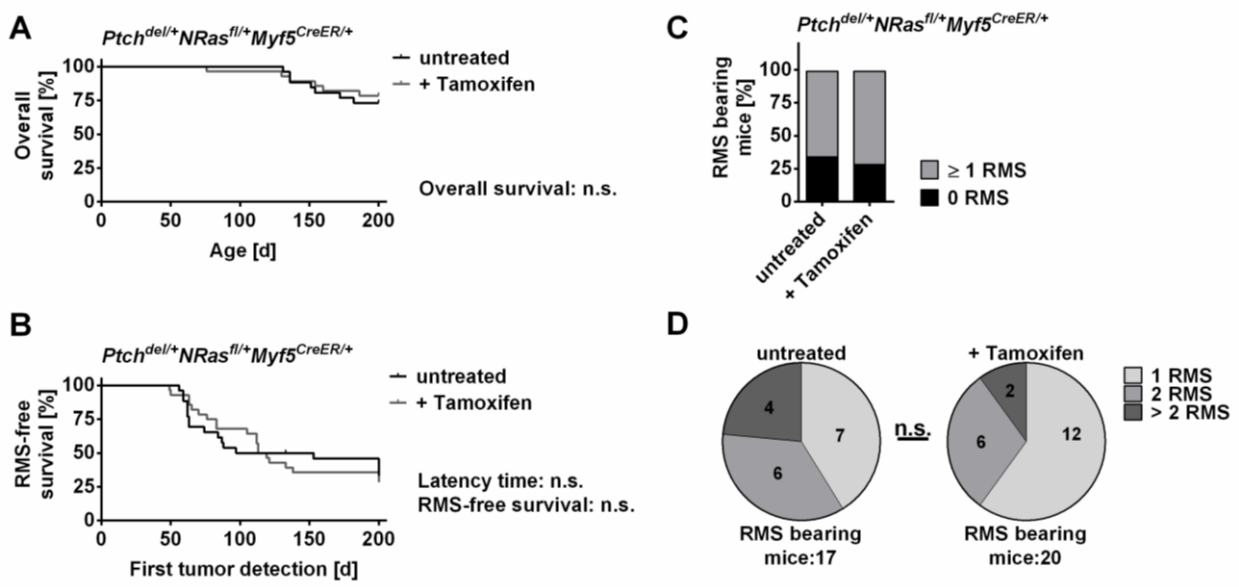

Figure 50: OncNRas does not influence ERMS-free survival, tumor incidence or multiplicity in *Ptch*$^{del/+}$ mice

Ptch$^{del/+}$*NRas*$^{fl/+}$*Myf5*$^{CreER/+}$ mice were injected with tamoxifen at the age of 4 weeks or left untreated. Mice were monitored until the age of approximately 200 days and the time point of first tumor detection and death were recorded. Respective Kaplan-Meier curves for overall (A) and ERMS-free (B) survival of untreated (black) and tamoxifen-treated (grey) *Ptch*$^{del/+}$*NRas*$^{fl/+}$*Myf5*$^{CreER/+}$ mice are shown. The data were analyzed by Gehan-Breslow-Wilcoxon test for statistical differences in overall and tumor free survival. The data were analyzed for differences in latency time using the Log-rank (Mantel-Cox) test. Differences in total tumor incidence (C) or tumor multiplicity (D) were analyzed with Chi square tests. For more details see Tab. 28.

6.3.2.5 OncHRas and oncKRas increase proliferation rate of ERMS in *Ptch*$^{del/+}$ mice, whereas oncNRas does not

Next, the impact of oncRas isoforms on proliferation of ERMS was analyzed by staining of paraffin sections for Ki67$^+$ nuclei (compare section 5.4.2).

Tamoxifen treatment did not influence proliferation of ERMS in *Ptch*$^{del/+}$ mice (Fig. 51A). In contrast, an increase in Ki67$^+$ nuclei in ERMS of tamoxifen-treated *Ptch*$^{del/+}$*HRas*$^{fl/+}$*Myf5*$^{CreER/+}$ (Fig. 51B) and *Ptch*$^{del/+}$*KRas*$^{fl/+}$*Myf5*$^{CreER/+}$ (Fig. 51C) mice was observed in comparison to untreated mice of the same cohort. OncNRas induction did not influence proliferation of ERMS in *Ptch*$^{del/+}$ mice (Fig. 51D). Thus, the mean of Ki67$^+$ nuclei in tumors of untreated mice from all cohorts ranged between 5.5 % and 6.5 % regardless of the genotype and did not differ significantly between the analyzed groups. In tumors of tamoxifen-treated mice the mean of Ki67$^+$ nuclei ranged between 6.0 % and 13 %. In contrast, tumors with oncHRas or oncKRas mutations showed a significantly higher proliferation rate than ERMS from tamoxifen-treated *Ptch*$^{del/+}$ mice and tumors with oncNRas mutations.

Additionally, the tumor weight and volume were assessed for ERMS from untreated and tamoxifen-treated *Ptch*$^{del/+}$*NRas*$^{fl/+}$*Myf5*$^{CreER/+}$ mice. However, oncNRas did not influence the respective parameters (data not shown).

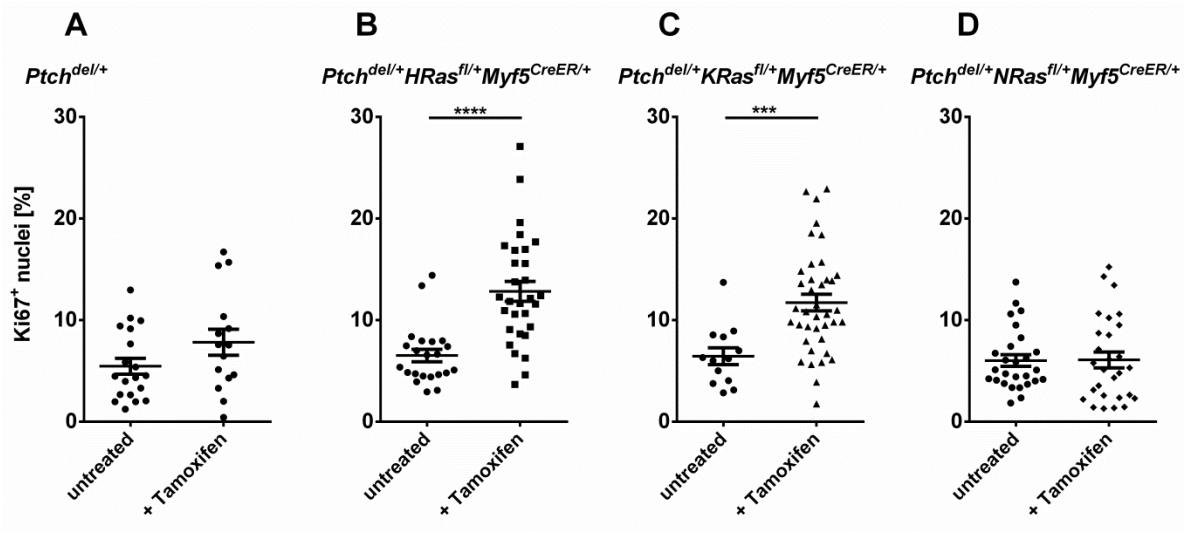

Figure 51: OncHRas and oncKRas increase the percentage of Ki67$^+$ nuclei in ERMS from *Ptch$^{del/+}$* mice
ERMS tissue sections from untreated (n= 19 ERMS from 10 mice) and tamoxifen-treated (n= 15 ERMS from 12 mice) *Ptch$^{del/+}$* mice (A), untreated (n= 22 ERMS from 13 mice) and tamoxifen-treated (n= 30 ERMS from 22 mice) *Ptch$^{del/+}$HRas$^{fl/+}$Myf5$^{CreER/+}$* mice (B), untreated (n= 14 ERMS from 10 mice) and tamoxifen-treated (n= 39 ERMS from 21 mice) *Ptch$^{del/+}$KRas$^{fl/+}$Myf5$^{CreER/+}$* mice (C) and untreated (n= 27 ERMS from 14 mice) and tamoxifen-treated (n= 28 ERMS from 19 mice) *Ptch$^{del/+}$NRas$^{fl/+}$Myf5$^{CreER/+}$* mice (D) were stained with a specific antibody against the proliferation marker Ki67. Number of all nuclei and Ki67$^+$ nuclei were counted manually in 10 pictures of each tumor and percentage of Ki67$^+$ nuclei was calculated. For statistical analyses non-parametric t-tests (Mann Whitney) were performed. ***p<0.001, ****p< 0.0001 compared to untreated *Ptch$^{del/+}$oncRas$^{fl/+}$Myf5$^{CreER/+}$* mice from the respective cohort.

6.3.2.6 OncRas isoforms do not change expression of Hh target genes in ERMS of *Ptch$^{del/+}$* mice

Next, SM and ERMS tissue samples were analyzed for the expression level of the major Hh target *Gli1* and of other downstream targets, namely *Gli2*, *Gli3*, *Ptch* and *Hhip* (Fig. 52). The expression of *18S rRNA* or *Tbp* was used for normalization. Furthermore, the expression of the respective gene is shown as fold induction over the expression level in SM of the same animal, which was set to 1. Unfortunately, only 2 freshly frozen tumor samples of untreated *Ptch$^{del/+}$KRas$^{fl/+}$Myf5$^{CreER/+}$* mice were available for the analyses. Hence, a statistical analysis was not possible for this cohort.

None of the comparisons showed significant differences (Fig. 52). Thus, tamoxifen itself did not have significant effects on Hh target gene expression in tumors of *Ptch$^{del/+}$* mice (Fig. 52A) and no significant differences between mRNA expression of tumors with and without oncRas were detected (Fig. 52B, Fig. 52C, Fig. 52D). Nevertheless, a tendency for downregulation of *Gli1* in oncRas-expressing tumors was observed. This is notable because a similar, but significant downregulation of *GLI1* was revealed in human ERMS cell lines (see section 6.1.2.1).

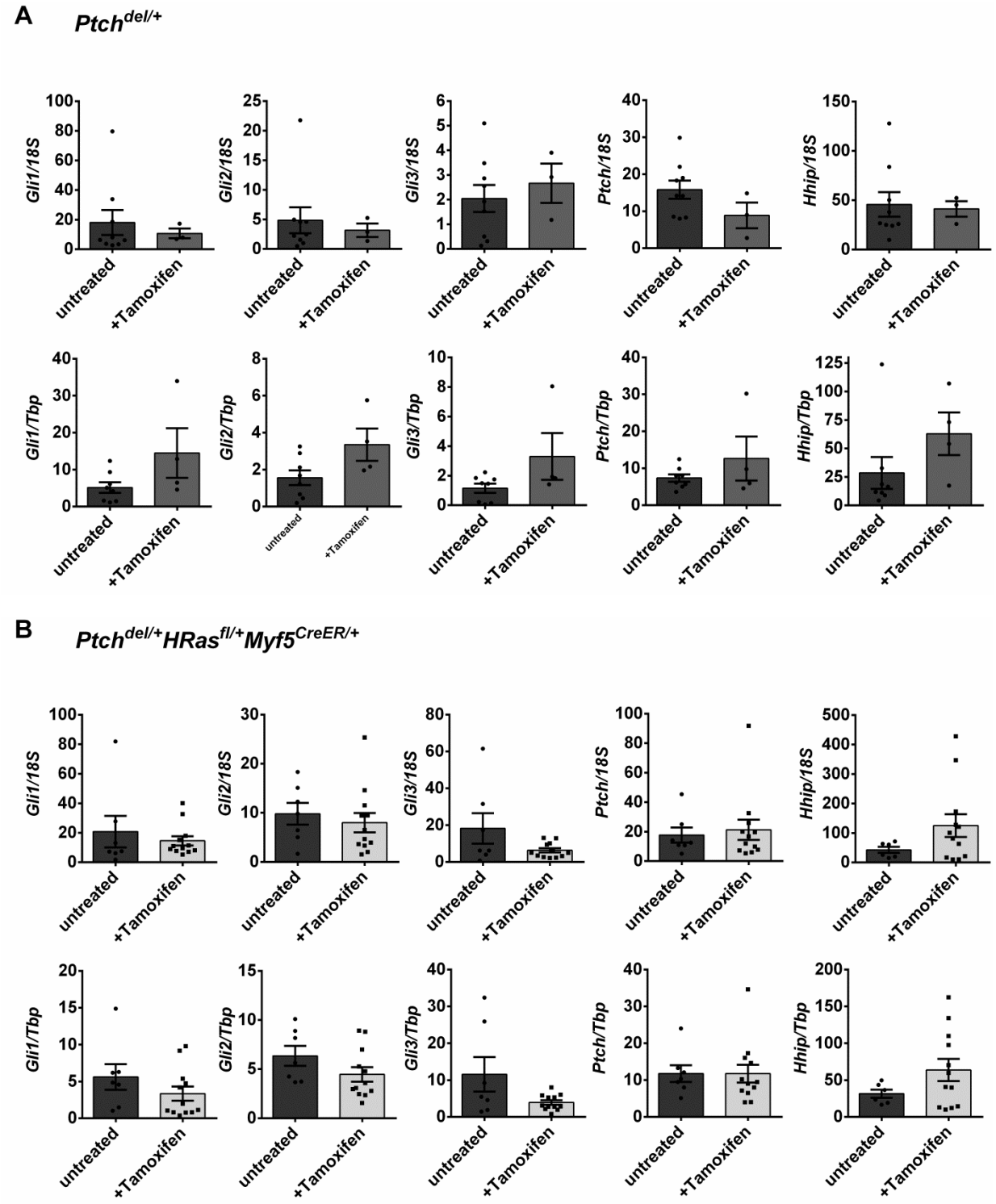
A
Ptch^del/+
Gli1/18S
Gli2/18S
Gli3/18S
Ptch/18S
Hhip/18S
Gli1/Tbp
Gli2/Tbp
Gli3/Tbp
Ptch/Tbp
Hhip/Tbp
untreated
+Tamoxifen
B
Ptch^del/+HRas^fl/+Myf5^CreER/+
Gli1/18S
Gli2/18S
Gli3/18S
Ptch/18S
Hhip/18S
Gli1/Tbp
Gli2/Tbp
Gli3/Tbp
Ptch/Tbp
Hhip/Tbp
untreated
+Tamoxifen

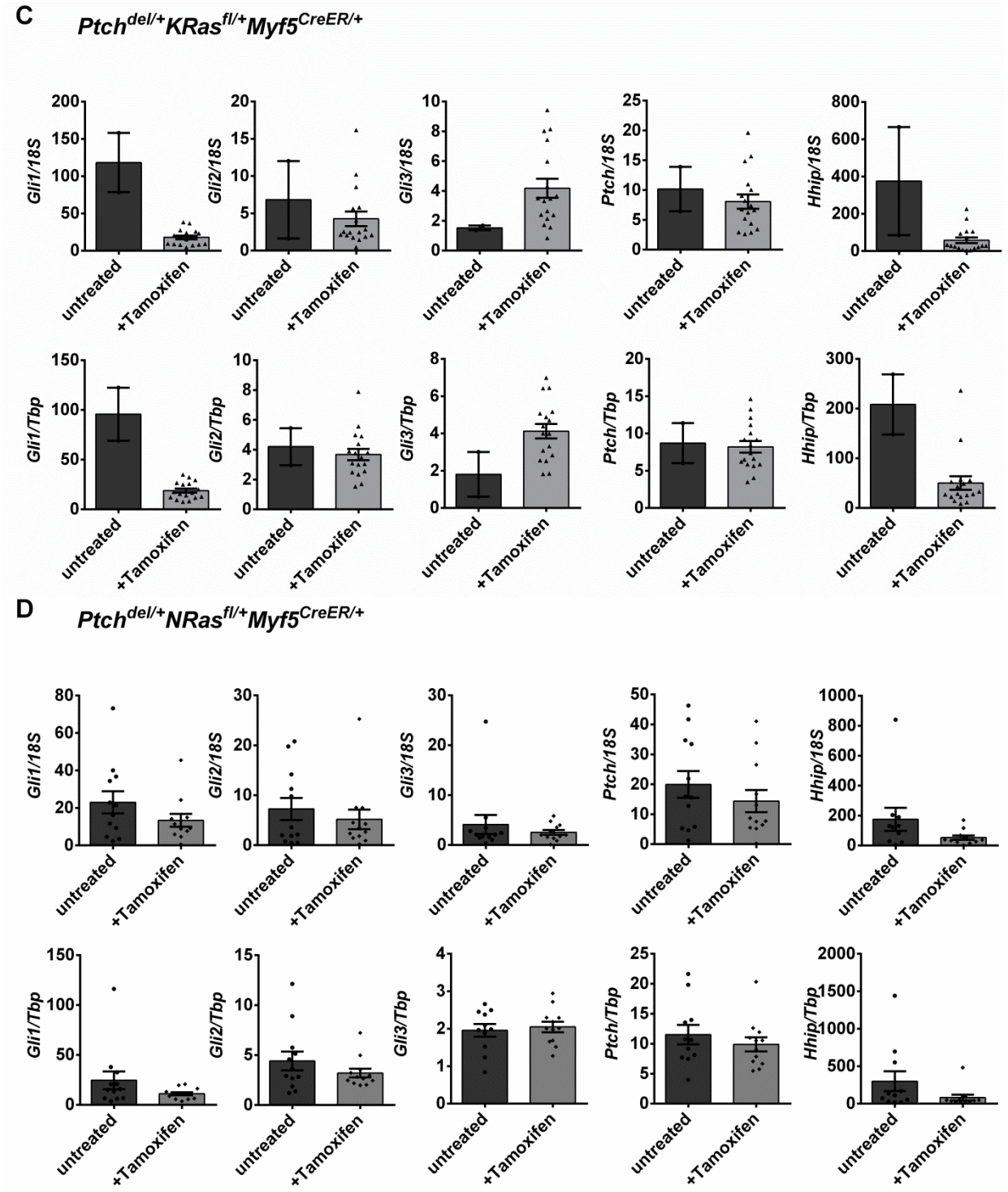

Figure 52: OncRas does not influence the expression of Hh signaling genes in ERMS

ERMS and skeletal muscle (SM) tissue samples were isolated from untreated (n= 9) and tamoxifen-treated (n= 4) *Ptch*$^{del/+}$ mice (A), untreated (n= 7) and tamoxifen-treated (n= 12) *Ptch*$^{del/+}$*HRas*$^{fl/+}$*Myf5*$^{CreER/+}$ mice (B), untreated (n= 2) and tamoxifen-treated (n= 17) *Ptch*$^{del/+}$*KRas*$^{fl/+}$*Myf5*$^{CreER/+}$ mice (C) and untreated (n= 12) and tamoxifen-treated (n= 12) *Ptch*$^{del/+}$*NRas*$^{fl/+}$*Myf5*$^{CreER/+}$ mice (D). Afterwards tissue samples were subjected to RNA isolation, cDNA synthesis and subsequent qRT-PCR analyses of the Hh signaling pathway genes *Gli1*, *Gli2*, *Gli3, Ptch1* and *Hhip*. The data were normalized to *18S rRNA* (18S, upper row) or *Tbp* (lower row) and are shown as fold expression to the expression of the same gene within SM of the respective mouse, which was set to 1. Bars show the mean ± SEM of one cohort and represent measurements in technical triplicates. For statistical analyses non-parametric t-tests (Mann Whitney) were performed in comparison to ERMS from untreated mice of the same cohort.

6.3.2.7 OncNRas, but not oncHRas or oncKRas, increases the expression of muscle differentiation markers in ERMS of *Ptch*$^{del/+}$ mice

Next, the expression of the muscle differentiation marker *MyoD*, *Myogenin*, *Tropomyosin 3* and *Myosin Heavy Chain (MyHC)* was analyzed in SM and ERMS samples by qRT-PCR. The expression of *18S rRNA* or *Tbp* was used for normalization. Again the data are shown in relation to the expression of the respective gene in SM tissue of the same animal that was set to 1. Data are shown for tamoxifen-treated *Ptch*$^{del/+}$ mice (Fig. 53A), *Ptch*$^{del/+}$*HRas*$^{fl/+}$*Myf5*$^{CreER/+}$ (Fig. 53B), *Ptch*$^{del/+}$*KRas*$^{fl/+}$*Myf5*$^{CreER/+}$ (Fig. 53C) and *Ptch*$^{del/+}$*NRas*$^{fl/+}$*Myf5*$^{CreER/+}$ (Fig. 53D) mice in comparison to the untreated controls.

The expression level of *MyoD* and *Myogenin* are reflective for proliferation and differentiation of muscle precursors during myogenesis and are considered to be early differentiation markers. The expression level of *Tropomyosin 3* and *MyHC* indicate differentiation of already established muscle cells and are considered to be late differentiation markers [341]. As demonstrated in Fig. 53A no significant differences in the expression of *MyoD*, *Myogenin, Tropomyosin 3* and *MyHC* mRNA level were detected in RMS from *Ptch*$^{del/+}$ mice after tamoxifen treatment (Fig. 53A) or upon expression of oncHRas or oncKRas (Fig. 53B, Fig. 53C). In contrast, oncNRas significantly increased mRNA expression of *Myogenin* (at least when the data was normalized to *18S rRNA*) and *Tropomyosin 3* (Fig. 53D). This implicates that oncNRas induces a higher differentiation status of ERMS and thus potentially a less aggressive phenotype.

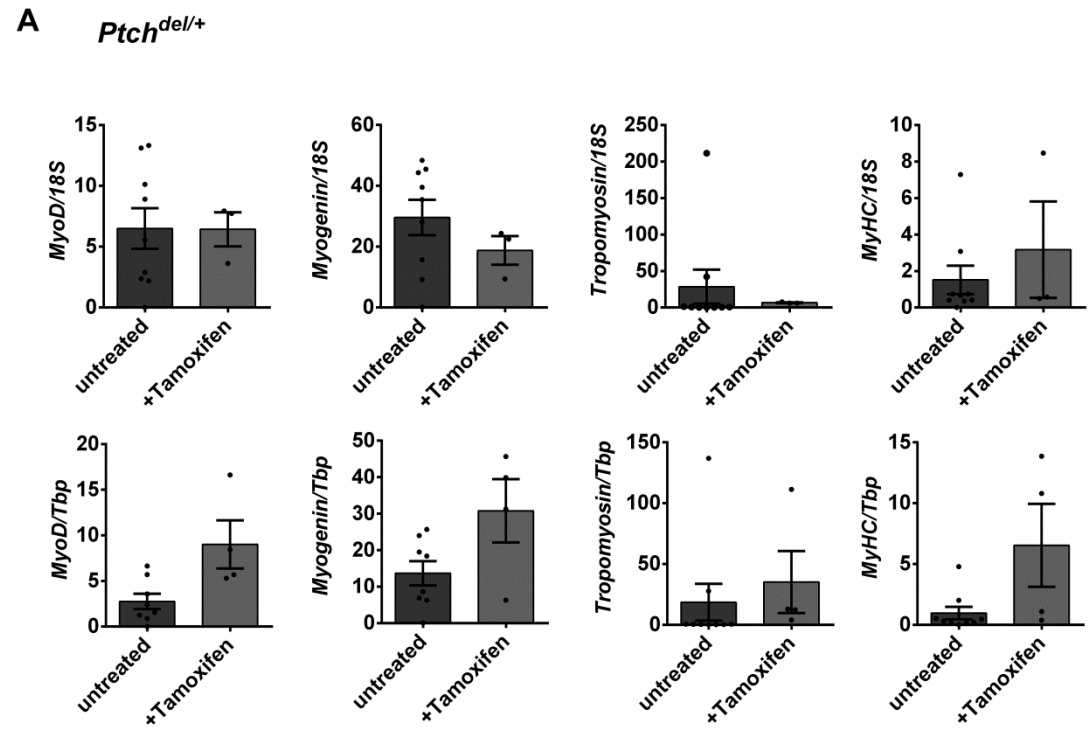

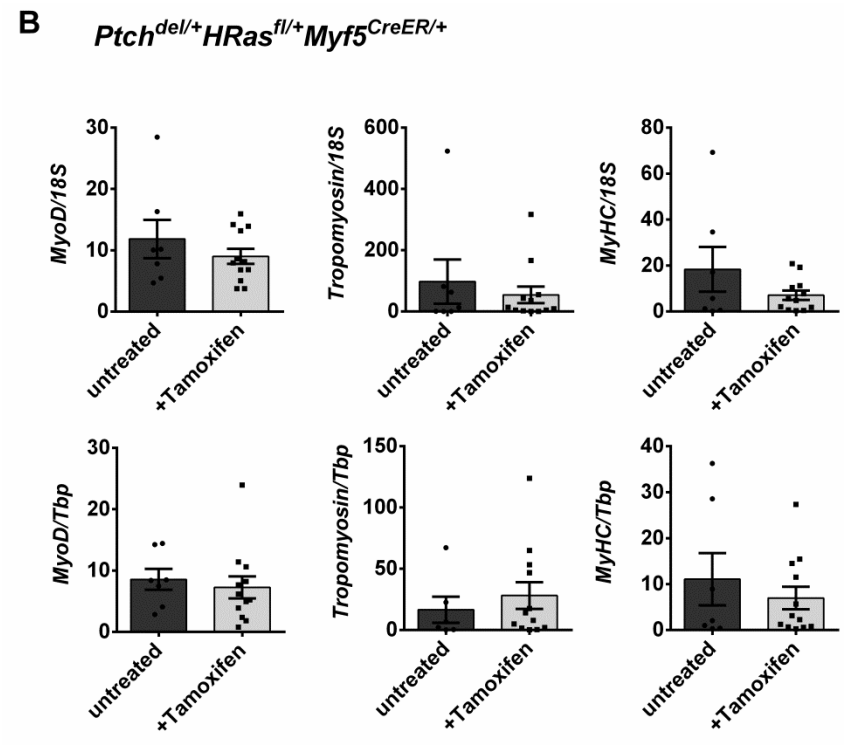
B
Ptch^del/+HRas^fl/+Myf5^CreER/+
MyoD/18S
Tropomyosin/18S
MyHC/18S
MyoD/Tbp
Tropomyosin/Tbp
MyHC/Tbp
untreated
+Tamoxifen

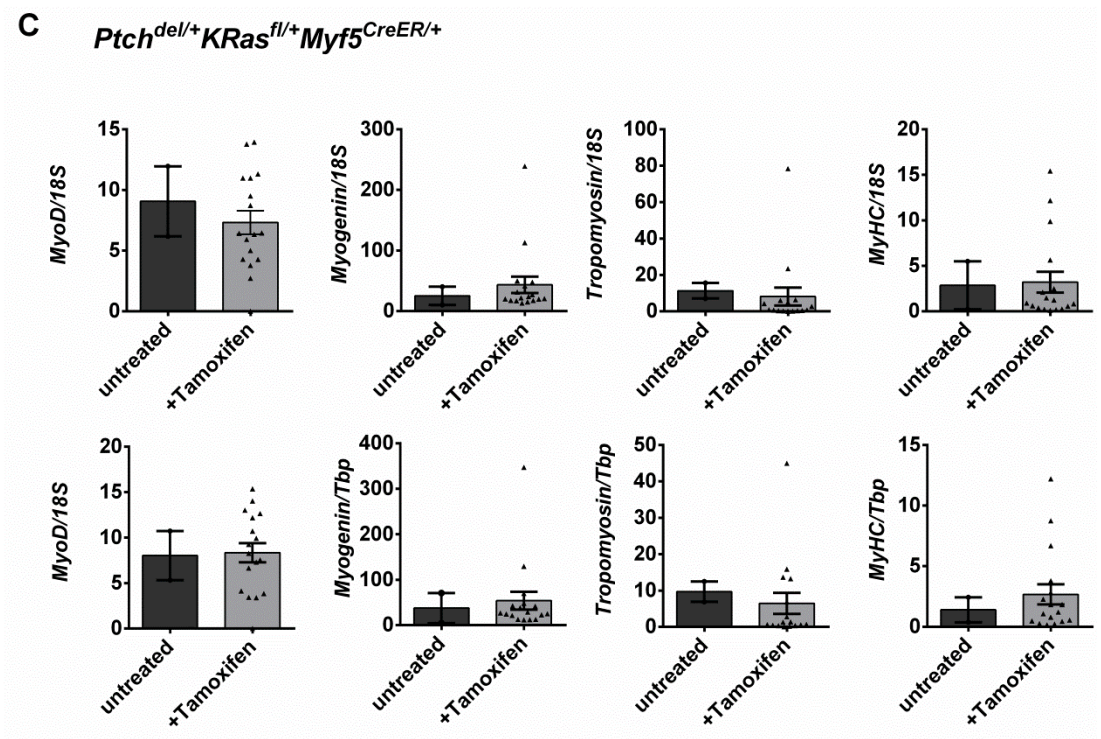
C
Ptch^del/+KRas^fl/+Myf5^CreER/+
MyoD/18S
Myogenin/18S
Tropomyosin/18S
MyHC/18S
MyoD/18S
Myogenin/Tbp
Tropomyosin/Tbp
MyHC/Tbp
untreated
+Tamoxifen

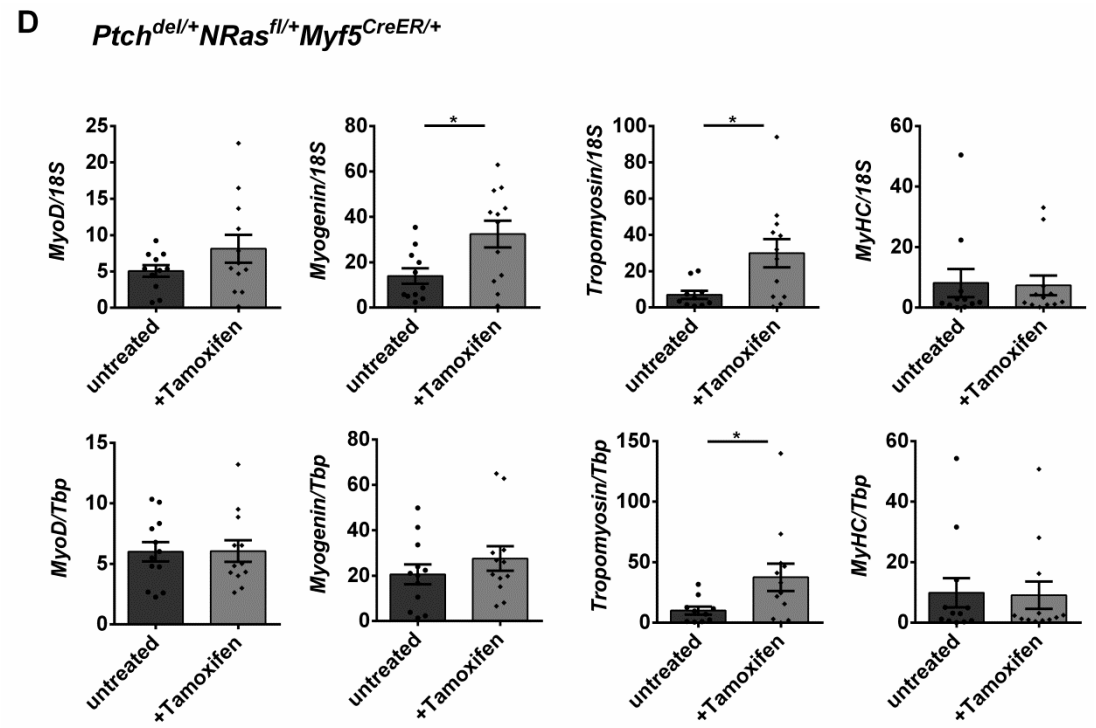

Figure 53: OncNRas induces expression of myogenic differentiation markers in ERMS, whereas oncHRas and oncKRas do not

ERMS and skeletal muscle (SM) tissue samples were isolated from untreated (n= 9) and tamoxifen-treated (n= 4) *Ptch*$^{del/+}$ mice (A), untreated (n= 7) and tamoxifen-treated (n= 12) *Ptch*$^{del/+}$*HRas*$^{fl/+}$*Myf5*$^{CreER/+}$ mice (B), untreated (n= 2) and tamoxifen-treated (n= 17) *Ptch*$^{del/+}$*KRas*$^{fl/+}$*Myf5*$^{CreER/+}$ mice (C) and untreated (n= 12) and tamoxifen-treated (n= 12) *Ptch*$^{del/+}$*NRas*$^{fl/+}$*Myf5*$^{CreER/+}$ mice (D). Afterwards tissue samples were subjected to RNA isolation, cDNA synthesis and subsequent qRT-PCR analyses of the myogenic differentiation markers *MyoD, Myogenin, Tropomyosin 3* and *Myosin Heavy Chain (MyHC).* The data were normalized to *18S rRNA* (18S, upper row) or *Tbp* (lower row) and are shown as fold expression to the expression of the same gene within SM of the respective mouse, which was set to 1. Bars show the mean ± SEM of one cohort and represent measurements in technical triplicates. For statistical analyses non-parametric t-tests (Mann Whitney) were performed in comparison to ERMS from untreated mice of the same cohort. *p<0.05 compared to untreated mice from the respective cohort

When the tumors were reviewed histologically by the pathologist Prof. Dr. med. Hans-Ulrich Schildhaus, no general differences between untreated and tamoxifen-treated tumors were detected. However, single tumor samples expressing oncRas were less differentiated than control tumors. In addition, single ERMS expressing oncKRas showed a more pleomorphic phenotype and more signs of necrosis in comparison to ERMS with oncHRas or oncNRas.

Due to these data, we also examined the expression of the cell cycle marker p21 that influences apoptosis, proliferation and cell cycle arrest [342]. However, no differences between the tumor samples were observed (data not shown).

6.3.2.8 No obvious changes in pAKT, pERK, pS6 or caspase 3 cleavage in oncRas-expressing ERMS of *Ptch*$^{del/+}$ mice

Finally, the protein expression level of phosphorylated Erk, Akt and S6 and cleavage of caspase 3 in SM and ERMS of untreated and tamoxifen-treated *Ptch*$^{del/+}$*HRas*$^{fl/+}$*Myf5*$^{CreER/+}$ and *Ptch*$^{del/+}$*KRas*$^{fl/+}$*Myf5*$^{CreER/+}$ mice was compared. In general, the results were very heterogeneous and no common differences between control ERMS and oncRas-expressing ERMS were detected (Fig. 54A and Fig. 54B).

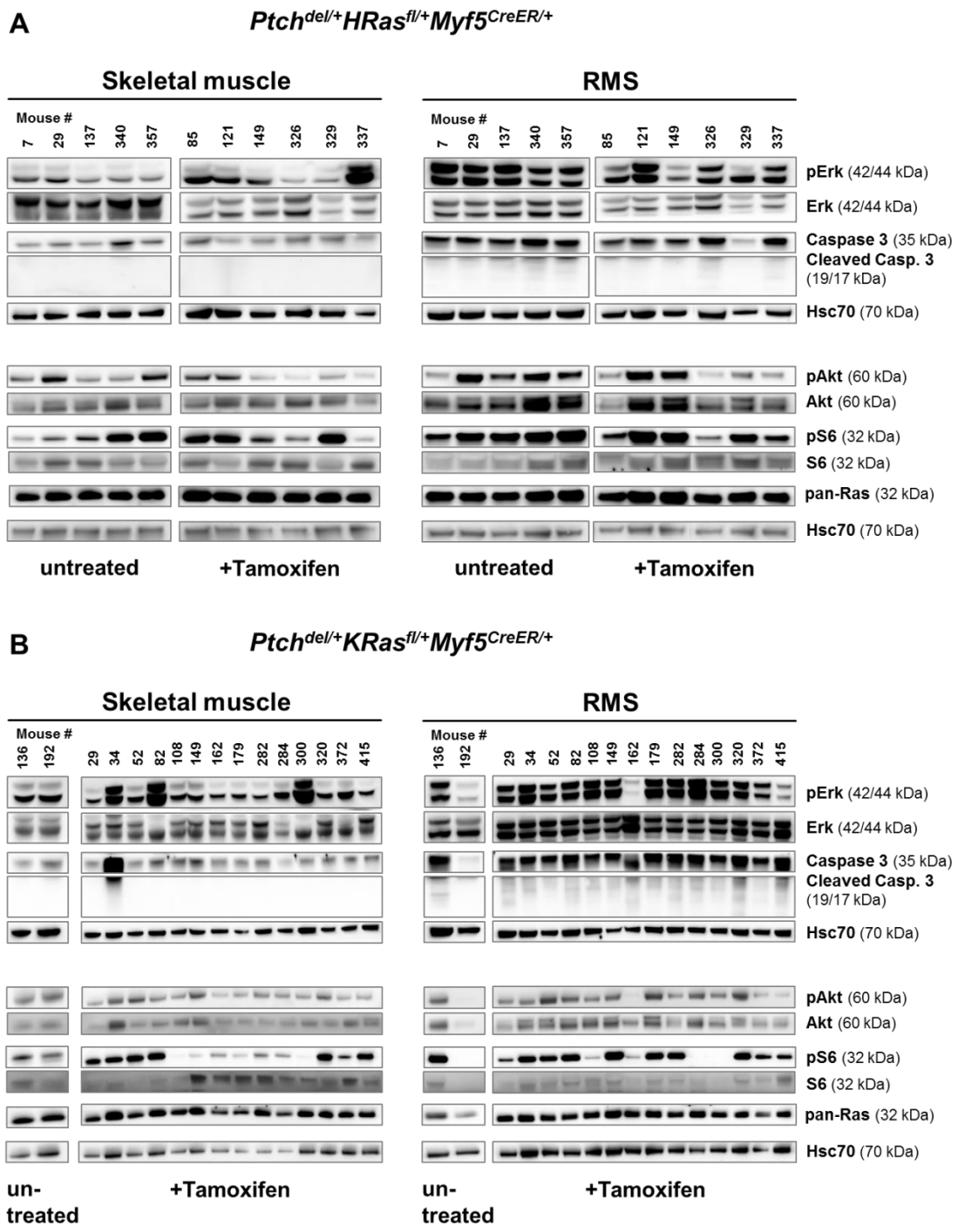

Figure 54: Impact of oncHRas and oncKRas on phosphorylation of Erk, Akt and S6 and caspase cleavage in ERMS of *Ptch*$^{del/+}$ mice

Protein was isolated from Skeletal muscle (SM) and ERMS (RMS) of untreated (n= 5) and tamoxifen-treated (n= 6) *Ptch*$^{del/+}$*HRas*$^{fl/+}$*Myf5*$^{CreER/+}$ (A) and untreated (n= 2) and tamoxifen-treated (n= 14) *Ptch*$^{del/+}$*KRas*$^{fl/+}$*Myf5*$^{CreER/+}$ (B) mice. Afterwards cell lysates were subjected to Western Blot analyses. Phosphorylation of Erk, Akt and S6 and cleavage of caspase 3 were detected using specific primary antibodies. Hsc70 served as reference protein and loading control. The Western Blots are representative for at least two independent technical replicates. Protein names and sizes in kDa are displayed on the right side of the Blots.

Unfortunately, only 2 control ERMS samples from untreated *Ptch*$^{del/+}$*KRas*$^{fl/+}$*Myf5*$^{CreER/+}$ mice were available for the analyses (Fig. 54B). Therefore, it is not possible to judge whether there are real differences between control ERMS and oncKRas-expressing ERMS in this cohort. Nevertheless, the results show that phosphorylation either of Erk, Akt or S6 as well as caspase 3 cleavage is generally higher in tumors compared to normal skeletal muscle.

These results are similar to those shown by our group in 2004 [138]. However, due to these heterogeneous results and the time-consuming procedure the analysis of tissue samples from *Ptch*$^{del/+}$ or *Ptch*$^{del/+}$*NRas*$^{fl/+}$*Myf5*$^{CreER/+}$ mice was set aside.

To sum up, the data within section 6.3.2 highlight that the expression of oncKRas and oncHRas accelerate Hh-associated ERMS formation, whereas oncNRas does not. This was measured by overall and ERMS-free survival, tumor incidence and the proliferation status of the tumors. Interestingly, oncNRas elevated the expression of specific muscle differentiation markers in ERMS, which thus correlates with the lack of increased aggressiveness of the tumors. In addition, oncRas seem to generally decrease the expression of *Gli1* in the tumors. Although the decrease was not significant, these results are similar to human ERMS cell lines.

6.3.3 Activation of oncRas in established ERMS

In a next study, oncRas mutations were induced in already established ERMS of *Ptch*$^{del/+}$ mice. For this purpose, mice with palpable tumors (diameter of approximately 0.5 cm) were subjected to µCT measurement to document the exact tumor size. Then the *Ptch*$^{del/+}$*oncRas*$^{fl/+}$*Myf5*$^{CreER/+}$ mice were injected i.p. 5 times with tamoxifen to induce Cre-mediated recombination and thereby oncRas expression in the tumor. Solvent-treated ERMS-bearing *Ptch*$^{del/+}$*oncRas*$^{fl/+}$*Myf5*$^{CreER/+}$ siblings served as controls. In addition, the ERMS growth of solvent or tamoxifen-treated *Ptch*$^{del/+}$ mice was analyzed. Seven weeks after tamoxifen injection the tumor volume was again analyzed by µCT.

6.3.3.1 OncRas isoforms do not influence growth of established ERMS of *Ptch*$^{del/+}$ mice

As stated above, the tumor volume of *Ptch*$^{del/+}$*oncRas*$^{fl/+}$*Myf5*$^{CreER/+}$ mice were analyzed by µCT before and 7 weeks after induction of oncRas expression. The relative tumor volumes at the first and last µCT measurement are shown in Fig. 55A. The data were plotted on a logarithmic scale with linear trend lines for assumed tumor growth curves. The relative tumor growth, calculated as percentage increase of the tumor volume when comparing the absolute tumor volume at the first and last µCT measurement, is displayed on logarithmic scale as well (Fig. 55B). Solvent-treated mice served as controls.

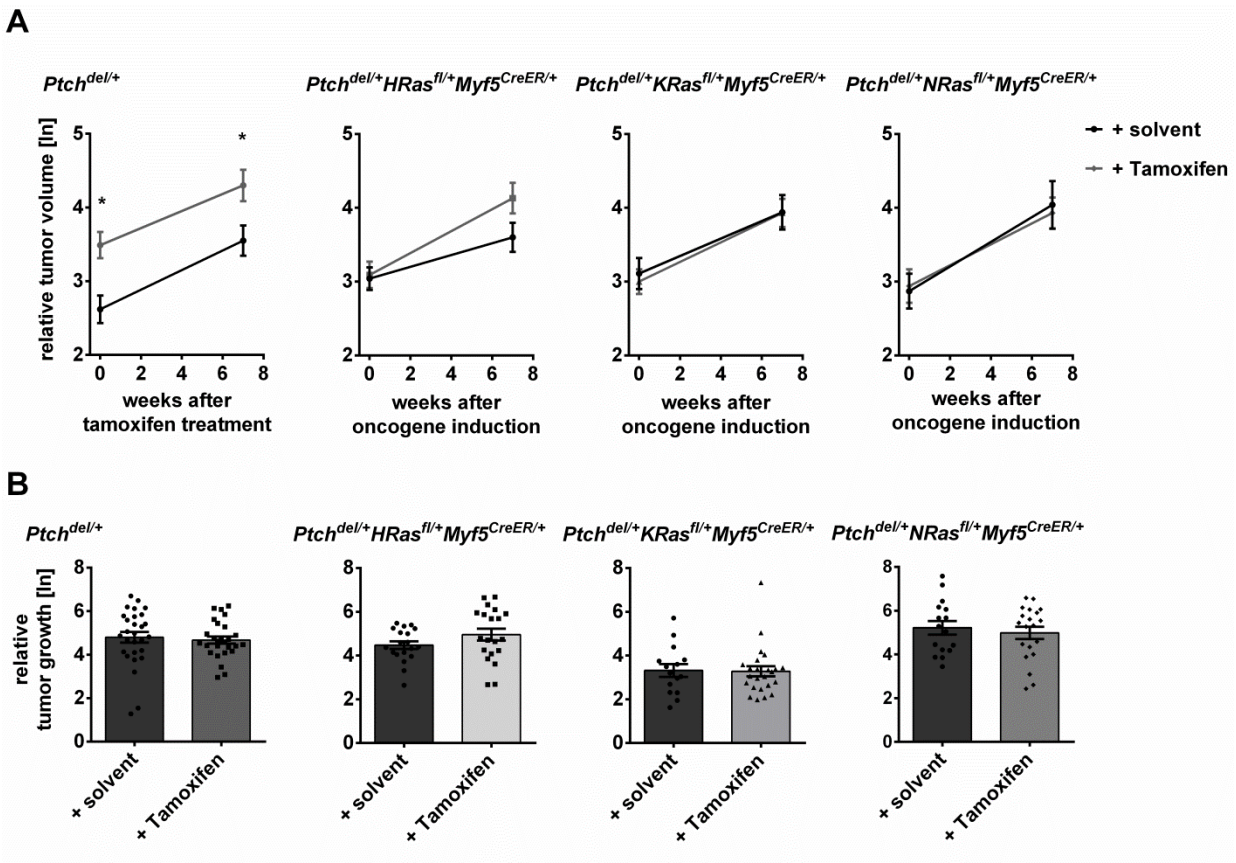

Figure 55: Tamoxifen treatment and oncRAS mutations do not influence growth of established ERMS of *Ptch*$^{del/+}$ mice

Mice with palpable tumors were subjected to µCT measurements before and 7 weeks after solvent or tamoxifen treatment and tumor volume was calculated (A). The relative percentage of increase was additionally calculated for each tumor (B). Solvent or tamoxifen treatment is represented by black or grey graphs, respectively. Multiple ERMS within the same mouse were analyzed as individual tumors. Data analyses was performed for solvent-treated (n= 29 ERMS from 17 mice) or tamoxifen-treated (n= 27 ERMS from 18 mice) *Ptch*$^{del/+}$ mice, solvent-treated (n= 19 ERMS from 12 mice) or tamoxifen-treated (n= 20 ERMS from 11 mice) *Ptch*$^{del/+}$*HRas*$^{fl/+}$*Myf5*$^{CreER/+}$ mice, solvent-treated (n= 15 ERMS from 12 mice) or tamoxifen-treated (n= 24 ERMS from 15 mice) *Ptch*$^{del/+}$*KRas*$^{fl/+}$*Myf5*$^{CreER/+}$ mice and solvent-treated (n= 16 ERMS from 11 mice) or tamoxifen-treated (n= 20 ERMS from 13 mice) *Ptch*$^{del/+}$*NRas*$^{fl/+}$*Myf5*$^{CreER/+}$ mice. The tumor volume at the start and the end of tumor growth measurement and percental increase of each tumor are displayed on a logarithmic scale. For statistical analyses Student's t-tests were performed in comparison to tumor volume from solvent-treated mice of the same cohort.

At the onset of the study the sizes of all RMS of the *Ptch*$^{del/+}$*oncRas*$^{fl/+}$*Myf5*$^{CreER/+}$ cohorts were almost identical. This was different in *Ptch*$^{del/+}$ control mice, in which the mean tumor volume of mice that underwent tamoxifen-injection was accidentally larger. Seven weeks after solvent or tamoxifen treatment, all tumors had grown. However, neither tamoxifen nor oncRas had significantly influenced ERMS growth (Fig. 55A). This is also demonstrated in Fig. 55B, which represents the relative tumor growth of individual tumors. Finally, a comparison between tumors expressing different oncRas isoforms also revealed no significant differences (data not shown).

6.3.3.2 OncRas isoforms do not influence proliferation of established ERMS of *Ptch*$^{del/+}$ mice

Next, all available tumor samples were analyzed for the expression of the proliferation marker Ki67. In all analyzed tumors the mean amount of Ki67$^+$ nuclei ranged between 2.5 % and 4.0 % and did not differ significantly between the cohorts (Fig. 56). Together with the data shown in section 6.3.2.1, the results demonstrate that oncRas isoforms have no impact on proliferation of established ERMS of *Ptch*$^{del/+}$ mice.

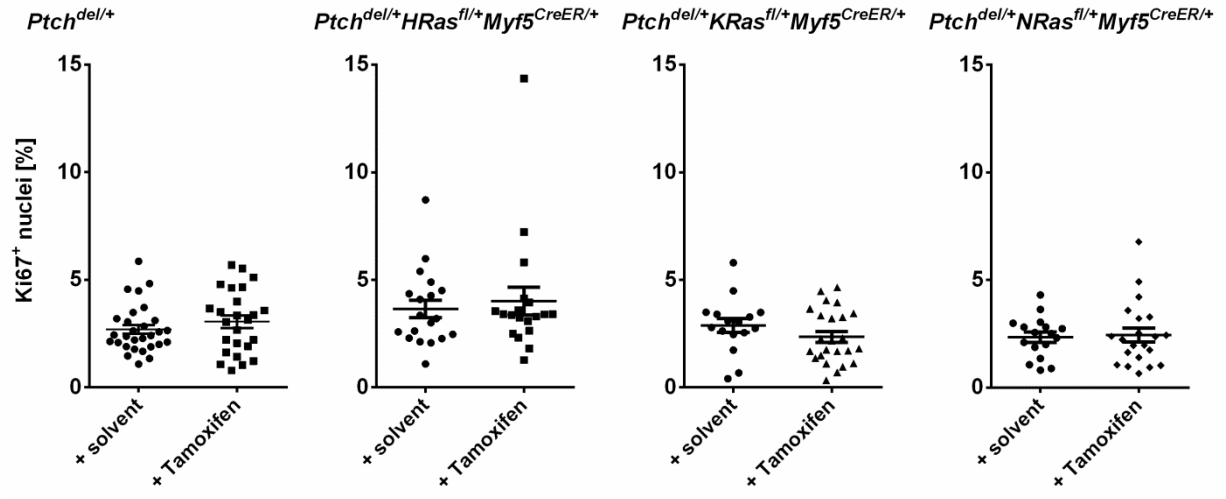

Figure 56: Percentage of Ki67$^+$ nuclei in established ERMS from *Ptch*$^{del/+}$ mice with and without oncRas
ERMS tissue sections from solvent-treated (n= 29 ERMS from 17 mice) and tamoxifen-treated (n= 27 ERMS from 18 mice) *Ptch*$^{del/+}$ mice, solvent-treated (n= 29 ERMS from 12 mice) and tamoxifen-treated (n= 20 ERMS from 11 mice) *Ptch*$^{del/+}$*HRas*$^{fl/+}$*Myf5*$^{CreER/+}$ mice, solvent-treated (n= 15 ERMS from 12 mice) and tamoxifen-treated (n= 24 ERMS from 15 mice) *Ptch*$^{del/+}$*KRas*$^{fl/+}$*Myf5*$^{CreER/+}$ mice and solvent-treated (n= 16 ERMS from 11 mice) and tamoxifen-treated (n= 20 ERMS from 13 mice) *Ptch*$^{del/+}$*NRas*$^{fl/+}$*Myf5*$^{CreER/+}$ mice were stained with a specific antibody against the proliferation marker Ki67. Number of all nuclei and Ki67$^+$ nuclei were counted manually in 6 pictures of each tumor and the percentage of Ki67$^+$ nuclei was calculated. For statistical analyses non-parametric t-tests (Mann Whitney) were performed.

6.3.3.3 OncRas does not change expression of Hh target genes in established ERMS

Afterwards, the expression level of the Hh genes *Gli1* and *Gli2* were analyzed in the SM and ERMS tissue samples (Fig. 57). The expression of *18S rRNA* or *Tbp* was used for normalization.

Again and as already mentioned, the expression of the respective gene in ERMS is shown relative to the expression in SM of the same animal and the expression level of the gene in SM was set to 1. However, the analyses revealed no significant differences in *Gli1* and *Gli2* mRNA expression between ERMS of solvent- or tamoxifen-treated *Ptch*$^{del/+}$*oncRas*$^{fl/+}$*Myf5*$^{CreER/+}$ mice. This was true for *Ptch*$^{del/+}$*HRas*$^{fl/+}$*Myf5*$^{CreER/+}$ (Fig. 57B), *Ptch*$^{del/+}$*KRas*$^{fl/+}$*Myf5*$^{CreER/+}$ (Fig. 57C) and *Ptch*$^{del/+}$*NRas*$^{fl/+}$*Myf5*$^{CreER/+}$ mice (Fig. 57C) and also for *Ptch*$^{del/+}$ mice (Fig. 57A).

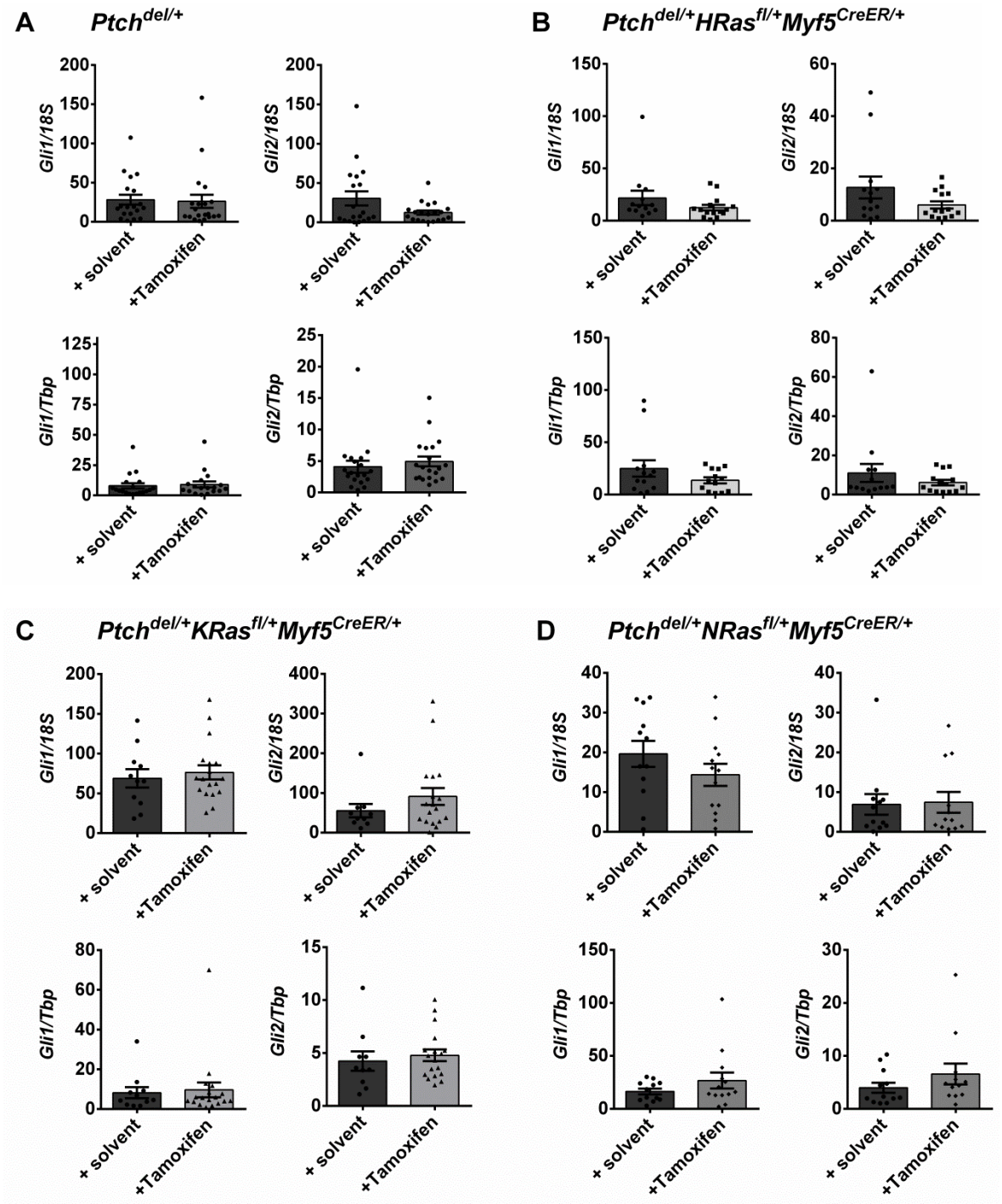

Figure 57: Tamoxifen treatment and oncRas mutations do not influence expression of *Gli1* and *Gli2* in established ERMS in *Ptch*$^{del/+}$ mice

ERMS and skeletal muscle (SM) tissue samples were isolated from solvent-treated (n= 19) and tamoxifen-treated (n= 20) *Ptch*$^{del/+}$ mice (A), solvent-treated (n= 13) and tamoxifen-treated (n=15) *Ptch*$^{del/+}$*HRas*$^{fl/+}$*Myf5*$^{CreER/+}$ mice (B), solvent-treated (n= 11) and tamoxifen-treated (n= 18) *Ptch*$^{del/+}$*KRas*$^{fl/+}$*Myf5*$^{CreER/+}$ mice (C) and solvent-treated (n= 12) and tamoxifen-treated (n=13) *Ptch*$^{del/+}$*NRas*$^{fl/+}$*Myf5*$^{CreER/+}$ mice (D). Afterwards tissue samples were subjected to RNA isolation, cDNA synthesis and subsequent qRT-PCR analyses of the Hh signaling genes *Gli1* and *Gli2.* The data were normalized to *18S rRNA* (18S, left) or *Tbp* (right) and are shown as fold expression to expression of the same gene within SM of the respective mouse, which was set to 1. Bars show the mean ± SEM of one cohort and represent measurements in technical triplicates. For statistical analyses non-parametric t-tests (Mann Whitney) were performed in comparison to RMS from untreated mice of the same cohort.

6.3.3.4 OncRas do not influence expression of muscle differentiation markers in established ERMS

Subsequently, the expression of the muscle differentiation markers *MyoD*, *Myogenin*, *Tropomyosin 3* and *MyHC* were analyzed in SM and ERMS. The analyses were done as described in the previous chapters.

The results show that there was no significant difference between mRNA expression of muscle differentiation markers in established tumors with and without tamoxifen treatment or with and without oncRas expression (Fig. 58A-Fig. 58D).

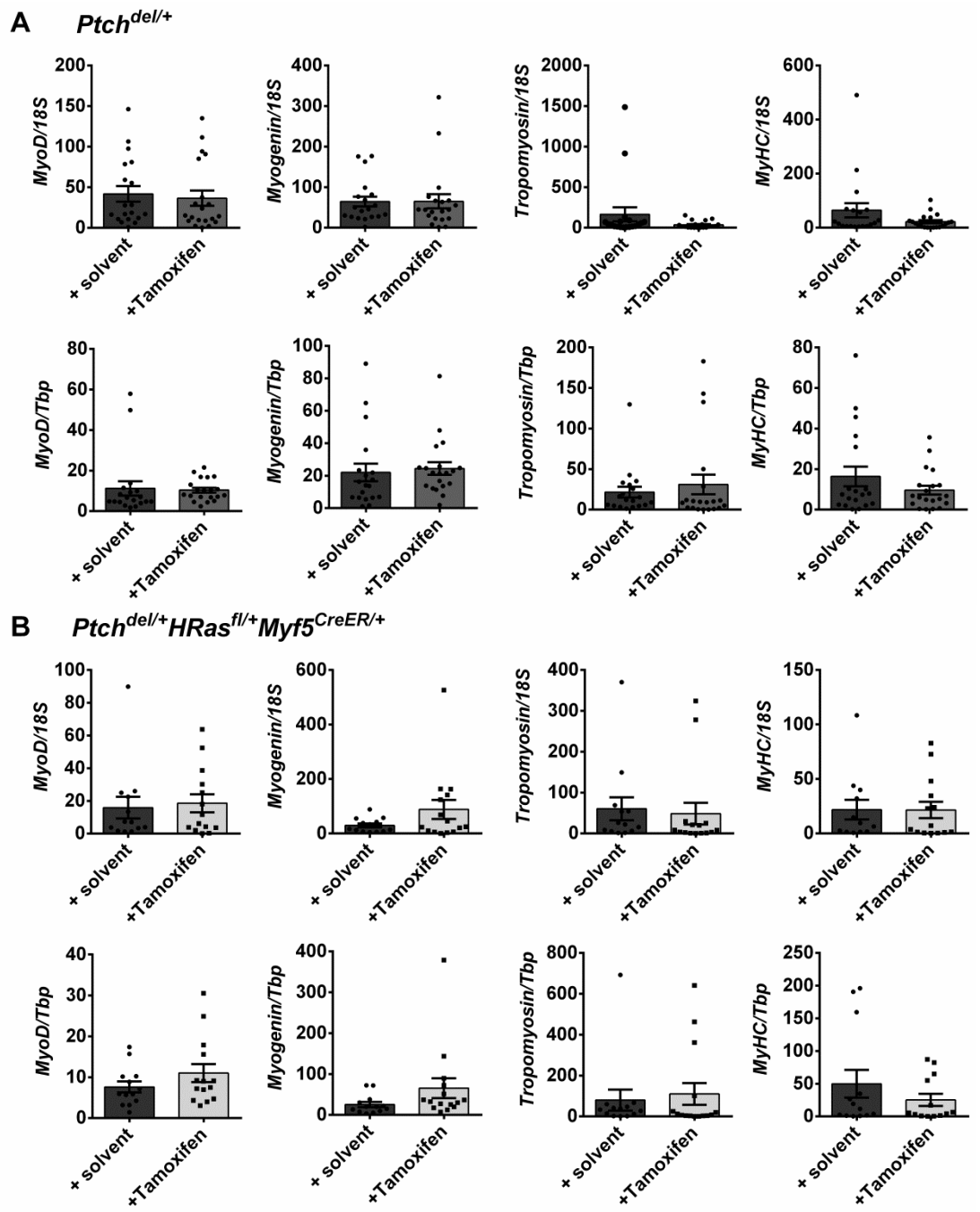

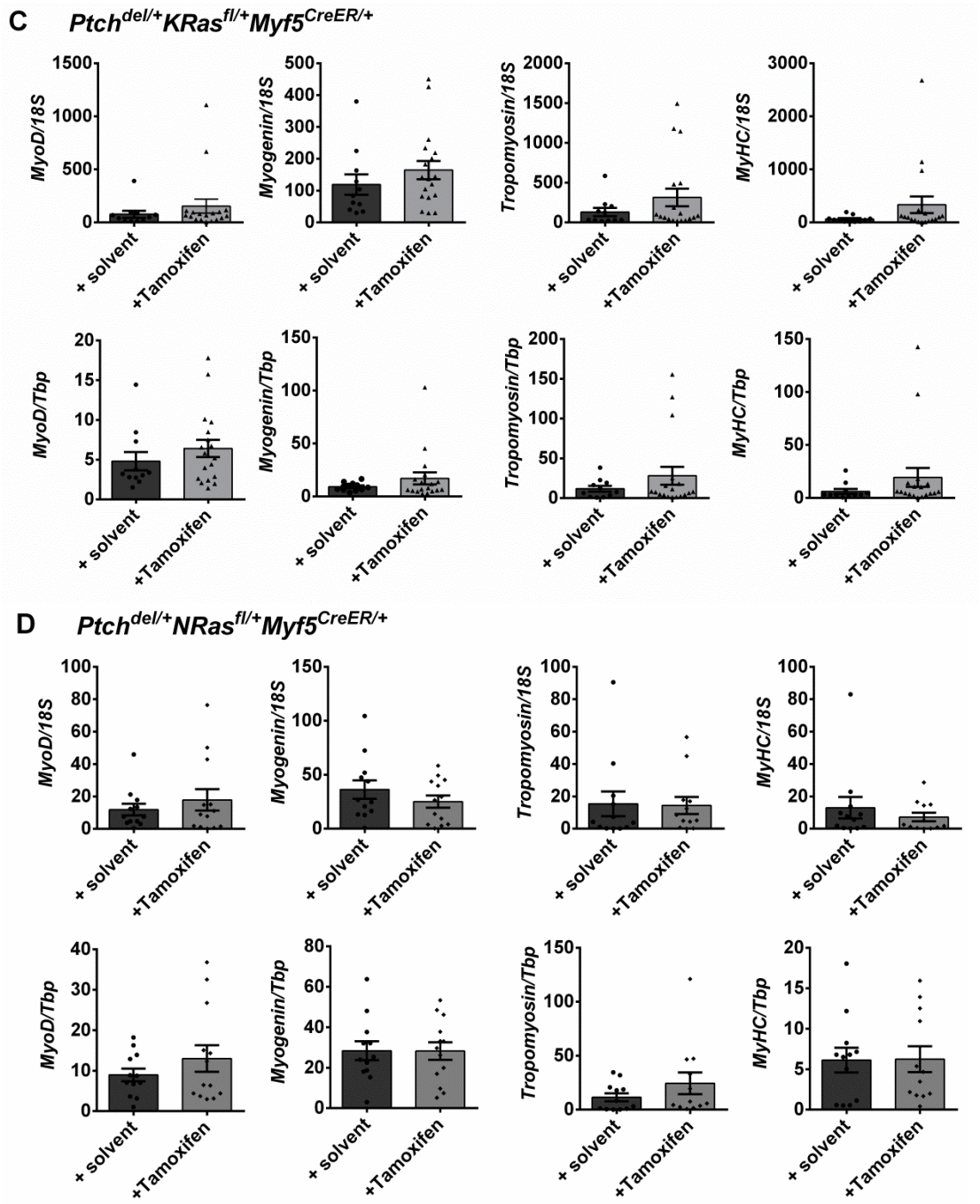

Figure 58: Tamoxifen treatment and oncRas mutations do not influence myogenic differentiation in established ERMS in *Ptch*$^{del/+}$ mice

ERMS and skeletal muscle (SM) tissue samples were isolated from solvent-treated (n= 19) and tamoxifen-treated (n= 20) *Ptch*$^{del/+}$ mice (A), solvent-treated (n= 13) and tamoxifen-treated (n= 15) *Ptch*$^{del/+}$*HRas*$^{fl/+}$*Myf5*$^{CreER/+}$ mice (B), solvent-treated (n= 11) and tamoxifen-treated (n= 18) *Ptch*$^{del/+}$*KRas*$^{fl/+}$*Myf5*$^{CreER/+}$ mice (C) and solvent-treated (n= 12) and tamoxifen-treated (n=13) *Ptch*$^{del/+}$*NRas*$^{fl/+}$*Myf5*$^{CreER/+}$ mice (D). Afterwards tissue samples were subjected to RNA isolation, cDNA synthesis and subsequent qRT-PCR analyses of the myogenic differentiation markers *MyoD, Myogenin, Tropomyosin 3* and *Myosin Heavy Chain (MyHC).* The data were normalized to *18S rRNA* (18S, upper row) or *Tbp* (lower row) and are shown as fold expression to the expression of the same gene within SM of the respective mouse which was set to 1. Bars show the mean ± SEM of one cohort and represent measurements in technical triplicates. For statistical analyses non-parametric t-tests (Mann Whitney) were performed.

To sum up, the results from chapter 6.3.3 indicate that oncRas do not influence growth, proliferation and thus aggressiveness of established ERMS. Furthermore, oncRas isoforms do not influence the expression of different muscle differentiation markers. Moreover, oncRas isoforms do not downregulate targets of Hh signaling such as *Gli1* and *Gli2*.

6.3.4 Chapter summary

Within chapter 6.3 the effect of oncRas on *Hh/Ptch*-driven ERMS in *Ptch*$^{del/+}$ mice is described. The data show that all 3 Ras isoforms are expressed in SM and ERMS of *Ptch*$^{del/+}$ mice and are not mutated. In addition, activity of the *Myf5*^{CreER} driver, which was used to conditionally activate oncRas isoforms, is indeed mainly active in ERMS. This is not only revealed by using *Ptch*$^{del/+}$*Myf5*$^{CreER/+}$*R26R*$^{+/-}$ mice, but also by recombination assays using normal SM and ERMS tissue samples and Ras activity assays using ERMS tissue samples from tamoxifen-treated *Ptch*$^{del/+}$ and *Ptch*$^{del/+}$*oncRas*$^{fl/+}$*Myf5*$^{CreER/+}$ mice.

The results reporting induction of oncRas in ERMS precursor lesions also show that oncKRas and most likely also oncHRas accelerate Hh-associated ERMS formation, whereas oncNRas or tamoxifen itself do not. Thus, tamoxifen-treated *Ptch*$^{del/+}$*HRas*$^{fl/+}$*Myf5*$^{CreER/+}$ and *Ptch*$^{del/+}$*KRas*$^{fl/+}$*Myf5*$^{CreER/+}$ mice show an increased ERMS incidence in comparison to untreated mice and oncKRas mutations even decrease overall survival of *Ptch*$^{del/+}$ mice. OncKRas and oncHRas also increase proliferation of tumor cells, whereas oncNRas does not. However, oncHRas, oncNRas, and most likely also oncKRas (please note that there were only 2 control samples available for analysis), do not significantly influence Hh signaling, although a tendency of downregulation of *Gli1* was detected. OncHRas and oncKRas also do not influence myogenic differentiation of ERMS, whereas oncNRas induces the expression of late myogenic differentiation markers in ERMS. Finally, the analyses of the phosphorylation status of Erk, Akt and S6 in SM and ERMS show very heterogeneous results and no unambiguous influence of the oncRas mutations. However, as already shown by our group before, the phosphorylation of the mentioned proteins was in generally higher in ERMS as in SM (please note that tamoxifen treatment itself did not modulate any of the mentioned parameters).

When expression of oncRas isoforms is induced in established ERMS, the relative tumor volume, relative tumor growth and proliferation of ERMS do not change. On molecular level, oncRas also do not modulate gene expression of *Gli1, Gli2, MyoD*, *Myogenin*, *Tropomyosin 3* and *MyHC*. Together, these results show that oncRas isoforms do not influence any of the analyzed parameters in established ERMS.

In summary, the results highlight that oncHRas and oncKRas mutations affect Hh-associated ERMS precursor lesions but not full-blown ERMS. This was most obvious when analyzing the aggressiveness of the tumors by proliferation, tumor incidence and ERMS-free survival. In contrast, oncNRas never influences these parameters but apparently induces a more differentiated ERMS phenotype. Finally, it has to be mentioned that the results differ from that of cultured ERMS cell lines, in which all oncRAS mutations induces a more aggressive tumor phenotype.

7 Discussion

RMS, the most common malignant soft tissue sarcoma in children, is currently treated with multimodal therapies. However, the efficiency is limited [3,4,13,23,25]. This indicates a need for a deeper understanding of the tumor's pathology to design improved therapies for the patients. Interestingly, human RMS, especially ERMS, frequently show an activation of the HH signaling cascade and mutations within the RAS signaling pathway [6,14,15,141-143]. Furthermore, interactions between these signaling pathways have been discovered [284,343]. In dependency of the cellular context and the experimental setting oncRas signaling can either activate or suppress Hh signaling activity [75,84,295,296,298] (for more details, see section 2.4). This shows a cooperation of both pathways in tumor development, maintenance or progression and led to the conclusion that the RAS and/or the HH signaling pathways could also be interesting therapeutic targets in RMS.

Indeed, recently our group has discovered a crosstalk between both pathways in RMS [299]. As already stated above, ERMS, but not ARMS, strongly express HH target genes and show oncRAS mutations. Therefore, the focus of this thesis was on unravelling the role of oncRAS mutations in regulation of genes implicated in the HH signaling pathway and associated cellular responses of ERMS. Moreover, the impact of a crosstalk between both pathways in ERMS pathogenesis, growth and aggressiveness was analyzed. For this purpose, oncRAS/oncRas signaling was activated in human cell lines derived from sporadic ERMS and in precursor lesions and full-blown ERMS of *Ptch*$^{del/+}$*oncRas*$^{fl/+}$*Myf5*$^{CreER/+}$ mice, which is a *Hh*/*Ptch*-driven ERMS mouse model. Finally, some of the already performed experiments of our group were validated.

7.1 OncRAS mutations stimulate growth of cell lines derived from sporadic ERMS despite inhibition of the major HH target *GLI1*

7.1.1 Differences and limitations of the utilized RMS cell lines

To unravel interactions between HH and RAS signaling, the human ERMS cell lines TE617.T and RUCH-2 and the human ARMS cell line RMS-13, all wt for *RAS*, were stably transduced with different oncRAS^{G12V} isoforms [299]. In addition to experiments with stably transduced cell lines, experiments were performed with the ERMS cell line RD that harbors an endogenous NRAS^{Q61H} mutation [312,326].

After generation of RMS cell lines that stably express oncRAS isoforms, a PCR-based assay detected that a TE617.T clone has been generated, which expresses both oncHRAS and oncNRAS (Fig. 9). This was probably due to a mistake during production. Nevertheless, these cells were analyzed in the same manner as the other cell clones. The analyses

showed that oncRAS-expressing TE617.T cells have an increased RAS activity (Fig. 11), measured by a pulldown assay with beads that are coated with the RBD of RAF-1 kinase that specifically binds to active RAS [344]. However, the cells do not show a strong activation of the MEK/ERK or the PI3K/AKT/mTOR axes (Fig. 10). Whether other RAS target pathways or molecules, such as JNK, p38 and ERK5, are activated by RAS/RAF is currently unknown. In contrast to TE617.T cells, oncRAS-transduced RUCH-2 and RMS-13 cell lines showed elevated levels of pERK (Fig. 10). Since RAS activity in these cells was high, whereas no changes in pAKT or pS6 levels were detected, the MEK/ERK axis must be the main, or at least one of the main active downstream effector of oncRAS in these cell lines.

As described in the results sections, culture experiments showed that the RMS cell lines also respond differently to e.g. ERK inhibition. To a certain extent, these findings can be explained by the origin of these cells and by their specific genetic make-up.

Thus, the TE617.T cell line was originally isolated from the connective tissue of a 1.7-year-old girl with ERMS [315,326]. Although this cell line is wt for *RAS*, it shows protein-changing mutations in M*AP3K14* (different splice variant) and MAP3K1 (threonine deletion at position 949) [345]. The *MAP3K14* gene encodes for the Nuclear factor “kappa-light-chain-enhancer” of activated B-cells (NFκB)-inducing kinase (NIK) and is involved in the alternative NFκB induction through tumor necrosis factor (TNF), CD95 and interleukin (IL)-1 24 [346]. *MAP3K1* encodes for the Mitogen-activated protein kinase kinase kinase 1 (MEKK1) and can activate the ERK and JNK kinase pathways by phosphorylation of MAPK8, MAP2K1 and MAP2K4 [347,348]. The indicated protein changes are not located within structural motifs, like the catalytic domain. Nevertheless, an effect on protein functionality and on the functionality function of the MAPK pathways cannot be excluded. Consequently, these mutations could be responsible for the effects discussed in sections 7.1.2 and 7.1.3.

The RUCH-2 cell line, which is also wt for *RAS*, was established from a primary ERMS of the botryoid type detected in the vagina of a 1.3-year-old girl and shows multiple chromosomal rearrangements [314,315,326,349]. Until now not many characteristics have been described for this cell line [326,349]. However, it is known that RUCH-2 cells originally expressed *MYF3* and *MYF5* but lost the expression of these markers during cell culture [314]. *MYF5,* together with *MYOD* and the calcineurin pathway, is known to activate the transcription of different *MyHC* genes [350]. This could explain why RUCH-2 cells do not express further myogenic markers, like *MyHC1* and *myogenic regulatory factor* (*MRF*). In addition, RUCH-2 cells show increased invasiveness at higher passages [314].

RD is the most commonly used RMS cell line and was isolated from an recurrent pelvic ERMS of a 7-year-old girl [312]. Besides a heterozygous $NRAS^{Q61H}$ mutation, the cells have an amplification of the *MYC* oncogene and a homozygous mutation of *TP53* [16,275,312,326,351]. Thus,

this cell line is a valid model system for ERMS since these characteristic mutations are also observed in human ERMS [14,15,141,231,232,267]. Nevertheless, due to the endogenous *NRAS* mutation, a comparison to “baseline” expression without oncRAS mutation of e.g. *GLI1* was not possible.

The RMS-13 cell line was isolated from a bone marrow metastasis of a 17-year-old boy and shows alveolar histology. The cell line is PAX3:FOXO1a fusion-positive, shows a *TP53* mutation and amplifications of *CDK4* and *GLI1* [313,352,353]. A limitation of the RMS-13 cell line is the fact that until now *RAS* mutations have not been described in fusion-positive ARMS [14,15,141]. Consequently, experiments with the fusion-positive ARMS cell line RMS-13 do not necessarily represent the biology of human ARMS. However, the focus of this thesis was on ERMS and only few experiments were done with this cell line.

Finally, cultured cells poorly mimic the conditions of primary tumors [354]. Hence, all cell culture experiments are limited to the specific characteristics of the utilized cell lines and do not necessarily reflect the situation *in vivo*.

7.1.2 Influence of oncRAS mutations on expression of *GLI1* and the related mechanisms

The data show that oncRAS mutations in general decrease the mRNA expression of the major HH target *GLI1* (Fig. 13). This effect was not only detected in cell culture, but also *in vivo* in transplanted oncRAS-expressing cells (Fig. 37, Fig. 39, Fig. 40). In cultured TE617.T cells the oncH-/NRAS-induced decrease of *GLI1* is dependent on the reference gene. The discrepancy in statistical significance is due to a higher SEM in gene expression of oncH-/NRAS-expressing TE617.T cells after normalization to *18S rRNA* (Fig. 13). Furthermore, an oncRAS-dependent decrease of *GLI1* was observed in RUCH-2 and RMS-13 cells and thereby confirmed previous results [299] (Fig. 13). In xenotransplants, an oncRAS-mediated downregulation of *GLI1* was also observed, which however was very weak and not significant. This effect can be explained by the tumor microenvironment, which is missing in cell culture.

Similar to RMS cell lines, a suppressive effect of oncKRAS on *GLI1* expression has been described for pancreatic cancer cells [84]. However, these findings are in contrast to other studies, which show that oncNRAS or oncHRAS can stimulate expression of *GLI1*. This has been shown in melanoma cells [75]. Additionally, oncHRAS and oncKRAS increase *GLI1* in thyroid cancer cells [298]. This shows that oncRAS-mediated modulation of *GLI1* can have oppositional effects in different tumor entities. Indeed, this is also suggested by the current experiments that show that oncRAS downregulate *GLI1* in RMS cell lines, but not in the MB cell line Daoy.

7.1.2.1 ERMS cell lines do not secrete HH ligands and are not HH-responsive

The ERMS cell lines TE617.T, RUCH-2 and RD generally express *SHH* but were not able to secrete this ligand, regardless if they harbor an oncRAS mutation or not (Fig. 16, Fig. 17 and [299]). In contrast, data published for pancreatic cancer cell lines suggest that onKRAS induces SHH expression and secretion, which results in activation of HH signaling activity in neighboring cells [84]. However, this was not the case in ERMS cell lines. One possible explanation is that cholesterol-dependent binding of SHH to DISP or an autocatalytic cleavage of the HH ligand (that is required for ligand secretion [355]), do not occur in ERMS cell lines. To test this hypothesis, a Western Blot to detect cleaved and precursor HH ligands could be performed with lysates from cells cultured in cholesterol-lacking or cholesterol-supplemented media. An additional explanation could be the lack of extracellular Scube proteins in the used ERMS cell lines. This group of proteins enhances the solubility of the cholesterol-modified HH ligands and is necessary for HH ligand secretion [355]. Western Blot analyses for Scube proteins could shed light on this question. Moreover, it is possible that the SHH protein is degraded in ERMS cell lines and therefore is not secreted. This could be tested in experiments with proteasome inhibitors, e.g. Bortezomib, which then should increase the intracellular level of SHH and could allow for SHH secretion as well.

Vice versa, stimulation with SHH did not significantly activate HH signaling in RUCH-2 cells with and without oncRAS mutation (Fig. 18). This was also seen in RD cells, which neither react to stimulation with SHH-CM nor to the SMO agonist SAG at the level of *GLI1*, *HHIP* or *PTCH* [159]. However, it has been reported that in RD cells, depletion of *IHH* or *DHH* results in a decrease of *GLI1*, whereas SHH downregulation does not affect *GLI1* expression [150]. Therefore, it is possible that IHH and DHH are more important in RMS than SHH. Nevertheless, the current data and data from our group using SMO inhibitors indicate that canonical HH signaling only plays a subordinate role in ERMS cell lines [159,337], regardless if they harbor an oncRAS mutation or not. This is partially conflicting with the expression of IHH and DHH in ERMS [150] (see above) and with other reports, showing that especially ERMS display elevated expression level of *GLI1*, *GLI2*, *GLI3* and *PTCH*, which actually is indicative for an active canonical HH signaling cascade [141,142]. However, HH target gene expression not always stands for an active HH signaling cascade, because the respective genes can also be regulated non-canonically (compare section 2.2.2). Indeed and as recently described by our group, a non-canonical regulation of the HH signaling pathway is supported by the fact that RUCH-2 and RD cells rarely develop cilia [159]. Cilia play a central role in canonical HH signal transduction [356]. Consequently, canonical HH signaling cannot be properly activated in RD and RUCH-2 cells.

7.1.2.2 OncRAS mutations decrease *GLI1*/GLI1 expression via the MEK/ERK axis in ERMS cells

The fact that it is not possible to stimulate or inhibit canonical HH signaling via the PTCH/SMO axis led to the hypothesis that oncRAS isoforms decrease the expression of *GLI1* in a non-canonical i.e. HH/PTCH/SMO-independent manner. Consequently, the expression of *GLI1* was measured in TE617.T and RUCH-2 cell lines with and without oncRAS after application of PI-103, UO126 or SCH772984 (Fig. 21, Fig. 22). Additionally, SCH772984 was applied to RD cells (Fig. 23). Finally, the expression of *GLI1* was measured after incubation of the cells with HhA. Ahead of the experiments, the inhibitor functionality was validated, and results are described and explained in section 6.1.4.

Treatment with HhA failed to decrease *GLI1* in any of the TE617.T cell lines. Similar results have been obtainend in other RMS cell lines [337], including RUCH-2 control cells. Since HhA is a SMO inhibitor, these observations underline the hypothesis, that canonical HH signaling plays only a minor role in ERMS cell lines (see section 7.1.2.1). Likewise, the application of PI-103 did not influence *GLI1* in any of the TE617.T cells. In contrast, treatment with UO126 or SCH772984 resulted in a significant increase of *GLI1* expression in all TE617.T cells. However, this is independent of oncRAS mutations, since the effect was also observed in control TE617.T cells. This might depend on the *MAP3K1* mutation in these cells. Assuming that this mutation is an activating one, this would result in an increased basal activation of ERK and consequently in an ERK-dependent suppression of *GLI1* in TE617.T control cells. The stable transduction with oncRAS isoforms could additionally increase ERK activity and thus strengthen the decrease of *GLI1*. Consequently, the application of SCH772984 would result in an increase of *GLI1* in all TE617.T cells. If this hypothesis is true, it would support the assumption that oncRAS isoforms downregulate *GLI1* expression and thus the HH signaling pathway through activation of the ERK axis.

Indeed, in RUCH-2 cells, in which HhA activates ERK, *GLI1* expression was downregulated. This effect was significant for oncRAS-expressing cells, but was also seen as a trend in wt cells. Nevertheless, downregulation of *GLI1* can also depend on SMO inhibition. Finally, it also can be explained by toxic effects of the drug because the used concentration of 10 µM decreases cell viability (measured by WST-1 assay) of oncRAS-expressing RUCH-2 [299,337]. In contrast, application of HhA to TE617.T cells did not influence cell viability (data not shown). A treatment with PI-103 decreased *GLI1* mRNA expression in RUCH-2 cell lines with and without oncRAS. This indicates that PI3K/mTOR signaling in general activates the expression of *GLI1* in RUCH-2 cells and is not involved in oncRAS-mediated downregulation of *GLI1*. It is possible that PI-103 decreases *GLI1* via AKT or S6, which are downstream of the inhibited kinases PI3K and mTOR. Thus, AKT can inactivate GSK3 and PKA and thereby decrease the inhibitory effects of these kinases on GLI1/2 activity [54,79,357]. In addition, S6

triggers S6K1-dependent phosphorylation of GLI1 and induced the release of GLI1 from SUFU [79]. On the other hand, downregulation of *GLI1* by PI-103 could be a toxic effect, because the same concentration of PI-103 decreased cell viability (measured by WST-1 assay) in oncRAS-expressing RUCH-2 cells [299]. However, because PI-103 also decreases cell viability of TE617.T cells (data not shown), but not the expression of *GLI1* (see above) the latter explanation this is rather unlikely. Finally, inhibition of ERK restored oncRAS-induced downregulation of *GLI1* back to basal level of RUCH-2 control cells. Similar results were obtained on protein level. Thus, oncRAS decreased the GLI1 protein level, which was reversed by ERK inhibition irrespective of the cellular compartment (Fig. 33). This confirms that oncRAS-mediated decrease of *GLI1*/GLI1 can be regulated by ERK in ERMS, which thus is different from pancreatitic ductal epithel cells, in which oncRAS (or at least oncKRAS) stabilizes GLI1 protein [297].

Like in oncRAS-expressing RUCH-2 cells, ERK also inhibited *GLI1* expression in RD cells (Fig. 23). This was supported by the fact that the transcriptional activity of a GLI reporter significantly increased after incubation with SCH772984 (Fig. 32).

Together, these data indicate an ERK-dependent regulation of *GLI1* in RUCH-2 and RD cells. Indeed and as already mentioned, non-canonical interactions between the HH and RAS signaling pathways via the MEK/ERK pathway have been described [71,284,343]. Thus, Gli1 was identified as a potential substrate of Erk and supposedly can be phosphorylated by this kinase in a Mek-dependent manner [286-288]. Therefore it was first hypothesized that ERK regulates *GLI1* through phosphorylation in ERMS and thereby prevents the translocation of the GLI transcrition factors into the nucleus. However, no differences between the GLI level in cytosol and nucleus were observed, at least not in RUCH-2 cells (Fig. 33, Fig. 34). Consequently, the oncRAS-dependent downregulation of GLI1 is most likely not due to the translocation of GLI^A and GLI^R forms into the nucleus. This result is in contrast to findings from melanoma model systems where oncNRAS or oncHRAS stimulate nuclear localization of GLI1 [75]. However, and as already described in the results section, GLI2 and GLI3 protein level were highly variable between biological replicates and were probably not regulated by the oncRAS/ERK axis. Thus, it is possible that GLI1 is selectively degradated by the proteasom in an ERK-dependent manner. This is supported by the finding that the MEK/ERK pathway can lead to selective protein degradation in other cellular settings [187]. To test this hypothesis, expression of GLI proteins in ERMS cell lines should be measured within time row experiments after application of a proteasome inhibitor. Another explanation for the decrease of *GLI1*/GLI1 in oncRAS-expressing RUCH-2 is an ERK-dependent regulation of *GLI1* transcription. This is even more likely than a proteasome-dependent regulation of GLI1, because GLI2 and GLI3 are in most likeliness not regulated by ERK. ERK itself, or its downstream targets ETS-like gene tyrosine kinase 1 (Elk1), c-Fos and c-Jun, that activate

the AP1 transcription factor [358], can regulate transcriptional activity of ERK target genes. However, it remains to be elucidated if the *GLI1* promotor is a direct target of ERK signaling. To confirm this hypothesis, the *GLI1* promotor sequence should be screened for ERK-specific (or Elk1-, c-Fos- c-Jun or AP1-specific) binding sites. Additionally, respective chromatin immunoprecipitation (ChIP) assays can be performed.

7.1.3 Influence of oncRAS mutations on expression of other genes implicated in the HH signaling cascade

In TE617.T cells, there is an insignificant trend for an oncKRAS- or oncH-/NRAS-dependent decrease of *GLI2* or *PTCH*, respectively, without affecting *HHIP* expression level (Fig. 14). ERK inhibits *PTCH* in TE617.T cells irrespective of an oncRAS mutation, whereas its impact in regulation of *GLI2* is not clear-cut (Fig. 24, Fig. 25, Fig. 26). In xenografts derived from TE617.T cells that express oncKRAS or oncH-/NRAS isoforms, the tumorintrinsic expression of *hGLI2* is not affected (Fig. 37). However, this differences might be explained by the presence of tumorextrinsic effects in xenografts through the tumor's micorenvironment.

In RUCH-2 cells, oncRAS isoforms reduce *GLI2* expression without affecting *HHIP* expression level (Fig. 15). Additionally, oncHRAS and oncKRAS increase *PTCH* expression in cultured RUCH-2 cells (Fig. 15) and ERK is not involved in the regulation of *PTCH* expression in this very cell line (Fig. 28, Fig. 29, Fig. 30). However and in contrast to cell cell culture experiments, oncKRAS or oncNRAS did not significantly decrease *hGLI2* in xenografts (Fig. 39, Fig. 40), which might be an effect of the xenograft microenvironment.

GLI1, *PTCH* and *HHIP* are considered to be mammalian HH target genes and *GLI2* is a positive regulator of HH signaling [31,69]. In a canonical regulation of *GLI1* through HH signaling, an oncRAS-dependent decrease of *GLI1* would be probably accompanied by a downregulation of *PTCH*, *HHIP* and also of *GLI2*. However, this was not the case, neither in cell culture nor in xenotransplants derived neither from TE617.T nor in RUCH-2 cells. These observations together with the fact that it is rather impossible to stimulate or to inhibit canonical HH signaling via the PTCH/SMO axis (see also chapter 7.1.2.1) strengthens the hypothesis, that oncRAS isoforms decrease the expression of *GLI1*/GLI1 in a non-canonical i.e. HH/PTCH/SMO-independent manner.

Moreover, the expression of *GLI3* was decreased in an oncNRAS-dependent manner in TE617.T and RUCH-2 cells (Fig. 14, Fig. 15). However and in contrast to *GLI1*, *GLI3* is not a HH target gene. In TE617.T and RUCH-2 cells, the oncNRAS-dependent downregulation of *GLI3* is independent of ERK (Fig. 26, Fig. 30). This is in contrast to RD cells, where ERK inhibits *GLI3* (Fig. 31). The differences between the cell lines might rely on cell line specific mutations (see section 7.1).

Despite a lack of HH ligand secretion, all ERMS cell lines show basal mRNA expression of *SHH*. In oncRAS-transduced TE617.T cell lines the expression of *SHH* was decreased in comparison to control cells (Fig. 14). Additionally, xenografts derived from TE617.T cells with oncKRAS or oncH-/NRAS also showed decreased tumorintrinsic expression of *hSHH*, which was however only significant for oncH-/NRAS tumors (Fig. 37). In general, transcriptional regulation of *SHH* is mechanistically not fully understood. However, it can be mediated via NFκB, which normally induces SHH expression [359-362]. Additionally, it is known that oncRAS isoforms can induce the activation of NFκB through the NIK(MAP3K14)/IKK-pathway [363,364]. In addition, NIK also can influence phosphorylation and thus activity of ERK [365]. The regulation becomes even more complicated because ERK can activate NFκB by IKK [366,367] or inhibit NFκB-driven transcription, which is dependent on the cellular context [368]. Thus, it is possible that the *MAP3K14* (NIK) mutation in TE617.T impairs the activity of both NFκB and ERK, which could also affect SHH expression in a specific, but so far unknown mechanism.

In contrast, RUCH-2 cells show an oncRAS-dependent increase of *SHH* in cell culture (Fig. 15). This similar to pancreatic cancer cells, in which oncKRAS also upregulates the expression of *SHH* [84,295]. Additionally, the data from this work show that this increase is ERK-dependent (Fig. 28, Fig. 29, Fig. 30). This is in line with findings from the literature, in which an enhanced *SHH* expression correlates with the oncRAS mutational status [84,369]. In contrast to the observation in cell culture, xenografts derived from RUCH-2 cells with oncKRAS or oncNRAS show a slightly decreased tumorintrinsic *SHH* expression (Fig. 39, Fig. 40). The discrepancy between *SHH* expression in cell culture experiments and xenografts can also be explained by microenvironmental effects that occur only in the *in vivo* setting. However, it is also possible that this relies on a difference in transcriptional regulation of the *SHH* promotor, which could be different between cultured and transplanted cells.

Despite the tumorintrinsic decrease of *SHH*, tumorextrinsic *mGli2* expression is increased in oncKRAS-expressing RUCH-2 xenografts. This indicates that the transplanted tumor cells may indeed secrete SHH (despite being downregulated). Nevertheless, this is against the finding, that *mGli1* is not upregulated in the tumor stroma and that RUCH-2 cells in general do not secrete SHH. However, and as already mentioned in section 7.1.2.1, it is still possible that RUCH-2 secrete IHH or DHH.

Besides the impact on HH signaling genes, these experiments show that different RAS proteins can have non-redundant (oncNRAS decreases *GLI3* expression in TE617.T and RUCH-2 cells, whereas oncH/-KRAS do not) or partially overlapping functions (both oncHRAS and oncKRAS increase the expression of *PTCH* in RUCH-2 cells) in ERMS cell lines. Isoform-specific functions of RAS proteins have also been described in other tumor entities. It is hypothesized that this is due to the different intracellular distribution of RAS

isoforms or to the induction of different biological responses through diverse downstream effectors [174,208,211-215] (compare also section 2.3.1).

Taken together, these results show that an ERK-dependent downregulation of *GLI1* is a common feature in ERMS cell lines with oncRAS mutation (compare section 7.1.2), whereas the expression of other HH target genes such as *PTCH*, *GLI2* or *HHIP* are either inhibited, activated or not affected by ERK. This depends on the used cell line and on the respective oncRAS isoform. Furthermore, these results are in support of a RAS/ERK-dependent regulation of *GLI1* expression on transcriptional level, which is independent of the SHH/PTCH/SMO/GLI2-3 axis (Fig. 59). One possibility to verify that the oncRAS-dependent regulation of *GLI1* is indeed non-canonical, the experiments could be repeated after inhibition of SUFU, a negative regulator of canonical HH signaling [59].

Finally, the differences between TE617.T, RUCH-2 and RD cell lines are hard to explain. Most likely they depend on the different activation status of the MAPK signaling pathway within the cells. As already mentioned, RD cells and oncRAS-expressing RUCH-2 cells show hyperactive MEK/ERK signaling, whereas oncRAS does not affect phosphorylation of ERK in TE617.T cells. However, TE617.T cells harbor protein-changing mutations in *MAP3K14* and *MAP3K1* [345,349]. These mutations might alter activation of ERK and of JNK, as well as of NFκB. Consequently, it is possible that the effects of oncRAS mutations or of MEK/ERK-inhibition are masked in this very cell line. This also would fit to the observation that oncRAS/MEK/ERK-associated downregulation of *GLI1* in TE617.T is weaker than in the other cell lines (Fig. 13). It is possible that elevated level of pERK were not detected in the TE617.T cell line due to a lack of sensitivity of the Western Blot. Immunoprecipitation of active ERK and *in vitro* kinase activity assays could help to prove this assumption.

The differences between RUCH-2 and RD cell lines in oncRAS-mediated regulation of other HH targets than *GLI1* can also be explained by the mutational status of the cell lines. For example, RD cells harbor a *TP53* mutation [16,275,312,326,351]. In melanoma, p53 can suppress GLI1 activity and *GLI1* expression [72] and a mutation in p53 would consequently increase *GLI1* transcription. On the other hand, MEK and ERK can transcriptionally activate p53 [370,371], which thus may contribute to suppression of *GLI1* transcription. However, the a final statement about the precise role of the p53 tumor suppressor in combination with oncRAS mutations in ERMS cell lines needs further investigations. Nevertheless, mutations such as *TP53* are likely to influence cellular signaling networks and thus may influence the effect of oncRAS mutations in ERMS.

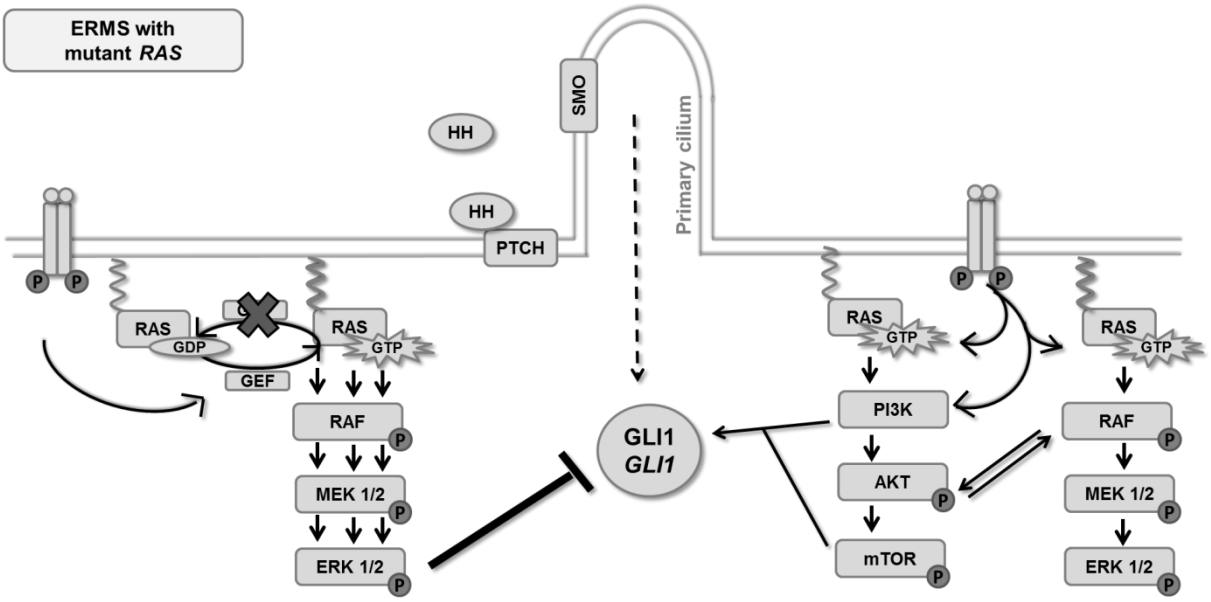

Figure 59: Model system for HH/RAS interactions in ERMS with oncRAS mutations
In ERMS with activating *RAS* mutations, the MEK/ERK axis is hyperactivated and *GLI1*/GLI1 is suppressed. Thereby the MEK/ERK axis negatively regulates *GLI1* transcription and GLI1 protein expression, whereas the PI3K/AKT/mTOR axis may positively regulate *GLI1* transcription (at least in RD and RUCH-2 cells). Canonical HH signaling seems to play a subordinate role in regulation of *GLI1*/GLI1 (dashed arrow). For more details, see text.

7.1.4 Influence of oncRAS mutations on proliferation

OncRas isoforms can promote deregulation of cell cycle progression and can have positive or negative effects on the regulation of apoptosis, depending on the cell type and other cellular factors [184,372]. Additionally, oncRas can promote malignant transformation, characterized by increased proliferation and desensitization to apoptosis [167]. However, oncRAS isoforms do not induce apoptosis and do not alter the cell cycle distribution in RMS cell lines (Fig. 10, Fig. 12). Nevertheless, the cells show a more aggressive phenotype as measured by proliferative capacity in cell culture (Fig. 35 and [299]) and tumorigenicity in xenografts (Fig. 36, Fig. 38 and [299]).

In TE617.T cells oncRAS isoforms strongly induce proliferation (Fig. 35) and additionally increase growth and weight of xenografts (Fig. 36). However, oncRAS do not change the cell cycle distribution in this cell line (Fig. 12). Experiments with RMS-13 cells showed similar results (Fig. 12 and [299]). These inconsistent results (i.e. strongly induced proliferation and tumorigenicity, but lack of increased cell numbers in S phase) can be explained by the fact that the cells were not synchronized ahead of the cell cycle analyses. During synchronization (e.g. by serum starvation or a double thymidine block [373]) distinct subpopulations of cells are in the same stages of the cell cycle, which makes shifts in cell cycle distribution more evident. Additionally, the protocol for cell cycle analyses should be optimized e.g. by inclusion of BrdU labeling of proliferating cells. This would make the analyses more precise because both, cell cycle distribution and the percentage of proliferating cells would be investigated [374].

RUCH-2 cells grow slowly in comparison to other RMS cell lines. OncHRAS or oncKRAS increased proliferation of cultured RUCH-2 cells, whereas oncNRAS had no impact on proliferation (Fig. 35). These findings are in contrast to previous observations from our group, in which oncRAS *decreased* proliferation 24 h after seeding [299]. However and as shown here, at least 48 – 72 hours are needed to detect an oncRAS-dependent increase of proliferation in this very cell line. For oncNRAS transduced cells an even a longer period might be necessary. Indeed, RUCH-2 xenografts that express oncKRAS or oncNRAS show a strongly increased growth and weight of the tumors (Fig. 38). Additionally, RUCH-2 xenotransplants with and without oncRAS mutations grow very efficiently when injected within a matrigel matrix but do marginally grow when injected in PBS (data not shown). This shows that microenvironmental effects might improve attachment and growth of RUCH-2 cells more efficiently than regular cell culture medium. Besides, these experiments verify the finding that oncRAS isoforms can increase proliferation of RUCH-2 cell lines.

It has to be mentioned that oncHRAS-expressing RUCH-2 cells did not grow *in vivo* (Fig. 38). In most likelyhood this observation is due to an experimental failure. However, it could also rely on oncHRAS-induced senescence, which has been described for the $HRAS^{G12V}$ mutation [174]. The induction of senescence occurs downstream of RAS, most likely via the $p53/p19^{ARF}$ and/or $p16^{INK4A}$ pathways and requires a high cell density [185]. Indeed, the cell density of oncHRAS-expressing cells is strongly elevated within tumor xenografts in comparison to cell culture experiments. This might explain why the cells grew normal in cell culture but failed to establish tumors in *Nu/Nu* mice. To test if oncHRAS-induced senescence indeed hampered tumor growth of RUCH-2 cells, tumor sections should be examined for senescence-associated β-galactosidase activity with X-Gal staining. Nevertheless, the transplantation experiment using oncHRAS-transduced RUCH-2 cells needs to be repeated.

The fact that all oncRAS mutations (with the exception of transplanted RUCH-2 oncHRAS cells; see above) strongly induce proliferation despite downregulation of *GLI1*/GLI1 indicate that the HH signaling pathway is not the main driver of growth and aggressiveness of cell lines derived from sporadic ERMS, like the TE617.T and RUCH-2 cells. However, aberrant activation of the HH pathway can drive the initiation of RMS, since heterozygous loss of *PTCH*/*Ptch* in humans and mice is associated with ERMS development [21,99,100,108,324,325,375]. On the other hand, *PTCH* mutations are a very rare event in human ERMS (compare section 2.2.4). Nevertheless, also established ERMS show high level of *GLI1* and *PTCH*, which is indicative for an active HH signaling cascade [141,142]. However, ERMS are insensitive to SMO-inhibition, at least if they do not harbor a mutation in *PTCH* [158,159]. Interestingly, they are sensitive to the specific GLI1/2 inhibitor GANT61, which reduces growth of ERMS cells *in vitro* and *in vivo* [155]. This indicates that GLI transcription factors indeed drive proliferative processes of ERMS, which are most likely independent of canonical HH signaling.

In this context and at the first glance, the results showing that oncRAS-mediated downregulation of *GLI1*/GLI1 is associated with a more aggressive ERMS growth, seems to be paradox. However, it is possible that oncRAS is such a potent proliferative stimulus that permits simultaneous downregulation of other proliferative stimuli such as *GLI1*/GLI1. Of whether a complete GLI1 knockdown would still allow for oncRAS-driven ERMS proliferation is unclear. This question could be answered by transfection of oncRAS-expressing ERMS cell lines with e.g. *GLI1* specific siRNA or by incubation of the cells with GANT61. In addition, it also would be interesting to see if the proliferative capacity of ERMS cell lines is dependent on the MEK/ERK axis. This could be done by inhibition of either MEK or ERK. To exclude that other signaling pathways are involved in cellular proliferation, GLI and MEK/ERK should be blocked simultaneously. If the cells indeed will stop to proliferate upon this co-treatment, this combinatory treatment should be tested as a therapeutic approach in e.g. ERMS xenografts.

Taken together, oncRAS isoforms increase proliferation despite a decrease of *GLI1* expression in human RMS cell lines. In the ERMS cell lines RUCH-2 and RD the downregulation of *GLI1* is ERK-dependent. Hence, it would be highly valuable to analyze, if the occurrence of high RAS signaling with concurrent low HH signaling is a general feature in human ERMS. This could be done by analysis of public available RMS microarray datasets, like [275]. If these data are consistent with the findings from cell culture, ERK should be considered as a target in future therapies in ERMS.

7.2 Specific oncRas mutations can increase *Hh/Ptch*-driven ERMS incidence and growth when expressed at an early tumor stage

To investigate the role of Ras signaling in *Hh/Ptch*-driven ERMS in an immunocompetent *in vivo* setting, a genetic approach was pursued. For this purpose, $Ptch^{del/+}$ mice, which spontaneously develop ERMS-like tumors with active Hh signaling [137,143,323,324], were bred to mice, which conditionally express one of the oncRas genes [220,303,304] and to $Myf5^{CreER}$ deleter mice [305]. The resulting $Ptch^{del/+}oncRas^{fl/+}Myf5^{CreER/+}$ mice were used to study the effect of oncRAS mutations in ERMS precursor lesions and full-blown ERMS.

$Ptch^{del/+}oncRas^{fl/+}Myf5^{CreER/+}$ mice are a suitable model to analyze Ras signaling in *Hh/Ptch*-driven ERMS because their tumors express wt*HRas*, wt*KRas* and wt*NRas* and because the $Myf5^{CreER}$ driver induces tamoxifen-mediated recombination primarily in tumor tissue (Fig. 41, Fig. 42). This was crucial because the expression of *Myf5* is detected in different muscle populations but is also found in non-muscle tissues, such as preadipocytes and neurons [376-378]. Indeed, an experiment utilizing *R26R* reporter mice, which conditionally can express lacZ and basically can show high β-galactosidase activity in every organ of the body [306], indicated that the tamoxifen-inducible $Myf5^{CreER}$ driver is primarily active in tumor tissue without

leakiness. However, the galactosidase activity visualized by X-Gal staining was not as strong as expected from literature [305]. This is most likely due to technical issues, such as an incorrect pH or temperature of the staining solutions or too much contact to light (X-gal is light sensitive). In addition to its ERMS-specificity, the *Myf5*^{CreER} driver also efficiently mediated recombination at the different *Ras* loci (Fig. 43, Fig. 44, Fig. 45). This was important, because differently floxed loci have different sensitivities to cre-mediated recombination [339,379]. Additionally, increased Ras activity was verified in ERMS of tamoxifen-treated *Ptch*$^{del/+}$*oncRas*$^{fl/+}$*Myf5*$^{CreER/+}$ mice (Fig. 46). Finally, the results revealed that tamoxifen itself (which is necessary to activate the CreER) has no impact on median overall survival, median tumor latency time, mean ERMS-free survival, tumor incidence or tumor multiplicity (Fig. 47, Tab. 25). Together, these experiments indicate that *Ptch*$^{del/+}$*oncRas*$^{fl/+}$*Myf5*$^{CreER/+}$ mice are a suitable model to study the role of Ras signaling in *Hh*/*Ptch*-driven ERMS.

7.2.1 Influence of oncRas mutations on *Hh/Ptch*-associated ERMS precursor lesions

The 3 different oncRas mutations were induced in ERMS precursor lesions of *Ptch*$^{del/+}$*oncRas*$^{fl/+}$*Myf5*$^{CreER/+}$ mice. Interestingly, oncHRas and oncKRas mutations influence the tumor growth, whereas oncNRas does not (Fig. 48, Fig. 49, Fig. 50). Thus, activation of oncHRas in ERMS precursor lesions significantly increased the tumor incidence and resulted in a trend to decrease mean ERMS-free survival. It however did not influence median overall survival, median tumor latency time or tumor multiplicity (Fig. 48, Tab. 26). In contrast, activation of oncKRas significantly decreased median overall survival, median tumor latency time, mean ERMS-free survival and significantly increases tumor incidence without affecting tumor multiplicity (Fig. 49, Tab. 27). These data indicate that both oncKRas and oncHRas increase the susceptibility to HH-associated ERMS formation. OncKRas also accelerates ERMS formation and thus decreases the ERMS-free survival and latency time until tumor detection. In addition, it significantly decreased the life span of the mice. At the first glance, these differences point out diverse roles or functions of the HRas and KRas oncogenes in ERMS pathogenesis. One explanation is the different expression levels of the *Ras* genes in SM and ERMS. Thus, the level of *HRas* expression are similar in SM and RMS, whereas *KRas* level are higher in RMS compared to SM (Fig. 42). A higher level of *KRas* most likely also results in a higher level of oncKRas, which may explain the faster tumor growth and thus the reduction of the latency time when the mutation was set in ERMS precursors. However, it is also possible that the tumor detection in the HRas cohort by manual palpation was not as efficient as in the KRas cohort, because several experimenters were involved in the tumor monitoring of the HRas cohort. Indeed, like ERMS with oncKRas, paraffin sections of ERMS with oncHRas show a significantly higher amount of Ki67^{+} nuclei than the respective controls, suggesting a faster tumor growth of the tumors with oncHRas. Unfortunately, the final tumor

size and tumor weight were not recorded, for neither the HRas nor the KRas cohorts. Consequently, it is very hard to judge if an oncKRas mutation indeed induces an ERMS growth behavior that is different from that of an oncHRas mutation. Nevertheless, oncKRas mutations in ERMS precursor lesions decreased the median overall survival, which was not observed in mice with oncHRas mutations. Since other tumors than ERMS occurred at similar numbers in both cohorts and since all mice were sacrificed when the tumors reached a size of 1.5 cm, the data indeed favor the idea that oncKRas induces a more aggressive ERMS growth compared to oncHRas.

In contrast, oncNRas mutations neither influenced median overall survival, median tumor latency time, mean ERMS-free survival, tumor incidence, tumor multiplicity nor proliferation of ERMS in *Ptch*$^{del/+}$ mice (Fig. 50, Tab. 28, Fig. 51). These results highlight that oncNRas mutations, which are set at a very early ERMS stages do not alter the aggressiveness of the tumors. This is similar to a mouse model for colon cancers, where oncKRas stimulates hyperproliferation in the colonic epithelium, whereas oncNRas does not alter the growth properties of the tissue [220]. Similar differences between Ras isoforms have been described for endodermal progenitor cells. OncKRas promotes proliferation and maintains stem cell characteristics and oncHRas promotes differentiation and growth arrest. In contrast, oncNRas has no impact on any of these parameters [221]. These findings underline that different oncRas isoforms can lead to different cellular fates. This can be due to collaborative effects between oncRas and different wtRas proteins, which contribute for the cancer phenotype [236,238,239]. For example, wtKRas and wtNRas promote oncHRas-dependent papilloma development [239]. However, in other settings, wtRas can act as a tumor suppressor in oncRas-expressing cancers [239-241]. An additional explanation for this non-redundant functions is the different cellular compartmentalization of Ras isoforms, which can influence the ability of Ras proteins to activate their downstream effectors [206]. However, whether one of these mechanisms is also involved in ERMS precursor lesions is not clear so far.

The observation that oncNRas mutations do not influence the growth of ERMS precursor lesions of *Ptch*$^{del/+}$ mice is suprising, because in human RMS, oncNRAS mutations are the most frequent RAS mutations [14,15,141]. However, it is possible that this modification is due to species-specific differences in tumor pathobiology. This has already been described for several other knockout mouse models [380]. For example, loss of the *RB* gene is associated with the development of retinoblastomas and osteosarcomas in humans, whereas mice that have a *Rb* deletion fail to develop these tumor types [381]. Similar, *NF2* mutations in humans lead to schwannomas, whereas conventional *Nf2* knockout mice develop osteosarcomas [382].

It has to be noted that tamoxifen-treated *Ptch*$^{del/+}$*oncRas*$^{fl/+}$*Myf5*$^{CreER/+}$ mice show similar tumor incidences (oncHRas: 74 %, oncKRas: 76 %, oncNRas: 71 %). However, whereas the tumor incidence of the oncHRas and oncKRas cohorts differed from the respective control

cohorts, that of the oncNRas cohort did not. This finding indicates that untreated *Ptch*$^{del/+}$*NRas*$^{fl/+}$*Myf5*$^{CreER/+}$ mice develop more tumors than other untreated *Ptch*$^{del/+}$*oncRas*$^{fl/+}$*Myf5*$^{CreER/+}$ mice. The underlying reason in most likelihood is the genetic background of the NRas cohort, since leakiness of the *Myf5*^{CreER} deleter and spontaneous recombination at the floxed *NRas* locus were precluded. In addition, all mice with suspect genotypes or recombination patterns (regardless of which cohort) were excluded from the analyses. The finding that ERMS from tamoxifen-treated *Ptch*$^{del/+}$*NRas*$^{fl/+}$*Myf5*$^{CreER/+}$ mice did not show a higher proliferation rate than ERMS from untreated mice together with the fact that the proliferation rate was similar to untreated *Ptch*$^{del/+}$*HRas*$^{fl/+}$*Myf5*$^{CreER/+}$ and *Ptch*$^{del/+}$*KRas*$^{fl/+}$*Myf5*$^{CreER/+}$ mice (Fig. 51) supports the conclusion that oncNRas mutations do not accelerate formation of (*Ptch/Hh*-associated) ERMS. Hence, the presence of an oncNRas mutation in ERMS does not necessarily reflect the individual tumor's aggressiveness, which could also be true for human tumors. Nevertheless, when considering the high prevalence of NRAS mutations in human ERMS, it is also possible that the *NRas*^{G12D} mutation in the mouse model is simply not functional. However, the fact that tumors, in which the oncNRas mutation was induced with tamoxifen, showed a higher Ras activity than the controls, strongly argues against this assumption (Fig. 46). Furthermore, it is also possible that the expression of the NRas^{Q61H} mutation, which is frequently seen in human ERMS [267], will be a more potent oncogene than the NRas^{G12D} mutation. However, the fact that the expression level of the muscle differentiation markers *Myogenin and Tropomyosin 3* were significantly higher in tamoxifen-treated *Ptch*$^{del/+}$*NRas*$^{fl/+}$*Myf5*$^{CreER/+}$ mice compared to the other cohorts (Fig. 53), strongly argues for the conclusion that oncNRas mutations indeed do not accelerate formation of (*Ptch/Hh*-associated) ERMS, at least in mice. It however induces myogenic differentiation, because myogenin is a reliable and specific marker for rhabdomyoblastic differentiation [383] and *Tropomyosin 3* encodes for a sarcomeric protein implicated in in skeletal muscle cell differentiation [384]. This is not the case for ERMS expressing oncHRas or oncKRas mutations (Fig. 53). Hence, oncNRas mutations may have a different role than oncHRas and oncKRas in ERMS. This would be similar to colonic tumors, in which oncKRas and oncNRas have differential effects on proliferation, differentiation and tumor progression. Thus, expression of oncKRas^{G12D} in the colonic epithelium stimulates hyperproliferation, whereas oncNRas^{G12D} does not alter the growth properties of the epithelium, but is able to confer resistance to apoptosis [220]. If oncNRas indeed has a different function than the other oncRas isoforms in *Ptch/Hh*-associated ERMS, this would be different from fusion-negative RMS cell lines, in which all oncRAS isoforms inhibit myogenic differentiation through an ERK-dependent inhibition of the myogenic transcription factor *MYOG* [385].

7.2.1.1 OncRas mutations do not influence the expression of Hh signaling genes or the phosphorylation status of Erk, Akt and S6 in ERMS

All oncRas-expressing ERMS show a moderate downregulation of *Gli1* when compared to the control. This is similar to cell culture and xenotransplantation experiments discussed in section 7.1.2. However, these results did not reach significance in murine ERMS. Thus, it is rather unlikely that oncRas mutations altered the Hh signaling pathway in the mouse, especially because the expression of *Gli2*, *Gli3*, *Ptch* and *Hhip* was also not modified in SM and RMS tissue samples (Fig. 52). Additionally, the phosphorylation status of Erk, Akt and S6 was very heterogeneous in in ERMS from mice with and without oncRas mutation (Fig. 54). The final statemant from Western Blot analyses, that phosphorylation of these proteins is generally higher in tumors compared to normal skeletal muscle, is similar to findings from the literature [138].

The result that oncRas isoforms rather do not influence Hh signaling or the mRNA expression of Hh signaling members in murine ERMS is in contrast to findings from cultured human ERMS cells. It is possible that this relies on the mutational status of the systems or on the tumor microenvironment. However, it is also possible that oncRas mutations simply do not play a role in regulation of Hh signaling genes in *Hh/Ptch*-associated ERMS. This suggests that the oncRAS-mediated changes of the tumor phenotype must be driven by other molecular mechanisms, which could be analyzed by RNA sequencing (RNAseq) of tumor samples from tamoxifen-treated, solvent-treated and untreated $Ptch^{del/+}oncRas^{fl/+}Myf5^{CreER/+}$ mice.

7.2.2 Influence of oncRas mutations on *Hh/Ptch*-associated full-blown ERMS

The impact of oncRas mutations was also analyzed in full-blown ERMS. For this purpose the expression of oncRas was induced in palpable tumors of $Ptch^{del/+}HRas^{fl/+}Myf5^{CreER/+}$, $Ptch^{del/+}KRas^{fl/+}Myf5^{CreER/+}$ or $Ptch^{del/+}NRas^{fl/+}Myf5^{CreER/+}$ mice. Controls were solvent-treated siblings of the same genotype, solvent-treated or tamoxifen-treated $Ptch^{del/+}$ mice, which all had palpable ERMS of approximately the same size. In this setting, none of the oncRas mutations did influence tumor growth (Fig. 55). OncRas mutations also did not alter proliferation of the tumors (Fig. 56). They also did not modulate the expression of the Hh target genes *Gli1* and *Gli2* (Fig. 57) or of muscle differentiation markers (Fig. 58).

7.2.2.1 Comparison of the role of oncRAS in *Hh/Ptch*-associated ERMS precursor lesions and full-blown ERMS

Together, the data from $Ptch^{del/+}oncRas^{fl/+}Myf5^{CreER/+}$ mice indicate that oncRAS mutations influence growth of *Hh*/*Ptch*-associated ERMS precursor lesion but not of full blown ERMS. This favors the hypothesis that oncRas are early events in ERMS development and that they might be a driver mutation in ERMS. However, oncRAS germline mutations do not predispose mice to the development of ERMS [277]. This strongly argues against the “ERMS-

driver" hypothesis (for further discussion see also section 7.3). In contrast, *Hh/Ptch*-associated ERMS of mice are initiated before birth [386], showing that *Ptch* mutations can be "ERMS-drivers". Nevertheless, in general oncRas mutations also seem to be early events in different other tumor entities. For example, *HRAS* mutations are early events during development and progression of bladder cancer [387]. Additionally, *KRAS* mutations occur in early stages during colorectal carcinoma progression [388]. Likewise, *NRAS* mutations are early events during melanoma development [389].

In contrast to *Hh/Ptch*-driven ERMS precursor lesions, full-blown ERMS do not care about the expression of oncRAS mutations. This indicates that ERMS cells at later stages of tumor progression are insensitive to oncRAS mutations because of their specific genetic make-up. However, it is also possible that this insensitivity is a matter of the used animal model or of e.g. the tumor stem cell population (for further discussion see section 7.3). Finally, it has to mentioned that oncHRas and oncKRas increase ERMS formation from *Hh/Ptch*-associated precursor lesions and increase the proliferative capacity of the tumors, without notably affecting the Hh signaling pathway. This again indicate that HH/Hh signaling is extremely important for growth of *Hh/Ptch*-mutant ERMS.

7.3 Potential roles of active Ras or Hh signaling in ERMS initiation and progression

As stated above, oncRas mutations differently affect aggressiveness of ERMS of $Ptch^{del/+}$ mice, cell culture experiments and xenografts. All oncRAS isoforms increase proliferation and tumorigenicity of cultured cells derived from sporadic ERMS (Fig. 35, Fig. 36, Fig. 38), whereas oncKRas and oncHRas accelerate growth of *Hh/Ptch*-driven ERMS precursor lesions (Fig. 48, Fig. 49) but not of full-blown ERMS (Fig. 55). This indicates that oncRas mutations differently effect diverse developmental stages of ERMS as discussed above.

Similarly, oncRAS mutations inhibit *GLI1* expression in a non-canonical manner in cell lines derived from sporadic ERMS, whereas this is rather not seen in *Hh/Ptch*-associated ERMS of $Ptch^{del/+}$ mice. These findings are summarized in Tab. 29.

Table 29: Overview of oncRas-dependent effects in cell lines derived from sporadic ERMS, *Hh/Ptch*-driven ERMS precursor lesions and full-blown ERMS
This table summarizes the discussed effects of different oncRas isoforms in ERMS. For more details, see sections 7.1 (ERMS cell lines), 7.2.1 (ERMS precursor lesions) and 7.2.2 (full-blown ERMS).
↑: increase; ↓: decrease; ↔: no effect

	ERMS cell lines derived from full-blown sporadic tumors			**ERMS precursor of *Ptch*$^{del/+}$ mice**			**Full-blown ERMS of *Ptch*$^{del/+}$ mice**		
Canonical HH signaling	Sporadic, *Ptch* wt ERMS which do not secrete HH ligands,are not HH-responsive and do not respond to SMO inhibition			*Hh/Ptch*-driven ERMS due to a heterozygous *Ptch* mutation			*Hh/Ptch*-driven ERMS due to a heterozygous *Ptch* mutation; respond to SMO inhibitors		
***RAS/Ras* mutation**	**Onc HRAS**	**Onc KRAS**	**Onc NRAS**	**Onc HRas**	**Onc KRas**	**Onc NRas**	**Onc HRas**	**Onc KRas**	**Onc NRas**
Non-canonical HH signaling	*GLI1*/GLI1 ↓ (ERK-dependent in RUCH-2 and RD)			insignificant oncRas-dependent reduction of *GLI1*			↔		
	PTCH ↑ (RUCH-2)	*GLI3* ↓ (RUCH-2, TE617.T)							
Myogenic differentiation markers	not applicable			↔		↑	↔		
Proliferation	↑ (cell culture, xenografts)			↑		↔	↔		
Overall survival	not applicable			↔	↓	↔	not applicable		
ERMS-free survival	not applicable			↔ (↓)	↓	↔	not applicable		
Tumor incidence	not applicable			↑	↑	↔	not applicable		

One hypothesis for the discrepancy of the role of oncRAS between sporadic and *Hh/Ptch*-driven tumors may be the mode of tumor formation. Whereas *Ptch*$^{del/+}$ mice develop ERMS due to a heterozygous *Ptch* mutation [21], activating mutations in *PTCH* or other genes of the HH pathway are very rare in sporadic ERMS. *PTCH* mutations have been excluded in RD cells and probably also do not occur in TE617.T and RUCH-2 cells [15,142,144,145,147,155]. Therefore, it is possible that the growth of already established *HH/PTCH (Hh/Ptch)*-associated tumors solely depend on active canonical HH/Hh signaling, whereas this pathway rather plays a subsidiary role in ERMS without *PTCH/Ptch* mutations. Indeed, recent work from our lab shows that full-blown *Hh/Ptch*-associated ERMS cells react to SMO inhibitors, whereas those without *PTCH* mutations do not [159]. *Vice versa*, it is possible that *RAS* mutations elicit different cellular responses in ERMS cells with and without *PTCH* mutation. However, this is pure speculation and should be verified by e.g. a *PTCH* knock-down in TE617.T and RUCH-2 cells with and without oncRAS mutations or in the RD cell line. However and as already mentioned above, it is likely that canonical HH signaling plays a

subordinate role in ERMS cell lines, which are wt for *PTCH*. Indeed, oncRAS decrease the expression of the main HH target GLI1/*GLI1* in a non-canonical manner via ERK, whereas cell proliferation is strongly enhanced. This shows that the HH pathway or at least GLI1 is not the main driver of ERMS that are wt for *PTCH*.

The data from the genetic experiments are highly interesting. The findings indicate that oncHRas and oncKRas mutations increase the aggressiveness of Hh-associated ERMS precursor lesions but do not affect proliferation of full-blown ERMS. In contrast, oncNRas does not influence proliferation and aggressiveness of ERMS in any of these settings, while inducing a more differentiated ERMS phenotype when activated in precursor lesion. Together, these findings indicate that oncRAS mutations in different isoforms affect diverse developmental stages of ERMS in a different manner. In the case of the oncNRas mutation it must be noticed that ERMS in the *Ptch*$^{del/+}$ model are derived from Delta1-positive, Myf5-negative, Myogenin-negative and Pax3-negative mesodermal progenitors that can undergo myogenic differentiation but lack stable lineage commitment [386]. Therefore it is possible that oncNRas pushes the cells into myogenic differentiation, whereas oncHRas and oncKRas rather keep the cells in a more undifferentiated stages and push proliferation of the ERMS precursors. The underlying molecular mechanisms must be specific for very early ERMS, because they do not operate at an advanced tumor stage.

In addition, and since *RAS* mutations usually occur at a very early stage during tumor development (see above) it is tempting to speculate that oncRas mutations are driver mutations. Indeed, this also has been suggested for ERMS. For example, oncRas mutations were proposed to be necessary to convert normal primary human skeletal muscle myoblasts into tumorigenic cells mimicking ERMS [278] (compare section 2.3.4). This is in line with genetic syndromes e.g. Costello and Noonan syndrome, in which RAS germline mutations can confer susceptibility to ERMS development [242,243]. However, this is apparently different in the mouse, in which *Ras* germline mutations do not result in ERMS [277]. It is also different from several reports, indicating that *RAS* mutations are rather modifiers in ERMS. Thus microarray-based data of human RMS samples show that an oncRAS signature only occurs in combination with other pathway signatures [275]. Nevertheless, the increased ERMS susceptibility in patients with e.g. Noonan syndrome strongly favors the “driver” hypothesis. However, the Noonan syndrome can be caused by KRAS^{P34R}, KRAS^{D153V} and KRAS^{F156L} mutations in the KRAS protein [256] or by NRAS^{G60E}, NRAS^{T71A}, NRAS^{C101T}, NRAS^{C149T} or NRAS^{G179A} mutations in the NRAS protein [257,390]. These mutations are different from the oncRAS^{G12}, oncRAS^{G13} and oncRAS^{Q61} mutations, which commonly occur in cancer [231,233]. This observation together with the fact, that mice with oncRas mutations alone do not develop ERMS [277], opens the intriguing possibility that the oncRAS mutations found in human sporadic ERMS are not ERMS driver mutations, but rather passenger mutations that,

dependent on the tumor stage or the affected cell subpopulation, can either accelerate or decelerate tumor progression. Indeed, whereas Xia *et al.* [20] and Chen *et al.* [15] reported a worse prognosis in ERMS patients with *RAS* mutations, another study shows the opposite. Martinelli *et al.* showed that gain-of-function mutations within the *RAS* genes occur more frequently in ERMS patients with a better outcome [267]. Similar findings were described for *NRAS* mutations in melanoma patients [391].

Hh/Ptch-associated ERMS of mice are initiated before birth. Thus, deletion of a single copy of the *Ptch* allele at E9.5 results in a tumor incidence of 88% but reaches only 44% and 12% when the *Ptch* allele is inactivated at E11.5 and E13.5, respectively [323]. Similarly, induction of the *Ptch* mutation at E9.5 also significantly shortens ERMS-free survival and results in an increased tumor multiplicity [323]. This shows that *Ptch* mutations are real ERMS-driver mutations, at least in the mouse. In contrast, oncRas mutations rather act as some kind of "passenger" mutations in ERMS. Thus, as already stated several times, they by themselves do not initiate ERMS at least not in the mouse. However, they can accelerate tumor growth or modify tumor differentiation of already initiated ERMS precursor lesions (oncHRas and oncKRas or oncNRas, respectively). They also can accelerate growth of cultured cells or xenotransplants derived from sporadic ERMS. This may indicate that oncRas mutations only affect already initiated ERMS precursor cells and/or cancer stem cells (CSCs) within the heterogeneous tumor mass, whereas they do not affect the total cancer cell population. This would be in line with oncRas being not an ERMS-predisposing mutation, but rather an advantageous mutation for ERMS. As suggested by Kuhner and colleagues, a mutation which is advantageous but not predisposing, is a mutation that occurs in a specific somatic cell and confers growth or survival advantage on this very cell lineage, but otherwise does not contribute to tissue invasion or metastasis [392]. These cells then might be selectively favored early during tumor development. If this hypothesis is true for ERMS, it could explain the high number of tumors showing *RAS* mutations (12 % [16], 22 % [266], 35 % [267] or even 46 % [141] of RMS, depending on the analyzed tumor subset). Intriguingly, one study shows that all ERMS (or fusion-negative RMS) with *RAS* mutations show LOH of 11p15.5 [393]. LOH results from uniparental disomy or trisomy, which is usually associated with loss of maternal genetic information and duplication of the paternal one [394]. 11p15.5 is the location of the *IGF2* gene, which is normally imprinted and is exclusively expressed from the paternal allele. Almost all RMS overexpress IGF2 [395,396], which is due either to loss of imprinting with re-expression of IGF2 from the normally silent maternal allele or results from LOH with paternal disomy or trisomy [4]. Although both, LOH of 11p15.5 and *RAS* mutations, apparently are very early events in the evolutionary history of fusion-negative RMS [393], it is possible that LOH with overexpression of IGF2 is the ERMS initiating event, whereas the *RAS* mutations are advantageous for ERMS growth. This could also be true for recurrent gains of chromosome 8 that are also described for all ERMS with *RAS* mutations [14].

It is also possible that *RAS* mutations only are advantageous when they occur in CSCs. CSCs are tumor cells that show self-renewal, clonal tumor initiation and clonal long-term repopulation potential [397]. In this context, it is interesting to know that Hh and Egfr signaling synergistically contribute to oncogenic transformation of keratinocytes via the Raf/Mek/Erk axis [289-291]. Thereby the pathways synergistically regulate the expression of the stem cell markers *Sox2*, *Sox9* and *Cxcr4*, which are also required for growth of BCC cells [292]. The total number of CSCs is variable depending on the cell line and tissue [397,398]. We assume that human ERMS cell lines derived from sporadic tumors carry a relatively high number of CSCs. Indeed, preliminary data of our lab using the putative CSCs marker in sarcoma cells CD133 [399,400] suggest the presence of a subpopulation with stem cell characteristics. Thus, transduction of ERMS cell lines with oncRAS might have targeted many CSCs, which could be selectively favored during tumor development. This can explain the increased proliferative capacity of oncRAS cells both *in vitro* and *in vivo* settings. However, if this is true, one would expect that targeting oncRas mutations to full-blown ERMS of $Ptch^{del/+}oncRas^{fl/+}Myf5^{CreER/+}$ mice would similarly enhance ERMS growth. However, this was not the case (see section 7.2.2.1). There are several explanations for this circumstance. One the one hand, it is possible that only few CSCs exist in *Hh/Ptch*-driven full-blown ERMS (whereas many of them exist in precursor lesions). On the other hand, it is possible that CSCs do not express Myf5. This would prevent the induction of oncRAS in these cells. Indeed, CSCs usually show a different gene expression pattern than the bulk tumor mass [401-403]. Finally, it is possible that CSCs in *Hh/Ptch*-driven ERMS are solely dependent on Hh signaling (the role of Hh signaling in CSCs is described in detail in [404-406]). To verify the existence of CSCs in full-blown ERMS of $Ptch^{del/+}$ mice the tumors should be screened for CD133, aldehyde dehydrogenase 1 (Aldh1) or Sox2 expression, which are all established CSCs marker for ERMS [400,407-409]. In addition and to verify the hypothesis that oncRAS/oncRas mutations selectively favor ERMS growth from CSCs, but not from the bulk tumor mass, one should test the proliferative capacity of CSCs and the bulk cells from ERMS cell lines with and without oncRas mutation. This can be done by FACS sorting of living cells and by subsequent BrdU proliferation assays and transplantation studies of the sorted cells.

8 Summary and Conclusion

This work aimed for a deeper unterstandig of the role of RAS signaling in *HH/PTCH*-associated ERMS and to study potential interactions between both pathways. Sporadic ERMS usually show high expression of HH target genes despite lacking mutations in members of the HH pathway. However, subsets of ERMS are HH-driven by e.g. inactivating PTCH mutations, which is mimicked in mice that are heterozygous for *Ptch*. The data from this work show that oncRAS mutations decrease the expression of the major HH target *GLI1* in cell lines that are derived from 3 sporadic ERMS and 1 sporadic ARMS. Furthermore, oncRAS can also regulate the expression of *PTCH*, *GLI2*, *GLI3* and *SHH,* which depends on the oncRAS isoform and the individual cell line, e.g. all oncRAS isoforms increase or decrease *GLI2* and *SHH,* respectively, in the ERMS cell line RUCH-2. Although oncRAS mutations can modify the expression of *SHH*, ERMS cell lines (TE617.T, RUCH-2 and RD) are in all likelihood not able to secret HH ligands. They are also not responsive to a HH stimulus. Together with results from other lab members, these data suggest a subordinate role of canonical HH/PTCH/SMO signaling in sporadic ERMS. They also suggest an oncRAS-dependent, non-canonical regulation of *GLI1* expression in ERMS. Indeed, experiments utilizing several kinase inhibitors show that the oncRAS-mediated downregulation of *GLI1* in RD and RUCH-2 cell lines is ERK-dependent. Similarly, oncRAS-mediated downregulation of *GLI1* in TE617.T also depends on ERK. However, this cell line already shows an intrinsic block of *GLI1* expression. Subsequent experiments revealed that the oncRAS/ERK-mediated downregulation of *GLI1* is also seen on protein level and occurs in the cytoplasm and in the nucleus of RUCH-2 cells. This indicates that oncRAS/ERK regulate GLI1/*GLI1* levels probably on transcriptional level. ERK is also involved in regulation of other HH pathway members (*GLI2*, *GLI3*, *PTCH* and *SHH),* which however is cell line-specific and probably depends on the individual genetic make-up of the individual cell line. Further experiments are needed to prove the latter findings and to complete the knowledge about the role of oncRAS isoforms in regulation of HH targets in sporadic ERMS.

Interestingly, oncRAS mutations induce proliferation of TE617.T and RUCH-2 cell lines despite downregulation of *GLI1*/GLI1 in cell culture. Increased proliferation is also seen in the respective xenografts. This indicates that *GLI1*/GLI1, and thereby HH signaling activity, is not associated with the proliferative capacity of ERMS cells. In addition, in xenotransplants, oncRAS isoforms tend to decrease tumorintrinsic *GLI1* and *SHH* expression, whereas tumorextrinsic expression of *Gli2* is increased in oncKRAS-expressing RUCH-2 xenografts. This indicates that specific oncRAS mutations might affect HH signaling activity in the tumor microenvironment. Further experiments are needed to verify this assumption.

In *Hh/Ptch*-driven ERMS of $Ptch^{del/+}$ mice, oncKRas and oncHRas accelerate Hh-associated ERMS formation as measured by tumor incidence, ERMS-free survival and the proliferation marker Ki67, whereas oncNRas does not. However, oncNRas induces myogenic differentiation. This indicates that oncRas isoform have divergent tumorigenic functions. Interestingly, and in contrast to ERMS precursor lesions, oncRas mutations do not influence growth and proliferation of full-blown tumors in $Ptch^{del/+}$ mice. This underlines that oncRas mutations have a different impact on different developmental stages of ERMS. However, irrespective of the tumor developmental stage, oncRas do not significantly modulate Hh signaling in murine ERMS, suggesting that the growth of the tumors depend on the latter pathway.

Since oncRas mutation themselves do not drive ERMS formation but can enhance tumor progression of ERMS precursor lesions, it is possible that oncRAS mutations act as a “passenger“ mutations in ERMS, which modulate the tumor’s aggressiveness at early stages of tumor development. This is different from *Ptch* mutations that drive ERMS formation. In already established ERMS, *Ras* mutations have no or only a minor impact on tumor aggressiveness. However, this has to be verified e.g. by treatment of ERMS-bearing mice with RAS inhibitors.

Finally, the difference of the oncRAS-mediated impact on growth of ERMS cell lines derived from sporadic full-blown ERMS and on full-blown *Hh/Ptch*-driven ERMS must be noted. At the first glance, it is tempting to speculate that this discrepancy is caused by the *Ptch/PTCH* mutation status of the tumors. However, the differences might also dependent on the impact of oncRAS/oncRas mutation on CSC subpopulations within ERMS cell lines and murine ERMS, which again fosters the “passenger” hypothesis. However, this must be elucidated in further experiment.

9 Bibliography

1 Ferrari, A. *et al.* The challenge of the management of adolescents and young adults with soft tissue sarcomas. *Pediatric blood & cancer* **65**, e27013, doi:10.1002/pbc.27013 (2018).

2 Ferrari, A. *et al.* Soft tissue sarcoma across the age spectrum: a population-based study from the Surveillance Epidemiology and End Results database. *Pediatric blood & cancer* **57**, 943-949, doi:10.1002/pbc.23252 (2011).

3 Miller, K. D. *et al.* Cancer treatment and survivorship statistics, 2016. *CA: a cancer journal for clinicians* **66**, 271-289, doi:10.3322/caac.21349 (2016).

4 Dagher, R. & Helman, L. Rhabdomyosarcoma: an overview. *The oncologist* **4**, 34-44 (1999).

5 El Demellawy, D., McGowan-Jordan, J., de Nanassy, J., Chernetsova, E. & Nasr, A. Update on molecular findings in rhabdomyosarcoma. *Pathology* **49**, 238-246, doi:10.1016/j.pathol.2016.12.345 (2017).

6 Parham, D. M. & Barr, F. G. Classification of rhabdomyosarcoma and its molecular basis. *Advances in anatomic pathology* **20**, 387-397, doi:10.1097/PAP.0b013e3182a92d0d (2013).

7 Parham, D. M. & Ellison, D. A. Rhabdomyosarcomas in adults and children: an update. *Arch Pathol Lab Med* **130**, 1454-1465, doi:10.1043/1543-2165(2006)130[1454:RIAACA]2.0.CO;2 (2006).

8 Egas-Bejar, D. & Huh, W. W. Rhabdomyosarcoma in adolescent and young adult patients: current perspectives. *Adolescent health, medicine and therapeutics* **5**, 115-125, doi:10.2147/AHMT.S44582 (2014).

9 Jo, V. Y. & Fletcher, C. D. WHO classification of soft tissue tumours: an update based on the 2013 (4th) edition. *Pathology* **46**, 95-104, doi:10.1097/PAT.0000000000000050 (2014).

10 Fletcher, C. D. M., Bridge, J.A., Hogendoorn, P., Mertens F. *WHO Classification of Tumours of Soft Tissue and Bone - 4th Edition*. (IARC Press, 2013).

11 Dodd, L. G., Bui, M. M. in *Soft tissue and bone pathology* (New York : Demos Medical, United States, 2015).

12 Galili, N. *et al.* Fusion of a fork head domain gene to PAX3 in the solid tumour alveolar rhabdomyosarcoma. *Nature genetics* **5**, 230-235, doi:10.1038/ng1193-230 (1993).

13 Williamson, D. *et al.* Fusion gene-negative alveolar rhabdomyosarcoma is clinically and molecularly indistinguishable from embryonal rhabdomyosarcoma. *J Clin Oncol* **28**, 2151-2158 (2010).

14 Shern, J. F. *et al.* Comprehensive genomic analysis of rhabdomyosarcoma reveals a landscape of alterations affecting a common genetic axis in fusion-positive and fusion-negative tumors. *Cancer discovery* **4**, 216-231, doi:10.1158/2159-8290.CD-13-0639 (2014).

15 Chen, X. *et al.* Targeting oxidative stress in embryonal rhabdomyosarcoma. *Cancer cell* **24**, 710-724, doi:10.1016/j.ccr.2013.11.002 (2013).

16 Shukla, N. *et al.* Oncogene mutation profiling of pediatric solid tumors reveals significant subsets of embryonal rhabdomyosarcoma and neuroblastoma with mutated genes in growth signaling pathways. *Clinical cancer research : an official journal of the American Association for Cancer Research* **18**, 748-757, doi:10.1158/1078-0432.CCR-11-2056 (2012).

17 Hennekam, R. C. Costello syndrome: an overview. *American journal of medical genetics. Part C, Seminars in medical genetics* **117C**, 42-48, doi:10.1002/ajmg.c.10019 (2003).

18 Miller, R. W. & Rubinstein, J. H. Tumors in Rubinstein-Taybi syndrome. *Am J Med Genet* **56**, 112-115, doi:10.1002/ajmg.1320560125 (1995).

19 Ferrari, A. *et al.* Soft-tissue sarcomas in children and adolescents with neurofibromatosis type 1. *Cancer* **109**, 1406-1412, doi:10.1002/cncr.22533 (2007).

20 Xia, S. J., Pressey, J. G. & Barr, F. G. Molecular pathogenesis of rhabdomyosarcoma. *Cancer biology & therapy* **1**, 97-104 (2002).

21 Hahn, H. *et al.* Rhabdomyosarcomas and radiation hypersensitivity in a mouse model of Gorlin syndrome. *Nat Med* **4**, 619-622 (1998).

22 Gorlin, R. J. & Peterson, W. C., Jr. Oral disease in man and animals based on analysis of 1,135 cases in a variety of species. *Arch Dermatol* **96**, 390-403 (1967).

23 Yang, L., Takimoto, T. & Fujimoto, J. Prognostic model for predicting overall survival in children and adolescents with rhabdomyosarcoma. *BMC Cancer* **14**, 654, doi:10.1186/1471-2407-14-654 (2014).

24 Hawkins, D. S., Gupta, A. A. & Rudzinski, E. R. What is new in the biology and treatment of pediatric rhabdomyosarcoma? *Curr Opin Pediatr* **26**, 50-56, doi:10.1097/MOP.0000000000000041 (2014).

25 Hettmer, S. *et al.* Rhabdomyosarcoma: current challenges and their implications for developing therapies. *Cold Spring Harbor perspectives in medicine* **4**, a025650, doi:10.1101/cshperspect.a025650 (2014).

26 Nusslein-Volhard, C. & Wieschaus, E. Mutations affecting segment number and polarity in Drosophila. *Nature* **287**, 795-801 (1980).

27 Lee, J. J., von Kessler, D. P., Parks, S. & Beachy, P. A. Secretion and localized transcription suggest a role in positional signaling for products of the segmentation gene hedgehog. *Cell* **71**, 33-50 (1992).

28 Mohler, J. & Vani, K. Molecular organization and embryonic expression of the hedgehog gene involved in cell-cell communication in segmental patterning of Drosophila. *Development* **115**, 957-971 (1992).

29 Tabata, T., Eaton, S. & Kornberg, T. B. The Drosophila hedgehog gene is expressed specifically in posterior compartment cells and is a target of engrailed regulation. *Genes & development* **6**, 2635-2645 (1992).

30 Teperino, R., Aberger, F., Esterbauer, H., Riobo, N. & Pospisilik, J. A. Canonical and non-canonical Hedgehog signalling and the control of metabolism. *Seminars in cell & developmental biology* **33**, 81-92, doi:10.1016/j.semcdb.2014.05.007 (2014).

31 Ingham, P. W. & McMahon, A. P. Hedgehog signaling in animal development: paradigms and principles. *Genes & development* **15**, 3059-3087, doi:10.1101/gad.938601 (2001).

32 Briscoe, J. & Therond, P. P. The mechanisms of Hedgehog signalling and its roles in development and disease. *Nature reviews. Molecular cell biology* **14**, 416-429, doi:10.1038/nrm3598 (2013).

33 Hammerschmidt, M., Brook, A. & McMahon, A. P. The world according to hedgehog. *Trends Genet* **13**, 14-21 (1997).

34 Heussler, H. S. & Suri, M. Sonic hedgehog. *Mol Pathol* **56**, 129-131 (2003).

35 Vortkamp, A. *et al.* Regulation of rate of cartilage differentiation by Indian hedgehog and PTH-related protein. *Science* **273**, 613-622 (1996).

36 Bitgood, M. J. & McMahon, A. P. Hedgehog and Bmp genes are coexpressed at many diverse sites of cell- cell interaction in the mouse embryo. *Developmental biology* **172**, 126-138 (1995).

37 Pathi, S. *et al.* Comparative biological responses to human Sonic, Indian, and Desert hedgehog. *Mechanisms of development* **106**, 107-117 (2001).

38 Porter, J. A. *et al.* Hedgehog patterning activity: role of a lipophilic modification mediated by the carboxy-terminal autoprocessing domain. *Cell* **86**, 21-34 (1996).

39 Burke, R. *et al.* Dispatched, a novel sterol-sensing domain protein dedicated to the release of cholesterol-modified hedgehog from signaling cells. *Cell* **99**, 803-815 (1999).

40 Porter, J. A. *et al.* The product of hedgehog autoproteolytic cleavage active in local and long-range signalling. *Nature* **374**, 363-366 (1995).

41 Goodrich, L. V., Johnson, R. L., Milenkovic, L., McMahon, J. A. & Scott, M. P. Conservation of the hedgehog/patched signaling pathway from flies to mice: induction of a mouse patched gene by Hedgehog. *Genes & development* **10**, 301-312 (1996).

42 Cohen, M. M., Jr. Hedgehog signaling update. *American journal of medical genetics. Part A* **152A**, 1875-1914, doi:10.1002/ajmg.a.32909 (2010).

43 Cohen, M. M., Jr. The hedgehog signaling network. *American journal of medical genetics. Part A* **123**, 5-28 (2003).

44 Allen, B. L. *et al.* Overlapping Roles and Collective Requirement for the Coreceptors GAS1, CDO, and BOC in SHH Pathway Function. *Dev Cell* **20**, 775-787 (2011).

45 Rohatgi, R., Milenkovic, L. & Scott, M. P. Patched1 regulates hedgehog signaling at the primary cilium. *Science* **317**, 372-376, doi:10.1126/science.1139740 (2007).

46 Hooper, J. E. & Scott, M. P. Communicating with Hedgehogs. *Nature reviews. Molecular cell biology* **6**, 306-317, doi:10.1038/nrm1622 (2005).

47 Alcedo, J., Ayzenzon, M., Von Ohlen, T., Noll, M. & Hooper, J. E. The Drosophila smoothened gene encodes a seven-pass membrane protein, a putative receptor for the hedgehog signal. *Cell* **86**, 221-232 (1996).

48 Ruiz i Altaba, A., Mas, C. & Stecca, B. The Gli code: an information nexus regulating cell fate, stemness and cancer. *Trends in cell biology* **17**, 438-447, doi:10.1016/j.tcb.2007.06.007 (2007).

49 Aberger, F. & Ruiz, I. A. A. Context-dependent signal integration by the GLI code: the oncogenic load, pathways, modifiers and implications for cancer therapy. *Seminars in cell & developmental biology* **33**, 93-104, doi:10.1016/j.semcdb.2014.05.003 (2014).

50 Lee, R. T., Zhao, Z. & Ingham, P. W. Hedgehog signalling. *Development* **143**, 367-372, doi:10.1242/dev.120154 (2016).

51 Pasca di Magliano, M. & Hebrok, M. Hedgehog signalling in cancer formation and maintenance. *Nat Rev Cancer* **3**, 903-911 (2003).

52 Rubin, L. L. & de Sauvage, F. J. Targeting the Hedgehog pathway in cancer. *Nature reviews. Drug discovery* **5**, 1026-1033, doi:10.1038/nrd2086 (2006).

53 Hui, C. C. & Angers, S. Gli proteins in development and disease. *Annual review of cell and developmental biology* **27**, 513-537, doi:10.1146/annurev-cellbio-092910-154048 (2011).

54 Niewiadomski, P. *et al.* Gli protein activity is controlled by multisite phosphorylation in vertebrate Hedgehog signaling. *Cell reports* **6**, 168-181, doi:10.1016/j.celrep.2013.12.003 (2014).

55 Jia, J. Phosphorylation regulation of Hedgehog signaling. *Vitamins and hormones* **88**, 253-272, doi:10.1016/B978-0-12-394622-5.00011-0 (2012).

56 Pan, Y., Bai, C. B., Joyner, A. L. & Wang, B. Sonic hedgehog signaling regulates Gli2 transcriptional activity by suppressing its processing and degradation. *Molecular and cellular biology* **26**, 3365-3377, doi:10.1128/MCB.26.9.3365-3377.2006 (2006).

57 Buttitta, L., Mo, R., Hui, C. C. & Fan, C. M. Interplays of Gli2 and Gli3 and their requirement in mediating Shh-dependent sclerotome induction. *Development* **130**, 6233-6243, doi:10.1242/dev.00851 (2003).

58 Bai, C. B., Stephen, D. & Joyner, A. L. All mouse ventral spinal cord patterning by hedgehog is Gli dependent and involves an activator function of Gli3. *Dev Cell* **6**, 103-115 (2004).

59 Cheng, S. Y. & Yue, S. Role and regulation of human tumor suppressor SUFU in Hedgehog signaling. *Adv Cancer Res* **101**, 29-43, doi:10.1016/S0065-230X(08)00402-8 (2008).

60 Ingham, P. W. Hedgehog signaling. *Cold Spring Harbor perspectives in biology* **4**, doi:10.1101/cshperspect.a011221 (2012).

61 Wang, B., Fallon, J. F. & Beachy, P. A. Hedgehog-regulated processing of Gli3 produces an anterior/posterior repressor gradient in the developing vertebrate limb. *Cell* **100**, 423-434 (2000).

62 Goetz, S. C., Ocbina, P. J. & Anderson, K. V. The primary cilium as a Hedgehog signal transduction machine. *Methods Cell Biol* **94**, 199-222, doi:10.1016/S0091-679X(08)94010-3 (2009).

63 Tukachinsky, H., Lopez, L. V. & Salic, A. A mechanism for vertebrate Hedgehog signaling: recruitment to cilia and dissociation of SuFu-Gli protein complexes. *J Cell Biol* **191**, 415-428, doi:10.1083/jcb.201004108 (2010).

64 Ruiz i Altaba, A. Hedgehog signaling and the Gli code in stem cells, cancer, and metastases. *Science signaling* **4**, pt9, doi:10.1126/scisignal.2002540 (2011).

65 Scales, S. J. & de Sauvage, F. J. Mechanisms of Hedgehog pathway activation in cancer and implications for therapy. *Trends Pharmacol Sci* (2009).

66 Hahn, H. *et al.* Patched target Igf2 is indispensable for the formation of medulloblastoma and rhabdomyosarcoma. *The Journal of biological chemistry* **275**, 28341-28344, doi:10.1074/jbc.C000352200 (2000).

67 Pandolfi, S. & Stecca, B. Cooperative integration between HEDGEHOG-GLI signalling and other oncogenic pathways: implications for cancer therapy. *Expert reviews in molecular medicine* **17**, e5, doi:10.1017/erm.2015.3 (2015).

68 Lee, J., Platt, K. A., Censullo, P. & Ruiz i Altaba, A. Gli1 is a target of Sonic hedgehog that induces ventral neural tube development. *Development* **124**, 2537-2552 (1997).

69 Stecca, B. & Ruiz, I. A. A. Context-dependent regulation of the GLI code in cancer by HEDGEHOG and non-HEDGEHOG signals. *J Mol Cell Biol* **2**, 84-95 (2010).

70 Robbins, D. J., Fei, D. L. & Riobo, N. A. The Hedgehog signal transduction network. *Science signaling* **5**, re6, doi:10.1126/scisignal.2002906 (2012).

71 Aberger, F., Kern, D., Greil, R. & Hartmann, T. N. Canonical and noncanonical Hedgehog/GLI signaling in hematological malignancies. *Vitamins and hormones* **88**, 25-54, doi:10.1016/B978-0-12-394622-5.00002-X (2012).

72 Stecca, B. & Ruiz i Altaba, A. A GLI1-p53 inhibitory loop controls neural stem cell and tumour cell numbers. *Embo J* **28**, 663-676 (2009).

73 Abe, Y. *et al.* Hedgehog signaling overrides p53-mediated tumor suppression by activating Mdm2. *Proc Natl Acad Sci U S A* **105**, 4838-4843, doi:10.1073/pnas.0712216105 (2008).

74 Dennler, S. *et al.* Induction of sonic hedgehog mediators by transforming growth factor-beta: Smad3-dependent activation of Gli2 and Gli1 expression in vitro and in vivo. *Cancer research* **67**, 6981-6986, doi:10.1158/0008-5472.CAN-07-0491 (2007).

75 Stecca, B. *et al.* Melanomas require HEDGEHOG-GLI signaling regulated by interactions between GLI1 and the RAS-MEK/AKT pathways. *Proc Natl Acad Sci U S A* **104**, 5895-5900 (2007).

76 Riobo, N. A., Lu, K., Ai, X., Haines, G. M. & Emerson, C. P., Jr. Phosphoinositide 3-kinase and Akt are essential for Sonic Hedgehog signaling. *Proc Natl Acad Sci U S A* **103**, 4505-4510 (2006).

77 Katoh, Y. & Katoh, M. Integrative genomic analyses on GLI1: positive regulation of GLI1 by Hedgehog-GLI, TGFbeta-Smads, and RTK-PI3K-AKT signals, and negative regulation of GLI1 by Notch-CSL-HES/HEY, and GPCR-Gs-PKA signals. *International journal of oncology* **35**, 187-192 (2009).

78 Zhou, J. *et al.* Non-canonical GLI1/2 activation by PI3K/AKT signaling in renal cell carcinoma: A novel potential therapeutic target. *Cancer letters* **370**, 313-323, doi:10.1016/j.canlet.2015.11.006 (2016).

79 Wang, Y. *et al.* The crosstalk of mTOR/S6K1 and Hedgehog pathways. *Cancer cell* **21**, 374-387, doi:10.1016/j.ccr.2011.12.028 (2012).

80 Agarwal, N. K., Qu, C., Kunkalla, K., Liu, Y. & Vega, F. Transcriptional regulation of serine/threonine protein kinase (AKT) genes by glioma-associated oncogene homolog 1. *The Journal of biological chemistry* **288**, 15390-15401, doi:10.1074/jbc.M112.425249 (2013).

81 Ehe, B. K. *et al.* Identification of a DYRK1A-mediated phosphorylation site within the nuclear localization sequence of the hedgehog transcription factor GLI1. *Biochemical and biophysical research communications* **491**, 767-772, doi:10.1016/j.bbrc.2017.07.107 (2017).

82 Mao, J. *et al.* Regulation of Gli1 transcriptional activity in the nucleus by Dyrk1. *The Journal of biological chemistry* **277**, 35156-35161, doi:10.1074/jbc.M206743200 (2002).

83 Varjosalo, M. *et al.* Application of active and kinase-deficient kinome collection for identification of kinases regulating hedgehog signaling. *Cell* **133**, 537-548, doi:10.1016/j.cell.2008.02.047 (2008).

84 Lauth, M. *et al.* DYRK1B-dependent autocrine-to-paracrine shift of Hedgehog signaling by mutant RAS. *Nat Struct Mol Biol* **17**, 718-725, doi:10.1038/nsmb.1833 (2010).

85 Gruber, W. *et al.* DYRK1B as therapeutic target in Hedgehog/GLI-dependent cancer cells with Smoothened inhibitor resistance. *Oncotarget*, doi:10.18632/oncotarget.6910 (2016).

86 Keramati, A. R. *et al.* A form of the metabolic syndrome associated with mutations in DYRK1B. *N Engl J Med* **370**, 1909-1919, doi:10.1056/NEJMoa1301824 (2014).

87 Singh, R., Dhanyamraju, P. K. & Lauth, M. DYRK1B blocks canonical and promotes non-canonical Hedgehog signaling through activation of the mTOR/AKT pathway. *Oncotarget* **8**, 833-845, doi:10.18632/oncotarget.13662 (2017).

88 Thibert, C. *et al.* Inhibition of neuroepithelial patched-induced apoptosis by sonic hedgehog. *Science* **301**, 843-846 (2003).

89 Chinchilla, P., Xiao, L., Kazanietz, M. G. & Riobo, N. A. Hedgehog proteins activate pro-angiogenic responses in endothelial cells through non-canonical signaling pathways. *Cell Cycle* **9**, 570-579, doi:10.4161/cc.9.3.10591 (2010).

90 Barnes, E. A., Kong, M., Ollendorff, V. & Donoghue, D. J. Patched1 interacts with cyclin B1 to regulate cell cycle progression. *Embo J* **20**, 2214-2223 (2001).

91 Takizawa, C. G. & Morgan, D. O. Control of mitosis by changes in the subcellular location of cyclin-B1-Cdk1 and Cdc25C. *Curr Opin Cell Biol* **12**, 658-665 (2000).

92 Polizio, A. H. *et al.* Heterotrimeric Gi proteins link Hedgehog signaling to activation of Rho small GTPases to promote fibroblast migration. *The Journal of biological chemistry* **286**, 19589-19596, doi:10.1074/jbc.M110.197111 (2011).

93 Bijlsma, M. F., Borensztajn, K. S., Roelink, H., Peppelenbosch, M. P. & Spek, C. A. Sonic hedgehog induces transcription-independent cytoskeletal rearrangement and migration regulated by arachidonate metabolites. *Cellular signalling* **19**, 2596-2604, doi:10.1016/j.cellsig.2007.08.011 (2007).

94 Yam, P. T., Langlois, S. D., Morin, S. & Charron, F. Sonic hedgehog guides axons through a noncanonical, Src-family-kinase-dependent signaling pathway. *Neuron* **62**, 349-362, doi:10.1016/j.neuron.2009.03.022 (2009).

95 Belgacem, Y. H. & Borodinsky, L. N. Sonic hedgehog signaling is decoded by calcium spike activity in the developing spinal cord. *Proc Natl Acad Sci U S A* **108**, 4482-4487, doi:10.1073/pnas.1018217108 (2011).

96 Brennan, D., Chen, X., Cheng, L., Mahoney, M. & Riobo, N. A. Noncanonical Hedgehog signaling. *Vitamins and hormones* **88**, 55-72, doi:10.1016/B978-0-12-394622-5.00003-1 (2012).

97 Ayers, K. L. & Therond, P. P. Evaluating Smoothened as a G-protein-coupled receptor for Hedgehog signalling. *Trends in cell biology* **20**, 287-298, doi:10.1016/j.tcb.2010.02.002 (2010).

98 Teperino, R. *et al.* Hedgehog partial agonism drives Warburg-like metabolism in muscle and brown fat. *Cell* **151**, 414-426, doi:10.1016/j.cell.2012.09.021 (2012).

99 Hahn, H. *et al.* Mutations of the human homolog of Drosophila patched in the nevoid basal cell carcinoma syndrome. *Cell* **85**, 841-851 (1996).

100 Johnson, R. L. *et al.* Human homolog of patched, a candidate gene for the basal cell nevus syndrome. *Science* **272**, 1668-1671 (1996).

101 Gorlin, R. J. & Goltz, R. W. Multiple nevoid basal-cell epithelioma, jaw cysts and bifid rib. A syndrome. *New Eng J Med* **262**, 908-912 (1960).

102 Gorlin, R. J. Nevoid basal cell carcinoma (Gorlin) syndrome: unanswered issues. *J Lab Clin Med* **134**, 551-552 (1999).

103 Xie, J., Bartels, C. M., Barton, S. W. & Gu, D. Targeting hedgehog signaling in cancer: research and clinical developments. *OncoTargets and therapy* **6**, 1425-1435, doi:10.2147/OTT.S34678 (2013).

104 Beddis, I. R., Mott, M. G. & Bullimore, J. Case report: nasopharyngeal rhabdomyosarcoma and Gorlin's naevoid basal cell carcinoma syndrome. *Med Pediatr Oncol* **11**, 178-179 (1983).

105 Cajaiba, M. M., Bale, A. E., Alvarez-Franco, M., McNamara, J. & Reyes-Mugica, M. Rhabdomyosarcoma, Wilms tumor, and deletion of the patched gene in Gorlin syndrome. *Nature clinical practice. Oncology* **3**, 575-580, doi:10.1038/ncponc0608 (2006).

106 Herzberger, J. J. & Wiskemann, A. Die fünfte Phakomatose. Basalzellnävus mit familiärer Belastung und Medulloblastom. *Dermatologica* **126**, 106-123 (1963).
107 Lo Muzio, L. Nevoid basal cell carcinoma syndrome (Gorlin syndrome). *Orphanet journal of rare diseases* **3**, 32, doi:10.1186/1750-1172-3-32 (2008).
108 Unden, A. B. *et al.* Mutations in the human homologue of Drosophila patched (PTCH) in basal cell carcinomas and the Gorlin syndrome: different in vivo mechanisms of PTCH inactivation. *Cancer research* **56**, 4562-4565 (1996).
109 Unden, A. B., Zaphiropoulos, P. G., Bruce, K., Toftg~ard, R. & St~ahle-Backdahl, M. Human patched (PTCH) mRNA is overexpressed consistently in tumor cells of both familial and sporadic basal cell carcinoma. *Cancer research* **57**, 2336-2340 (1997).
110 Wolter, M., Reifenberger, J., Sommer, C., Ruzicka, T. & Reifenberger, G. Mutations in the human homologue of the Drosophila segment polarity gene patched (PTCH) in sporadic basal cell carcinomas of the skin and primitive neuroectodermal tumors of the central nervous system. *Cancer research* **57**, 2581-2585 (1997).
111 Gailani, M. R. *et al.* The role of the human homologue of Drosophila patched in sporadic basal cell carcinomas [see comments]. *Nature genetics* **14**, 78-81 (1996).
112 Pietsch, T. *et al.* Medulloblastomas of the desmoplastic variant carry mutations of the human homologue of Drosophila patched. *Cancer research* **57**, 2085-2088 (1997).
113 Yang, L., Xie, G., Fan, Q. & Xie, J. Activation of the hedgehog-signaling pathway in human cancer and the clinical implications. *Oncogene* **29**, 469-481, doi:10.1038/onc.2009.392 (2010).
114 Xie, J. *et al.* Activating Smoothened mutations in sporadic basal-cell carcinoma. *Nature* **391**, 90-92 (1998).
115 Lam, C. W. *et al.* A frequent activated smoothened mutation in sporadic basal cell carcinomas. *Oncogene* **18**, 833-836 (1999).
116 Reifenberger, J. *et al.* Somatic mutations in the PTCH, SMOH, SUFUH and TP53 genes in sporadic basal cell carcinomas. *Br J Dermatol* **152**, 43-51 (2005).
117 Reifenberger, J. *et al.* Missense mutations in SMOH in sporadic basal cell carcinomas of the skin and primitive neuroectodermal tumors of the central nervous system. *Cancer research* **58**, 1798-1803 (1998).
118 Shou, Y. *et al.* A five-gene hedgehog signature developed as a patient preselection tool for hedgehog inhibitor therapy in medulloblastoma. *Clinical cancer research : an official journal of the American Association for Cancer Research* **21**, 585-593, doi:10.1158/1078-0432.CCR-13-1711 (2015).
119 Kijima, C., Miyashita, T., Suzuki, M., Oka, H. & Fujii, K. Two cases of nevoid basal cell carcinoma syndrome associated with meningioma caused by a PTCH1 or SUFU germline mutation. *Familial cancer* **11**, 565-570, doi:10.1007/s10689-012-9548-0 (2012).
120 Brastianos, P. K. *et al.* Genomic sequencing of meningiomas identifies oncogenic SMO and AKT1 mutations. *Nature genetics* **45**, 285-289, doi:10.1038/ng.2526 (2013).
121 Singh, R. R. *et al.* Sonic hedgehog signaling pathway is activated in ALK-positive anaplastic large cell lymphoma. *Cancer research* **69**, 2550-2558, doi:10.1158/0008-5472.CAN-08-1808 (2009).
122 Watkins, D. N. *et al.* Hedgehog signalling within airway epithelial progenitors and in small-cell lung cancer. *Nature* **422**, 313-317 (2003).
123 Collins, V. P. Gene amplification in human gliomas. *Glia* **15**, 289-296, doi:10.1002/glia.440150309 (1995).
124 Kinzler, K. W. *et al.* Identification of an amplified, highly expressed gene in a human glioma. *Science* **236**, 70-73 (1987).
125 Kar, S. *et al.* Intricacies of hedgehog signaling pathways: a perspective in tumorigenesis. *Experimental cell research* **318**, 1959-1972, doi:10.1016/j.yexcr.2012.05.015 (2012).
126 Berman, D. M. *et al.* Widespread requirement for Hedgehog ligand stimulation in growth of digestive tract tumours. *Nature* **425**, 846-851 (2003).
127 Watkins, D. N. & Peacock, C. D. Hedgehog signalling in foregut malignancy. *Biochemical pharmacology* **68**, 1055-1060 (2004).

128 Thayer, S. P. *et al.* Hedgehog is an early and late mediator of pancreatic cancer tumorigenesis. *Nature* **425**, 851-856, doi:10.1038/nature02009 (2003).

129 Fei, D. L. *et al.* Hedgehog signaling regulates bladder cancer growth and tumorigenicity. *Cancer research* **72**, 4449-4458, doi:10.1158/0008-5472.CAN-11-4123 (2012).

130 Shin, K. *et al.* Hedgehog signaling restrains bladder cancer progression by eliciting stromal production of urothelial differentiation factors. *Cancer cell* **26**, 521-533, doi:10.1016/j.ccell.2014.09.001 (2014).

131 Geng, L. *et al.* Hedgehog signaling in the murine melanoma microenvironment. *Angiogenesis* **10**, 259-267 (2007).

132 Das, S. *et al.* The hedgehog pathway transcription factor GLI1 promotes malignant behavior of cancer cells by up-regulating osteopontin. *The Journal of biological chemistry* **284**, 22888-22897, doi:10.1074/jbc.M109.021949 (2009).

133 Alexaki, V. I. *et al.* GLI2-mediated melanoma invasion and metastasis. *Journal of the National Cancer Institute* **102**, 1148-1159, doi:10.1093/jnci/djq257 (2010).

134 Sheng, T. *et al.* Activation of the hedgehog pathway in advanced prostate cancer. *Molecular cancer* **3**, 29, doi:10.1186/1476-4598-3-29 (2004).

135 Kasper, M., Jaks, V., Fiaschi, M. & Toftgard, R. Hedgehog signalling in breast cancer. *Carcinogenesis* **30**, 903-911, doi:10.1093/carcin/bgp048 (2009).

136 Zhao, H. *et al.* The Hedgehog signaling pathway is associated with poor prognosis in breast cancer patients with the CD44+/CD24 phenotype. *Molecular medicine reports* **14**, 5261-5270, doi:10.3892/mmr.2016.5856 (2016).

137 Kappler, R. *et al.* Molecular characterization of Patched-associated rhabdomyosarcoma. *The Journal of pathology* **200**, 348-356, doi:10.1002/path.1361 (2003).

138 Kappler, R. *et al.* Profiling the molecular difference between Patched- and p53-dependent rhabdomyosarcoma. *Oncogene* **23**, 8785-8795, doi:10.1038/sj.onc.1208133 (2004).

139 Lee, Y. *et al.* Loss of suppressor-of-fused function promotes tumorigenesis. *Oncogene* **26**, 6442-6447, doi:10.1038/sj.onc.1210467 (2007).

140 Mao, J. *et al.* A novel somatic mouse model to survey tumorigenic potential applied to the Hedgehog pathway. *Cancer research* **66**, 10171-10178 (2006).

141 Paulson, V. *et al.* High-resolution array CGH identifies common mechanisms that drive embryonal rhabdomyosarcoma pathogenesis. *Genes, chromosomes & cancer* **50**, 397-408, doi:10.1002/gcc.20864 (2011).

142 Tostar, U. *et al.* Deregulation of the hedgehog signalling pathway: a possible role for the PTCH and SUFU genes in human rhabdomyoma and rhabdomyosarcoma development. *The Journal of pathology* **208**, 17-25, doi:10.1002/path.1882 (2006).

143 Zibat, A. *et al.* Activation of the hedgehog pathway confers a poor prognosis in embryonal and fusion gene-negative alveolar rhabdomyosarcoma. *Oncogene* **29**, 6323-6330, doi:10.1038/onc.2010.368 (2010).

144 Pressey, J. G., Anderson, J. R., Crossman, D. K., Lynch, J. C. & Barr, F. G. Hedgehog pathway activity in pediatric embryonal rhabdomyosarcoma and undifferentiated sarcoma: A report from the Children's Oncology Group. *Pediatric blood & cancer* (2011).

145 Teot, L. A. *et al.* Clinical and mutational spectrum of highly differentiated, paired box 3:forkhead box protein o1 fusion-negative rhabdomyosarcoma: A report from the Children's Oncology Group. *Cancer* **124**, 1973-1981, doi:10.1002/cncr.31286 (2018).

146 Bridge, J. A. *et al.* Genomic gains and losses are similar in genetic and histologic subsets of rhabdomyosarcoma, whereas amplification predominates in embryonal with anaplasia and alveolar subtypes. *Genes, chromosomes & cancer* **33**, 310-321 (2002).

147 Bridge, J. A. *et al.* Novel genomic imbalances in embryonal rhabdomyosarcoma revealed by comparative genomic hybridization and fluorescence in situ hybridization: an intergroup rhabdomyosarcoma study. *Genes, chromosomes & cancer* **27**, 337-344 (2000).

148 Calzada-Wack, J. *et al.* Analysis of the PTCH coding region in human rhabdomyosarcoma. *Human mutation* **20**, 233-234, doi:10.1002/humu.9056 (2002).
149 Ragazzini, P. *et al.* Amplification of CDK4, MDM2, SAS and GLI genes in leiomyosarcoma, alveolar and embryonal rhabdomyosarcoma. *Histol Histopathol* **19**, 401-411 (2004).
150 Almazan-Moga, A. *et al.* Ligand-dependent Hedgehog pathway activation in Rhabdomyosarcoma: the oncogenic role of the ligands. *Br J Cancer* **117**, 1314-1325, doi:10.1038/bjc.2017.305 (2017).
151 Satheesha, S. *et al.* Targeting hedgehog signaling reduces self-renewal in embryonal rhabdomyosarcoma. *Oncogene*, doi:10.1038/onc.2015.267 (2015).
152 Oue, T., Uehara, S., Yamanaka, H., Nomura, M. & Usui, N. Hedgehog signal inhibitors suppress the invasion of human rhabdomyosarcoma cells. *Pediatric surgery international* **29**, 1153-1158, doi:10.1007/s00383-013-3369-6 (2013).
153 Lauth, M., Bergstrom, A., Shimokawa, T. & Toftgard, R. Inhibition of GLI-mediated transcription and tumor cell growth by small-molecule antagonists. *Proc Natl Acad Sci U S A* **104**, 8455-8460, doi:10.1073/pnas.0609699104 (2007).
154 Srivastava, R. K. *et al.* GLI inhibitor GANT-61 diminishes embryonal and alveolar rhabdomyosarcoma growth by inhibiting Shh/AKT-mTOR axis. *Oncotarget* **5**, 12151-12165 (2014).
155 Tostar, U., Toftgard, R., Zaphiropoulos, P. G. & Shimokawa, T. Reduction of human embryonal rhabdomyosarcoma tumor growth by inhibition of the hedgehog signaling pathway. *Genes & cancer* **1**, 941-951, doi:10.1177/1947601910385449 (2010).
156 Lauth, M. *et al.* Antipsychotic drugs regulate hedgehog signaling by modulation of 7-dehydrocholesterol reductase levels. *Molecular pharmacology* **78**, 486-496, doi:10.1124/mol.110.066431 (2010).
157 Kawabata, N. *et al.* Pharmacological inhibition of the Hedgehog pathway prevents human rhabdomyosarcoma cell growth. *International journal of oncology* **39**, 899-906, doi:10.3892/ijo.2011.1076 (2011).
158 Ecke, I. *et al.* Cyclopamine treatment of full-blown Hh/Ptch-associated RMS partially inhibits Hh/Ptch signaling, but not tumor growth. *Molecular carcinogenesis* **47**, 361-372, doi:10.1002/mc.20394 (2008).
159 Geyer, N. *et al.* Different Response of Ptch Mutant and Ptch Wildtype Rhabdomyosarcoma Toward SMO and PI3K Inhibitors. *Frontiers in oncology* **8**, doi:10.3389/fonc.2018.00396 (2018).
160 Geyer, N. *Targeting the Hedgehog and PI3K/AKT/mTOR signaling pathways in rhabdomyosarcoma*, Georg-August-University Goettingen (2018).
161 Malumbres, M. & Barbacid, M. RAS oncogenes: the first 30 years. *Nature reviews. Cancer* **3**, 459-465, doi:10.1038/nrc1097 (2003).
162 Barbacid, M. ras genes. *Annual review of biochemistry* **56**, 779-827, doi:10.1146/annurev.bi.56.070187.004023 (1987).
163 Schafer, W. R. *et al.* Genetic and pharmacological suppression of oncogenic mutations in ras genes of yeast and humans. *Science* **245**, 379-385 (1989).
164 Schafer, W. R. *et al.* Enzymatic coupling of cholesterol intermediates to a mating pheromone precursor and to the ras protein. *Science* **249**, 1133-1139 (1990).
165 Hancock, J. F., Magee, A. I., Childs, J. E. & Marshall, C. J. All ras proteins are polyisoprenylated but only some are palmitoylated. *Cell* **57**, 1167-1177 (1989).
166 Hancock, J. F., Cadwallader, K., Paterson, H. & Marshall, C. J. A CAAX or a CAAL motif and a second signal are sufficient for plasma membrane targeting of ras proteins. *Embo J* **10**, 4033-4039 (1991).
167 Downward, J. Targeting RAS signalling pathways in cancer therapy. *Nature reviews. Cancer* **3**, 11-22, doi:10.1038/nrc969 (2003).
168 Gideon, P. *et al.* Mutational and kinetic analyses of the GTPase-activating protein (GAP)-p21 interaction: the C-terminal domain of GAP is not sufficient for full activity. *Molecular and cellular biology* **12**, 2050-2056 (1992).
169 Wolfman, A. & Macara, I. G. A cytosolic protein catalyzes the release of GDP from p21ras. *Science* **248**, 67-69 (1990).

170 Downward, J., Riehl, R., Wu, L. & Weinberg, R. A. Identification of a nucleotide exchange-promoting activity for p21ras. *Proc Natl Acad Sci U S A* **87**, 5998-6002 (1990).

171 Bos, J. L., Rehmann, H. & Wittinghofer, A. GEFs and GAPs: critical elements in the control of small G proteins. *Cell* **129**, 865-877, doi:10.1016/j.cell.2007.05.018 (2007).

172 Daub, H., Weiss, F. U., Wallasch, C. & Ullrich, A. Role of transactivation of the EGF receptor in signalling by G-protein-coupled receptors. *Nature* **379**, 557-560, doi:10.1038/379557a0 (1996).

173 Bos, J. L. ras oncogenes in human cancer: a review. *Cancer research* **49**, 4682-4689 (1989).

174 Hobbs, G. A., Der, C. J. & Rossman, K. L. RAS isoforms and mutations in cancer at a glance. *Journal of cell science* **129**, 1287-1292, doi:10.1242/jcs.182873 (2016).

175 Ponting, C. P. & Benjamin, D. R. A novel family of Ras-binding domains. *Trends Biochem Sci* **21**, 422-425 (1996).

176 Chang, L. & Karin, M. Mammalian MAP kinase signalling cascades. *Nature* **410**, 37-40. (2001).

177 Marais, R., Light, Y., Paterson, H. F., Mason, C. S. & Marshall, C. J. Differential regulation of Raf-1, A-Raf, and B-Raf by oncogenic ras and tyrosine kinases. *The Journal of biological chemistry* **272**, 4378-4383 (1997).

178 Kolch, W. Meaningful relationships: the regulation of the Ras/Raf/MEK/ERK pathway by protein interactions. *The Biochemical journal* **351 Pt 2**, 289-305 (2000).

179 Yan, M. & Templeton, D. J. Identification of 2 serine residues of MEK-1 that are differentially phosphorylated during activation by raf and MEK kinase. *The Journal of biological chemistry* **269**, 19067-19073 (1994).

180 Kyriakis, J. M. *et al.* Raf-1 activates MAP kinase-kinase. *Nature* **358**, 417-421, doi:10.1038/358417a0 (1992).

181 Zheng, C. F., Ohmichi, M., Saltiel, A. R. & Guan, K. L. Growth factor induced MEK activation is primarily mediated by an activator different from c-raf. *Biochemistry* **33**, 5595-5599 (1994).

182 Zhang, W. & Liu, H. T. MAPK signal pathways in the regulation of cell proliferation in mammalian cells. *Cell research* **12**, 9-18, doi:10.1038/sj.cr.7290105 (2002).

183 Chang, F. *et al.* Regulation of cell cycle progression and apoptosis by the Ras/Raf/MEK/ERK pathway (Review). *International journal of oncology* **22**, 469-480 (2003).

184 Downward, J. Ras signalling and apoptosis. *Current opinion in genetics & development* **8**, 49-54 (1998).

185 Dimauro, T. & David, G. Ras-induced senescence and its physiological relevance in cancer. *Current cancer drug targets* **10**, 869-876 (2010).

186 Sears, R., Leone, G., DeGregori, J. & Nevins, J. R. Ras enhances Myc protein stability. *Molecular cell* **3**, 169-179 (1999).

187 Deschenes-Simard, X. *et al.* Tumor suppressor activity of the ERK/MAPK pathway by promoting selective protein degradation. *Genes & development* **27**, 900-915, doi:10.1101/gad.203984.112 (2013).

188 Courtois-Cox, S., Jones, S. L. & Cichowski, K. Many roads lead to oncogene-induced senescence. *Oncogene* **27**, 2801-2809 (2008).

189 Castellano, E. & Downward, J. RAS Interaction with PI3K: More Than Just Another Effector Pathway. *Genes & cancer* **2**, 261-274, doi:10.1177/1947601911408079 (2011).

190 Manning, B. D. & Toker, A. AKT/PKB Signaling: Navigating the Network. *Cell* **169**, 381-405, doi:10.1016/j.cell.2017.04.001 (2017).

191 Dibble, C. C. & Cantley, L. C. Regulation of mTORC1 by PI3K signaling. *Trends in cell biology* **25**, 545-555, doi:10.1016/j.tcb.2015.06.002 (2015).

192 Engelman, J. A. Targeting PI3K signalling in cancer: opportunities, challenges and limitations. *Nature reviews. Cancer* **9**, 550-562, doi:10.1038/nrc2664 (2009).

193 Hemmings, B. A. & Restuccia, D. F. PI3K-PKB/Akt pathway. *Cold Spring Harbor perspectives in biology* **4**, a011189, doi:10.1101/cshperspect.a011189 (2012).

194 Aksamitiene, E., Kiyatkin, A. & Kholodenko, B. N. Cross-talk between mitogenic Ras/MAPK and survival PI3K/Akt pathways: a fine balance. *Biochem Soc Trans* **40**, 139-146, doi:10.1042/BST20110609 (2012).

195 Kelley, G. G., Reks, S. E., Ondrako, J. M. & Smrcka, A. V. Phospholipase C(epsilon): a novel Ras effector. *Embo J* **20**, 743-754, doi:10.1093/emboj/20.4.743 (2001).

196 Aspenstrom, P. Integration of signalling pathways regulated by small GTPases and calcium. *Biochimica et biophysica acta* **1742**, 51-58, doi:10.1016/j.bbamcr.2004.09.029 (2004).

197 Matsui, M. S., Chew, S. L. & DeLeo, V. A. Protein kinase C in normal human epidermal keratinocytes during proliferation and calcium-induced differentiation. *The Journal of investigative dermatology* **99**, 565-571 (1992).

198 Porat-Shliom, N., Kloog, Y. & Donaldson, J. G. A unique platform for H-Ras signaling involving clathrin-independent endocytosis. *Mol Biol Cell* **19**, 765-775, doi:10.1091/mbc.e07-08-0841 (2008).

199 Tall, G. G., Barbieri, M. A., Stahl, P. D. & Horazdovsky, B. F. Ras-activated endocytosis is mediated by the Rab5 guanine nucleotide exchange activity of RIN1. *Dev Cell* **1**, 73-82 (2001).

200 Leblanc, V., Tocque, B. & Delumeau, I. Ras-GAP controls Rho-mediated cytoskeletal reorganization through its SH3 domain. *Molecular and cellular biology* **18**, 5567-5578 (1998).

201 Hall, A. Ras-related GTPases and the cytoskeleton. *Mol Biol Cell* **3**, 475-479, doi:10.1091/mbc.3.5.475 (1992).

202 Leon, J., Guerrero, I. & Pellicer, A. Differential expression of the ras gene family in mice. *Molecular and cellular biology* **7**, 1535-1540 (1987).

203 Muller, R. *et al.* Transcription of c-onc genes c-rasKi and c-fms during mouse development. *Molecular and cellular biology* **3**, 1062-1069 (1983).

204 Lampson, B. L. *et al.* Rare codons regulate KRas oncogenesis. *Current biology : CB* **23**, 70-75, doi:10.1016/j.cub.2012.11.031 (2013).

205 Pershing, N. L. *et al.* Rare codons capacitate Kras-driven de novo tumorigenesis. *J Clin Invest* **125**, 222-233, doi:10.1172/JCI77627 (2015).

206 Jura, N., Scotto-Lavino, E., Sobczyk, A. & Bar-Sagi, D. Differential modification of Ras proteins by ubiquitination. *Molecular cell* **21**, 679-687, doi:10.1016/j.molcel.2006.02.011 (2006).

207 Lau, K. S. & Haigis, K. M. Non-redundancy within the RAS oncogene family: insights into mutational disparities in cancer. *Molecules and cells* **28**, 315-320, doi:10.1007/s10059-009-0143-7 (2009).

208 Castellano, E. & Santos, E. Functional specificity of ras isoforms: so similar but so different. *Genes & cancer* **2**, 216-231, doi:10.1177/1947601911408081 (2011).

209 Buhrman, G. *et al.* Analysis of binding site hot spots on the surface of Ras GTPase. *Journal of molecular biology* **413**, 773-789, doi:10.1016/j.jmb.2011.09.011 (2011).

210 Hancock, J. F. Ras proteins: different signals from different locations. *Nature reviews. Molecular cell biology* **4**, 373-384, doi:10.1038/nrm1105 (2003).

211 Walsh, A. B. & Bar-Sagi, D. Differential activation of the Rac pathway by Ha-Ras and K-Ras. *The Journal of biological chemistry* **276**, 15609-15615, doi:10.1074/jbc.M010573200 (2001).

212 Yan, J., Roy, S., Apolloni, A., Lane, A. & Hancock, J. F. Ras isoforms vary in their ability to activate Raf-1 and phosphoinositide 3-kinase. *The Journal of biological chemistry* **273**, 24052-24056 (1998).

213 Voice, J. K., Klemke, R. L., Le, A. & Jackson, J. H. Four human ras homologs differ in their abilities to activate Raf-1, induce transformation, and stimulate cell motility. *The Journal of biological chemistry* **274**, 17164-17170 (1999).

214 Hamilton, M. & Wolfman, A. Ha-ras and N-ras regulate MAPK activity by distinct mechanisms in vivo. *Oncogene* **16**, 1417-1428, doi:10.1038/sj.onc.1201653 (1998).

215 Omerovic, J., Hammond, D. E., Clague, M. J. & Prior, I. A. Ras isoform abundance and signalling in human cancer cell lines. *Oncogene* **27**, 2754-2762, doi:10.1038/sj.onc.1210925 (2008).

216 Keller, J. W. *et al.* Oncogenic K-RAS subverts the antiapoptotic role of N-RAS and alters modulation of the N-RAS:gelsolin complex. *Oncogene* **26**, 3051-3059, doi:10.1038/sj.onc.1210103 (2007).

217 Khokhlatchev, A. *et al.* Identification of a novel Ras-regulated proapoptotic pathway. *Current biology : CB* **12**, 253-265 (2002).

218 Maher, J., Baker, D. A., Manning, M., Dibb, N. J. & Roberts, I. A. Evidence for cell-specific differences in transformation by N-, H- and K-ras. *Oncogene* **11**, 1639-1647 (1995).

219 Whitwam, T. *et al.* Differential oncogenic potential of activated RAS isoforms in melanocytes. *Oncogene* **26**, 4563-4570, doi:10.1038/sj.onc.1210239 (2007).

220 Haigis, K. M. *et al.* Differential effects of oncogenic K-Ras and N-Ras on proliferation, differentiation and tumor progression in the colon. *Nature genetics* **40**, 600-608, doi:10.1038/ng.115 (2008).

221 Quinlan, M. P., Quatela, S. E., Philips, M. R. & Settleman, J. Activated Kras, but not Hras or Nras, may initiate tumors of endodermal origin via stem cell expansion. *Molecular and cellular biology* **28**, 2659-2674, doi:10.1128/MCB.01661-07 (2008).

222 Johnson, L. *et al.* K-ras is an essential gene in the mouse with partial functional overlap with N-ras. *Genes & development* **11**, 2468-2481 (1997).

223 Koera, K. *et al.* K-ras is essential for the development of the mouse embryo. *Oncogene* **15**, 1151-1159, doi:10.1038/sj.onc.1201284 (1997).

224 Esteban, L. M. *et al.* Targeted genomic disruption of H-ras and N-ras, individually or in combination, reveals the dispensability of both loci for mouse growth and development. *Molecular and cellular biology* **21**, 1444-1452, doi:10.1128/MCB.21.5.1444-1452.2001 (2001).

225 Khalaf, W. F. *et al.* K-Ras is essential for normal fetal liver erythropoiesis. *Blood* **105**, 3538-3541, doi:10.1182/blood-2004-05-2021 (2005).

226 Potenza, N. *et al.* Replacement of K-Ras with H-Ras supports normal embryonic development despite inducing cardiovascular pathology in adult mice. *EMBO Rep* **6**, 432-437, doi:10.1038/sj.embor.7400397 (2005).

227 Nakamura, K. *et al.* Partial functional overlap of the three ras genes in mouse embryonic development. *Oncogene* **27**, 2961-2968, doi:10.1038/sj.onc.1210956 (2008).

228 Ise, K. *et al.* Targeted deletion of the H-ras gene decreases tumor formation in mouse skin carcinogenesis. *Oncogene* **19**, 2951-2956, doi:10.1038/sj.onc.1203600 (2000).

229 Umanoff, H., Edelmann, W., Pellicer, A. & Kucherlapati, R. The murine N-ras gene is not essential for growth and development. *Proc Natl Acad Sci U S A* **92**, 1709-1713 (1995).

230 Perez de Castro, I. *et al.* Mice deficient for N-ras: impaired antiviral immune response and T-cell function. *Cancer research* **63**, 1615-1622 (2003).

231 Bamford, S. *et al.* The COSMIC (Catalogue of Somatic Mutations in Cancer) database and website. *Br J Cancer* **91**, 355-358, doi:10.1038/sj.bjc.6601894 (2004).

232 Forbes, S. A. *et al.* COSMIC: exploring the world's knowledge of somatic mutations in human cancer. *Nucleic acids research* **43**, D805-811, doi:10.1093/nar/gku1075 (2015).

233 Cox, A. D., Fesik, S. W., Kimmelman, A. C., Luo, J. & Der, C. J. Drugging the undruggable RAS: Mission possible? *Nature reviews. Drug discovery* **13**, 828-851, doi:10.1038/nrd4389 (2014).

234 Prior, I. A., Lewis, P. D. & Mattos, C. A comprehensive survey of Ras mutations in cancer. *Cancer research* **72**, 2457-2467, doi:10.1158/0008-5472.CAN-11-2612 (2012).

235 Fotiadou, P. P., Takahashi, C., Rajabi, H. N. & Ewen, M. E. Wild-type NRas and KRas perform distinct functions during transformation. *Molecular and cellular biology* **27**, 6742-6755, doi:10.1128/MCB.00234-07 (2007).

236 Jeng, H. H., Taylor, L. J. & Bar-Sagi, D. Sos-mediated cross-activation of wild-type Ras by oncogenic Ras is essential for tumorigenesis. *Nature communications* **3**, 1168, doi:10.1038/ncomms2173 (2012).

237 Grabocka, E. *et al.* Wild-type H- and N-Ras promote mutant K-Ras-driven tumorigenesis by modulating the DNA damage response. *Cancer cell* **25**, 243-256, doi:10.1016/j.ccr.2014.01.005 (2014).
238 Young, A., Lou, D. & McCormick, F. Oncogenic and wild-type Ras play divergent roles in the regulation of mitogen-activated protein kinase signaling. *Cancer discovery* **3**, 112-123, doi:10.1158/2159-8290.CD-12-0231 (2013).
239 To, M. D., Rosario, R. D., Westcott, P. M., Banta, K. L. & Balmain, A. Interactions between wild-type and mutant Ras genes in lung and skin carcinogenesis. *Oncogene* **32**, 4028-4033, doi:10.1038/onc.2012.404 (2013).
240 Bremner, R. & Balmain, A. Genetic changes in skin tumor progression: correlation between presence of a mutant ras gene and loss of heterozygosity on mouse chromosome 7. *Cell* **61**, 407-417 (1990).
241 Weyandt, J. D. *et al.* Wild-Type Hras Suppresses the Earliest Stages of Tumorigenesis in a Genetically Engineered Mouse Model of Pancreatic Cancer. *PloS one* **10**, e0140253, doi:10.1371/journal.pone.0140253 (2015).
242 Rauen, K. A. The RASopathies. *Annual review of genomics and human genetics* **14**, 355-369, doi:10.1146/annurev-genom-091212-153523 (2013).
243 Fernandez-Medarde, A. & Santos, E. Ras in cancer and developmental diseases. *Genes & cancer* **2**, 344-358, doi:10.1177/1947601911411084 (2011).
244 Wallace, M. R. *et al.* Type 1 neurofibromatosis gene: identification of a large transcript disrupted in three NF1 patients. *Science* **249**, 181-186 (1990).
245 Viskochil, D. *et al.* Deletions and a translocation interrupt a cloned gene at the neurofibromatosis type 1 locus. *Cell* **62**, 187-192 (1990).
246 Eerola, I. *et al.* Capillary malformation-arteriovenous malformation, a new clinical and genetic disorder caused by RASA1 mutations. *American journal of human genetics* **73**, 1240-1249, doi:10.1086/379793 (2003).
247 Niihori, T. *et al.* Germline KRAS and BRAF mutations in cardio-facio-cutaneous syndrome. *Nature genetics* **38**, 294-296, doi:10.1038/ng1749 (2006).
248 Rodriguez-Viciana, P. *et al.* Germline mutations in genes within the MAPK pathway cause cardio-facio-cutaneous syndrome. *Science* **311**, 1287-1290, doi:10.1126/science.1124642 (2006).
249 Brems, H. *et al.* Germline loss-of-function mutations in SPRED1 cause a neurofibromatosis 1-like phenotype. *Nature genetics* **39**, 1120-1126, doi:10.1038/ng2113 (2007).
250 Aoki, Y. *et al.* Germline mutations in HRAS proto-oncogene cause Costello syndrome. *Nature genetics* **37**, 1038-1040, doi:10.1038/ng1641 (2005).
251 Cordeddu, V. *et al.* Mutation of SHOC2 promotes aberrant protein N-myristoylation and causes Noonan-like syndrome with loose anagen hair. *Nature genetics* **41**, 1022-1026, doi:10.1038/ng.425 (2009).
252 Martinelli, S. *et al.* Heterozygous germline mutations in the CBL tumor-suppressor gene cause a Noonan syndrome-like phenotype. *American journal of human genetics* **87**, 250-257, doi:10.1016/j.ajhg.2010.06.015 (2010).
253 Tartaglia, M. *et al.* Mutations in PTPN11, encoding the protein tyrosine phosphatase SHP-2, cause Noonan syndrome. *Nature genetics* **29**, 465-468, doi:10.1038/ng772 (2001).
254 Tartaglia, M. *et al.* Gain-of-function SOS1 mutations cause a distinctive form of Noonan syndrome. *Nature genetics* **39**, 75-79, doi:10.1038/ng1939 (2007).
255 Razzaque, M. A. *et al.* Germline gain-of-function mutations in RAF1 cause Noonan syndrome. *Nature genetics* **39**, 1013-1017, doi:10.1038/ng2078 (2007).
256 Schubbert, S. *et al.* Biochemical and functional characterization of germ line KRAS mutations. *Molecular and cellular biology* **27**, 7765-7770, doi:10.1128/MCB.00965-07 (2007).
257 Cirstea, I. C. *et al.* A restricted spectrum of NRAS mutations causes Noonan syndrome. *Nature genetics* **42**, 27-29, doi:10.1038/ng.497 (2010).
258 Pandit, B. *et al.* Gain-of-function RAF1 mutations cause Noonan and LEOPARD syndromes with hypertrophic cardiomyopathy. *Nature genetics* **39**, 1007-1012, doi:10.1038/ng2073 (2007).

259 Kratz, C. P., Rapisuwon, S., Reed, H., Hasle, H. & Rosenberg, P. S. Cancer in Noonan, Costello, cardiofaciocutaneous and LEOPARD syndromes. *American journal of medical genetics. Part C, Seminars in medical genetics* **157C**, 83-89, doi:10.1002/ajmg.c.30300 (2011).

260 Salem, B., Hofherr, S., Turner, J., Doros, L. & Smpokou, P. Childhood Rhabdomyosarcoma in Association With a RASopathy Clinical Phenotype and Mosaic Germline SOS1 Duplication. *Journal of pediatric hematology/oncology* **38**, e278-e282, doi:10.1097/MPH.0000000000000566 (2016).

261 Sanchez-Montenegro, C. *et al.* Costello Syndrome and Umbilical Ligament Rhabdomyosarcoma in Two Pediatric Patients: Case Reports and Review of the Literature. *Case reports in genetics* **2017**, 1587610, doi:10.1155/2017/1587610 (2017).

262 Chen, Y. *et al.* Mutations of the PTPN11 and RAS genes in rhabdomyosarcoma and pediatric hematological malignancies. *Genes, chromosomes & cancer* **45**, 583-591, doi:10.1002/gcc.20322 (2006).

263 Bisogno, G., Murgia, A., Mammi, I., Strafella, M. S. & Carli, M. Rhabdomyosarcoma in a patient with cardio-facio-cutaneous syndrome. *Journal of pediatric hematology/oncology* **21**, 424-427 (1999).

264 Innes, A. M. & Chudley, A. E. Rhabdomyosarcoma in a patient with Cardio-Facio-Cutaneous syndrome. *Journal of pediatric hematology/oncology* **22**, 546-547 (2000).

265 Heney, D., Lockwood, L., Allibone, E. B. & Bailey, C. C. Nasopharyngeal rhabdomyosarcoma and multiple lentigines syndrome: a case report. *Med Pediatr Oncol* **20**, 227-228 (1992).

266 Stratton, M. R., Fisher, C., Gusterson, B. A. & Cooper, C. S. Detection of point mutations in N-ras and K-ras genes of human embryonal rhabdomyosarcomas using oligonucleotide probes and the polymerase chain reaction. *Cancer research* **49**, 6324-6327 (1989).

267 Martinelli, S. *et al.* RAS signaling dysregulation in human embryonal Rhabdomyosarcoma. *Genes, chromosomes & cancer* **48**, 975-982, doi:10.1002/gcc.20702 (2009).

268 Seki, M. *et al.* Integrated genetic and epigenetic analysis defines novel molecular subgroups in rhabdomyosarcoma. *Nature communications* **6**, 7557, doi:10.1038/ncomms8557 (2015).

269 Dolgikh, N., Hugle, M., Vogler, M. & Fulda, S. NRAS-Mutated Rhabdomyosarcoma Cells Are Vulnerable to Mitochondrial Apoptosis Induced by Coinhibition of MEK and PI3Kalpha. *Cancer research*, doi:10.1158/0008-5472.CAN-17-1737 (2018).

270 Graab, U., Hahn, H. & Fulda, S. Identification of a novel synthetic lethality of combined inhibition of hedgehog and PI3K signaling in rhabdomyosarcoma. *Oncotarget* **6**, 8722-8735 (2015).

271 Guenther, M. K., Graab, U. & Fulda, S. Synthetic lethal interaction between PI3K/Akt/mTOR and Ras/MEK/ERK pathway inhibition in rhabdomyosarcoma. *Cancer letters* **337**, 200-209, doi:10.1016/j.canlet.2013.05.010 (2013).

272 Renshaw, J. *et al.* Dual blockade of the PI3K/AKT/mTOR (AZD8055) and RAS/MEK/ERK (AZD6244) pathways synergistically inhibits rhabdomyosarcoma cell growth in vitro and in vivo. *Clinical cancer research : an official journal of the American Association for Cancer Research* **19**, 5940-5951, doi:10.1158/1078-0432.CCR-13-0850 (2013).

273 Hettmer, S. *et al.* Sarcomas induced in discrete subsets of prospectively isolated skeletal muscle cells. *Proc Natl Acad Sci U S A* **108**, 20002-20007, doi:10.1073/pnas.1111733108 (2011).

274 Langenau, D. M. *et al.* Effects of RAS on the genesis of embryonal rhabdomyosarcoma. *Genes & development* **21**, 1382-1395, doi:10.1101/gad.1545007 (2007).

275 Rubin, B. P. *et al.* Evidence for an Unanticipated Relationship between Undifferentiated Pleomorphic Sarcoma and Embryonal Rhabdomyosarcoma. *Cancer Cell* **19**, 177-191 (2011).

276 Zhu, B. & Davie, J. K. New insights into signalling-pathway alterations in rhabdomyosarcoma. *Br J Cancer* **112**, 227-231, doi:10.1038/bjc.2014.471 (2015).
277 Kashi, V. P., Hatley, M. E. & Galindo, R. L. Probing for a deeper understanding of rhabdomyosarcoma: insights from complementary model systems. *Nature reviews. Cancer* **15**, 426-439, doi:10.1038/nrc3961 (2015).
278 Linardic, C. M. & Counter, C. M. Genetic modeling of Ras-induced human rhabdomyosarcoma. *Methods Enzymol* **438**, 419-427, doi:10.1016/S0076-6879(07)38028-2 (2008).
279 Jacks, T. *et al.* Tumor spectrum analysis in p53-mutant mice. *Current biology : CB* **4**, 1-7. (1994).
280 Harvey, M. *et al.* Spontaneous and carcinogen-induced tumorigenesis in p53-deficient mice. *Nature genetics* **5**, 225-229, doi:10.1038/ng1193-225 (1993).
281 Doyle, B. *et al.* p53 mutation and loss have different effects on tumourigenesis in a novel mouse model of pleomorphic rhabdomyosarcoma. *The Journal of pathology* **222**, 129-137, doi:10.1002/path.2748 (2010).
282 Tsumura, H., Yoshida, T., Saito, H., Imanaka-Yoshida, K. & Suzuki, N. Cooperation of oncogenic K-ras and p53 deficiency in pleomorphic rhabdomyosarcoma development in adult mice. *Oncogene* **25**, 7673-7679, doi:10.1038/sj.onc.1209749 (2006).
283 Blum, J. M. *et al.* Distinct and overlapping sarcoma subtypes initiated from muscle stem and progenitor cells. *Cell reports* **5**, 933-940, doi:10.1016/j.celrep.2013.10.020 (2013).
284 Brechbiel, J., Miller-Moslin, K. & Adjei, A. A. Crosstalk between hedgehog and other signaling pathways as a basis for combination therapies in cancer. *Cancer treatment reviews* **40**, 750-759, doi:10.1016/j.ctrv.2014.02.003 (2014).
285 Chang, H., Li, Q., Moraes, R. C., Lewis, M. T. & Hamel, P. A. Activation of Erk by sonic hedgehog independent of canonical hedgehog signalling. *Int J Biochem Cell Biol* **42**, 1462-1471, doi:10.1016/j.biocel.2010.04.016 (2010).
286 Riobo, N. A., Haines, G. M. & Emerson, C. P., Jr. Protein kinase C-delta and mitogen-activated protein/extracellular signal-regulated kinase-1 control GLI activation in hedgehog signaling. *Cancer research* **66**, 839-845, doi:10.1158/0008-5472.CAN-05-2539 (2006).
287 Whisenant, T. C. *et al.* Computational prediction and experimental verification of new MAP kinase docking sites and substrates including Gli transcription factors. *PLoS computational biology* **6**, doi:10.1371/journal.pcbi.1000908 (2010).
288 Bardwell, L., Bardwell, J.A., Wu, B., Waterman, M. in *Experimental Biology Abstracts 2016* Vol. 30 (The FASEB Journal, 2016).
289 Kasper, M. *et al.* Selective modulation of Hedgehog/GLI target gene expression by epidermal growth factor signaling in human keratinocytes. *Molecular and cellular biology* **26**, 6283-6298, doi:10.1128/MCB.02317-05 (2006).
290 Schnidar, H. *et al.* Epidermal growth factor receptor signaling synergizes with Hedgehog/GLI in oncogenic transformation via activation of the MEK/ERK/JUN pathway. *Cancer research* **69**, 1284-1292, doi:10.1158/0008-5472.CAN-08-2331 (2009).
291 Mangelberger, D., Kern, D., Loipetzberger, A., Eberl, M. & Aberger, F. Cooperative Hedgehog-EGFR signaling. *Front Biosci (Landmark Ed)* **17**, 90-99 (2012).
292 Eberl, M. *et al.* Hedgehog-EGFR cooperation response genes determine the oncogenic phenotype of basal cell carcinoma and tumour-initiating pancreatic cancer cells. *EMBO molecular medicine* **4**, 218-233, doi:10.1002/emmm.201100201 (2012).
293 Chabu, C., Li, D. M. & Xu, T. EGFR/ARF6 regulation of Hh signalling stimulates oncogenic Ras tumour overgrowth. *Nature communications* **8**, 14688, doi:10.1038/ncomms14688 (2017).
294 Seto, M. *et al.* Regulation of the hedgehog signaling by the mitogen-activated protein kinase cascade in gastric cancer. *Molecular carcinogenesis* **48**, 703-712, doi:10.1002/mc.20516 (2009).

295 Mills, L. D. *et al.* Loss of the transcription factor GLI1 identifies a signaling network in the tumor microenvironment mediating KRAS oncogene-induced transformation. *The Journal of biological chemistry* **288**, 11786-11794, doi:10.1074/jbc.M112.438846 (2013).

296 Rajurkar, M. *et al.* The activity of Gli transcription factors is essential for Kras-induced pancreatic tumorigenesis. *Proc Natl Acad Sci U S A* **109**, E1038-1047, doi:10.1073/pnas.1114168109 (2012).

297 Ji, Z., Mei, F. C., Xie, J. & Cheng, X. Oncogenic KRAS activates hedgehog signaling pathway in pancreatic cancer cells. *The Journal of biological chemistry* **282**, 14048-14055, doi:10.1074/jbc.M611089200 (2007).

298 Parascandolo, A. *et al.* A dual mechanism of activation of the Sonic Hedgehog pathway in anaplastic thyroid cancer: crosstalk with RAS-BRAF-MEK pathway and ligand secretion by tumor stroma. *Oncotarget* **9**, 4496-4510, doi:10.18632/oncotarget.23388 (2018).

299 Cuvelier, N. *The interaction between Hedgehog/Patched and Ras signaling in Rhabdomyosarcoma* Georg-August University Goettingen (2016).

300 Beer, C., Buhr, P., Hahn, H., Laubner, D. & Wirth, M. Gene expression analysis of murine cells producing amphotropic mouse leukaemia virus at a cultivation temperature of 32 and 37 degrees C. *The Journal of general virology* **84**, 1677-1686, doi:10.1099/vir.0.18871-0 (2003).

301 Fritsch, A. *Analysen zu Interaktionen zwischen dem Vitamin-D-Rezeptor Signalweg und der Hedgehog Signalkaskade*, Georg-August-Universität, (2014).

302 Uhmann, A. *et al.* The Hedgehog receptor Patched controls lymphoid lineage commitment. *Blood* **110**, 1814-1823, doi:10.1182/blood-2007-02-075648 (2007).

303 Chen, X. *et al.* Endogenous expression of Hras(G12V) induces developmental defects and neoplasms with copy number imbalances of the oncogene. *Proc Natl Acad Sci U S A* **106**, 7979-7984, doi:10.1073/pnas.0900343106 (2009).

304 Tuveson, D. A. *et al.* Endogenous oncogenic K-ras(G12D) stimulates proliferation and widespread neoplastic and developmental defects. *Cancer cell* **5**, 375-387 (2004).

305 Biressi, S. *et al.* Myf5 expression during fetal myogenesis defines the developmental progenitors of adult satellite cells. *Developmental biology* **379**, 195-207, doi:10.1016/j.ydbio.2013.04.021 (2013).

306 Soriano, P. Generalized lacZ expression with the ROSA26 Cre reporter strain. *Nature genetics* **21**, 70-71, doi:10.1038/5007 (1999).

307 Uhmann, A. *et al.* Antitumoral effects of calcitriol in basal cell carcinomas involve inhibition of hedgehog signaling and induction of vitamin D receptor signaling and differentiation. *Molecular cancer therapeutics* **10**, 2179-2188, doi:10.1158/1535-7163.MCT-11-0422 (2011).

308 Jacobsen, P. F., Jenkyn, D. J. & Papadimitriou, J. M. Establishment of a human medulloblastoma cell line and its heterotransplantation into nude mice. *Journal of neuropathology and experimental neurology* **44**, 472-485 (1985).

309 Graham, F. L., Smiley, J., Russell, W. C. & Nairn, R. Characteristics of a human cell line transformed by DNA from human adenovirus type 5. *The Journal of general virology* **36**, 59-74, doi:10.1099/0022-1317-36-1-59 (1977).

310 Chen, J. K., Taipale, J., Young, K. E., Maiti, T. & Beachy, P. A. Small molecule modulation of Smoothened activity. *Proc Natl Acad Sci U S A* **99**, 14071-14076, doi:10.1073/pnas.182542899 (2002).

311 Jainchill, J. L., Aaronson, S. A. & Todaro, G. J. Murine sarcoma and leukemia viruses: assay using clonal lines of contact-inhibited mouse cells. *Journal of virology* **4**, 549-553 (1969).

312 McAllister, R. M., Melnyk, J., Finkelstein, J. Z., Adams, E. C., Jr. & Gardner, M. B. Cultivation in vitro of cells derived from a human rhabdomyosarcoma. *Cancer* **24**, 520-526 (1969).

313 Roberts, W. M., Douglass, E. C., Peiper, S. C., Houghton, P. J. & Look, A. T. Amplification of the gli gene in childhood sarcomas. *Cancer Res* **49**, 5407-5413 (1989).

314 Scholl, F. A., Betts, D. R., Niggli, F. K. & Schafer, B. W. Molecular features of a human rhabdomyosarcoma cell line with spontaneous metastatic progression. *Br J Cancer* **82**, 1239-1245, doi:10.1054/bjoc.1999.1069 (2000).

315 Missiaglia, E. *et al.* Genomic imbalances in rhabdomyosarcoma cell lines affect expression of genes frequently altered in primary tumors: an approach to identify candidate genes involved in tumor development. *Genes, chromosomes & cancer* **48**, 455-467, doi:10.1002/gcc.20655 (2009).

316 Zibat, A. *et al.* Time-point and dosage of gene inactivation determine the tumor spectrum in conditional Ptch knockouts. *Carcinogenesis* **30**, 918-926, doi:10.1093/carcin/bgp068 (2009).

317 Jackson, E. L. *et al.* Analysis of lung tumor initiation and progression using conditional expression of oncogenic K-ras. *Genes & development* **15**, 3243-3248, doi:10.1101/gad.943001 (2001).

318 Cordier, A. C. & Haumont, S. M. Development of thymus, parathyroids, and ultimobranchial bodies in NMRI and nude mice. *The American journal of anatomy* **157**, 227-263, doi:10.1002/aja.1001570303 (1980).

319 Pelleitier, M. & Montplaisir, S. The nude mouse: a model of deficient T-cell function. *Methods and achievements in experimental pathology* **7**, 149-166 (1975).

320 Schindelin, J. *et al.* Fiji: an open-source platform for biological-image analysis. *Nature methods* **9**, 676-682, doi:10.1038/nmeth.2019 (2012).

321 Abcam. *Subcellular fractionation protocol*, https://www.abcam.com/protocols/subcellular-fractionation-protocol

322 Yu, Z., Huang, Z. and Lung, M. L. Subcellular Fractionation of Cultured Human Cell Lines. *Bio-protocol* **3**, e754 (2013).

323 Nitzki, F. *et al.* Uncommitted precursor cells might contribute to increased incidence of embryonal rhabdomyosarcoma in heterozygous Patched1-mutant mice. *Oncogene* **30**, 4428-4436, doi:10.1038/onc.2011.157 (2011).

324 Hahn, H. *et al.* Genetic mapping of a Ptch1-associated rhabdomyosarcoma susceptibility locus on mouse chromosome 2. *Genomics* **84**, 853-858, doi:10.1016/j.ygeno.2004.07.002 (2004).

325 Nitzki, F., Kruger, A., Reifenberg, K., Wojnowski, L. & Hahn, H. Identification of a genetic contamination in a commercial mouse strain using two panels of polymorphic markers. *Laboratory animals* **41**, 218-228, doi:10.1258/002367707780378104 (2007).

326 Sokolowski, E., Turina, C. B., Kikuchi, K., Langenau, D. M. & Keller, C. Proof-of-concept rare cancers in drug development: the case for rhabdomyosarcoma. *Oncogene* **33**, 1877-1889, doi:10.1038/onc.2013.129 (2014).

327 Gotschel, F. *et al.* Synergism between Hedgehog-GLI and EGFR signaling in Hedgehog-responsive human medulloblastoma cells induces downregulation of canonical Hedgehog-target genes and stabilized expression of GLI1. *PloS one* **8**, e65403, doi:10.1371/journal.pone.0065403 (2013).

328 Lemma, S., Avnet, S., Salerno, M., Chano, T. & Baldini, N. Identification and Validation of Housekeeping Genes for Gene Expression Analysis of Cancer Stem Cells. *PloS one* **11**, e0149481, doi:10.1371/journal.pone.0149481 (2016).

329 Park, S. *et al.* PI-103, a dual inhibitor of Class IA phosphatidylinositide 3-kinase and mTOR, has antileukemic activity in AML. *Leukemia* **22**, 1698-1706, doi:10.1038/leu.2008.144 (2008).

330 Favata, M. F. *et al.* Identification of a novel inhibitor of mitogen-activated protein kinase. *The Journal of biological chemistry* **273**, 18623-18632 (1998).

331 Morris, E. J. *et al.* Discovery of a novel ERK inhibitor with activity in models of acquired resistance to BRAF and MEK inhibitors. *Cancer discovery* **3**, 742-750, doi:10.1158/2159-8290.CD-13-0070 (2013).

332 Williams, J. A. *et al.* Identification of a small molecule inhibitor of the hedgehog signaling pathway: Effects on basal cell carcinoma-like lesions. *Proc Natl Acad Sci U S A* (2003).

333 Zhou, J. *et al.* Cucurbitacin B and SCH772984 exhibit synergistic anti-pancreatic cancer activities by suppressing EGFR, PI3K/Akt/mTOR, STAT3 and ERK signaling. *Oncotarget* **8**, 103167-103181, doi:10.18632/oncotarget.21704 (2017).

334 Normanno, N. *et al.* The MEK/MAPK pathway is involved in the resistance of breast cancer cells to the EGFR tyrosine kinase inhibitor gefitinib. *Journal of cellular physiology* **207**, 420-427, doi:10.1002/jcp.20588 (2006).

335 Turke, A. B. *et al.* MEK inhibition leads to PI3K/AKT activation by relieving a negative feedback on ERBB receptors. *Cancer research* **72**, 3228-3237, doi:10.1158/0008-5472.CAN-11-3747 (2012).

336 Carracedo, A. *et al.* Inhibition of mTORC1 leads to MAPK pathway activation through a PI3K-dependent feedback loop in human cancer. *J Clin Invest* **118**, 3065-3074, doi:10.1172/JCI34739 (2008).

337 Ridzewski, R. *et al.* Hedgehog Inhibitors in Rhabdomyosarcoma: A Comparison of Four Compounds and Responsiveness of Four Cell Lines. *Frontiers in oncology* **5**, 130, doi:10.3389/fonc.2015.00130 (2015).

338 Feil, S., Valtcheva, N. & Feil, R. Inducible Cre mice. *Methods Mol Biol* **530**, 343-363, doi:10.1007/978-1-59745-471-1_18 (2009).

339 Hayashi, S. & McMahon, A. P. Efficient recombination in diverse tissues by a tamoxifen-inducible form of Cre: a tool for temporally regulated gene activation/inactivation in the mouse. *Developmental biology* **244**, 305-318, doi:10.1006/dbio.2002.0597 (2002).

340 Vooijs, M., Jonkers, J. & Berns, A. A highly efficient ligand-regulated Cre recombinase mouse line shows that LoxP recombination is position dependent. *EMBO Rep* **2**, 292-297, doi:10.1093/embo-reports/kve064 (2001).

341 Chal, J. & Pourquie, O. Making muscle: skeletal myogenesis in vivo and in vitro. *Development* **144**, 2104-2122, doi:10.1242/dev.151035 (2017).

342 Gartel, A. L. & Tyner, A. L. The role of the cyclin-dependent kinase inhibitor p21 in apoptosis. *Molecular cancer therapeutics* **1**, 639-649 (2002).

343 Lauth, M. RAS and Hedgehog--partners in crime. *Front Biosci (Landmark Ed)* **16**, 2259-2270 (2011).

344 Cytoskeleton. *Ras Pull-down Activation Assay Biochem Kit (bead pull-down format)*, https://www.cytoskeleton.com/bk008

345 Barretina, J. *et al.* The Cancer Cell Line Encyclopedia enables predictive modelling of anticancer drug sensitivity. *Nature* **483**, 603-607, doi:10.1038/nature11003 (2012).

346 Malinin, N. L., Boldin, M. P., Kovalenko, A. V. & Wallach, D. MAP3K-related kinase involved in NF-kappaB induction by TNF, CD95 and IL-1. *Nature* **385**, 540-544, doi:10.1038/385540a0 (1997).

347 Xia, Y., Wu, Z., Su, B., Murray, B. & Karin, M. JNKK1 organizes a MAP kinase module through specific and sequential interactions with upstream and downstream components mediated by its amino-terminal extension. *Genes & development* **12**, 3369-3381 (1998).

348 Ye, B., Yu, W. P., Thomas, G. M. & Huganir, R. L. GRASP-1 is a neuronal scaffold protein for the JNK signaling pathway. *FEBS letters* **581**, 4403-4410, doi:10.1016/j.febslet.2007.08.008 (2007).

349 Hinson, A. R. *et al.* Human rhabdomyosarcoma cell lines for rhabdomyosarcoma research: utility and pitfalls. *Frontiers in oncology* **3**, 183, doi:10.3389/fonc.2013.00183 (2013).

350 Beylkin, D. H., Allen, D. L. & Leinwand, L. A. MyoD, Myf5, and the calcineurin pathway activate the developmental myosin heavy chain genes. *Developmental biology* **294**, 541-553, doi:10.1016/j.ydbio.2006.02.049 (2006).

351 Kouraklis, G., Triche, T. J., Wesley, R. & Tsokos, M. Myc oncogene expression and nude mouse tumorigenicity and metastasis formation are higher in alveolar than embryonal rhabdomyosarcoma cell lines. *Pediatric research* **45**, 552-558, doi:10.1203/00006450-199904010-00015 (1999).

352 Khan, J. *et al.* Gene expression profiling of alveolar rhabdomyosarcoma with cDNA microarrays. *Cancer Res* **58**, 5009-5013. (1998).

353 Chen, Y. *et al.* Mutation and expression analyses of the MET and CDKN2A genes in rhabdomyosarcoma with emphasis on MET overexpression. *Genes, chromosomes & cancer* **46**, 348-358, doi:10.1002/gcc.20416 (2007).

354 Lopes-Ramos, C. M. *et al.* Regulatory network changes between cell lines and their tissues of origin. *BMC genomics* **18**, 723, doi:10.1186/s12864-017-4111-x (2017).
355 Tukachinsky, H., Kuzmickas, R. P., Jao, C. Y., Liu, J. & Salic, A. Dispatched and scube mediate the efficient secretion of the cholesterol-modified hedgehog ligand. *Cell reports* **2**, 308-320, doi:10.1016/j.celrep.2012.07.010 (2012).
356 Wheway, G., Nazlamova, L. & Hancock, J. T. Signaling through the Primary Cilium. *Frontiers in cell and developmental biology* **6**, 8, doi:10.3389/fcell.2018.00008 (2018).
357 Fang, X. *et al.* Phosphorylation and inactivation of glycogen synthase kinase 3 by protein kinase A. *Proc Natl Acad Sci U S A* **97**, 11960-11965, doi:10.1073/pnas.220413597 (2000).
358 Yordy, J. S. & Muise-Helmericks, R. C. Signal transduction and the Ets family of transcription factors. *Oncogene* **19**, 6503-6513, doi:10.1038/sj.onc.1204036 (2000).
359 Nakashima, H. *et al.* Nuclear factor-kappaB contributes to hedgehog signaling pathway activation through sonic hedgehog induction in pancreatic cancer. *Cancer research* **66**, 7041-7049, doi:10.1158/0008-5472.CAN-05-4588 (2006).
360 Gu, D., Schlotman, K. E. & Xie, J. Deciphering the role of hedgehog signaling in pancreatic cancer. *Journal of biomedical research* **30**, 353-360, doi:10.7555/JBR.30.20150107 (2016).
361 ten Haaf, A. *et al.* Paradox of sonic hedgehog (SHH) transcriptional regulation: Alternative transcription initiation overrides the effect of downstream promoter DNA methylation. *Epigenetics : official journal of the DNA Methylation Society* **6**, 465-477 (2011).
362 Cui, W. *et al.* Expression and regulation mechanisms of Sonic Hedgehog in breast cancer. *Cancer science* **101**, 927-933, doi:10.1111/j.1349-7006.2010.01495.x (2010).
363 Kim, B. Y., Gaynor, R. B., Song, K., Dritschilo, A. & Jung, M. Constitutive activation of NF-kappaB in Ki-ras-transformed prostate epithelial cells. *Oncogene* **21**, 4490-4497, doi:10.1038/sj.onc.1205547 (2002).
364 Mayo, M. W., Norris, J. L. & Baldwin, A. S. Ras regulation of NF-kappa B and apoptosis. *Methods Enzymol* **333**, 73-87 (2001).
365 Dhawan, P. & Richmond, A. A novel NF-kappa B-inducing kinase-MAPK signaling pathway up-regulates NF-kappa B activity in melanoma cells. *The Journal of biological chemistry* **277**, 7920-7928, doi:10.1074/jbc.M112210200 (2002).
366 Nakano, H. *et al.* Differential regulation of IkappaB kinase alpha and beta by two upstream kinases, NF-kappaB-inducing kinase and mitogen-activated protein kinase/ERK kinase kinase-1. *Proc Natl Acad Sci U S A* **95**, 3537-3542 (1998).
367 Zhao, Q. & Lee, F. S. Mitogen-activated protein kinase/ERK kinase kinases 2 and 3 activate nuclear factor-kappaB through IkappaB kinase-alpha and IkappaB kinase-beta. *The Journal of biological chemistry* **274**, 8355-8358 (1999).
368 Carter, A. B. & Hunninghake, G. W. A constitutive active MEK --> ERK pathway negatively regulates NF-kappa B-dependent gene expression by modulating TATA-binding protein phosphorylation. *The Journal of biological chemistry* **275**, 27858-27864, doi:10.1074/jbc.M003599200 (2000).
369 Yauch, R. L. *et al.* A paracrine requirement for hedgehog signalling in cancer. *Nature* (2008).
370 Persons, D. L., Yazlovitskaya, E. M. & Pelling, J. C. Effect of extracellular signal-regulated kinase on p53 accumulation in response to cisplatin. *The Journal of biological chemistry* **275**, 35778-35785, doi:10.1074/jbc.M004267200 (2000).
371 Fung, M. K. *et al.* Role of MEK/ERK pathway in the MAD2-mediated cisplatin sensitivity in testicular germ cell tumour cells. *Br J Cancer* **95**, 475-484, doi:10.1038/sj.bjc.6603284 (2006).
372 Cox, A. D. & Der, C. J. The dark side of Ras: regulation of apoptosis. *Oncogene* **22**, 8999-9006, doi:10.1038/sj.onc.1207111 (2003).
373 Banfalvi, G. Overview of cell synchronization. *Methods Mol Biol* **761**, 1-23, doi:10.1007/978-1-61779-182-6_1 (2011).
374 Cecchini, M. J., Amiri, M. & Dick, F. A. Analysis of cell cycle position in mammalian cells. *Journal of visualized experiments : JoVE*, doi:10.3791/3491 (2012).

375 Hasenpusch-Theil, K. *et al.* Gorlin syndrome: identification of 4 novel germ-line mutations of the human patched (PTCH) gene. *Human mutation* **11**, 480 (1998).
376 Francetic, T. & Li, Q. Skeletal myogenesis and Myf5 activation. *Transcription* **2**, 109-114, doi:10.4161/trns.2.3.15829 (2011).
377 Ott, M. O., Bober, E., Lyons, G., Arnold, H. & Buckingham, M. Early expression of the myogenic regulatory gene, myf-5, in precursor cells of skeletal muscle in the mouse embryo. *Development* **111**, 1097-1107 (1991).
378 Summerbell, D. *et al.* The expression of Myf5 in the developing mouse embryo is controlled by discrete and dispersed enhancers specific for particular populations of skeletal muscle precursors. *Development* **127**, 3745-3757 (2000).
379 Liu, J. *et al.* Non-parallel recombination limits Cre-LoxP-based reporters as precise indicators of conditional genetic manipulation. *Genesis* **51**, 436-442, doi:10.1002/dvg.22384 (2013).
380 Rangarajan, A. & Weinberg, R. A. Comparative biology of mouse versus human cells: modelling human cancer in mice. *Nature Reviews Cancer* **3**, 952, doi:10.1038/nrc1235 (2003).
381 Robanus-Maandag, E. *et al.* p107 is a suppressor of retinoblastoma development in pRb-deficient mice. *Genes & development* **12**, 1599-1609 (1998).
382 Giovannini, M. *et al.* Conditional biallelic Nf2 mutation in the mouse promotes manifestations of human neurofibromatosis type 2. *Genes & development* **14**, 1617-1630 (2000).
383 Kumar, S., Perlman, E., Harris, C. A., Raffeld, M. & Tsokos, M. Myogenin is a specific marker for rhabdomyosarcoma: an immunohistochemical study in paraffin-embedded tissues. *Mod Pathol* **13**, 988-993 (2000).
384 Muthuchamy, M., Pajak, L., Howles, P., Doetschman, T. & Wieczorek, D. F. Developmental analysis of tropomyosin gene expression in embryonic stem cells and mouse embryos. *Molecular and cellular biology* **13**, 3311-3323 (1993).
385 Yohe, M. E. *et al.* MEK inhibition induces MYOG and remodels super-enhancers in RAS-driven rhabdomyosarcoma. *Science translational medicine* **10**, doi:10.1126/scitranslmed.aan4470 (2018).
386 Nitzki, F. *et al.* Hedgehog/Patched-associated rhabdomyosarcoma formation from delta1-expressing mesodermal cells. *Oncogene*, doi:10.1038/onc.2015.346 (2015).
387 Castillo-Martin, M., Domingo-Domenech, J., Karni-Schmidt, O., Matos, T. & Cordon-Cardo, C. Molecular pathways of urothelial development and bladder tumorigenesis. *Urologic oncology* **28**, 401-408, doi:10.1016/j.urolonc.2009.04.019 (2010).
388 Nash, G. M. *et al.* KRAS mutation and microsatellite instability: two genetic markers of early tumor development that influence the prognosis of colorectal cancer. *Annals of surgical oncology* **17**, 416-424, doi:10.1245/s10434-009-0713-0 (2010).
389 Omholt, K. *et al.* Screening of N-ras codon 61 mutations in paired primary and metastatic cutaneous melanomas: mutations occur early and persist throughout tumor progression. *Clinical cancer research : an official journal of the American Association for Cancer Research* **8**, 3468-3474 (2002).
390 Denayer, E. *et al.* NRAS Mutations in Noonan Syndrome. *Molecular syndromology* **3**, 34-38, doi:10.1159/000338467 (2012).
391 Ugurel, S. *et al.* B-RAF and N-RAS mutations are preserved during short time in vitro propagation and differentially impact prognosis. *PloS one* **2**, e236-e236, doi:10.1371/journal.pone.0000236 (2007).
392 Kuhner, M. K., Kostadinov, R. & Reid, B. J. Limitations of the Driver/Passenger Model in Cancer Prevention. *Cancer prevention research (Philadelphia, Pa.)* **9**, 335-338, doi:10.1158/1940-6207.capr-15-0343 (2016).
393 Chen, L. *et al.* Clonality and evolutionary history of rhabdomyosarcoma. *PLoS genetics* **11**, e1005075, doi:10.1371/journal.pgen.1005075 (2015).
394 Makishima, H. & Maciejewski, J. P. Pathogenesis and consequences of uniparental disomy in cancer. *Clinical cancer research : an official journal of the American Association for Cancer Research* **17**, 3913-3923, doi:10.1158/1078-0432.ccr-10-2900 (2011).

395 Krskova, L. *et al.* Rhabdomyosarcoma: molecular analysis of Igf2, MyoD1 and Myogenin expression. *Neoplasma* **58**, 415-423 (2011).
396 Makawita, S. *et al.* Expression of insulin-like growth factor pathway proteins in rhabdomyosarcoma: IGF-2 expression is associated with translocation-negative tumors. *Pediatric and developmental pathology : the official journal of the Society for Pediatric Pathology and the Paediatric Pathology Society* **12**, 127-135 (2009).
397 Plaks, V., Kong, N. & Werb, Z. The cancer stem cell niche: how essential is the niche in regulating stemness of tumor cells? *Cell stem cell* **16**, 225-238, doi:10.1016/j.stem.2015.02.015 (2015).
398 Kondo, T. Stem cell-like cancer cells in cancer cell lines. *Cancer biomarkers : section A of Disease markers* **3**, 245-250 (2007).
399 Veselska, R., Skoda, J. & Neradil, J. Detection of Cancer Stem Cell Markers in Sarcomas. *Klinicka onkologie Journal* **25**, 2s16–12s20 (2012).
400 Dela Cruz, F. S. Cancer stem cells in pediatric sarcomas. *Frontiers in oncology* **3**, 168, doi:10.3389/fonc.2013.00168 (2013).
401 Rich, J. N. Cancer stem cells: understanding tumor hierarchy and heterogeneity. *Medicine* **95**, S2-S7, doi:10.1097/md.0000000000004764 (2016).
402 Baccelli, I. & Trumpp, A. The evolving concept of cancer and metastasis stem cells. *The Journal of cell biology* **198**, 281-293, doi:10.1083/jcb.201202014 (2012).
403 Kreso, A. & Dick, John E. Evolution of the Cancer Stem Cell Model. *Cell stem cell* **14**, 275-291, doi: 10.1016/j.stem.2014.02.006 (2014).
404 Merchant, A. A. & Matsui, W. Targeting Hedgehog--a cancer stem cell pathway. *Clinical cancer research : an official journal of the American Association for Cancer Research* **16**, 3130-3140, doi:10.1158/1078-0432.ccr-09-2846 (2010).
405 Cochrane, C. R., Szczepny, A., Watkins, D. N. & Cain, J. E. Hedgehog Signaling in the Maintenance of Cancer Stem Cells. *Cancers* **7**, 1554-1585, doi:10.3390/cancers7030851 (2015).
406 Takebe, N. *et al.* Targeting Notch, Hedgehog, and Wnt pathways in cancer stem cells: clinical update. *Nature Reviews Clinical Oncology* **12**, 445, doi:10.1038/nrclinonc.2015.61 (2015).
407 Pressey, J. G. *et al.* CD133 marks a myogenically primitive subpopulation in rhabdomyosarcoma cell lines that are relatively chemoresistant but sensitive to mutant HSV. *Pediatric blood & cancer* **60**, 45-52, doi:10.1002/pbc.24117 (2013).
408 Walter, D. *et al.* CD133 positive embryonal rhabdomyosarcoma stem-like cell population is enriched in rhabdospheres. *PloS one* **6**, e19506, doi:10.1371/journal.pone.0019506 (2011).
409 Nakahata, K. *et al.* Aldehyde Dehydrogenase 1 (ALDH1) Is a Potential Marker for Cancer Stem Cells in Embryonal Rhabdomyosarcoma. *PloS one* **10**, e0125454, doi:10.1371/journal.pone.0125454 (2015).

Acknowledgements

It has been a long way to finish this thesis and it would not have been possible without the continuous support of all the people, which have been involved during this process.

First, I would like to express my deep gratitude to Prof. Dr. Heidi Hahn, my research supervisor, for her patient guidance, useful critiques and encouragement throughout this work. Thank you for your support, continuous mentoring, constructive discussions and proofreading of this work. Especially I would like to thank you for the confidence you have placed in me and for giving me the opportunity to work on exciting research projects.

In addition, I would like to express my great appreciation to Prof. Dr. Matthias Dobbelstein and Prof. Dr. Dieter Kube for their valuable and constructive suggestions during our thesis committee meetings. Thank you for your advice and ideas.

My grateful thanks go to Dr. Christian Dullin for his help with the µCT measurements. Additionally, I would like to thank Dr. Verena Reupke, Christina Malowsky, Sarah Garbode and Jonas Albers for enabling me to perform all the µCT measurements on time. Thanks for your competent work and the pleasant atmosphere during several measurements. In addition, my sincere thanks go to Prof. Dr. Hans-Ulrich Schildhaus for reviewing and evaluating numerous histological slides. Thank you for your interpretation and helpful explanations. Special thanks go to Dr. Kai Dittmann, who supported me with acquisition and interpretation of flow cytometry data. Thank you for your help and the nice atmosphere. Furthermore, I would like to thank Dr. Albert Rosenberger for statistical advice.

My special thanks are extended to Prof. Dr. Fritz Aberger, Dominik Elmer and Christina Sternberg. Thank you for the initial Western Blot analyses of my samples, the helpful assistance in the establishment of the GLI Western Blots, the stable transduction of Daoys and the opportunity to visit Salzburg and learn your method at first hand. In addition, I would like to acknowledge Prof. Dr. James A. Fagin for providing the *Hras*^{tm1Jaf} mice and thereby supporting this work. Furthermore, I would like to thank Prof. Dr. Thomas A. Rando, who kindly provided the *Myf5*$^{tm1(cre/Esr1*)Trdo}$ mice. Many thanks go to Prof. Dr. Dieter Saur for generously providing *Kras*^{tm4Tyj} mice to our lab.

Many people accompanied me on my way to complete this study and I am very grateful to all members of the department. Sincere thanks go to all present and former members of our working group for creating an atmosphere I enjoyed to work in. In particular, I would like to thank PD. Dr. Anja Uhmann for having a sympathetic ear for all the questions and problems that accompany a PhD. Thank you for inspiring discussions on scientific and non-scientific issues, technical advice and helpful suggestions, sharing your knowledge and experiences and always being supportive and reliable. Without our small coffee breaks, this PhD would

not have been the same. Moreover, I especially would like to thank Dr. Natalie Geyer and Dominik Botermann for the time we spent together at the µCT and on the way to the clinics and back. I additionally wish to acknowledge all the further support provided by Dominik Botermann. Thank you for being a great laboratory partner and taking care of my mice when I was not around. Moreover, I thank Dr. Nicole Cuvelier for the guidance at the beginning of my project. My grateful thanks go to our technicians for their help and technical support in everyday lab work. Especially, I would like to thank Anke Frommhold for taking the time to prepare tissue sections, her assistance with stainings and the immense support in the collection of my Ki67 data. Similar, my gratitude goes to Ina Heß for her support in second genotyping. Many thanks also go to all the other past and present lab members: Dr. Benedikt Linder, Dr. Marco Becker, Dr. Rosalie Ridzewski, Dr. Julia Dräger, Dr. Joanna Pyczek and Nadine Brandes. I am grateful for being part of such a wonderful working group. Thank you so much for all the support in the regular duties and responsibilities of the lab work, the various scientific and non-scientific discussions, a lot of fun and laughter in long hours of experiments, helpful encouragement in hard moments and sometimes being more than just colleagues. Thanks to the animal caretakers, especially Lea Piontek, Shari Bötticher and Susann Peter, who always had an eye on all the mice and thereby supported this work. Additionally, I would like to thank some of the “short-term” members of our working group. Thanks to Wiebke Maurer and Maria Kuzyakova for the nice time, we shared in the lab. Thanks to Simran, Soraia and Lukas for showing me what it means to be a supervisor.

Most importantly, I wish to thank my family for their endless support and encouragement throughout my studies and this thesis. Without you this would not have been possible and I am very grateful that you have faith in everything I do. Loving thanks go to my parents, Silvia and Karl-Heinz, for the countless ways in which, throughout my life, they have supported me. Thank you Nils, for providing the soundtrack to the good and bad days, for distraction from problems and the daily routine and being the best brother one could imagine. Additionally, many thanks go to my friends, who were always there for me and excused so many unplanned delays.

Finally, I gratefully thank my husband and best friend Sven. I thank you from the bottom of my heart for your patience, for celebrating each small progress, for cheering me up in critical phases, for your calming influence and for being around whenever I needed you. Your love was the greatest support throughout this thesis. Thank you!